Modelling of Controlled Source Electromagnetic Data

Lars Ole Løseth

Thesis presented for the degree
Doctor of Philosophy
at the
Norwegian University of Science and Technology
Department of Physics
March 2007

Summary

This work treats modelling of electromagnetic fields from controlled sources in geophysical applications. The focus is on modelling the marine CSEM (controlled source electromagnetic) method in planarly layered media. The recent introduction of SeaBed Logging (SBL) as an application of the marine CSEM method for direct hydrocarbon identification has resulted in increased survey activity, and expanded as well as renewed the interest for investigating electromagnetic field propagation in the subsurface of the earth.

The material within this document consists of a short introduction to the CSEM and SBL methods and four self-contained papers:

- **Low-frequency electromagnetic fields in applied geophysics: Waves or diffusion?** treats propagation of low-frequency fields in conductive media, and compares their behaviour to nondistorted field propagation in lossless media.
- **The first test of the SeaBed Logging method** describes the first laboratory test of this method. The scaled experiment was performed in order to validate if the detection of thin resistive layers within conductive surrounding media is possible.
- **Asymptotic evaluations of the marine CSEM field integrals** elaborates on how electromagnetic signals propagate in an idealized stratified earth model. To this end, the method of steepest descents is applied in order to separate the various wavemodes.
- **Electromagnetic fields in planarly layered anisotropic media** formulates a mathematical description of the field propagation in stratified media with arbitrary anisotropy. The field equations are solved by using the matrix propagator technique.

Even if electromagnetic field propagation in layered media is a rather mature research subject, the current development of the CSEM and SBL methods demands reinvestigations and new theoretical insights. Optimal survey planning and solid interpretation rely on a thorough understanding of the signal propagation in the subsurface. The main motivation in this thesis is to contribute to increased knowledge of how electromagnetic fields travel in the earth.

Preface

This document has been manufactured in order to satisfy the requirements for the degree "Doctor of Philosophy" (PhD) at the Norwegian University of Science and Technology (NTNU). The presented work has been carried out during four years from January 2003 to December 2006 at the Department of Physics. The first three years were financed by VISTA [Statoil's basic research programme conducted in collaboration with the Norwegian Academy of Science and Letters (www.vista.no)]. The final year has been financed by NTNU in return for teaching assignments at the Physics Department. I would like to thank both VISTA and NTNU for providing the finances necessary to conduct the research. I am grateful to Kåre Olaussen, Jakob J. Stamnes, and José M. Carcione for serving in the evaluation committee.

In January 2000 I was looking for a subject for my diploma thesis at NTNU and was fortunate to be introduced to the topic of electromagnetic wave propagation in layered media by Hans Magne Pedersen. After an excursion into the world of IT, I was a couple of years later given the opportunity to do a PhD in the same field of research much thanks to him. Hans Magne died in November 2004, and his company and knowledge have been greatly missed.

Bjørn Ursin and Ola Hunderi have been my supervisors the final two years of the PhD programme. I am grateful to both, and especially Bjørn for many inspiring and enlightening discussions. I furthermore thank Lasse Amundsen at Statoil ASA for constructive cooperation and for being a helpful contact person towards the VISTA programme. Also deserving special thanks are Terje Eidesmo and Svein Ellingsrud for employing me in ElectroMagnetic GeoServices (emgs) AS right after the company had been founded. The experience gained by working with collecting and processing SBL data before becoming a PhD student has been valuable, and it has been a privilege to work part time for emgs during the studies. I am indebted to many emgs employees (present and previous) for educational discussions; Rune Mittet and Ingve Simonsen deserve credit in particular.

I would also like to thank the staff at the Physics Department for providing a nice and comfortable working environment. I thank my former office neighbours Ole Johan Løkberg and Trude Støren for many interesting conversations about optics. The staff at SINTEF deserve credit for treating coffee, and Frantz for helping to drink their coffee (as well as Eirik

for leaving his share to us).

Finally, I thank family and friends for reminding me that there are more important things in life than a PhD.

Trondheim, December 2006

Lars O. Løseth

Contents

Chapter 1

Thesis introduction

The purpose of this introduction is to give a brief review of the marine CSEM (controlled source electromagnetic) and SBL (SeaBed Logging) methods. The main contents of the papers are furthermore outlined, and I have attempted to put the contribution from each paper into perspective as well as to explain the motivation for writing them.

1.1 Electromagnetic methods in geophysics

The history of scientific research of electromagnetism started with Ørsted's discovery of the fundamental relation between electricity and magnetism, and furthermore Ampère's explanation of Ørsted's findings (Hofmann, 2006). Darrigol (2000) presents a review of the development of electrodynamics in the 19th century, e.g., Ampère's formulations, Faraday's field concept, Maxwell's equations, Hertz' production of Maxwell's predicted waves, and Einstein's solution to the discrepancy between Newtonian and Maxwellian physics.

A summary of the early history of electromagnetic exploration in geophysics can be found in Ward (1980). Presumably the most successful application for hydrocarbon exploration has been well logging which was introduced by the Schlumberger brothers (Johnson, 1962). For the variety of remote sensing methods that were introduced during the 20th century, it seems that the more or less futile struggle to find a direct hydrocarbon-detection technique made electromagnetic methods of minor importance compared to seismic methods in the petroleum industry. The activity in electromagnetic exploration has however not been nonexistent, and in the 1980s, improved equipment and increasing data-processing power led to extensive development. Of particular interest to the work presented in this thesis is the development of marine exploration methods such as the marine CSEM and the marine magnetotelluric (MT) method (Chave et al., 1991).

Most of the electromagnetic applications in geophysics attempt to measure the resistivity of the earth materials. Numerous different names are used for more or less the same

resistivity-measurement methods as is evident in Nabighian (1987). The variety of methods reflects the possibility to vary the source type (e.g., magnetic or electric dipole) and source signal (e.g., direct current, time-harmonic, or transient).

The electromagnetic properties of a medium are described by the electric permittivity, magnetic permeability, and electric conductivity (resistivity is the reciprocal of conductivity). Since the earth is conductive, the attenuation of propagating waves becomes more severe as the signal frequency increases (frequencies in the optical window excepted). For example the use of radio frequencies in the ground penetrating radar (GPR) method thus implies that this method is employed for sensing the near surface. Both the electric permittivity and conductivity are important electromagnetic properties for the field propagation in GPR. The electric permittivity is also important in induced polarization methods where one seeks to measure the capacitance of the earth materials. In most of the exploration methods, except for e.g., magnetic ore-body prospecting, the possible variation of the magnetic permeability has so far not been recognized as important.

All of the methods that use human-made signal sources can in principle be referred to as CSEM methods. Contrary to the CSEM method, the MT method uses naturally occurring electromagnetic signals in the magnetosphere and ionosphere to measure the earth's apparent resistivity. The source signal in MT contains a spectrum of frequencies. The lower frequencies can be used to get a rough estimate of the deep subsurface resistivity profile, and the higher frequencies can be used to determine the resistivity profile in the near subsurface. The resolution of a subsurface image from MT increases as the applied source frequency increases. The MT method was introduced by Cagniard in the 1950's (Cagniard, 1953). The same receiver equipment can be used for both the CSEM and MT methods.

Every application of electromagnetic methods in geophysics obeys the same fundamental electromagnetic equations and can thus be compared to exploitation of electromagnetic phenomena in other technological disciplines such as for example communication technology. The application of antennas that operate at extremely low frequencies used in submarines, and the theoretical investigations in this subject (Burrows, 1978), are thus closely related to the marine CSEM application and corresponding research.

1.2 The CSEM and SBL methods

In 2000 the first SBL survey was performed offshore Angola (Ellingsrud et al., 2002). The survey was a result of successful laboratory testing (presented in Chapter 3 in this document), and since then, the interest in electromagnetic methods for subsurface exploration has increased. Today, six years after, electromagnetic methods are attractive for the petroleum industry as complementary tools to seismic methods, or even standalone tools, for remote sensing of the subsurface.

1.2 The CSEM and SBL methods

The SBL operation offshore Angola used the same apparatus as a standard marine CSEM survey. Even if the application of marine CSEM for hydrocarbon exploration had been investigated (Chave et al., 1991), the idea that the guiding of electromagnetic energy in hydrocarbon reservoirs is detectable, had not been pursued before Eidesmo et al. (2002) suggested using marine CSEM for direct hydrocarbon identification. The marine CSEM method was introduced by Cox et al. (1971), and has since then been successfully applied to study the oceanic lithosphere and active spreading centres (Young and Cox, 1981; Cox et al., 1986; Chave et al., 1990; Evans et al., 1994; Constable and Cox, 1996; MacGregor and Sinha, 2000).

In a marine CSEM experiment, a dipole antenna is used as source. Normally, a horizontal electric dipole source is used since this configuration results in the strongest response from the subsurface. The dipole emits a low-frequency signal (could be many frequency components, typically in the range 0.1 Hz to 10 Hz) into the surrounding media, and the signal is usually recorded by stationary seafloor receivers having both magnetic and electric dipole antennas.

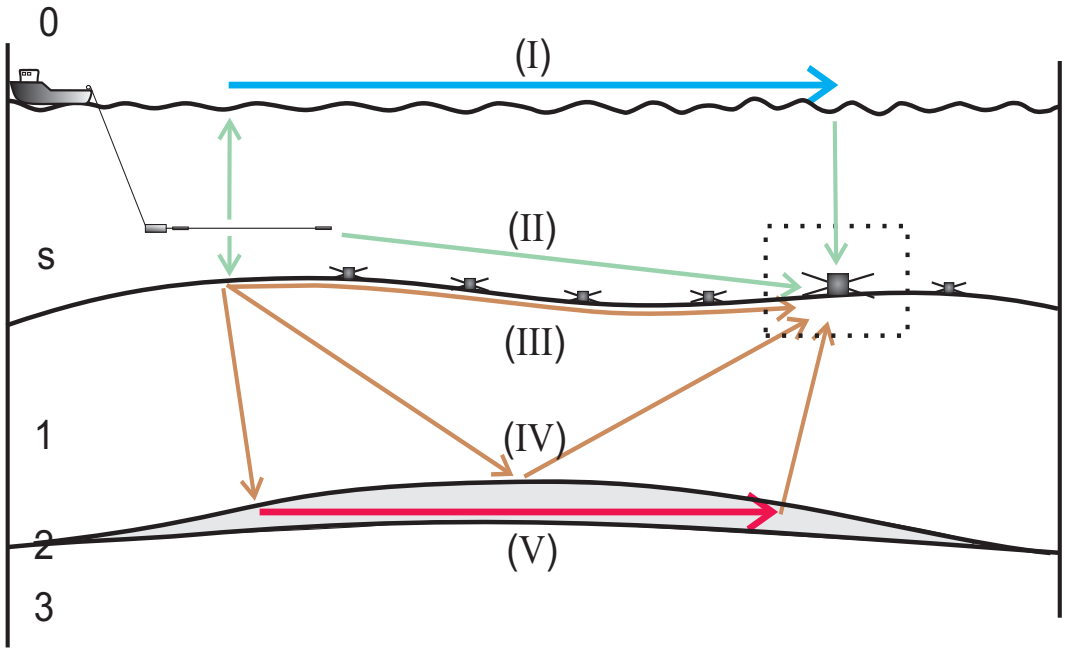

Figure 1.1: A sketch of a basic marine CSEM/SBL survey layout. The source antenna is towed behind the vessel, and the receivers are situated on the seabed. The signal propagation is indicated assuming that a hydrocarbon reservoir is present. The main contributions to the total response come from the sea-surface (I), direct field (II), seabed (III), "ray" reflection (IV), and guiding (V).

A typical CSEM/SBL survey layout is sketched in Figure 1.1 along with the basic signal propagation. The model that is presented consists of an air halfspace (region 0), a seawater layer (layer s), an overburden (layer 1), a thin resistive reservoir (layer 2), and an underburden (region 3). The conductivity of the seawater is larger than the conductivity of the overburden. The overburden conductivity is more or less equal to the underburden conductivity. The thin layer (e.g., hydrocarbons) is more resistive than the surrounding media and is normally referred to as a resistive layer. The term resistive layer might be a bit misleading since the layer is actually very conductive. Thus, the conduction current in Ampère's law dominates the displacement current for this medium also. However, the thin layer is resistive compared to the conductive surroundings which justifies the use of nomenclature.

Figure 1.1 furthermore contains a vessel that is towing a horizontal electric dipole source. In order to get as much energy down into the subsurface as possible, the source must be towed close to the seafloor. In a typical survey the source antenna has a length of 200 m and the receivers, which are situated on the seafloor, have a separation distance of approximately 1 km. The illustrated signal paths between the source and one of the receivers are: the sea-surface response (I), the direct field (II), the lateral wave along the seabed (III), the "ray" reflection from the thin layer (IV), and the guided wave in the resistive reservoir (V). The notion of the thin resistive layer as a "waveguide" stems from a description of the subsurface layers as stratified. In 3-D structures, the term "lossy resonator" might be more appropriate (cf. Jackson, 1998).

At short offsets (< 2 km) between a source and receiver, the direct field (path II) dominates the received signal. At longer offsets, the dominating contributions are due to the resistor (path V) and sea-surface (path I). These contributions contain multiple reflections in the water column which are not illustrated (cf. Chapter 4). In deep waters, the response from the sea-surface will be less due to the heavy damping of the signal in the water column. If the reservoir is not resistive, the guiding effect will not be present, and in this case, the dominating signal from the subsurface in Figure 1.1 will be from the lateral wave along the seabed (path III).

Along with doing a marine CSEM survey, a marine MT survey can be carried out simultaneously (when the controlled source is not active) since the same receiving equipment is used for both methods. The additional information from MT can be used as a supplement to the CSEM responses (Hoversten et al., 2006) when processing the survey data.

In the last few years, the terms marine CSEM and SBL have been used somewhat differently due to the development of SBL as an application of marine CSEM for direct hydrocarbon detection. At present, many workers refer to all types of offshore hydrocarbon exploration with controlled sources as marine CSEM.

1.3 Short review of the work

The thesis consists of four papers. The focus has been on the propagation of electromagnetic fields in stratified media, and the sources of the electromagnetic fields have been considered in 3-D space for all of the presented work. Proper handling of the inversion and migration problem relies on a thorough understanding of the mechanisms behind the field propagation. A numerical solution to Maxwell's equations for 3-D structures follows more or less directly from the equations. However, the formulation of a specific problem in an appropriate manner requires knowledge of the signal behaviour. It is thus believed that the contribution here is of value when considering modelling of 3-D structures, and also when treating the inverse problem and migration. Moreover, the equations for layered media are often useful when applying approximation methods to more complicated structures.

The first paper (Chapter 2) can be read as an introduction to electromagnetic field propagation in conductive media. The second paper (Chapter 3) presents the first test of the SBL method. This chapter should be of interest both as a historical documentation and an introduction to the basic concepts in the marine CSEM and SBL methods. The last two chapters constitute the main body of the thesis. Chapter 4 evaluates how the electromagnetic signals propagate in a planarly layered model, and Chapter 5 treats stratified media with arbitrary anisotropy. In the following the papers are reviewed in more detail.

In **Chapter 2**, the paper **Low-frequency electromagnetic fields in applied geophysics: Waves or diffusion?** is presented. It was written together with Hans Magne Pedersen, Bjørn Ursin, Lasse Amundsen, and Svein Ellingsrud. The paper was published by *Geophysics* in July 2006. The version presented in the thesis is slightly rewritten in order to be more consistent with the notation and language in the rest of the document.

The paper is a review of basic electromagnetic field propagation in dispersive and conductive media as well as nondispersive and nonconductive media. Maxwell's equations are considered in the frequency domain, and basic plane-wave analysis, asymptotic ray theory, and propagation in layered media are subjects of discussion along with Green's functions and electric dipole radiation in homogeneous regions. The common frequency-domain description of electromagnetic fields is used to calculate the time-domain characteristics of the fields for single-frequency-component signals and transients. For nonconductive media, this is shown to give basic sinusoidal wave propagation and pulse propagation, respectively. For conductive media, the paper demonstrates the attenuated wave propagation for the time-harmonic signal and the diffusion-like spreading for the transient signal.

The motivation for writing the paper was an apparent reluctance of some workers in the geophysical community to accept the term wave propagation in association with low-frequency field propagation in conductive media; they prefer to use the notion of diffusion

for such field propagation. The conclusion from our review is that both the term diffusion and wave propagation can be used, but that both terms should be used with some care. Independent of the choice of naming convention, the paper demonstrates that the well-known mathematical techniques in wave theory can be used for low-frequency fields in applied geophysics.

Chapter 3 presents **The first test of the SeaBed Logging method**. The paper is a result of collaboration with Hans Magne Pedersen, Tor Schaug-Pettersen, Svein Ellingsrud, and Terje Eidesmo. It has been submitted to the *Journal of Applied Geophysics*, and it describes the first laboratory test of the SBL method. The scaled experiment was performed in order to validate if the detection of thin resistive layers within conductive surrounding media is possible. The presented results show very good agreement between measured and modelled data. The modelled data were produced by a modelling tool for stratified media that can contain a dipole source in one of the layers. That 1-D modelling tools are sufficient for many model configurations is confirmed by Constable and Weiss (2006) who consider 1-D modelling of thin resistors and conclude that this often give satisfactory answers when compared to 3-D modelling.

The incentive for writing a summary of the initial test of the SBL method was to document the central idea and history behind the SBL method. In the thesis, the paper also introduces basic concepts and formulas that are further developed in the following two chapters. It might be in order to mention that the implications of the results of the tank experiment have been substantial. The successful test led to the first SBL survey offshore Angola in 2000 (Ellingsrud et al., 2002), and was an important part of the process that resulted in the establishment of the company emgs AS. The current growth in electromagnetic exploration activity in the petroleum industry is thus much obliged to the successful results in the tank experiment.

In **Asymptotic evaluations of the marine CSEM field integrals** presented in **Chapter 4**, I consider propagation of low-frequency electromagnetic fields in conductive media in terms of their wavemodes. The paper has been submitted to *IEEE Transactions on Geoscience and Remote Sensing*. The expressions that describe the electromagnetic fields in layered media can be written as integrals over a spectrum of plane waves in terms of Hankel functions and transfer functions. The evaluation of these integrals by the method of steepest descents leads to a description of the wave propagation in terms of the various wavemodes. This technique is well known and has e.g., been used to describe propagation of radio waves along the surface of the earth. Wait (1998) gives a review of the history of the so-called ground wave. Brekhovskikh (1960), Stamnes (1986), Kong (2000), and Felsen and Marcuvitz (2003) investigate asymptotic evaluation methods of integrals that describe wave

propagation.

When using the method of steepest descents, the wavemodes are results of the behaviour of the integrand in the complex wavenumber domain, and they can roughly be divided into the following categories: The reflected or transmitted ray is described by the saddle-point contribution, a possible lateral wave is described by branch points, and surface waves or guided waves are due to poles. The method of steepest descents is most often used for wave propagation in lossless media, but some investigations have also been done for propagation in conductive regions. Baños (1966) presents a thorough analysis of a medium configuration of two halfspaces where one is conductive. Wait (1966) considers propagation in a multilayered earth. Both authors describe the propagation in terms of electromagnetic potentials. In the contribution presented in Chapter 4, the investigation is done for the field integrals directly. The asymptotic approximations are accurate and provide a thorough basis for a better understanding of the signal propagation in typical marine CSEM models. The results explain why, for instance, the MT method will not detect thin layers in the manner that the CSEM technique is able to (since the source signal in the MT method can be regarded as plane waves). For the migration problem, the wavemode considerations suggest how the standard reflector problem from seismics (Claerbout, 1971) must be modified in CSEM in order to account for the lateral and guided wavemodes.

The results from the asymptotic evaluation should be valuable for optimizing the survey setup in marine CSEM and SBL as well as when processing and interpreting the collected data. The conclusions in the paper suggest that collection of data could focus on the ability to split the contribution into the TE- and TM-polarization modes. By using the asymptotic field expressions, one should then look for characteristic contributions from the different wavemodes in the data set. The investigations in the paper also imply that, provided that the polarization modes can be separated in acquisition or data processing, shallow water conditions may result in enhanced subsurface response.

Although the results from the paper lead to many potential improvements in the way marine CSEM data can be collected and rendered, it must be noted that the theoretical investigations have been done for an idealized stratified model. In order to be applicable in real CSEM scenarios, careful adaptation must be made.

The last part of the thesis, **Chapter 5**, treats **Electromagnetic fields in planarly layered anisotropic media**. This paper was cowritten with Bjørn Ursin, and has been accepted for publication in *Geophysical Journal International*. The main focus is the formulation of field propagation from dipoles in stratified media with general anisotropy. Many useful equations are obtained in the process of deriving the field equations. Several relations in Ursin (1983) are for the electromagnetic problem generalized to arbitrary anisotropic media. Reflection and transmission responses at planar interfaces between anisotropic regions

are derived. The reciprocity relations as presented in Chapman (1994) for elastic wave propagation are in our paper derived for the electromagnetic problem. The paper furthermore contains a procedure for iteratively calculating reflection and transmission responses through a stack of layers. A similar formulation can be found in e.g., Ursin and Stovas (2002) for elastic wave propagation. The reflectivity method, originally introduced by Kennett (Chapman, 2004), avoids exponentially growing terms that would result if the propagators were calculated directly. In addition to reflection and transmission for piecewise homogeneous media, reflection and transmission are also considered for inhomogeneous media. The results are useful for example when considering media with slow variation in terms of the WKB method.

The matrix propagator method separates the wavefield into upgoing and downgoing waves. This can be exploited when processing real CSEM data as described in Amundsen et al. (2006). By carefully choosing the eigenvector matrices that are used for the transformation of the wavefield into its upgoing and downgoing constituents, the up/down-separation can be done in terms of the polarization modes of the fields. The possibility to remove stacks of layers above or below the position of the measured field follows. In marine CSEM or SBL this implies the ability to remove the seawater layer or the sea-surface interface provided appropriate collection of data.

Following the theoretical derivations, an application of the propagator matrix method is demonstrated on some marine CSEM models with various anisotropies. This reveals that the presence of anisotropy may mislead interpreters of CSEM/SBL data if the anisotropy effects are not carefully taken into account. A modelling code for stratified media that can handle general anisotropy configurations should be a helpful tool in survey planning and data rendering.

Chapter 2

Low-frequency electromagnetic fields in applied geophysics: Waves or diffusion?

L. O. Løseth, H. M. Pedersen, B. Ursin, L. Amundsen, and S. Ellingsrud
Published in Geophysics 71(4), July-August 2006

Summary

Low-frequency electromagnetic signal propagation in geophysical applications is sometimes referred to as diffusion and sometimes as waves. In the following we discuss the mathematical and physical approaches behind the use of the different terms. The basic theory of electromagnetic wave propagation is reviewed. From a frequency-domain description it is shown that all the well-known mathematical tools of wave theory, including an asymptotic ray-series description, can be applied both for nondispersive waves in nonconductive materials and low-frequency waves in conductive materials. We consider the electromagnetic field from an electric dipole source and show that a common frequency-domain description yields both the nondistorted pulses in nonconductive materials and the strongly distorted pulses in conductive materials. We also show that the diffusion-equation approximation of low-frequency electromagnetic fields in conductive materials gives the correct mathematical description, and that this equation has wave solutions. Having considered both a wave-picture approach and a diffusion approach to the problem, we discuss the possible confusion that the use of these terms might lead to.

2.1 Introduction

Electromagnetic methods have been used for a long time and for different purposes in applied geophysics, cf. the extensive treatment in Nabighian (1987). The electromagnetic methods in

geophysics are based on the theory of classic electrodynamics in conductive materials which is treated in well-known textbooks in electromagnetic theory (Stratton, 1941; Adler et al., 1960; Jackson, 1998; Griffiths, 1999; Kong, 2000; Ulaby, 2001) and optics [cf. the chapter on metal optics in Born and Wolf (1999)]. Ward and Hohmann (1987) give a comprehensive review of the theory for geophysical applications.

Since its introduction as an additional hydrocarbon-exploration technique some years ago, SeaBed Logging (SBL) has become an important complementary tool to seismic exploration methods in the detection and characterization of possible hydrocarbon-filled layers in sedimentary environments. SBL is a variety of the marine controlled source electromagnetic (CSEM) method that uses an electric dipole source and array of seabed receiver antennas in a manner suggested by Cox et al. (1971) and Young and Cox (1981). SBL exploits the guiding of electromagnetic energy that occurs in resistive layers located in a more conductive environment (Eidesmo et al., 2002; Ellingsrud et al., 2002).

Eidesmo et al. (2002) refer to electromagnetic signal propagation as both diffusion and waves. They furthermore talk about flowing inductive and galvanic currents as well as an equivalent picture of a respective TE and TM mode of electromagnetic field propagation (Born and Wolf, 1999). In a variety of geophysical literature it is common to refer to the propagation of electromagnetic fields in conductive media as diffusion. Spies (1989) discusses the depth of penetration of various electromagnetic sounding experiments with different source signatures. The propagation is referred to as diffusion; both transient signals and a related time-domain diffusion depth in addition to single-frequency components and their skin depths are considered. Raiche and Gallagher (1985) use the concept of a diffusion velocity for transient electromagnetic signals in the conductive earth, and Lee et al. (1989) consider a fictious wavefield representation of the diffusive electromagnetic field. Virieux et al. (1994) refer to electromagnetic signal propagation in the earth as a diffusion process, whereas Nekut (1994) discusses ray-trace tomography for low-frequency fields in the conductive earth, a well-known wave-theory technique. He refers to the propagation of the fields as diffusive electromagnetic waves. Carcione (2006) applies wave concepts to the electromagnetic diffusion equation. Ward and Hohmann (1987) elaborate on wave propagation of fields in conductive media. They further refer to the differential equations that describe electromagnetic fields in conductive media as both diffusion equations and wave equations.

The propagation of low-frequency electromagnetic fields in conductive media is hence sometimes referred to as diffusion and sometimes referred to as waves. It might be interesting to ask if one naming convention is better than the other. What is the motivation for referring to the propagation as waves, and what is the motivation for the diffusion picture? Is there any physical understanding connected to the words that calls for some care when using either of the terms? In the following we show that propagation of electromagnetic fields in conductive materials is well described within the framework of standard theory of electromagnetic wave

propagation. We demonstrate that the wave equation in the frequency domain contains the diffusion-like equation in the high loss approximation, and that this equation has wave solutions which are attenuated as shown by Ward and Hohmann (1987). Moreover, we find that there is no sharp boundary between propagation of fields in a wave-like manner and a diffusion-like manner. Based on these observations, both terms can be used. However, it is interesting to discuss both the diffusion and wave picture connected to low-frequency electromagnetic fields in conductive materials. We consider the simple cases of an electric dipole in a homogeneous nonconductive medium and a conductive medium. In both cases time-harmonic and transient source signatures are considered. During the discussion, it will become evident that picturing low-frequency propagation of electromagnetic fields in conductive media as waves and diffusion calls for some caution.

We first review Maxwell's equations in the frequency domain. The purpose of the basic mathematical review is to show that a common frequency-domain description contains both the physics behind high-frequency propagation in nonconductive regions and low-frequency propagation in conductive regions. We introduce a complex wavenumber and impedance before we derive inhomogeneous wave equations that describe electromagnetic wave propagation in inhomogeneous media. The reason for treating the equations in the frequency domain becomes evident as we compare the frequency-domain and time-domain differential equations. The vector wave equation without damping term is a hyperbolic partial differential equation, and the vector diffusion equation is a parabolic partial differential equation (Sommerfeld, 1967; Davison and Doeschl, 2004). A vector wave equation with a damping term is either one or the other of these types depending on the material parameters involved. In the frequency domain these partial differential equations reduce to an elliptic equation. We review the simple plane-wave solutions of the frequency-domain wave equation and discuss the relation between the electric and magnetic fields and the wavenumber's dependence on frequency for these waves. The theory for reflection and refraction of plane waves at an interface between two homogeneous media is reviewed in Appendix 2.A.

Next, we look at approximate solutions of the inhomogeneous wave equations by applying asymptotic ray theory, which is well known and extensively used in fields like optics (Born and Wolf, 1999), seismics (Červený and Hron, 1980), and ocean-wave modelling (Svendsen and Jonsson, 1976). The eikonal equation which we derive from our ray-solution ansatz is complex and frequency dependent. We show that it becomes real and frequency independent for the two extreme cases of nondispersive waves in nonconductive materials and the highly dispersive, low-frequency waves in conductive materials. Even if ray theory is a high-frequency approach, it is also applicable in conductive media for low frequencies, as shown by Nekut (1994).

We briefly consider the standard theory of wave propagation in horizontally layered media (Born and Wolf, 1999; Brekhovskikh, 1960; Wait, 1962; Chave and Cox, 1982; Ursin, 1983)

and simplify to homogeneous media where the wave equations are solved in terms of Green's functions. We calculate the Green's functions and use them to derive an expression for the radiated electromagnetic field from an electric dipole source. We consider dipole radiation in homogeneous media and show that the simple frequency-domain description gives a nondispersive wave in nonconductive materials and an attenuated wave in conductive materials for a time-harmonic source current. When regarding a radiated pulse, we get the simple pulse propagation in nonconductive materials and the highly dispersive, distorted diffusion-like pulses in conductive materials. Thus, as expected, we get a separate behaviour depending on the dispersion relation for the two extreme cases. Having presented a unified mathematical treatment of classic electrodynamics, we discuss some basic differences between a diffusion picture and a wave picture of the propagation of fields in conductive regions.

2.2 Electromagnetic fields in the frequency domain

We introduce the Fourier transform pair

$$\boldsymbol{\Psi}(\omega) = \int_{-\infty}^{\infty} dt\, \boldsymbol{\psi}(t)\, \mathrm{e}^{i\omega t} \quad \text{and} \quad \boldsymbol{\psi}(t) = \frac{1}{2\pi} \int_{-\infty}^{\infty} d\omega\, \boldsymbol{\Psi}(\omega)\, \mathrm{e}^{-i\omega t}, \tag{2.1}$$

where $i = \sqrt{-1}$, t denotes time, ω denotes angular frequency, $\boldsymbol{\Psi}$ is a field vector in the frequency domain, and $\boldsymbol{\psi}$ is a field vector in the time domain. Let $\mathbf{E}(\mathbf{x}, \omega)$ represent the complex electric field and $\mathbf{H}(\mathbf{x}, \omega)$ the complex magnetic field; $\mathbf{x}$ is the position vector. The electromagnetic fields in the time and frequency domains are interrelated by the Fourier transform pair defined in equation 2.1. We restrict our discussion to linear and isotropic media throughout this paper. The constitutive relation between the electric displacement $\mathbf{D}$ and the electric field $\mathbf{E}$ then becomes $\mathbf{D} = \tilde{\varepsilon}(\mathbf{x}, \omega)\mathbf{E}$, where $\tilde{\varepsilon}$ is the scalar complex electric permittivity which includes a possible conductive property of the medium. The relation between the magnetic induction $\mathbf{B}$ and magnetic field $\mathbf{H}$ becomes $\mathbf{B} = \mu(\mathbf{x}, \omega)\mathbf{H}$, where μ is the scalar magnetic permeability. In the constitutive relations we neglect the possible nonlocal effects in space of the material parameters since these effects normally become important above optical frequencies. The complex electromagnetic field obeys Maxwell's equations which now become (cf. Stratton, 1941; Jackson, 1998)

$$\nabla \cdot (\tilde{\varepsilon}\mathbf{E}) = \rho_0, \tag{2.2a}$$

$$\nabla \cdot (\mu\mathbf{H}) = 0, \tag{2.2b}$$

$$\nabla \times \mathbf{E} = i\omega\mu\mathbf{H}, \tag{2.2c}$$

$$\nabla \times \mathbf{H} = \mathbf{J}_0 - i\omega\tilde{\varepsilon}\mathbf{E}, \tag{2.2d}$$

where $\mathbf{J}_0$ is a source-current density and ρ_0 is a source-charge density. The macroscopic averages of the electromagnetic properties in a surrounding medium are described by μ and $\tilde{\varepsilon}$

only. The local conduction-current density is normally well described by Ohm's law, $\mathbf{J}_c = \sigma\mathbf{E}$, where σ is the electric conductivity. The displacement current is given as $\mathbf{J}_d = -i\omega\varepsilon\mathbf{E}$, where ε is the electric permittivity. The term $\mathbf{J} = -i\omega\tilde{\varepsilon}\mathbf{E}$ includes both the conduction current and the displacement current, and the complex electric permittivity becomes $\tilde{\varepsilon} = \varepsilon + i\sigma/\omega$. This way of writing the conductivity is consistent with the electron model of Drude (Jackson, 1998). Note that it is a matter of convention if one writes the ohmic term as a standalone term or in a combination with the dielectricity. The charge-conservation equation becomes $i\omega\rho_0 = \nabla \cdot \mathbf{J}_0$, where $\mathbf{J}_0 \neq 0$ only at the source antenna.

The material properties can be expressed by two secondary parameters that characterize the interaction of the electromagnetic field at a specific frequency with the properties of the medium. These are the complex wavenumber,

$$k = \omega\sqrt{\mu\tilde{\varepsilon}} = \sqrt{\omega^2\mu\varepsilon + i\omega\mu\sigma}, \tag{2.3}$$

and the characteristic impedance,

$$\eta = \sqrt{\mu/\tilde{\varepsilon}} = \sqrt{\mu/(\varepsilon + i\sigma/\omega)}. \tag{2.4}$$

From Maxwell's equations the wave equations for inhomogeneous media can be derived:

$$\nabla^2\mathbf{E} + k^2\mathbf{E} + \nabla\left[\mathbf{E}\cdot\nabla\left(\ln\tilde{\varepsilon}\right)\right] + i\omega\nabla\mu\times\mathbf{H} = -i\omega\mu\left[\mathbf{J}_0 + \tfrac{\nabla(\nabla\cdot\mathbf{J}_0)}{k^2}\right] + \tfrac{\nabla\cdot\mathbf{J}_0}{i\omega}\nabla\left(\tfrac{1}{\tilde{\varepsilon}}\right), \tag{2.5a}$$

$$\nabla^2\mathbf{H} + k^2\mathbf{H} + \nabla\left[\mathbf{H}\cdot\nabla\left(\ln\mu\right)\right] - i\omega\nabla\tilde{\varepsilon}\times\mathbf{E} = -\nabla\times\mathbf{J}_0. \tag{2.5b}$$

2.2.1 Plane waves

In order to get an understanding of electromagnetic wave propagation, it is useful to consider plane waves. Many problems involving spherical waves or cylindrical waves can be simplified by expanding the waves into a spectrum of plane waves (Sommerfeld, 1909; Weyl, 1919), and in asymptotic theory the assumption of local plane waves can provide useful simplifications. Expressions for reflection and transmission of electromagnetic fields at boundaries are easily derived if we restrict to plane waves at planar boundaries (cf. Appendix 2.A). We here look at some elementary properties of electromagnetic plane waves and consider a source-free homogeneous medium ($\mathbf{J}_0 = 0$). Then the wave equations 2.5a and 2.5b simplify to

$$\nabla^2\boldsymbol{\Psi} + k^2\boldsymbol{\Psi} = 0, \tag{2.6}$$

where $\boldsymbol{\Psi}$ can represent either the electric or magnetic field. The wavenumber k is given by the dispersion relation in equation 2.3 where the medium parameters in this case are space invariant. Equation 2.6 has the plane-wave solution

$$\boldsymbol{\Psi}(\mathbf{x}) = \boldsymbol{\Psi}_0 \mathrm{e}^{i\mathbf{k}\cdot\mathbf{x}}. \tag{2.7}$$

The wavenumber k is complex if the medium is conductive. When the direction of propagation coincides with the direction of attenuation, i.e., for uniform plane waves, $\mathbf{k} = k\hat{\mathbf{s}}$, where $\hat{\mathbf{s}}$ is a unit vector in the propagation direction. Maxwell's equations (2.2c and 2.2d) then imply that, in source-free regions, the three vectors $\hat{\mathbf{s}}$, $\mathbf{E}$ and $\mathbf{H}$ form a right-handed, orthogonal system and are interrelated by

$$\mathbf{E}(\mathbf{x}) = -\eta\hat{\mathbf{s}} \times \mathbf{H}(\mathbf{x}), \quad \mathbf{H}(\mathbf{x}) = \frac{1}{\eta}\hat{\mathbf{s}} \times \mathbf{E}(\mathbf{x}). \tag{2.8}$$

Thus, the electric and magnetic field are transverse to each other and the direction of propagation.

We find it illustrative to consider the wavenumber's dependence on frequency, permittivity and conductivity. Assuming for simplicity that the material parameters are independent of frequency, we express the wavenumber in terms of a phase velocity c_p and an attenuation coefficient k_i. Then $k = \omega/c_p + ik_i$, where k_i is often given in terms of a skin depth $\delta = 1/k_i$. From the dispersion relation in equation 2.3, we see that the phase velocity and attenuation coefficient have the same frequency dependence:

$$c_p = \frac{1}{\sqrt{\mu\varepsilon}} f\left(\frac{\omega}{\omega_0}\right), \quad k_i = \frac{1}{2}\sigma\sqrt{\frac{\mu}{\varepsilon}} f\left(\frac{\omega}{\omega_0}\right), \tag{2.9}$$

where $\omega_0 = \sigma/\varepsilon$ is the characteristic frequency at which the magnitude of the displacement current equals that of the conduction current and

$$f(\chi) = \chi\sqrt{2\left(\sqrt{1+\frac{1}{\chi^2}} - 1\right)} \cong \begin{cases} 1 & \text{for} \quad \chi \gg 1\,, \\ \sqrt{2\chi} & \text{for} \quad \chi \ll 1\,. \end{cases} \tag{2.10}$$

This function is illustrated in Figure 2.1. The asymptotic limits are seen to be very good for $\chi > 10$ and $\chi < 0.1$, respectively.

Consider a plane wave in the z-direction ($z = \hat{\mathbf{s}} \cdot \mathbf{x}$). The wave can be described in terms of the phase velocity and attenuation factor as $\mathbf{\Psi}(z) = \mathbf{\Psi}_0 \exp(-k_i z) \exp(i\omega z/c_p)$. In the time domain a time-harmonic plane wave at frequency ω is thus given as:

$$\boldsymbol{\psi}(z,t) = \boldsymbol{\psi}_0 \mathrm{e}^{-k_i z} \cos\left[\omega\left(\frac{z}{c_p} - t\right)\right]. \tag{2.11}$$

We observe that the attenuation increases and that the phase velocity decreases with increasing conductivity. Moreover, the attenuation and phase velocity are seen to be frequency dependent except when $\omega\varepsilon/\sigma \gg 1$.

2.2.2 Asymptotic ray theory

In inhomogeneous media, asymptotic ray-series solution methods are an alternative to pure numerical methods for modelling the electromagnetic fields described by Maxwell's equations.

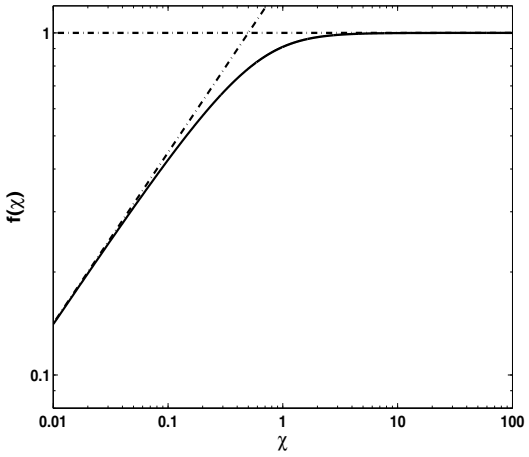

Figure 2.1: The function $f(\chi)$ defined in equation 2.10 in log-log scale. The asymptotic limits for $\chi \gg 1$ and $\chi \ll 1$ are very good for $\chi > 10$ and $\chi < 0.1$, respectively.

In ray theory the energy is regarded as being transported along rays. The approximation of wave propagation where one actually neglects the wave character is often referred to as geometrical optics. In the classic works of Brekhovskikh (1960), Wait (1962), and Baños (1966), the geometrical optics solutions are obtained when exact integral representations of the fields are evaluated by the asymptotic method of steepest descents. When the paths of integration are deformed into the paths of steepest descent, branch cuts and poles of the reflection and transmission coefficients may yield lateral waves (head waves) and waveguide modes (channel waves) in addition to the geometrical optics contributions. Baños (1966) gives a comprehensive treatment of that approach applied to dipole radiation in the presence of a sea-surface interface and develops accurate expressions for all field components with a dipole source in different orientations and at different positions in the two regions.

In the following we demonstrate that we can treat asymptotic ray theory in a unified framework for both dielectric and conductive media and that the description simplifies in the two special cases of either high frequency and low conductivity or low frequency and high conductivity. We assume slow spatial variation of the medium properties and consider source-free regions. Then equations 2.5a and 2.5b are both reduced to homogeneous Helmholtz equations. Taking $\mathbf{\Psi}$ to represent either the electric or magnetic field, we get

$$\nabla^2 \mathbf{\Psi} + k^2(\mathbf{x})\mathbf{\Psi} = \mathbf{0}. \tag{2.12}$$

We use the well-known solution ansatz

$$\mathbf{\Psi}(\mathbf{x}) = \mathrm{e}^{ik_0 W(\mathbf{x})} \sum_{m=0}^{N} \frac{\mathbf{\Psi}_m(\mathbf{x})}{(ik_0)^m}, \tag{2.13}$$

where all the terms might be frequency dependent, but where the spatial variation is described by the phase term $W(\mathbf{x})$ and the slowly varying amplitudes $\mathbf{\Psi}_m(\mathbf{x})$. In the sum we have indicated an upper limit N because infinite asymptotic series usually diverge. The parameter k_0 is the wavenumber for a reference medium.

In our solution ansatz the underlying assumption is that only one geometrical wave front passes through each point in space (Born and Wolf, 1999). In regions where several rays pass through the same point in space, we often need to use a more general solution ansatz which contains sums over raypaths. A thorough discussion of an analogous case from seismic modelling can be found in Chapman (2004). Inserting our ansatz into equation 2.12 and solving for powers of ik_0 as the magnitude of k_0 becomes large, we get

$$(\nabla W)^2 = (k/k_0)^2\,, \tag{2.14a}$$

$$\nabla^2 W\mathbf{\Psi}_0 + 2\,(\nabla W\cdot\nabla)\,\mathbf{\Psi}_0 = \mathbf{0}, \tag{2.14b}$$

$$\nabla^2 W\mathbf{\Psi}_m + 2\,(\nabla W\cdot\nabla)\,\mathbf{\Psi}_m + \nabla^2\mathbf{\Psi}_{m-1} = \mathbf{0}, \quad m\geq 1, \tag{2.14c}$$

where it is implicit that k_0 and k must have the same order of magnitude. Equation 2.14a is the eikonal equation, and equation 2.14b is the transport equation. In the eikonal equation, k/k_0 is a normalized slowness. In optics this is equivalent to a refraction index $n=\sqrt{\mu_r\tilde{\varepsilon}_r}=k/k_0$, where μ_r and $\tilde{\varepsilon}_r$ denote relative permeability and relative complex permittivity, respectively, and it is common to use vacuum as the reference medium. If we use only the first term in the ray expansion, the eikonal equation describes the raypaths whereas the transport equation describes how the slow geometrical amplitude variations must be to satisfy energy conservation.

The eikonal equation (2.14a) is complex and frequency dependent. However, in two cases of particular interest, it becomes real and frequency independent. In the asymptotic limit $\chi > 10$ (cf. Figure 2.1) or in nonconducting media, the wavenumber reduces to $k(\mathbf{x}) = \omega\sqrt{\mu(\mathbf{x})\varepsilon(\mathbf{x})}$. With $k_0=\omega\sqrt{\mu_0\varepsilon_0}$, where the index zero refers to values in a chosen reference medium, we see that $(\nabla W)^2=\mu(\mathbf{x})\varepsilon(\mathbf{x})/(\mu_0\varepsilon_0)$. In the solution ansatz in equation 2.13, we can in this case alternatively choose $i\omega W'(\mathbf{x})$ in the exponential. Then the eikonal equation becomes $(\nabla W')^2=\mu(\mathbf{x})\varepsilon(\mathbf{x})$, where $\nabla W'$ now describes slowness.

In conducting media, low-frequency signals are approximated well by the dispersion relation $k(\mathbf{x})=\sqrt{i\omega\mu(\mathbf{x})\sigma(\mathbf{x})}$. This corresponds to the asymptotic limit $\chi<0.1$ in Figure 2.1. With $k_0=\sqrt{i\omega\mu_0\sigma_0}$ the eikonal equation 2.14a is real and frequency independent for this case as well: $(\nabla W)^2=\mu(\mathbf{x})\sigma(\mathbf{x})/(\mu_0\sigma_0)$. In the solution ansatz in equation 2.13, we can in this case alternatively choose $-\sqrt{-i\omega}W''(\mathbf{x})$ in the exponential. Then the eikonal equation becomes $(\nabla W'')^2=\mu(\mathbf{x})\sigma(\mathbf{x})$, which is the solution approach found in Virieux et al. (1994).

2.2.3 Layered media

In both geophysics and optics, it is often of interest to consider electromagnetic fields in layered media. Then the medium varies only in one direction, and the spatial components orthogonal to this direction are well suited for a Fourier expansion. We consider a stack of homogeneous layers and decompose the wavenumber into $k^2 = k_x^2 + k_y^2 + k_z^2$. We choose the variation to be along the z-direction. After the Fourier expansion: $\partial_x \rightarrow ik_x$ and $\partial_y \rightarrow ik_y$, and each Fourier component represents a superposition of upgoing and downgoing plane waves in each layer. Introducing $p_x = k_x/\omega$ and $p_y = k_y/\omega$, which represent slownesses in the x- and y-directions, respectively, and following the formalism of Ursin (1983), we can express Maxwell's equations as

$$\frac{d\boldsymbol{b}}{dz} = -i\omega \boldsymbol{A}\boldsymbol{b} + \boldsymbol{s}, \tag{2.15}$$

with field vector $\boldsymbol{b} = (E_x \;\; E_y \;\; -H_y \;\; H_x)^T$ where T denotes transpose, source vector $\boldsymbol{s} = (p_x J_z/\tilde{\varepsilon} \;\; p_y J_z/\tilde{\varepsilon} \;\; J_x \;\; J_y)^T$, and system matrix $\boldsymbol{A} = (\mathbf{0} \;\; \boldsymbol{A}_1 \,; \; \boldsymbol{A}_2 \;\; \mathbf{0})$, where

$$\boldsymbol{A}_1 = \frac{1}{\tilde{\varepsilon}} \begin{pmatrix} \mu\tilde{\varepsilon} - p_x^2 & -p_x p_y \\ -p_x p_y & \mu\tilde{\varepsilon} - p_y^2 \end{pmatrix} \quad \text{and} \quad \boldsymbol{A}_2 = \frac{1}{\mu} \begin{pmatrix} \mu\tilde{\varepsilon} - p_y^2 & p_x p_y \\ p_x p_y & \mu\tilde{\varepsilon} - p_x^2 \end{pmatrix}. \tag{2.16}$$

At interfaces we introduce mathematical idealizations that lead to discontinuities of the material parameters. The boundary conditions state continuity of $\boldsymbol{b}$, which leads to the Fresnel reflection and transmission coefficients for two orthogonal states of polarization: transverse electric (TE) and transverse magnetic (TM). Explicit expressions for the Fresnel coefficients are derived in Appendix 2.A. The propagator theory of multilayer systems can be used to compute the overall TE- and TM-reflection and/or transmission responses from several layers. One finally obtains the total response from the multilayered system by an inverse Fourier transform (Ward and Hohmann, 1987; Løseth, 2000). Most modelling codes for horizontally layered media are based on this theory and, for low-frequency waves in conductive materials, the formulas in Chave and Cox (1982) are readily obtained from this formalism.

2.2.4 Green's functions

From Green's theorem stems the concept of Green's functions (Green, 1828), which define the impulse response of a medium. These functions can be used to solve inhomogeneous differential equations with boundary conditions. In electromagnetic theory they provide an alternative solution method to vector potential techniques. The dyadic Green's functions for the electric field $\mathbf{G}_E$ and magnetic field $\mathbf{G}_H = \nabla \times \mathbf{G}_E$ characterize the electromagnetic response resulting from a directional point source. Once the Green's functions are constructed, the electromagnetic field due to a source distribution can be determined, and the electric and

magnetic fields outside the source region are given as volume integrals over the source and their respective Green's function:

$$\mathbf{E}(\mathbf{x},\omega) = i\omega\mu \int_{V_0} d\mathbf{x}_0 \mathbf{G}_E(\mathbf{x},\omega,\mathbf{x}_0)\mathbf{J}_0(\mathbf{x}_0,\omega), \tag{2.17a}$$

$$\mathbf{H}(\mathbf{x},\omega) = \int_{V_0} d\mathbf{x}_0 \mathbf{G}_H(\mathbf{x},\omega,\mathbf{x}_0)\mathbf{J}_0(\mathbf{x}_0,\omega). \tag{2.17b}$$

The Green's function for the electric field obeys the reciprocity relation (Felsen and Marcuvitz, 2003)

$$\mathbf{G}_E(\mathbf{x},\omega,\mathbf{x}_0) = \mathbf{G}_E^T(\mathbf{x}_0,\omega,\mathbf{x}). \tag{2.18}$$

This means that the m'th component of a signal at $\mathbf{x}$ caused by a unit impulse applied in the n'th direction at $\mathbf{x}_0$ equals the n'th component of a signal at $\mathbf{x}_0$ caused by a unit impulse applied in the m'th direction at $\mathbf{x}$. The reciprocity relation (equation 2.18) then gives us the conditions for interchanging source and receiver without affecting the measured signal.

2.2.5 Analytic solution in a homogeneous medium

In homogeneous media, the terms containing derivatives of the medium parameters in equation 2.5 vanish. The electric and magnetic fields are then solutions of inhomogeneous Helmholtz equations where the wavenumber, k, found in equation 2.3, is now space invariant. Following Tai (1994) the dyadic Green's functions for the electric and magnetic field are then solutions of

$$\nabla^2\mathbf{G}_E + k^2\mathbf{G}_E = -\left[\mathbf{I} + \frac{1}{k^2}\nabla\nabla\right]\delta\left(\mathbf{x}-\mathbf{x}_0\right), \tag{2.19a}$$

$$\nabla^2\mathbf{G}_H + k^2\mathbf{G}_H = -\nabla\times\left[\mathbf{I}\delta\left(\mathbf{x}-\mathbf{x}_0\right)\right]. \tag{2.19b}$$

Here, $\nabla\times$ denotes curl of a dyadic function, $\nabla\nabla$ is a dyadic operator, and $\mathbf{I}$ is the unit diagonal dyad. The solutions of the Green's functions are:

$$\mathbf{G}_E = \frac{\mathrm{e}^{ikr}}{4\pi r^3}\begin{pmatrix} r^2h_1+(x-x_0)^2h_2 & (x-x_0)(y-y_0)h_2 & (x-x_0)(z-z_0)h_2 \\ (x-x_0)(y-y_0)h_2 & r^2h_1+(y-y_0)^2h_2 & (y-y_0)(z-z_0)h_2 \\ (x-x_0)(z-z_0)h_2 & (y-y_0)(z-z_0)h_2 & r^2h_1+(z-z_0)^2h_2 \end{pmatrix}, \tag{2.20a}$$

$$\mathbf{G}_H = \frac{(ikr-1)\mathrm{e}^{ikr}}{4\pi r^3}\begin{pmatrix} 0 & -(z-z_0) & (y-y_0) \\ (z-z_0) & 0 & -(x-x_0) \\ -(y-y_0) & (x-x_0) & 0 \end{pmatrix}, \tag{2.20b}$$

where $r = |\mathbf{x}-\mathbf{x}_0| = \left[(x-x_0)^2+(y-y_0)^2+(z-z_0)^2\right]^{1/2}$ and

$$h_1 = \left(1 - \frac{1}{ikr} - \frac{1}{(kr)^2}\right), \quad h_2 = \left(-1 + \frac{3}{ikr} + \frac{3}{(kr)^2}\right). \tag{2.21}$$

These equations are equivalent to the dyadic Green's functions found in Ward and Hohmann (1987), but here they are not restricted to a conductive medium. In the special case of a homogeneous medium it can be seen from equation 2.20 that the Green's functions, in addition to obeying the general law of reciprocity (equation 2.18), obey the symmetry relation $\mathbf{G}_E(\mathbf{x}, \omega, \mathbf{x}_0) = \mathbf{G}_E(\mathbf{x}_0, \omega, \mathbf{x})$ and $\mathbf{G}_H(\mathbf{x}, \omega, \mathbf{x}_0) = -\mathbf{G}_H(\mathbf{x}_0, \omega, \mathbf{x})$.

2.3 Dipole radiation

We consider dipole radiation in a homogeneous medium in order to illustrate that the unified description in the frequency domain yields the correct expressions in the time domain for nondispersive waves in nonconductive media and dispersive waves in conductive media.

An infinitesimal electric dipole antenna can be represented by a line current of length $l \ll \lambda$ with current amplitude $I(\omega)$. This gives the dipole current moment Il. For simplicity we use spherical coordinates with the source located at the origin and pointing in the z-direction. Then the source-current density becomes $\mathbf{J}_0 = Il\delta(\mathbf{r})\hat{\mathbf{z}}$. Let θ denote the angle between the z-axis and the radial vector $\mathbf{r}$, and let ϕ denote the angle between the x-axis and a projection of $\mathbf{r}$ into the xy-plane. The coordinate systems, with the source included, are shown in Figure 2.2. The electromagnetic field in the frequency domain from such a source-current distribution is easily found with the aid of the Green's functions in equation 2.20 and the relation between the fields and their Green's functions (equation 2.17). After a transform from Cartesian to spherical coordinates, the radiated dipole field is expressed as

$$\mathbf{E}(\mathbf{r}, \omega) = \frac{ik\eta Il}{4\pi r} \mathrm{e}^{ikr} \left[-\left(1 - \frac{1}{ikr} + \frac{1}{(ikr)^2}\right) \hat{\boldsymbol{\theta}} \sin\theta + \left(\frac{1}{ikr} - \frac{1}{(ikr)^2}\right) 2\hat{\mathbf{r}} \cos\theta \right], \quad (2.22a)$$

$$\mathbf{H}(\mathbf{r}, \omega) = \frac{ikIl}{4\pi r} \mathrm{e}^{ikr} \left(1 - \frac{1}{ikr}\right) (-\hat{\boldsymbol{\phi}} \sin\theta), \quad (2.22b)$$

where $\omega\mu = k\eta$ and where η is the impedance as defined in equation 2.4. The exact expressions for a Hertzian dipole are excellent approximations for the fields from a physical dipole at distances $r \gg l$ and are found in a variety of works (cf. Baños, 1966; Burrows, 1978). The magnetic field is circulating around the z-axis (in the $\hat{\boldsymbol{\phi}}$ direction), the electric field is in the plane defined by the z-axis and the radial distance (in the $\mathbf{r}$ and $\hat{\boldsymbol{\theta}}$ directions), and the signal level is determined by the dipole current moment Il. The radiation pattern is rotationally symmetric about the dipole axis, and the maximum radiation is in the normal direction ($\theta = 90°$). A more thorough investigation of the radiation pattern can be found in Appendix 2.B. We observe that the exact dipole formulas in equation 2.22 are ray-series expansions of the same kind as in equation 2.13. In this case the ray-series method actually yields exact results with $N = 2$ for the electric field and $N = 1$ for the magnetic field.

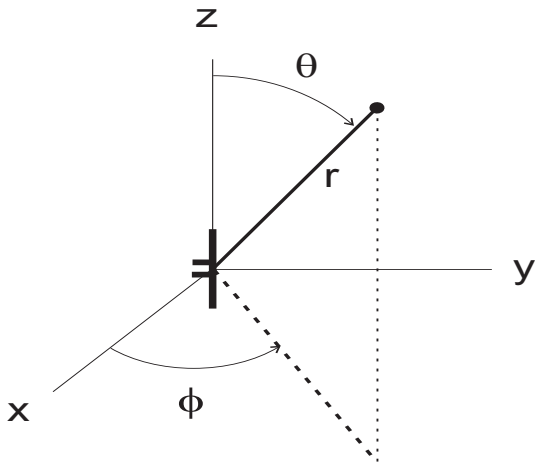

Figure 2.2: The Cartesian and spherical coordinate systems are shown with the dipole antenna included. The antenna is oriented in the z-direction. The elevation angle θ is in the plane spanned by $\mathbf{r}$ and $\hat{\mathbf{z}}$. The azimuth angle ϕ is in the xy-plane.

2.4 Time-domain signals

The electromagnetic field in the time domain from an electric dipole source is found by applying an inverse Fourier transform to the frequency-domain fields in equation 2.22:

$$\mathbf{e}(\mathbf{r},t) = \frac{\mu}{4\pi r}\left\{e_0(r,t)(\hat{\boldsymbol{\theta}}\sin\theta) + [e_1(r,t)+e_2(r,t)]\,(2\hat{\mathbf{r}}\cos\theta + \hat{\boldsymbol{\theta}}\sin\theta)\right\}, \tag{2.23a}$$

$$\mathbf{h}(\mathbf{r},t) = \frac{1}{4\pi r}\left\{h_0(r,t)+h_1(r,t)\right\}(\hat{\boldsymbol{\phi}}\sin\theta), \tag{2.23b}$$

where the real electric field is represented by $\mathbf{e}(\mathbf{r},t)$ and the real magnetic field by $\mathbf{h}(\mathbf{r},t)$. The two far-field terms are

$$e_0(r,t) = -\frac{il}{2\pi}\int_{-\infty}^{\infty} d\omega\, \omega I(\omega)\mathrm{e}^{i(kr-\omega t)}, \quad h_0(r,t) = -\frac{l}{2\pi}\int_{-\infty}^{\infty} d\omega\, ikI(\omega)\mathrm{e}^{i(kr-\omega t)}. \tag{2.24}$$

The electric near-field terms $e_1(r,t)$ and $e_2(r,t)$ are described by integrals over the two higher-order terms in the dipole expansion. The two integrals are given by consecutive multiplication of the frequency-domain far-field term by the factor $-1/(ikr)$. The magnetic near-field term $h_1(r,t)$ is an integral over the magnetic far-field term times this factor. Note that an additional factor $1/(ik)$ in the integrals in equation 2.24 equals an integration that can be carried out in the time domain:

$$\int_{-\infty}^{\infty} d\omega\, \frac{f(\omega)}{ik}\mathrm{e}^{ikr} = -\int_{r}^{\infty}\int_{-\infty}^{\infty} dr' d\omega\, f(\omega)\mathrm{e}^{ikr'}. \tag{2.25}$$

Let us consider the radiated electromagnetic field from an electric dipole in a nonconductive medium and a conductive medium. We first look at the resulting electromag-

netic field from a simple time-harmonic current source $I(t) = I_0 \cos(\omega_0 t)$ and next derive the step response, i.e., the electromagnetic field from a constant current turned on at $t = 0$. The frequency-domain representation of the two current distributions are $I(\omega) = I_0\pi[\delta(\omega + \omega_0) + \delta(\omega - \omega_0)]$ and $I(\omega) = I_0[\pi\delta(\omega) - 1/i\omega]$, where $\delta(\omega)$ represents the Dirac delta function.

2.4.1 Nondispersive and nonconductive media

For nondispersive waves in nonconducting materials, we have the dispersion relation $k(\omega) = \omega/c$, where $c = 1/\sqrt{\mu\varepsilon}$ is the velocity in the medium. The radiated electromagnetic field from a dipole source for a time-harmonic current distribution then becomes

$$\mathbf{e}(\mathbf{r},t) = \frac{\mu\omega_0 I_0 l \sin\varphi}{4\pi r}\hat{\boldsymbol{\theta}}\sin\theta + \frac{I_0 l}{4\pi\varepsilon r^2}\left[\frac{1}{c}\cos\varphi - \frac{1}{\omega_0 r}\sin\varphi\right](\hat{\boldsymbol{\theta}}\sin\theta + 2\hat{\mathbf{r}}\cos\theta), \tag{2.26a}$$

$$\mathbf{h}(\mathbf{r},t) = \frac{I_0 l}{4\pi r}\left[\frac{\omega_0}{c}\sin\varphi + \frac{1}{r}\cos\varphi\right]\hat{\boldsymbol{\phi}}\sin\theta, \tag{2.26b}$$

where $\varphi = \omega_0(r/c - t)$.

In the step-response calculations the well-known result with a perfect but delayed delta pulse is obtained:

$$\mathbf{e}(\mathbf{r},t) = \frac{\mu I_0 l}{4\pi r}\delta(t - r/c)\hat{\boldsymbol{\theta}}\sin\theta + \frac{I_0 l t}{4\pi\varepsilon r^3}H(t - r/c)(\hat{\boldsymbol{\theta}}\sin\theta + 2\hat{\mathbf{r}}\cos\theta), \tag{2.27a}$$

$$\mathbf{h}(\mathbf{r},t) = \frac{I_0 l}{4\pi r}\left[\frac{1}{c}\delta(t - r/c) - \frac{1}{r}H(t - r/c)\right]\hat{\boldsymbol{\phi}}\sin\theta, \tag{2.27b}$$

where $H(t)$ is the Heaviside step function. Note that the electric field has a near-field contribution only for times $t \geq r/c$. This is a contribution equal to the static dipole field from the charges $\pm q_0 = \pm I_0 t$ accumulated on the dipole ends in a nonconductive material. For the magnetic field, the first term is the radiated far-field pulse, but for $t \geq r/c$ the near-field term yields a static magnetic field caused by the constant source current. The far-field term has the same time dependence as the electric field since the impedance η is independent of frequency in nonconductive materials.

2.4.2 Conductive media

For low frequencies and conductive media, we use $k(\omega) = (1 + i)\sqrt{\omega\mu\sigma/2}$ as the dispersion relation. In this expression the real (k_r) and imaginary (k_i) parts of the wavenumber are

equal. A time-harmonic source current then yields

$$\mathbf{e}(\mathbf{r},t) = \frac{\mu\omega_0 I_0 l}{4\pi r}\mathrm{e}^{-\kappa r}\sin(\varphi_c)(\hat{\boldsymbol{\theta}}\sin\theta) + \frac{I_0 l}{4\pi r^2}\mathrm{e}^{-\kappa r}\left[\sqrt{\frac{\mu\omega_0}{\sigma}}\cos(\varphi_c-\pi/4)+\frac{1}{\sigma r}\cos\varphi_c\right](2\hat{\mathbf{r}}\cos\theta+\hat{\boldsymbol{\theta}}\sin\theta), \tag{2.28a}$$

$$\mathbf{h}(\mathbf{r},t) = \frac{I_0 l}{4\pi r}\mathrm{e}^{-\kappa r}\left[\sqrt{\mu\sigma\omega_0}\cos(\varphi_c-\pi/4)+\frac{1}{r}\cos\varphi_c\right](\hat{\boldsymbol{\Phi}}\sin\theta), \tag{2.28b}$$

where $\kappa = k_r = k_i = \sqrt{\omega_0\mu\sigma/2}$, and $\varphi_c = (\kappa r - \omega_0 t)$.

When calculating the step response, we evaluate the integrals asymptotically. That is, since the main contribution to the integrals comes from the low-frequency regime, we approximate the integrals by integrating up to a cutoff frequency where the low-frequency wavenumber approximation for conductive media is valid. We then use this approximation and expand the integration limits to infinity again. The approximation is justified by the heavy attenuation of the higher frequencies in highly conducting media, which implies that the measurable part of the signal is in the low-frequency region. A formal correct mathematical treatment should include the entire dispersion relation given in equation 2.3. This would lead to a solution containing weighted sums of heavily attenuated delta pulses for higher frequencies. A discussion of pulse propagation in dispersive media can be found in the classic papers of Sommerfeld (1914) and Brillouin (1914). A thorough treatment is also given in Stratton (1941). Morse and Feshbach (1953) solve the expression in equation 2.24 and the higher-order terms for the complete dispersion relation. However, our goal here is to demonstrate the calculation that leads to the quasi-static approximation.

To solve the first integral in equation 2.24 for the step response, we introduce a new variable $\xi = \sqrt{\omega t/2}$ and use that $\cos(-\xi) = \cos(\xi)$. Then

$$e_0(r,t) \cong \frac{4I_0 l}{\pi t}\int_0^\infty d\xi\,\xi\exp\left(-\sqrt{\frac{\mu\sigma r^2}{t}}\xi\right)\cos\left[\sqrt{\frac{\mu\sigma r^2}{t}}\xi - 2\xi^2\right]. \tag{2.29}$$

This integral is tabulated in equation 3.966.2 in Gradshteyn and Ryzhik (1980). The result is

$$e_0(r,t) \cong I_0 l\sqrt{\frac{\mu\sigma r^2}{4\pi t^3}}\exp\left(-\frac{\mu\sigma r^2}{4t}\right). \tag{2.30}$$

For the higher-order terms that constitute the near-field, we use the method in equation 2.25. We then obtain by repeated integration

$$e_1(r,t) \cong \frac{I_0 l}{r\sqrt{\pi\mu\sigma t}}\exp\left(-\frac{\mu\sigma r^2}{4t}\right), \quad e_2(r,t) \cong \frac{I_0 l}{\mu\sigma r^2}\left[1-\mathrm{erf}\left(\sqrt{\frac{\mu\sigma r^2}{4t}}\right)\right], \tag{2.31}$$

where the error function is

$$\mathrm{erf}(z) = \frac{2}{\sqrt{\pi}}\int_0^z d\xi\exp(-\xi^2). \tag{2.32}$$

To determine the magnetic field, we note that since we are using the dispersion relation $k^2 = i\omega\mu\sigma$, the terms in the expression for the magnetic field only differ from the higher-order terms of the electric field by the factor σr.

For convenience we express the dipole step response in terms of a scaled time $\tau = t/t_d$, where $t_d = \mu\sigma r^2/4$. In terms of these parameters the electromagnetic field becomes

$$\mathbf{e}(\mathbf{r},t) \cong \frac{I_0 l}{4\pi\sigma r^3}\left[f_1\left(\frac{t}{t_d}\right)\hat{\boldsymbol{\theta}}\sin\theta + f_2\left(\frac{t}{t_d}\right)\left(\hat{\boldsymbol{\theta}}\sin\theta + 2\hat{\mathbf{r}}\cos\theta\right)\right], \tag{2.33a}$$

$$\mathbf{h}(\mathbf{r},t) \cong \frac{I_0 l}{4\pi r^2} f_2\left(\frac{t}{t_d}\right)\hat{\boldsymbol{\phi}}\sin\theta, \tag{2.33b}$$

where

$$f_1(\tau) = \frac{4}{\sqrt{\pi\tau^3}}\exp\left(-\frac{1}{\tau}\right) \tag{2.34}$$

is the far-field step response for the electric field, and

$$f_2(\tau) = 1 + \frac{2}{\sqrt{\pi\tau}}\exp\left(-\frac{1}{\tau}\right) - \operatorname{erf}\left(\frac{1}{\sqrt{\tau}}\right) \tag{2.35}$$

is the step response of the two near-field terms for the electric field. These step responses are shown in Figure 2.3.

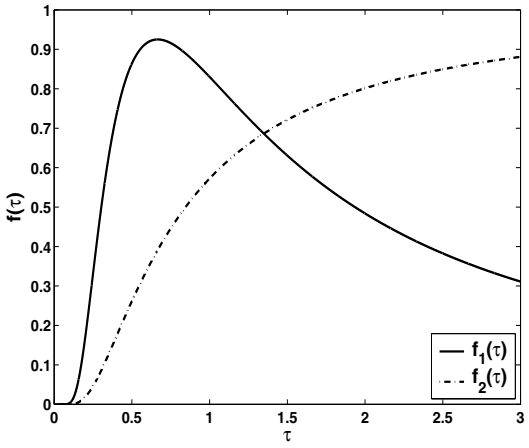

Figure 2.3: Step responses for dipole radiation in conductive materials: far-field response $f_1(\tau)$ and near-field response $f_2(\tau)$. The far-field response is largest for $\tau < 1.4$.

The step response for the magnetic field is given by $f_2(\tau)$. If we consider the magnetic field and split $f_2(\tau)$ into the far-field term and near-field term, we get a relation between the two components that is similar to the relation between $f_1(\tau)$ and $f_2(\tau)$. To illustrate our point, it is thus sufficient to consider $f_1(\tau)$ and $f_2(\tau)$. When doing so, we see that although

the far-field term arrives first and dominates for $t < t_d$, we cannot neglect the near-field term. We also have the same geometrical r-dependence for both the near-field and the far-field. In contrast to the frequency domain, there is thus no clear distinction between the far-field and the near-field. In a conductive material, for $t \gg t_d$, the near-field term yields a constant, static dipole field:

$$\mathbf{e}_{\text{DC}}(\mathbf{r}) = \frac{I_0 l}{4\pi\sigma r^3}(\hat{\boldsymbol{\theta}}\sin\theta + 2\hat{\mathbf{r}}\cos\theta), \quad \mathbf{h}_{\text{DC}}(\mathbf{r}) = \frac{I_0 l}{4\pi r^2}\hat{\boldsymbol{\phi}}\sin\theta. \tag{2.36}$$

With a current impulse $q_0\delta(t)$ of total charge q_0 at $t = 0$, the frequency-domain current amplitude is $I_0 = q_0$, and the resulting impulse response is obtained from the step response by a simple time differentiation:

$$\mathbf{e}(\mathbf{r}, t) \cong \frac{q_0 l}{\pi\mu\sigma^2 r^5}\left[g_1\left(\frac{t}{t_d}\right)\hat{\boldsymbol{\theta}}\sin\theta + g_2\left(\frac{t}{t_d}\right)(\hat{\boldsymbol{\theta}}\sin\theta + 2\hat{\mathbf{r}}\cos\theta)\right], \tag{2.37a}$$

$$\mathbf{h}(\mathbf{r}, t) \cong \frac{q_0 l}{\pi\mu\sigma r^4} g_2\left(\frac{t}{t_d}\right)\hat{\boldsymbol{\phi}}\sin\theta, \tag{2.37b}$$

where $g_j = df_j(\tau)/d\tau$ $(j = 1, 2)$ are the derivatives of the functions in equations 2.34 and 2.35. These time responses are shown in Figure 2.4. We see that the far-field response arrives first and has a peak value more than three times that of the near-field response, but at later times the near-field term cannot be neglected.

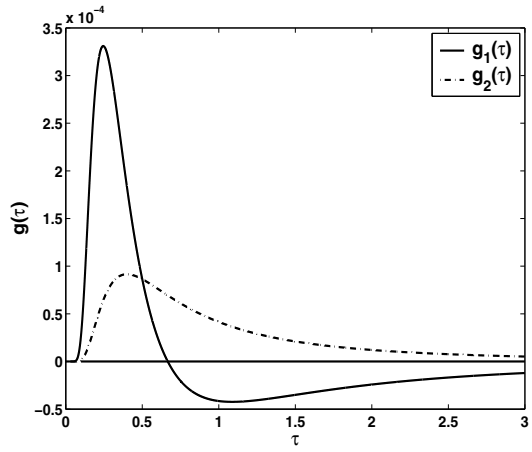

Figure 2.4: Impulse responses for dipole radiation in conductive materials: far-field response $g_1(\tau)$ and near-field response $g_2(\tau)$. The far-field response is largest for $\tau < 0.5$.

2.5 Discussion

In SBL and marine CSEM, the signal sources are towed electrical dipole antennas, and they are very well approximated by Hertzian dipoles at the frequencies and wavelengths involved. Detectable signal transmission is only obtained at very low frequencies, $\omega \ll \omega_0 = \sigma/\varepsilon$. In this limit the contribution from the displacement current can be ignored and equation 2.28 describes propagation of single-frequency components in homogeneous media. Compared to time-harmonic signal propagation in nonconductive media (equation 2.26), the propagation of a low-frequency signal in conductive materials is characterized by the damping term and the frequency-dependent phase velocity. In addition, the phase behaviour between the electric and magnetic fields differs in conductive media. The wavelength is $\lambda = 2\pi\delta$ where δ is the skin depth; thus, we have 54.6 dB attenuation per wavelength, and in most cases it is only possible to detect signals that are transmitted a few wavelengths. One then normally wants to use very low frequencies and long wavelengths ($\lambda > 1$ km) to reach down to deeply buried layers.

In exploration configurations where one uses transient source signals, one gets responses that resemble the strongly distorted pulse forms in Figures 2.3 and 2.4. The propagation has the same characteristics as in many diffusion processes. The far-field and the near-field terms in equations 2.33 and 2.37 have the same geometrical r-dependence. The difference between the time-domain step responses in nonconductive and conductive materials is caused by the strong dispersion and frequency-dependent attenuation in conductive materials.

We observe that the frequency-domain treatment of signal propagation in homogeneous media leads to the correct mathematical description of time-harmonic signals and transients for both conductive media and nonconductive media. A correct time-domain approach would of course lead to the same equations. If we derive the wave equation from Maxwell's equations in the time domain, assuming that the permeability, permittivity, and conductivity are independent of frequency, we get the following damped wave equation both for the electric field and magnetic field when we ignore the source term:

$$\nabla^2\boldsymbol{\psi} = \mu\sigma\frac{\partial\boldsymbol{\psi}}{\partial t} + \mu\varepsilon\frac{\partial^2\boldsymbol{\psi}}{\partial t^2}. \tag{2.38}$$

The term involving conductivity represents a damping term in the wave equation. Without damping, we would have the wave equation

$$\nabla^2\boldsymbol{\psi} = \mu\varepsilon\frac{\partial^2\boldsymbol{\psi}}{\partial t^2}, \tag{2.39}$$

which describes nondispersive waves in nonconductive materials. If the damping term becomes completely dominant as is the case for low-frequency signals in conductive materials, the wave equation is well approximated by

$$\nabla^2\boldsymbol{\psi} = \mu\sigma\frac{\partial\boldsymbol{\psi}}{\partial t}, \tag{2.40}$$

which is the diffusion equation one gets if the displacement current in Maxwell's equations is ignored, i.e., the speed of light is assumed infinite. This is often referred to as the quasi-static limit (e.g., Jackson, 1998). The equation has the same form as diffusion equations found in various literature (e.g., Crank, 1975).

The hyperbolic wave equation and the parabolic diffusion equation are both transformed into an elliptic equation when moving from the time domain into the frequency domain (Sommerfeld, 1967). In the frequency domain, the propagation is characterized by the position of the wavenumber k in the complex plane. The position might vary from the real axis to a line rotated by 45° with respect to the real axis. The first case of the two extremes corresponds to propagation of an undamped wave, whereas the second case represents highly attenuated propagating waves. Between these two cases there is a gradual change from undamped wave propagation to highly attenuated wave propagation or diffusion. Thus, the diffusion equation has wave solutions. Moreover, the diffusion equation 2.40 is a vector equation. Depending on what one means by a diffusion process, one should be careful about thinking of the physical *process* as a diffusion process since the notion of diffusion often is characterized by random motion which constitutes a probability distribution that describes diffusive transport (cf. Einstein's 1905 paper on Brownian motion). The conservation of direction and polarization of the electromagnetic field might not easily be related to this physical picture [cf. Milne's problem (Morse and Feshbach, 1953)].

On the other hand, when one thinks of the propagation of low-frequency fields in conductive media in terms of waves, one must consider that these waves are strongly attenuated and highly dispersive. Thus, the concept of time reversal, which is often used in processing of seismic data (Claerbout, 1971), cannot be directly applied. Moreover, the concept of group velocity loses its traditional significance (Stratton, 1941).

As stated above, there is nothing wrong in using equation 2.40 as the starting point for treating low-frequency electromagnetic fields in conducting media (assuming frequency-independent material parameters). This quasi-static approach is often used in connection with low-frequency electromagnetic fields in conductive media. The concept of looking at field propagation in terms of currents follows from this. However, we have also seen that by considering electromagnetic fields in the frequency domain, we can treat wave propagation in both nonconducting media and conducting media. Thus, the two apparently very different cases of nondispersive wave propagation and low-frequency highly dispersive wave propagation can be treated within a unified mathematical framework. In fact, all the well-established tools of wave theory can be directly applied. Moreover, there is no clear transition zone from one "process type" to the other as can be observed from Figure 2.1. An example of a unified treatment is for example found in the modelling of electromagnetic wave propagation in layered media. The well-known description of reflection and refraction of plane electromagnetic waves at planar interfaces and associated division of the fields into TE and TM modes

implies that both nondispersive waves in nonconductive materials and low-frequency waves in conductive materials obey the same equations (cf. Appendix 2.A). Thus, layers that are dominantly dispersive and layers that are dominantly dissipative can be treated on an equal footing. Within this picture the electromagnetic response from buried highly resistive layers can be explained in terms of the characteristic difference between the TE and TM polarization. In SBL, this characteristic difference is used to detect buried hydrocarbon layers by orienting the dipole source and receiver antennas in specific directions. However, in many other applications which use low-frequency electromagnetic fields, it might be advantageous to consider the problem from the quasi-static point of view.

2.6 Conclusion

The basic theory of electromagnetic wave propagation has been reviewed and used to develop a unified frequency-domain description that applies for nondispersive waves in nonconductive materials and highly dispersive low-frequency waves in conductive materials.

We have considered the time-domain responses for an infinitesimal electric dipole antenna and shown that a unified description in the frequency domain yields both the undistorted pulses in nonconductive materials and the highly distorted diffusive pulses for low-frequency signals in conductive materials. In the latter case both the step response and the impulse response are strongly attenuated and distorted.

The question of whether electromagnetic field propagation in conductive materials can be referred to as diffusion or wave propagation has been discussed. We have shown that the approximation that results in a diffusion-like equation is valid. We have also shown that the wave-propagation description provides the correct mathematical formulation. We conclude that one might call low-frequency propagation of electromagnetic fields in conductive media what one prefers, but when one characterizes the field propagation as diffusion, it might be clarifying to add that one is not referring to the random motion usually affiliated with diffusion processes. When the field propagation is characterized as wave propagation, it should be kept in mind that the waves are highly dispersive and strongly attenuated.

2.7 Acknowledgments

We are grateful to Ingve Simonsen, Rune Mittet, Tor Schaug-Pettersen and Ola Hunderi for interesting discussions and comments. We also thank one of the reviewers for useful suggestions. The research is supported by the Norwegian Research Council, Norsk Hydro ASA, Statoil ASA, and ElectroMagnetic GeoServices AS. L.O.L. is grateful to Statoil's VISTA programme for financial support.

2.A Reflection and refraction of plane waves

At an interface between two homogeneous media the boundary conditions for the tangential components of **E** and **H** become (Stratton, 1941)

$$\mathbf{n} \times (\mathbf{E}_2 - \mathbf{E}_1) = 0, \quad \mathbf{n} \times (\mathbf{H}_2 - \mathbf{H}_1) = \mathbf{K}, \tag{2.A-1}$$

where **K** is a surface current and **n** is a unit vector normal to the surface. The subscripts 1 and 2 denote the fields in medium 1 and 2, respectively. When the conductivities of the media are finite, there is no surface current, and we may assume that the tangential components of both **E** and **H** are continuous.

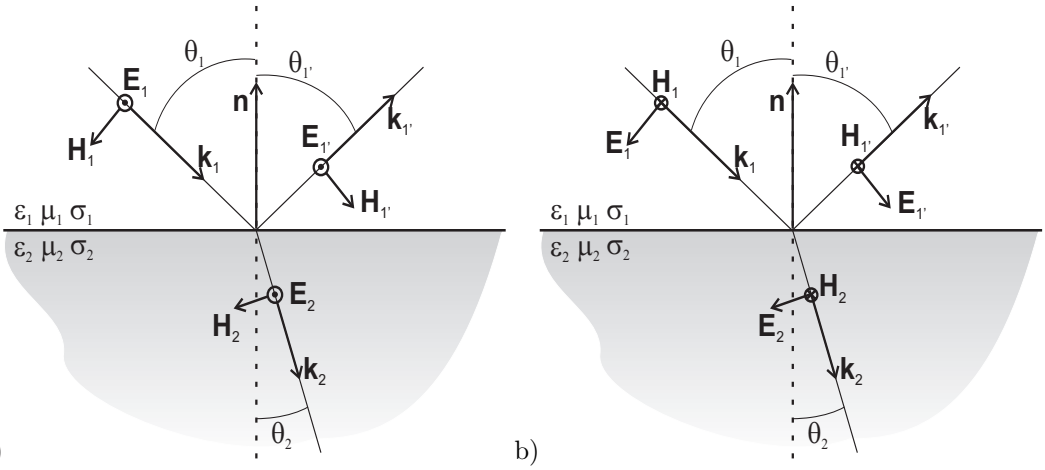

Figure 2.5: Reflection and transmission of a plane wave described by rays at a planar interface. The wavenumber vector **k**, electric field **E**, and magnetic field **H** form a right-handed system. For the TE mode the electric field is perpendicular to the plane of incidence as shown in Figure a. For the TM mode, shown in Figure b, the magnetic field is perpendicular to the plane of incidence. The incoming electric and magnetic fields have subscript 1, the reflected electric and magnetic fields have subscript $1'$, and the transmitted electric and magnetic fields have subscript 2. The angle of incidence is denoted θ_1, the angle of reflection equals the angle of incidence and is denoted $\theta_{1'}$, and the refracted angle is denoted θ_2. The wavenumber is $k_1 = k_{1'}$ in medium 1 and k_2 in medium 2. The unit vector **n** is normal to the interface.

Now, consider plane waves impinging at a planar interface. As depicted in Figure 2.5 we denote the incoming, reflected, and transmitted electric and magnetic fields with the

subscripts 1, 1′ and 2, respectively. Phase-matching conditions at the interface are now seen to give Snell's law and the law of reflection since the incoming, reflected and transmitted fields must have equal phases at the interface. These laws can be expressed as

$$\sin\theta_1 = \sin\theta_{1'}, \tag{2.A-2a}$$

$$k_1 \sin\theta_1 = k_2 \sin\theta_2, \tag{2.A-2b}$$

where $\theta_1 (= \theta_{1'})$ denotes the angle between the incoming (reflected) ray and interface normal, and θ_2 denotes the angle between the transmitted ray and the opposite direction of the interface normal. The wavenumbers in medium 1 and medium 2 are denoted by k_1 and k_2, respectively. When considering the relations between the amplitudes of the incident, reflected and transmitted fields, we get

$$\mathbf{n} \times (\mathbf{E}_1 + \mathbf{E}_{1'}) = \mathbf{n} \times \mathbf{E}_2, \tag{2.A-3a}$$

$$\mathbf{n} \times (\mathbf{H}_1 + \mathbf{H}_{1'}) = \mathbf{n} \times \mathbf{H}_2. \tag{2.A-3b}$$

Now we resolve the electric field into one component that is normal to the plane of incidence (cf. Figure 2.5a). This component is parallel to the interface and known in optics as s-polarization (Vašíček, 1960). Here we refer to it as transverse electric (TE) polarization (Born and Wolf, 1999). The TE-mode decomposition leads to the following relations between the incident, reflected, and transmitted transverse electric field components:

$$\mathbf{E}_{1'} = \frac{\mu_2 k_1 \cos\theta_1 - \mu_1 k_2 \cos\theta_2}{\mu_2 k_1 \cos\theta_1 + \mu_1 k_2 \cos\theta_2} \mathbf{E}_1, \tag{2.A-4a}$$

$$\mathbf{E}_2 = \frac{2\mu_2 k_1 \cos\theta_1}{\mu_2 k_1 \cos\theta_1 + \mu_1 k_2 \cos\theta_2} \mathbf{E}_1. \tag{2.A-4b}$$

For the other component the electric field is in the plane of incidence (cf. Figure 2.5b). Thus the magnetic field is normal to the plane of incidence and parallel to the interface. This is referred to as p-polarization or transverse magnetic (TM) polarization. The TM-mode decomposition leads to the following relations between the incident, reflected, and transmitted transverse magnetic field components:

$$\mathbf{H}_{1'} = \frac{\tilde{\varepsilon}_2 k_1 \cos\theta_1 - \tilde{\varepsilon}_1 k_2 \cos\theta_2}{\tilde{\varepsilon}_2 k_1 \cos\theta_1 + \tilde{\varepsilon}_1 k_2 \cos\theta_2} \mathbf{H}_1, \tag{2.A-5a}$$

$$\mathbf{H}_2 = \frac{2\tilde{\varepsilon}_2 k_1 \cos\theta_1}{\tilde{\varepsilon}_2 k_1 \cos\theta_1 + \tilde{\varepsilon}_1 k_2 \cos\theta_2} \mathbf{H}_1. \tag{2.A-5b}$$

As seen from Figure 2.5, we have $k_{z1} = k_1 \cos\theta_1$ and $k_{z2} = k_2 \cos\theta_2$. In general, $k_z = \sqrt{k^2 - k_\rho^2}$, where $k_\rho^2 = k_x^2 + k_y^2$. In the double-valued square root the condition $\mathrm{Im}(k_z) > 0$ must be satisfied. We furthermore observe that the reflected tangential components of the electric and magnetic fields will have opposite signs. Thus, the reflection and transmission

coefficients for the TE- and TM-polarization components of the horizontal electric field are:

$$r_{TE} = \frac{\mu_2 k_{z1} - \mu_1 k_{z2}}{\mu_2 k_{z1} + \mu_1 k_{z2}}, \qquad r_{TM} = \frac{\tilde{\varepsilon}_1 k_{z2} - \tilde{\varepsilon}_2 k_{z1}}{\tilde{\varepsilon}_2 k_{z1} + \tilde{\varepsilon}_1 k_{z2}}, \tag{2.A-6a}$$

$$t_{TE} = \frac{2\mu_2 k_{z1}}{\mu_2 k_{z1} + \mu_1 k_{z2}}, \qquad t_{TM} = \frac{2\tilde{\varepsilon}_1 k_{z2}}{\tilde{\varepsilon}_2 k_{z1} + \tilde{\varepsilon}_1 k_{z2}}. \tag{2.A-6b}$$

Note that $1 + r_{TE} = t_{TE}$ and $1 + r_{TM} = t_{TM}$. For the horizontal magnetic field components, the reflection and transmission coefficients are:

$$r'_{TE} = -r_{TE} = \frac{\mu_1 k_{z2} - \mu_2 k_{z1}}{\mu_2 k_{z1} + \mu_1 k_{z2}}, \qquad r'_{TM} = -r_{TM} = \frac{\tilde{\varepsilon}_2 k_{z1} - \tilde{\varepsilon}_1 k_{z2}}{\tilde{\varepsilon}_2 k_{z1} + \tilde{\varepsilon}_1 k_{z2}}, \tag{2.A-6c}$$

$$t'_{TE} = 1 + r'_{TE} = \frac{2\mu_1 k_{z2}}{\mu_2 k_{z1} + \mu_1 k_{z2}}, \qquad t'_{TM} = 1 + r'_{TM} = \frac{2\tilde{\varepsilon}_2 k_{z1}}{\tilde{\varepsilon}_2 k_{z1} + \tilde{\varepsilon}_1 k_{z2}}. \tag{2.A-6d}$$

The vertical magnetic field component is a pure TE mode and has the same reflection and transmission coefficients as the horizontal electric TE component. The vertical electric field component is a pure TM mode and has the same reflection and transmission coefficients as the horizontal magnetic TM component.

The coefficients in equation 2.A-6 are valid for both conductive and nonconductive media. The absolute value of the squared reflection coefficient represents reflected energy, whereas the absolute value of the squared transmission coefficient represents transmitted energy. Snell's law describes ray propagation across interfaces, and the law of reflection describes ray reflection at an interface. In the general case, Snell's law describes a relation between complex quantities. However, in the two cases of nondispersive waves in nonconductive media and low-frequency waves in conductive media, Snell's law is a relation between real quantities.

2.B Radiation Pattern

The complex Poynting vector $\mathbf{S}$ is defined as (Stratton, 1941; Jackson, 1998)

$$\mathbf{S} = \frac{1}{2}\mathbf{E} \times \mathbf{H}^*. \tag{2.B-7}$$

The time-averaged power density in a harmonic electromagnetic field is

$$< \mathbf{S} >= \frac{1}{2}\mathrm{Re}(\mathbf{E} \times \mathbf{H}^*). \tag{2.B-8}$$

The magnetic field from the electric dipole considered in this paper has a component in the $\hat{\boldsymbol{\phi}}$-direction only. In order to determine the radiation pattern of the dipole we need to evaluate the complex Poynting vector

$$\mathbf{S} = \frac{1}{2}\left(E_\theta H_\phi^* \hat{\mathbf{r}} - E_r H_\phi^* \hat{\boldsymbol{\theta}}\right). \tag{2.B-9}$$

Using equation 2.22, the products in equation 2.B-9 become

$$E_\theta H_\phi^* = \frac{kk^*\eta|Il|^2}{(4\pi r)^2}\mathrm{e}^{-2\mathrm{Im}(k)r}\left[1+\frac{i(k^*-k)}{kk^*r}+\frac{k-k^*}{k^2k^*r^2}+\frac{i}{k^2k^*r^3}\right]\sin^2\theta, \tag{2.B-10a}$$

$$E_r H_\phi^* = -\frac{kk^*\eta|Il|^2}{(4\pi r)^2}\mathrm{e}^{-2\mathrm{Im}(k)r}\frac{1}{ikr}\left[1+\frac{i(k^*-k)}{kk^*r}+\frac{1}{kk^*r^2}\right]\sin 2\theta, \tag{2.B-10b}$$

where $|Il|^2 = II^*l^2$ is the absolute value of the dipole current moment squared; k and k^* are the wavenumber and its complex conjugate, respectively; and η is the impedance. In a nonconductive medium where $k = \omega\sqrt{\mu\varepsilon}$, the complex Poynting vector becomes

$$\mathbf{S} = \frac{k^2\eta|Il|^2}{32\pi^2}\frac{\sin^2\theta}{r^2}\hat{\mathbf{r}} - i\frac{k\eta|Il|^2}{32\pi^2}\frac{\sin 2\theta}{r^3}\hat{\boldsymbol{\theta}} + i\frac{\eta|Il|^2}{32\pi^2 k}\frac{1}{r^5}\left(\sin^2\theta\hat{\mathbf{r}} - \sin 2\theta\hat{\boldsymbol{\theta}}\right). \tag{2.B-11}$$

Using that $\sqrt{\mu\varepsilon} = 1/c$, where c is the velocity in the medium, the time-averaged power density becomes

$$< \mathbf{S} >= \frac{\omega^2\mu|Il|^2}{32\pi^2 c}\frac{\sin^2\theta}{r^2}\hat{\mathbf{r}}. \tag{2.B-12}$$

When considering low-frequency radiation in conductive media, we use the dispersion relation $k = (1+i)\sqrt{(\mu\omega\sigma)/2}$. The complex Poynting vector is in this case

$$\begin{aligned}\mathbf{S} = {} & \frac{\omega\mu\kappa|Il|^2}{32\pi^2}\frac{\mathrm{e}^{-2\kappa r}}{r^2}\left\{\left[1+\frac{1}{\kappa r}+\frac{1}{\kappa^2 r^2}\right]\sin^2\theta\hat{\mathbf{r}} - \left[\frac{1}{\kappa r}+\frac{1}{2\kappa^3 r^3}\right]\sin 2\theta\hat{\boldsymbol{\theta}}\right\} \\ & - i\frac{\omega\mu\kappa|Il|^2}{32\pi^2}\frac{\mathrm{e}^{-2\kappa r}}{r^2}\left\{\left[\frac{1}{\kappa r}+\frac{1}{\kappa^2 r^2}-\frac{1}{2\kappa^3 r^3}\right]\sin^2\theta\hat{\mathbf{r}} + \frac{\sin 2\theta}{\kappa^2 r^2}\hat{\boldsymbol{\theta}}\right\},\end{aligned} \tag{2.B-13}$$

where $\kappa = \sqrt{\omega\mu\sigma/2}$. The real part of the Poynting vector now becomes

$$< \mathbf{S} >= \frac{\omega\mu\kappa|Il|^2}{32\pi^2}\frac{\mathrm{e}^{-2\kappa r}}{r^2}\left\{\left[1+\frac{1}{\kappa r}+\frac{1}{\kappa^2 r^2}\right]\sin^2\theta\hat{\mathbf{r}} - \left[\frac{1}{\kappa r}+\frac{1}{2\kappa^3 r^3}\right]\sin 2\theta\hat{\boldsymbol{\theta}}\right\}. \tag{2.B-14}$$

Observe that the conductive case yields an attenuation term as well as terms for higher negative powers of r. Note also that the time-averaged power density in this case has a component in the $\hat{\boldsymbol{\theta}}$-direction.

In nonconductive media, the total radiated power P_r is calculated by integrating $\hat{\mathbf{r}}\cdot < \mathbf{S} >$ over a sphere of radius r. The integration gives

$$P_r = \int_0^{2\pi} d\phi \int_0^{\pi} d\theta\ \sin\theta\, r^2 < S_r >= \frac{\omega^2\mu|Il|^2}{12\pi c}. \tag{2.B-15}$$

If we normalize the power density $< S_r(\theta,\phi) >$ on the total radiated power averaged over all angles, we get the directive gain $G(\theta,\phi)$:

$$G(\theta,\phi) = \frac{< S_r >}{P_r/4\pi r^2} = \frac{3}{2}\sin^2\theta. \tag{2.B-16}$$

A plot of the directive gain is shown in Figure 2.6.

For the conductive case the presence of absorption represented by the attenuation term indicates that we cannot find the total radiated power by simply integrating over a sphere. In this case one would rather consider the time-averaged power density at the coordinates of interest. The radiation *pattern*, normally understood to describe the pattern of the radiated power in the far-field, can however still be represented by Figure 2.6.

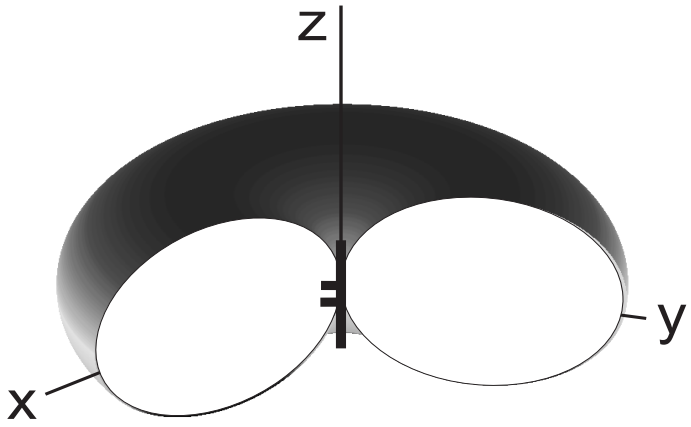

Figure 2.6: Radiation pattern for the electric dipole. The radiation is symmetric around the dipole axis and largest normal to the dipole axis.

Chapter 3

The first test of the SeaBed Logging method

L. O. Løseth, H. M. Pedersen, T. Schaug-Pettersen, S. Ellingsrud, and T. Eidesmo
Submitted to Journal of Applied Geophysics

Summary

SeaBed Logging (SBL) is an application of the marine controlled source electromagnetic (CSEM) method that is used to directly detect and characterize possible hydrocarbon-bearing prospects. Although the CSEM method has been used by academia for more than three decades, the application as a direct hydrocarbon indicator was first introduced about five years ago. The central idea of SBL is the guiding of electromagnetic energy in thin resistive layers within conductive sediments. Even if it has been well known for a long time that electromagnetic signals can propagate from a conductive region to another via resistive regions such as air or resistive parts of the lithosphere, the application to hydrocarbon exploration has not been developed until recently. This might be due to the uncertainty of getting any significant response from thin resistive layers such as hydrocarbon reservoirs since electromagnetic energy is highly attenuated in conductive sediments. Thus, during the early development phase of the SBL technique, a scaled laboratory experiment was performed to validate if a thin resistive layer (hydrocarbons) buried within conductive media (sediments) could be remotely detected by using electric dipoles as sources and receivers. Data from this experiment were compared to a forward modelling code for layered media, and the comparison showed good agreement between experimental and theoretical results. This suggested that thin resistive layers buried in conductive media are detectable due to the guiding of the electromagnetic field within the resistor. The successful results were vital for realizing the application of marine CSEM as a hydrocarbon exploration technique. We here present the results of the first scaled SBL experiment.

3.1 Introduction

Information about resistivity variations beneath the seafloor is crucial in offshore hydrocarbon exploration. Although various electromagnetic methods for remote mapping of resistivity in marine environments exist cf. Chave et al. (1991), until recently, sub-seafloor resistivity data in the oil and gas industry were obtained almost exclusively by wire-line logging of wells. In the last few years, a new application of the marine controlled source electromagnetic method (CSEM) called SeaBed Logging (SBL) has become an important complementary tool to seismic exploration methods to evaluate and rank possible hydrocarbon-bearing prospects. The basic idea behind the SBL method is to exploit lossy guiding of electromagnetic energy in resistive bodies within conductive media for direct detection and characterization of hydrocarbon-filled reservoirs.

In a marine CSEM experiment an electric dipole antenna is used as source. The dipole emits a low-frequency signal into the surrounding media, and the signal is normally recorded by stationary seafloor receivers having both magnetic and electric dipole antennas. The marine CSEM technique was introduced by Cox et al. (1971), and has since then been successfully applied to study the oceanic lithosphere and active spreading centres (Young and Cox, 1981; Cox et al., 1986; Chave et al., 1990; Evans et al., 1994; Constable and Cox, 1996; MacGregor and Sinha, 2000).

It has long been known that electromagnetic signals can propagate fairly long distances in conductive regions, e.g., seawater, by the aid of a resistive halfspace, e.g., air (Kraichman, 1970), or a resistive waveguide (Wait, 1966). However, although the marine magnetotelluric (MT) method has been used for hydrocarbon exploration (Constable et al., 1998), the marine CSEM method had not been applied as a direct hydrocarbon indicator before the SBL application was introduced about five years ago. The basic theory behind the SBL method is described in Eidesmo et al. (2002), and a summary of the first SBL survey can be found in Ellingsrud et al. (2002). This survey was performed owing to successful testing during the early development phase of the method. A scaled experiment was performed in the spring of 1999 in a large water tank at the Statoil Research Centre in Trondheim (Ellingsrud et al., 2000) in order to confirm the theoretical predictions that a signal guided in a resistive layer within conductive surroundings could be remotely detected. Along with the experiment some basic modelling studies had been performed using a forward modelling code (Løseth, 2000), and the data from the experiment and the modelling results showed a very good agreement.

In this paper we present the results from the first SBL experiment. The experimental setup of the water tank is explained, and the skin depths, wavelengths and phase velocities in the tank are discussed since these parameters are important when interpreting the experimental results. In order to relate the results to a full-scale experiment, the scaling between the tank-experiment configuration and a typical realistic setting for an SBL survey is consid-

ered. Next, the electromagnetic field equations are discussed, followed by a basic modelling study in order to illustrate some important aspects of the signal behaviour. Finally, the results from the experiment, i.e., the measured electric field components in the inline and broadside directions of the source antenna, are presented along with numerical results from the implementation of the field equations.

The theory for electromagnetic field propagation in planarly layered media is well known (Born and Wolf, 1999; Brekhovskikh, 1960; Wait, 1962; Chave and Cox, 1982; Ward and Hohmann, 1987; Chew, 1995). For completeness of the paper, we however briefly review the derivation of the field equations in the appendix. We keep the displacement current in the equations since we find this more convenient when handling the sea-surface interface. In air one might approximate both the displacement and conduction currents to zero in marine CSEM modelling, but we prefer not to do this (cf. King et al., 1992). Another reason for taking displacement currents into account, is the need to model effects of other highly resistive layers that are present in the apparatus used in the experiment.

3.2 Experimental setup

The experimental setup consisted of a large indoor water tank as shown in Figure 3.1. The tank had a surface area of 9 m by 6 m, and depth of 8 m. A conductive environment was created by filling the entire tank with seawater. A resistive layer was constructed by fitting 8 king-size waterbed mattresses into a wooden framework. This construction had a length of 7.50 m, width of 4.25 m, and thickness of 0.25 m. The mattresses were filled with tap water and could be held in a horizontal position at any desired depth beneath the seawater surface. Two identical electric dipole antennas were used as source and receiver. These antennas were constructed from two 15 cm $\times$ 15 cm brass plates mounted on an epoxy substrate. Each plate was connected to a coaxial cable, and the antenna impedance was approximately 50 Ω. A series of measurements with a time-harmonic signal in the frequency range between 30 kHz and 830 kHz with an interval of 4 kHz were performed. The dynamic range of the analyzer was from 0 dBm to approximately -100 dBm in this frequency range. The separation distance between the source and receiver (offset) was varied from 0.4 m up to 4 m with 0.2 m subintervals. The series of measurements were furthermore done with the antennas 25 cm and 65 cm below the seawater surface. We will refer to these as the *shallow* and *deep* configurations, respectively.

Two different orientations of the source and receiver were used throughout the experiment both being in the horizontal plane with respect to the layered system. The configuration that will be referred to as the *inline* measurement means that the separation distance between the source and receiver antennas is parallel to the direction of the antennas. The configuration that will be referred to as the *broadside* measurement implies that the separation direction

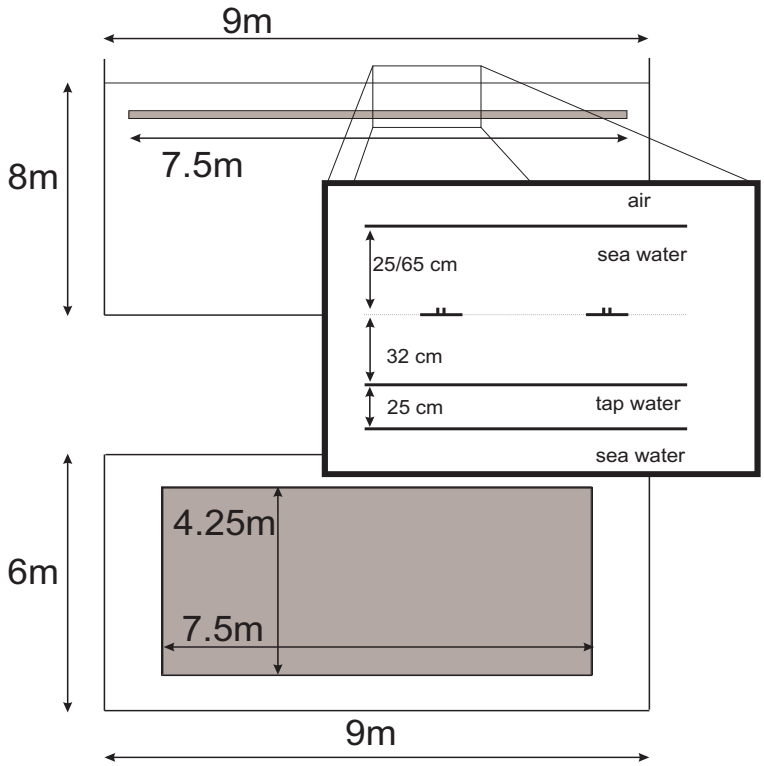

Figure 3.1: A sketch of the water tank seen from the side and above. In the excerpt, the details of the setup are shown.

is normal to the direction of the antennas. As well as measurements for the inline and broadside configurations, control measurements were done for the antennas at right angles to each other.

3.2.1 Wavelengths, skin depths, and phase velocities

The electromagnetic properties of a medium are described by the electric permittivity ε, magnetic permeability μ, and electric conductivity σ. Consider propagation of a time-harmonic plane wave with frequency f (angular frequency $\omega = 2\pi f$). The propagation can be described in terms of a wavenumber

$$k = \omega\sqrt{\mu\varepsilon + i\mu\sigma/\omega} = \omega/c_p + i/\delta, \tag{3.1}$$

where $i = \sqrt{-1}$, c_p is the phase velocity, and δ is the skin depth. The skin depth is a measure of how far the wave will penetrate into the medium. In the wavenumber expression in terms of the material parameters, the first part inside the square root is related to the displacement

currents in Maxwell's equations, and the second part to conduction currents. Thus, it can be observed from equation 3.1 that the conduction current dominates the displacement current if $\sigma/\omega\varepsilon > 1$. The frequency where the displacement current and conduction current contribute equally to the wavenumber ($\sigma/\omega\varepsilon = 1$), will be referred to as the critical frequency.

For water the relative electric permittivity is $\varepsilon_r = 80$. This means that for seawater with conductivity 5.2 S/m, the critical frequency is 1.2 GHz. For tap water with conductivity 0.013 S/m, the critical frequency is 3 MHz. The displacement current can thus be ignored when considering field propagation in the seawater and tap water for the frequencies (in the kHz domain) used in the tank experiment. The wavenumber in equation 3.1 can thus be written as

$$k \approx (1+i)\sqrt{\frac{\omega\mu\sigma}{2}}. \tag{3.2}$$

From this approximation and the relation in equation 3.1, the skin depth, phase velocity, and wavelength λ for low-frequency propagation in conductive media become:

$$\delta \approx \sqrt{\frac{2}{\mu\sigma\omega}}, \quad c_p \approx \sqrt{\frac{2\omega}{\mu\sigma}}, \quad \lambda = \frac{2\pi c_p}{\omega} \approx 2\pi\delta. \tag{3.3}$$

The skin depth, phase velocity, and wavelength for seawater and tap water for frequencies of 50 kHz, 100 kHz and 200 kHz are shown in Table 3.1.

Table 3.1: Skin depths, phase velocities, and wavelengths at 50 kHz, 100 kHz, and 200 kHz for seawater and tap water.

f (kHz)	σ (S/m)	δ (m)	c_p (m/s)	λ (m)
50	5.200	0.99	3.10×10^5	6.20
50	0.013	19.73	6.20×10^6	123.96
100	5.200	0.70	4.38×10^5	4.38
100	0.013	13.95	8.77×10^6	87.65
200	5.200	0.49	6.20×10^5	3.01
200	0.013	9.86	1.24×10^7	61.98

3.2.2 Scaling between the experiment and a realistic SBL setting

The purpose of the experimental setup was to create a stratified structure with a sublayer of low-loss material (the "hydrocarbon" layer) embedded in a medium with high loss ("overburden"). The conductivity of the seawater was measured to 5.2 S/m (resistivity 0.2 Ωm) during the experiment, and the conductivity of the tap water was measured to 0.013 S/m

(resistivity 80 Ωm). The conductivity contrast was thus close to 400. It was important that the distances and frequencies used in the tank experiment could be scaled up to realistic distances and frequencies that can be encountered in a real SBL survey. The choice of geometry and frequencies was thus based on the following consideration: If the frequencies (in the kHz domain) are scaled down by a factor 2×10^5, and the conductivities by a factor 5, the seawater corresponds to a typical overburden with resistivity approximately 1.0 Ωm, and the tap-water layer corresponds to a hydrocarbon layer with resistivity 400 Ωm. The dimensions are then scaled up by a factor $\delta_2/\delta_1 \approx 1000$, where δ_1 and δ_2 are skin depths related to corresponding layers in the tank experiment and a typical full-scale SBL experiment, respectively.

3.3 Field expressions

The electromagnetic field from an infinitesimal electric dipole source contained within a stratified medium was calculated by solving Maxwell's equations in terms of electromagnetic potentials. Since the medium properties change in one direction only, the spherical-wave expression in the vector potential can be expanded into a spectrum of plane waves. At the interfaces, a plane-wave constituent obeys the boundary conditions which lead to the Fresnel reflection coefficients for two orthogonal states of polarization. These are referred to as the transverse electric (TE) mode meaning that the electric field component is normal to the plane of incidence (and parallel to the interface), and the transverse magnetic (TM) mode meaning that the magnetic field component is normal to the plane of incidence (Stratton, 1941). For both polarization modes, the reflection response from an arbitrary number of layers is obtained by an iterative combination of the reflection and propagation in each layer. The total reflection response within the source layer is obtained by combining the responses from the two stacks of layers above and below the source antenna. The derivation of the electromagnetic field expressions is presented in Appendix 3.A.

In order to compare data from the experiment to theoretical predictions, we need to know the electric field from a horizontal electric dipole (HED) source in isotropic media:

$$E_\rho(\rho,\beta,z) = -\frac{Il_x}{4\pi}\cos\beta\left[\ \mathcal{I}^{TM}_{A0} + \frac{1}{\rho}\left(\mathcal{I}^{TE}_{A1} - \mathcal{I}^{TM}_{A1}\right)\right], \tag{3.4a}$$

$$E_\beta(\rho,\beta,z) = -\frac{Il_x}{4\pi}\sin\beta\left[-\mathcal{I}^{TE}_{A0} + \frac{1}{\rho}\left(\mathcal{I}^{TE}_{A1} - \mathcal{I}^{TM}_{A1}\right)\right], \tag{3.4b}$$

where E_ρ and E_β are frequency-domain representations of the complex horizontal electric field components. Their magnitude is determined by the dipole current moment Il_x where I is the source current and l_x is the length of the dipole. The symbols $\mathcal{I}$ in equation 3.4

represent integrals over a spectrum of plane waves:

$$\mathcal{I}^{TE}_{A0}(\rho,z) = \omega\mu \int_0^\infty dk_\rho \, \frac{k_\rho}{k_z} J_0(k_\rho\rho) \left[\mathrm{e}^{ik_z|z|} + R^{TE}_A(k_\rho,z) \right], \tag{3.5a}$$

$$\mathcal{I}^{TE}_{A1}(\rho,z) = \omega\mu \int_0^\infty dk_\rho \, \frac{1}{k_z} J_1(k_\rho\rho) \left[\mathrm{e}^{ik_z|z|} + R^{TE}_A(k_\rho,z) \right], \tag{3.5b}$$

$$\mathcal{I}^{TM}_{A0}(\rho,z) = \frac{\omega\mu}{k^2} \int_0^\infty dk_\rho \, k_z k_\rho J_0(k_\rho\rho) \left[\mathrm{e}^{ik_z|z|} + R^{TM}_A(k_\rho,z) \right], \tag{3.5c}$$

$$\mathcal{I}^{TM}_{A1}(\rho,z) = \frac{\omega\mu}{k^2} \int_0^\infty dk_\rho \, k_z J_1(k_\rho\rho) \left[\mathrm{e}^{ik_z|z|} + R^{TM}_A(k_\rho,z) \right]. \tag{3.5d}$$

By definition the medium properties have discontinuities in the vertical direction only. Thus, it is advantageous to write the equations in terms of cylindrical coordinates. The horizontal wavenumber component is given by k_ρ, and the vertical wavenumber component is described by $k_z = \sqrt{k^2 - k_\rho^2}$. The corresponding spatial components are ρ and z, respectively; whereas β describes the angle between the HED and ρ. The source is situated in the origin of the coordinate system. The field equations are written in terms of integrals containing Bessel functions of the first (J_0) and second (J_1) order so that double integrals in terms of the horizontal wavenumber components k_x and k_y are avoided in the numerical implementation.

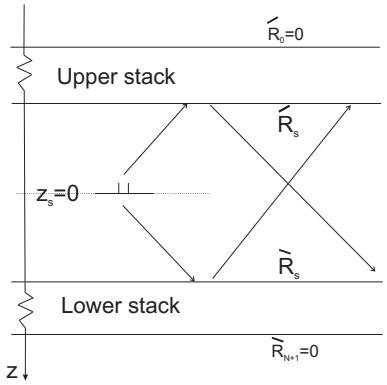

Figure 3.2: The source antenna situated between an upper and a lower stack of layers with reflection responses $\acute{R}_s$ and $\grave{R}_s$, respectively. Note that these are the reflection responses from the stacks at $z_s = 0$.

It can be observed that the electromagnetic field expressions consist of a direct field, which is the field that would be observed in a homogeneous wholespace, and a reflection response given by R_A. This reflection response is obtained by combining the reflection responses from an upper stack $\acute{R}_s$ and a lower stack $\grave{R}_s$ as illustrated in Figure 3.2. The subscript s means that the stack responses are to be calculated at the source position $z_s = 0$. The appropriate

summation of the reflection responses from the upper and lower stacks gives:

$$R_A(k_\rho, z) = \frac{\grave{R}_s(1+\acute{R}_s)\mathrm{e}^{-ik_z z} + \acute{R}_s(1+\grave{R}_s)\mathrm{e}^{ik_z z}}{1-\acute{R}_s\grave{R}_s}. \tag{3.6}$$

The reflection coefficient from a stack is obtained by a recursive combination of reflections from all the layers in the stack as shown in Chew (1995) or Løseth and Ursin (2007):

$$R_m = \frac{r_m + R_{m+1}}{1 + r_m R_{m+1}}\,\mathrm{e}^{2ik_{zm}d_m}, \tag{3.7}$$

where d_m is the thickness of the m'th layer, k_{zm} is the vertical wavenumber in the m'th layer, $R_M = 0$, r_m is the Fresnel coefficient for reflection between the m'th and $(m+1)$'th layer and $m = 1, 2, ..., M$. The iteration procedure is illustrated in Figure 3.3. At a single interface between two homogeneous regions, denoted by the subscripts 1 and 2 and where the incoming field is found in medium 1, the reflection coefficients for the TE and TM modes are (Stratton, 1941; Jackson, 1998):

$$r_{TE} = \frac{\mu_2 k_{z1} - \mu_1 k_{z2}}{\mu_2 k_{z1} + \mu_1 k_{z2}}, \quad \text{and} \quad r_{TM} = \frac{\tilde{\varepsilon}_1 k_{z2} - \tilde{\varepsilon}_2 k_{z1}}{\tilde{\varepsilon}_1 k_{z2} + \tilde{\varepsilon}_2 k_{z1}}, \tag{3.8}$$

where $\tilde{\varepsilon} = \varepsilon + i\sigma/w$.

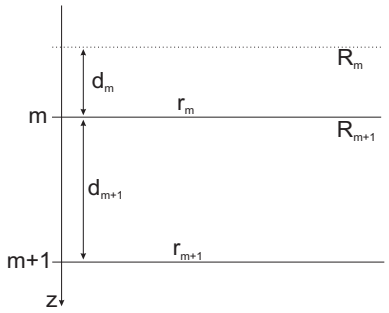

Figure 3.3: An illustration of how the reflection response from a stack is calculated. The response just below the m'th interface in layer $m+1$ is R_{m+1}, and r_m is the Fresnel coefficient.

The field expressions were implemented in Fortran 90 using an adaptive Gauss-Legendre quadrature and the Euler summation-acceleration method (Press et al., 1997).

3.4 Modelling study

The effects on the signal propagation when varying the conductivity, thickness, and depth of the resistive layer were investigated (cf. Figure 3.4). With a source frequency of 100 kHz, the variation in responses for different conductivities and thicknesses of the resistive layer was

looked at separately. In these cases the air halfspace was not included. The effect of the air halfspace was considered by modelling responses from the shallow and deep configurations, i.e., by varying d_0 in Figure 3.4.

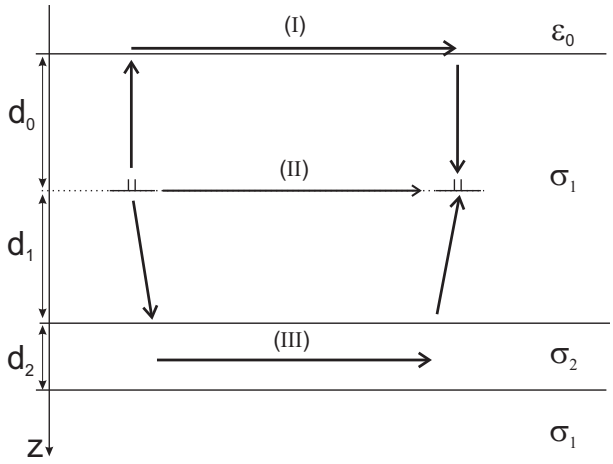

Figure 3.4: A sketch of the signal propagation. The contributions to the total response come from the sea-surface (I), direct field (II), and guiding (III).

In all the modelling cases, the resulting electric field components in the inline and broadside directions were studied. The results are shown in Figure 3.5 and 3.6. For the inline configuration E_ρ with $\beta = 0$ is plotted (dash-dot lines), and for the broadside configuration E_β with $\beta = 90°$ is plotted (solid lines). In both cases, the presentation of the results is in terms of magnitude versus offset (MVO) and phase versus offset (PVO).

In Figure 3.5a-b the magnitudes and phases of the electric field are shown for various conductivity contrasts. The green lines show the direct field which is the response one would measure in a homogeneous wholespace. Note that in this case the broadside component has the largest magnitude. For a three layer model (resistive layer in a conductive background medium), the responses from models with background-medium conductivity 5.2 S/m and thin-layer conductivities of 0.13 S/m, 0.065 S/m, and 0.013 S/m (conductivity contrasts of $\sigma_r = 40$, $\sigma_r = 80$ and $\sigma_r = 400$) are represented by yellow, magenta, and black lines, respectively. The resulting plots can be separated into three regions. In the first region the direct field dominates. In the next, the response from the more resistive layer is noticeable, whereas in the last and most interesting region, the energy that has been guided in the resistive layer dominates the response. Note that the inline configuration has the largest response in this region.

In Figure 3.5c-d the magnitudes and phases of the electric field for various thicknesses of the resistive layer are shown. For reference, the response from a homogeneous wholespace

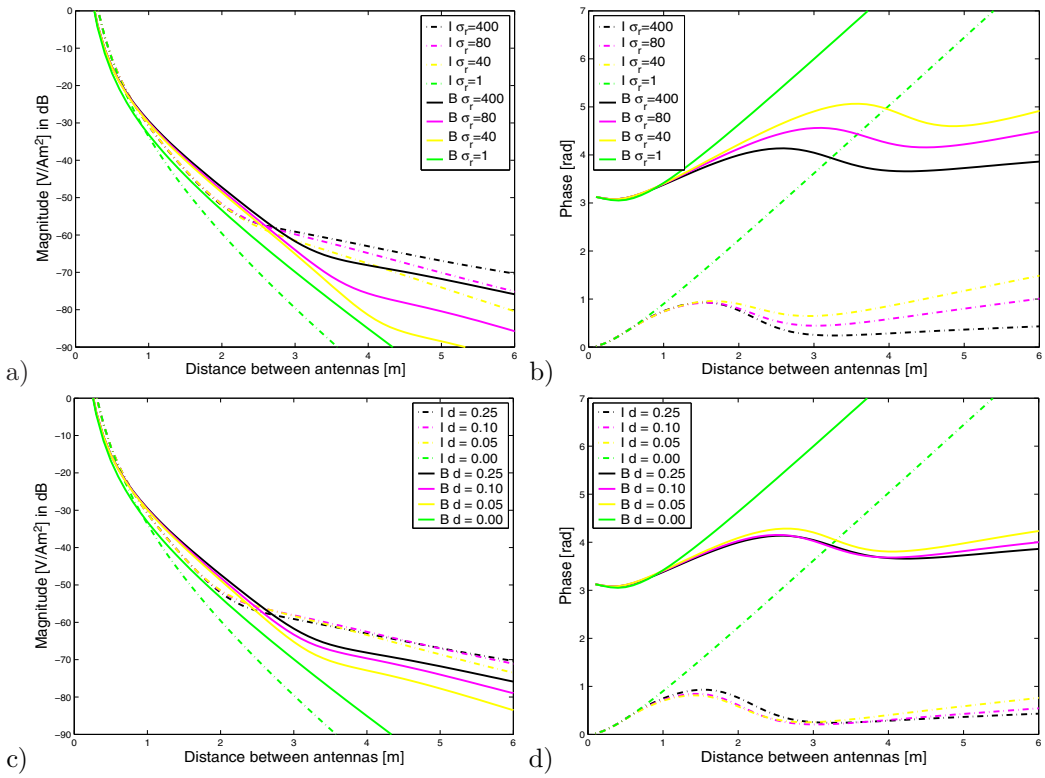

Figure 3.5: MVO plots for various conductivity contrasts σ_r are shown in Figure a, whereas Figure b shows the respective PVO plots. In Figure c and d the differences in responses for various thicknesses d_2 are shown. I and B denote inline and broadside antenna configurations, respectively.

is included and shown by the green curves. The yellow, magenta and black lines represent responses from a resistive layer of thickness 0.05 cm, 0.10 cm, and 0.25 cm, respectively. The plots indicate that the inline configuration is not as sensitive to a variation in thickness as it is to a variation in conductivity contrast. The broadside configuration is more sensitive to a variation in thickness than the inline configuration.

The effect of an air halfspace above the antennas is demonstrated in Figure 3.6. Again the green curves represent the direct field, and the response without the presence of the sea-surface interface ($d_0 = \infty$ in Figure 3.4) is plotted in yellow. These reference curves can be compared to the curves for the responses from the so-called deep configuration ($d_0 = 65$ cm) represented in magenta, and the shallow configuration ($d_0 = 25$ cm) shown in black.

It can be observed that the responses are larger at shallower depths, but that the response from the lossy waveguide is still present in the modelled data. The interpretation of the

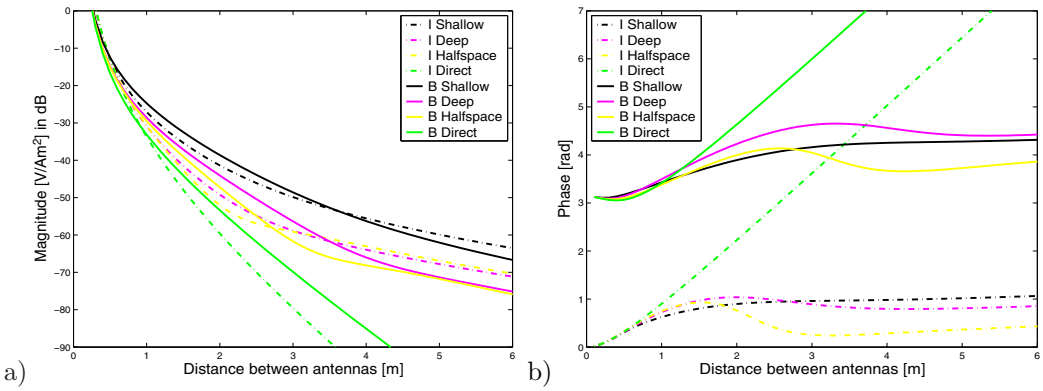

a) b)

Figure 3.6: Modelled response for various seawater depths.

phase plots might become more complicated than the interpretation of the magnitude plots in shallow water. It can be observed that the response from the sea-surface interface is significant at all distances where the signal is not dominated by the direct wave. Moreover the combination ("interference") between the response from above and below the antenna might lower the overall signal response. Note that one in a common SBL setting has one more layer that represents the seawater/overburden interface, and that the "interference" effects may become more complicated here.

3.4.1 TE and TM modes

From equation 3.4 we see that the TE-polarization component will dominate the signal in the far-field for the broadside configuration since the contribution from the TM mode vanishes as $\rho \to \infty$. By the same argument, the TM-polarization component will dominate the signal in the far-field for the inline configuration. However, in a marine CSEM or SBL experiment, one cannot neglect the near-field. Thus, both components contribute to the overall signal response both for the inline and broadside configurations. Moreover, the TM mode is sensitive to thin resistive layers whereas the TE mode does not "see" thin layers (Løseth, 2007). When a resistive layer becomes thick however, the contribution from the TE mode becomes significant.

In the geophysics literature the TM mode is often referred to as galvanic coupling between layers whereas the response due to the TE mode is referred to as inductive coupling (MacGregor and Sinha, 2000). The TM and TE modes are also sometimes referred to as TM and PM modes, respectively, then meaning toroidal and poloidal magnetic modes (Chave et al., 1991).

3.5 Results

In order to compare the measured responses in the tank to modelled responses, we plot the measured inline and broadside data along with the corresponding modelled data in Figure 3.7, 3.8, and 3.9. In all the figures the *measured* inline (broadside) data are represented by

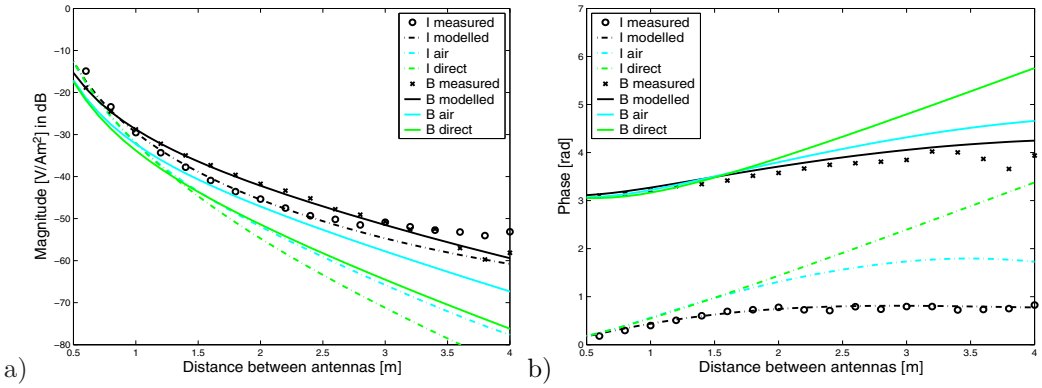

a) b)

Figure 3.7: Calculated and measured response for a 50 kHz source frequency at 65 cm depth.

o's (x's). The *modelled* inline (broadside) data are represented by dash-dot (solid) lines. For comparison, the modelled response from a seawater wholespace (green) and two halfspaces consisting of seawater and air (cyan) are shown. We denote the latter as the halfspace model. Figure 3.7 shows measured and calculated magnitude and phase responses for a signal of 50 kHz with the deep configuration. It can be observed that the modelled data fit the measured data very well at intermediate distances, and that the responses are substantially larger than the response from the halfspace model. In Figure 3.8, responses at shallow

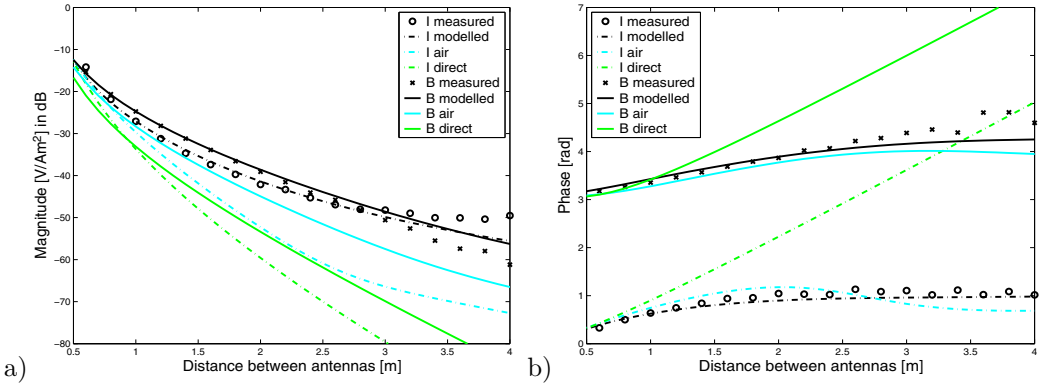

a) b)

Figure 3.8: Calculated and measured response at 100 kHz and 25 cm depth.

depth for a 100 kHz signal are shown. This figure shows a large halfspace response, but

the modelled data fit the real data very well for intermediate distances. One is thus able to "see" the tap-water layer at the shallow depth as well. The deep configuration at 200 kHz is shown in Figure 3.9. Here, the magnitude data fit the modelled data even better than for lower frequencies at large distances. For the inline case however, the phase data do not fit the modelled data as well as for the lower frequencies.

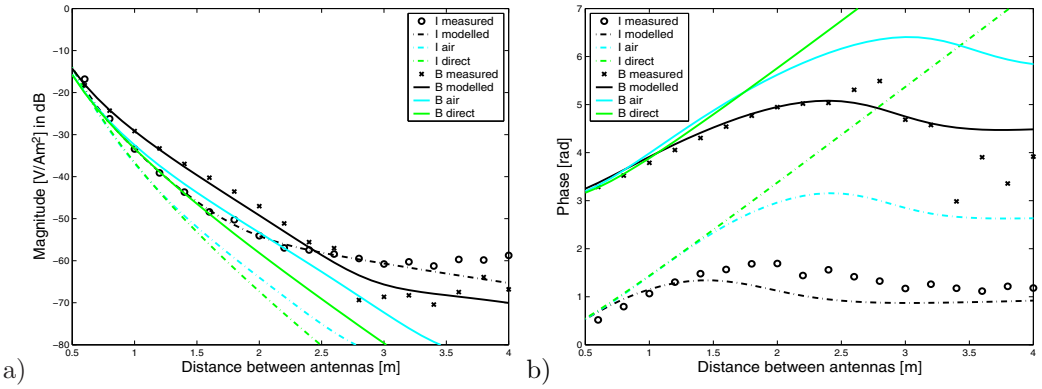

a) b)

Figure 3.9: Modelled and real data for a 200 kHz source frequency at 65 cm depth.

3.6 Discussion

As seen from Figure 3.7, 3.8, and 3.9, the agreement between the modelled and experimental results was very good. For small offsets however, the fact that the physical antenna has finite size does not correspond to the Hertzian dipole approach followed in the modelling code. This deviation is not large and is of minor importance in the overall picture.

At large offsets, disagreements between modelled and measured data will be due to the walls and finite bottom of the water tank. Response from the bottom of the water tank is however avoided by the large distance from the bottom to the tap-water layer (approximately 7 m). As seen from Table 3.1, the skin depth in tap water is much larger than the lateral size of the tap-water layer for low frequencies. Thus, we expect that reflections from the end of the mattresses will influence the data, and that these effects will be evident at far offsets. At higher frequencies, the attenuation is larger, and the end effects will not influence the data that much. Note also that, at the largest offsets, the receiver is operating near its detection limit.

The above considerations imply that the experimentally and theoretically obtained curves should be compared at intermediate source-receiver separation distances. The modelling code for stratified media is well suited to investigate the measured data at these offsets.

If one was to try to get an exact match between the modelled data and measured data,

one would have to take into account the coating of the mattresses that leads to very thin nonconductive layers in the model. From modelling investigations, it was seen that this would alter the responses only slightly. One should also take into account the wooden framework and the intermediate separation between the 8 mattresses in the tank. These parameters will however give only a slight mismatch in the phase plots at higher frequencies (cf. Figure 3.9b). At these frequencies, the phase is more influenced by the tap-water layer than at lower frequencies.

A determination of the *details* of the tank was however not the purpose of the experiment. The goal was to validate that the guiding of electromagnetic energy in thin resistive layers within conductive media is detectable by electric dipole antennas. The experiment indicated that the detection of a lossy waveguide (1-D modelling), or rather lossy resonator (experiment), is possible. The results also confirmed that, if one only has the opportunity to acquire some data, and if one looks for thin layers; one might want to use the inline configuration. Moreover, one might use the difference in response between the inline and broadside configurations to look for thin resistive layers. For thick layers, the increased sensitivity of the broadside configuration might become useful if one has a scenario that includes both a thin reservoir and a thick resistive layer.

A concern about the experimental setup compared to a real SBL or CSEM setting, is the lack of the "seabed" interface. When the experiment is scaled into a realistic setting, the seawater layer corresponds to an overburden, and one might argue that the presence of another layer in the experiment would have masked the response from the thin resistive layer. However, as discussed in Løseth (2007), the characteristic TM-mode response from the thin resistive layer would be altered only slightly in case of having an additional interface with relatively weak contrast to the source layer. Thus, the tank experiment gives valuable information about the detectability of the guiding effect in the thin resistor even without the seabed interface.

3.7 Conclusion

The purpose of the water-tank experiment was to investigate if a thin resistive layer (representing a hydrocarbon-filled reservoir) buried in a conductive medium would give a directly detectable electromagnetic response. The experiment showed that such detection was indeed possible. Moreover, it was confirmed that the sensitivity of the measurements was larger for certain configurations of the antennas. The results from the experiment and modelling study suggested that the inline configuration is the preferred configuration for detection of thin resistive layers. Moreover, the experiment verified that the difference in the response for the inline and broadside configurations can be used to identify thin layers. Even if a modelling study of a realistic SBL scenario would require full 3-D modelling, the results from

the experiment showed that 1-D modelling provides a useful approach to understanding the basic behaviour of the SBL signals.

3.8 Acknowledgments

The research was supported by VISTA, Statoil ASA, and emgs AS. The authors are grateful to Bjørn Ursin and Rune Mittet for useful discussions and suggestions.

3.A Derivation of the field expressions

In order to solve Maxwell's equations, the magnetic flux-density vector $\mathbf{B}$ can be expressed in terms of a vector potential as $\mathbf{B} = \nabla \times \mathbf{A}$ (Stratton, 1941). By applying the Lorenz gauge (Kong, 2000), the following Helmholtz equation for the vector potential from a source with current density $\mathbf{J}_0$ is obtained:

$$\nabla^2 \mathbf{A} + k^2 \mathbf{A} = -\mu \mathbf{J}_0, \tag{3.A-1}$$

where k is the wavenumber given in equation 3.1. The complex electric field $\mathbf{E}$ and magnetic field $\mathbf{H}$ in the frequency domain are then described in terms of the vector potential as

$$\mathbf{E}(\mathbf{r}, \omega) = i\omega \left\{ \mathbf{A}(\mathbf{r}, \omega) + \frac{\nabla \left[\nabla \cdot \mathbf{A}(\mathbf{r}, \omega) \right]}{k^2} \right\}, \tag{3.A-2a}$$

$$\mathbf{H}(\mathbf{r}, \omega) = \frac{1}{\mu} \nabla \times \mathbf{A}(\mathbf{r}, \omega), \tag{3.A-2b}$$

where $\mathbf{r}$ is the radial vector. An infinitesimal electric dipole source can be represented by a length vector $|\mathbf{l}| \ll \lambda$ with current amplitude $I(\omega)$. This gives the source current density $\mathbf{J}_0(\omega) = I(\omega)\mathbf{l}\delta(\mathbf{r})$. For such a source, the vector potential is found by solving equation 3.A-1:

$$\mathbf{A}(\mathbf{r}, \omega) = \frac{\mu I(\omega)\mathbf{l}}{4\pi |\mathbf{r}|} \exp\left(ik|\mathbf{r}|\right). \tag{3.A-3}$$

In a stratified medium with the electric dipole source situated between two layered stacks and the medium variations in the z-direction as shown in Figure 3.2, the coordinate system can be chosen with the dipole antenna located at the origin and in the plane defined by the x- and z-axis. This means that the source current distribution can be written as $\mathbf{J}_0(\omega) = I(\omega)[l_x \delta(\mathbf{r})\hat{\mathbf{x}} + l_z \delta(\mathbf{r})\hat{\mathbf{z}}]$. The x-component of the antenna will be referred to as a horizontal electric dipole (HED) and the z-component as a vertical electric dipole (VED).

In order to calculate reflection and transmission at the interfaces in the layered system, the spherical wave in the expression for the vector potential in equation 3.A-3 can be expanded into plane waves (Weyl, 1919):

$$\frac{\exp(ikr)}{r} = \frac{i}{2\pi} \int_{-\infty}^{\infty} dk_x dk_y \, \frac{\exp\left[i\left(k_x x + k_y y + k_z |z|\right)\right]}{k_z}, \tag{3.A-4}$$

where k_x and k_y are the spatial frequencies in the x- and y-direction, respectively; $k_\rho^2 = k_x^2 + k_y^2$; and $k_z = \sqrt{k^2 - k_\rho^2}$. The double-valued square root is made unique by the following physical consideration: Since k is complex and k_x and k_y are real, k_z is a complex quantity. To ensure that the field vanishes for $|z| \to \infty$, one must require that $\mathrm{Im}(k_z) > 0$. The inhomogeneous plane waves are thus exponentially damped with increasing $|z|$.

By using equation 3.A-2 and 3.A-4, the electromagnetic field in the frequency domain can now be expressed as:

$$\mathbf{\Psi}(\mathbf{r}) = \frac{1}{4\pi^2} \int_{-\infty}^{\infty} dk_x dk_y \, \mathbf{\Psi}(k_x, k_y, z) \, \mathrm{e}^{ik_x x + ik_y y} \,, \tag{3.A-5}$$

where $\mathbf{\Psi} = \{\mathbf{E}, \mathbf{H}\}$ and

$$\mathbf{E}(k_x, k_y, z) = -\frac{\mu\omega I}{2k_z} \left(\mathbf{l} - \frac{\mathbf{k}'(\mathbf{k}' \cdot \mathbf{l})}{k^2} \right) \mathrm{e}^{ik_z|z|}, \tag{3.A-6a}$$

$$\mathbf{H}(k_x, k_y, z) = -\frac{I}{2k_z} \left(\mathbf{k}' \times \mathbf{l} \right) \mathrm{e}^{ik_z|z|}, \tag{3.A-6b}$$

where $\mathbf{k}' = [k_x, k_y, \mathrm{sgn}(z)k_z]$. The delta-function contribution at the source position for the E_z-component is ignored. Equation 3.A-5 describes a 2-D inverse Fourier transform from the wavenumber domain into the spatial domain.

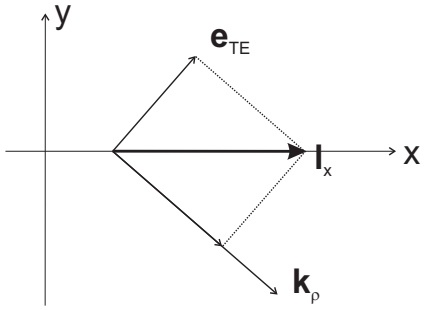

Figure 3.10: TE-polarization component for a plane wave. The TE part of the quantity $\mathbf{l} - \mathbf{k}'(\mathbf{k}' \cdot \mathbf{l})/k^2$ is denoted $\mathbf{e}_{TE}$, and $\mathbf{l}_x$ corresponds to a HED.

In order to calculate the reflection response from each interface in layered media, the quantities in equation 3.A-6 need to be decomposed into the transverse electric (TE) polarization component and the transverse magnetic (TM) polarization component. The term transverse here means that a plane-wave constituent is normal to the plane of incidence. The plane of incidence is defined by the wavenumber direction $\mathbf{k}$ and the z-direction (interface normal). The TE mode is obtained by considering the electric field component normal to the wavenumber in the horizontal plane that contains the HED as shown in Figure 3.10. Thus,

the field components in terms of the TE- and TM-polarization modes become:

$$E_x^{TE}(k_x,k_y,z) = c_h \frac{\mu\omega k_y^2}{k_z(k_x^2+k_y^2)}\left(\mathrm{e}^{ik_z|z|}+R_A^{TE}\right), \tag{3.A-7a}$$

$$E_x^{TM}(k_x,k_y,z) = c_h \frac{\mu\omega k_x^2 k_z}{k^2(k_x^2+k_y^2)}\left(\mathrm{e}^{ik_z|z|}+R_A^{TM}\right), \tag{3.A-7b}$$

$$E_y^{TE}(k_x,k_y,z) = -c_h \frac{\mu\omega k_x k_y}{k_z(k_x^2+k_y^2)}\left(\mathrm{e}^{ik_z|z|}+R_A^{TE}\right), \tag{3.A-7c}$$

$$E_y^{TM}(k_x,k_y,z) = c_h \frac{\mu\omega k_x k_y k_z}{k^2(k_x^2+k_y^2)}\left(\mathrm{e}^{ik_z|z|}+R_A^{TM}\right), \tag{3.A-7d}$$

$$H_x^{TE}(k_x,k_y,z) = c_h \frac{k_x k_y}{k_x^2+k_y^2}\left(\tfrac{z}{|z|}\mathrm{e}^{ik_z|z|}+R_D^{TE}\right), \tag{3.A-7e}$$

$$H_x^{TM}(k_x,k_y,z) = -c_h \frac{k_x k_y}{k_x^2+k_y^2}\left(\tfrac{z}{|z|}\mathrm{e}^{ik_z|z|}+R_D^{TM}\right), \tag{3.A-7f}$$

$$H_y^{TE}(k_x,k_y,z) = c_h \frac{k_y^2}{k_x^2+k_y^2}\left(\tfrac{z}{|z|}\mathrm{e}^{ik_z|z|}+R_D^{TE}\right), \tag{3.A-7g}$$

$$H_y^{TM}(k_x,k_y,z) = c_h \frac{k_x^2}{k_x^2+k_y^2}\left(\tfrac{z}{|z|}\mathrm{e}^{ik_z|z|}+R_D^{TM}\right), \tag{3.A-7h}$$

$$E_z(k_x,k_y,z) = -c_h \frac{\mu\omega k_x}{k^2}\left(\tfrac{z}{|z|}\mathrm{e}^{ik_z|z|}+R_D^{TM}\right), \tag{3.A-7i}$$

$$H_z(k_x,k_y,z) = -c_h \frac{k_y}{k_z}\left(\mathrm{e}^{ik_z|z|}+R_A^{TE}\right), \tag{3.A-7j}$$

where $c_h = -Il_x/2$. Note that the E_z-component is a pure TM mode, and that the H_z-component has a TE mode only. The exponential term describes the direct field, R_A is the reflection response given in equation 3.6, and

$$R_D(k_\rho,z) = \frac{-\grave{R}_s(1+\acute{R}_s)\mathrm{e}^{-ik_z z}+\acute{R}_s(1+\grave{R}_s)\mathrm{e}^{ik_z z}}{1-\acute{R}_s\grave{R}_s}. \tag{3.A-8}$$

The difference in sign from R_A is due to the antisymmetric radiation characteristics for the field components with the sgn(z)-term and the sign of the Fresnel coefficients being opposite compared to the definitions in equation 3.8.

From Figure 3.10 it can be deduced that the VED has no TE-polarization component.

Thus:

$$E_x^v(k_x,k_y,z) = -c_v\frac{\mu\omega k_x}{k^2}\left(\tfrac{z}{|z|}\mathrm{e}^{ik_z|z|}+R_B^{TM}\right), \tag{3.A-9a}$$

$$E_y^v(k_x,k_y,z) = -c_v\frac{\mu\omega k_y}{k^2}\left(\tfrac{z}{|z|}\mathrm{e}^{ik_z|z|}+R_B^{TM}\right), \tag{3.A-9b}$$

$$H_x^v(k_x,k_y,z) = c_v\frac{k_y}{k_z}\left(\mathrm{e}^{ik_z|z|}+R_C^{TM}\right), \tag{3.A-9c}$$

$$H_y^v(k_x,k_y,z) = -c_v\frac{k_x}{k_z}\left(\mathrm{e}^{ik_z|z|}+R_C^{TM}\right), \tag{3.A-9d}$$

$$E_z^v(k_x,k_y,z) = c_v\frac{\mu\omega(k_x^2+k_y^2)}{k_z k^2}\left(\mathrm{e}^{ik_z|z|}+R_C^{TM}\right), \tag{3.A-9e}$$

where $c_v = -Il_z/2$, $H_z = 0$, and the reflection responses are:

$$R_B(k_\rho,z) = \frac{\grave{R}_s(1-\acute{R}_s)\mathrm{e}^{-ik_z z}-\acute{R}_s(1-\grave{R}_s)\mathrm{e}^{ik_z z}}{1-\acute{R}_s\grave{R}_s}, \tag{3.A-10a}$$

$$R_C(k_\rho,z) = \frac{-\grave{R}_s(1-\acute{R}_s)\mathrm{e}^{-ik_z z}-\acute{R}_s(1-\grave{R}_s)\mathrm{e}^{ik_z z}}{1-\acute{R}_s\grave{R}_s}. \tag{3.A-10b}$$

The explanation of the sign differences in R_A, R_B, R_C, and R_D can be summarized as follows: The horizontal components of the electric (magnetic) field have positive (negative) reflection coefficients in terms of the definitions in equation 3.8. The reflection coefficient is negative (positive) for the vertical electric (magnetic) field. The radiation from a HED is symmetric above and below the antenna for the horizontal components of the electric field and vertical component of the magnetic field. The radiation is antisymmetric for the horizontal components of the magnetic field and the vertical component of the electric field. For the VED the horizontal components of the magnetic field and vertical component of the electric field are symmetric, whereas the horizontal components of the electric field are antisymmetric.

The Fourier transform of the expressions in equation 3.A-7 and 3.A-9 into the spatial domain must be done numerically. In order to do the calculations efficiently, the double integral can be reduced to a single integral by using cylindrical coordinates. Thus, the expressions must be written in terms of Bessel functions. Let α represent the angle between $k_\rho = \sqrt{k_x^2+k_y^2}$ and the k_x-component so that $k_x = k_\rho\cos\alpha$ and $k_y = k_\rho\sin\alpha$. The corresponding cylindrical spatial variable is the angle β between the HED and the polar radius ρ. The exponential term in the integral that describes the plane-wave expansion (equation 3.A-4) can be rewritten as

$$\exp\left(ik_x x + ik_y y\right) = \exp\left(ik_\rho\rho\sin\xi\right), \tag{3.A-11}$$

where $\xi = \alpha - \beta + \pi/2$. Equation 3.A-11 can be expressed by a series of Bessel functions

(Gradshteyn and Ryzhik, 1980):

$$\exp\left(ik_\rho\rho\sin\xi\right)=\sum_{-\infty}^{\infty}J_n(k_\rho\rho)\,\mathrm{e}^{in\xi}, \tag{3.A-12}$$

where $J_{-n}\left(k_\rho\rho\right)=(-1)^n\,J_n\left(k_\rho\rho\right)$. From this, one obtains the representation:

$$J_0(k_\rho\rho)=\frac{1}{2\pi}\int_0^{2\pi}d\xi\,\mathrm{e}^{ik_\rho\rho\sin\xi}\,, \tag{3.A-13a}$$

$$J_1(k_\rho\rho)=\frac{1}{2\pi i}\int_0^{2\pi}d\xi\,\sin\xi\,\mathrm{e}^{ik_\rho\rho\sin\xi}\,, \tag{3.A-13b}$$

$$J_2(k_\rho\rho)=\frac{1}{2\pi}\int_0^{2\pi}d\xi\,\cos 2\xi\,\mathrm{e}^{ik_\rho\rho\sin\xi}\,, \tag{3.A-13c}$$

where the following relationship between J_0, J_1, and J_2 holds:

$$J_0(k_\rho\rho)+J_2(k_\rho\rho)=\frac{2}{k_\rho\rho}J_1(k_\rho\rho). \tag{3.A-14}$$

In order to rewrite the expressions in equations 3.A-7 and 3.A-9 in terms of Bessel functions, the relations

$$\cos\alpha=\cos\left(\xi+\beta-\pi/2\right)=\sin\xi\cos\beta+\cos\xi\sin\beta, \tag{3.A-15a}$$

$$\sin\alpha=\sin\left(\xi+\beta-\pi/2\right)=-\cos\xi\cos\beta+\sin\xi\sin\beta, \tag{3.A-15b}$$

$$\cos 2\alpha=\cos\left(2\xi+2\beta-\pi\right)=-\cos 2\xi\cos 2\beta+\sin 2\xi\sin 2\beta, \tag{3.A-15c}$$

$$\sin 2\alpha=\sin\left(2\xi+2\beta-\pi\right)=-\sin 2\xi\cos 2\beta-\cos 2\xi\sin 2\beta, \tag{3.A-15d}$$

are needed. Note that terms involving $\cos\xi$ and $\sin 2\xi$ do not contribute to the Bessel expansion. In order to rewrite the Cartesian field components into cylindrical components, the following relations are used:

$$E_\rho=E_x\cos\beta+E_y\sin\beta\quad\text{and}\quad E_\beta=-E_x\sin\beta+E_y\cos\beta. \tag{3.A-16}$$

The horizontal electric field components due to a HED are as given in equation 3.4. The corresponding E_z component is

$$E_z(\rho,\beta,z)=\frac{i\omega\mu Il_x}{4\pi k^2}\cos\beta\int_0^{\infty}dk_\rho\,k_\rho^2J_1(k_\rho\rho)\left[\tfrac{z}{|z|}\mathrm{e}^{ik_z|z|}+R_D^{TM}(k_\rho,z)\right], \tag{3.A-17}$$

and the magnetic field can be written as

$$H_\rho(\rho,\beta,z)=+\frac{Il_x}{4\pi}\sin\beta\left[-\mathcal{I}_{D0}^{TE}+\frac{1}{\rho}\left(\mathcal{I}_{D1}^{TE}-\mathcal{I}_{D1}^{TM}\right)\right], \tag{3.A-18a}$$

$$H_\beta(\rho,\beta,z)=-\frac{Il_x}{4\pi}\cos\beta\left[\;\mathcal{I}_{D0}^{TM}+\frac{1}{\rho}\left(\mathcal{I}_{D1}^{TE}-\mathcal{I}_{D1}^{TM}\right)\right], \tag{3.A-18b}$$

$$H_z(\rho,\beta,z)=\;\frac{iIl_x}{4\pi}\sin\beta\int_0^{\infty}dk_\rho\,\frac{k_\rho^2}{k_z}J_1(k_\rho\rho)\left[\mathrm{e}^{ik_z|z|}+R_A^{TE}(k_\rho,z)\right], \tag{3.A-18c}$$

where

$$\mathcal{I}_{D0}^{TE}(\rho,z)=\int_0^\infty dk_\rho\, k_\rho\, J_0(k_\rho\rho)\left[\tfrac{z}{|z|}\mathrm{e}^{ik_z|z|}+R_D^{TE}(k_\rho,z)\right], \tag{3.A-19a}$$

$$\mathcal{I}_{D1}^{TE}(\rho,z)=\int_0^\infty dk_\rho\, J_1(k_\rho\rho)\left[\tfrac{z}{|z|}\mathrm{e}^{ik_z|z|}+R_D^{TE}(k_\rho,z)\right], \tag{3.A-19b}$$

$$\mathcal{I}_{D0}^{TM}(\rho,z)=\int_0^\infty dk_\rho\, k_\rho\, J_0(k_\rho\rho)\left[\tfrac{z}{|z|}\mathrm{e}^{ik_z|z|}+R_D^{TM}(k_\rho,z)\right], \tag{3.A-19c}$$

$$\mathcal{I}_{D1}^{TM}(\rho,z)=\int_0^\infty dk_\rho\, J_1(k_\rho\rho)\left[\tfrac{z}{|z|}\mathrm{e}^{ik_z|z|}+R_D^{TM}(k_\rho,z)\right]. \tag{3.A-19d}$$

The field components due to a VED are:

$$E_\rho^v(\rho,\beta,z)=\frac{i\mu\omega Il_z}{4\pi k^2}\int_0^\infty dk_\rho\, k_\rho^2\, J_1(k_\rho\rho)\left[\tfrac{z}{|z|}\mathrm{e}^{ik_z|z|}+R_B^{TM}(k_\rho,z)\right], \tag{3.A-20a}$$

$$H_\beta^v(\rho,\beta,z)=\frac{iIl_z}{4\pi}\int_0^\infty dk_\rho\,\frac{k_\rho^2}{k_z}\, J_1(k_\rho\rho)\left[\mathrm{e}^{ik_z|z|}+R_C^{TM}(k_\rho,z)\right], \tag{3.A-20b}$$

$$E_z^v(\rho,\beta,z)=-\frac{\mu\omega Il_z}{4\pi k^2}\int_0^\infty dk_\rho\,\frac{k_\rho^3}{k_z}\, J_0(k_\rho\rho)\left[\mathrm{e}^{ik_z|z|}+R_C^{TM}(k_\rho,z)\right]. \tag{3.A-20c}$$

Chapter 4

Asymptotic evaluations of the marine CSEM field integrals

L. O. Løseth
Submitted to IEEE Transactions on Geoscience and Remote Sensing

Summary

In marine controlled source electromagnetics (CSEM) or SeaBed Logging (SBL) one explores the subsurface by emitting low-frequency signals from an electric dipole source close to the seabed. The signals are recorded by receivers that are usually positioned on the seafloor. The main goal is to detect and describe possible thin resistive layers within the conductive surroundings beneath the seabed. A simple geological model from an exploration case includes an air halfspace, a water column, and a thin layer in the subsurface. The electromagnetic response from such a plane-layered model is easily calculated using standard modelling tools. However, in order to improve our understanding of the physics of marine CSEM, it is of interest to analyze how the electromagnetic signals propagate. In an isotropic stratified earth model, the electromagnetic field is given in terms of integrals over TE- and TM-polarized field constituents in the wavenumber domain. An analysis of the signal propagation can then be performed by an asymptotic evaluation of the field integrals. This results in closed-form space-domain expressions for the field contributions in terms of the TE and TM modes. In the first part of this paper, asymptotic expressions have been derived for three separate models that consist of: two halfspaces with air and seawater, two conductive halfspaces, and a thin resistive layer within a conductive background medium. By using the saddle-point method of evaluation, where the large parameter in the expansion is the propagation distance of the fields, the lateral wave responses from the sea-surface and seabed, due to branch points in the complex integration plane, have been obtained. It is shown that the response from the

sea-surface is dominated by the TE mode. It is furthermore shown that the response from a thin resistive layer is accounted for by a TM-mode pole in the complex wavenumber domain. Hence one may consider the thin-layer response as caused by a waveguide. In the second part of the paper, a complete model that consists of a sea-surface interface, a seabed interface, and a thin resistive layer in the subsurface has been considered. For this case is it shown that the TM response from the thin resistive layer and the TE response from the sea-surface account well for the total field response for the source and receiver offsets of main interest in conventional marine CSEM surveying for hydrocarbons. In shallow water, the TE response from the sea-surface and the TM response from the resistive layer normally increase. The effects introduced by the water column can be interpreted in terms of a larger effective source strength and an additional amplification of the signal at the receiver.

4.1 Introduction

In marine CSEM or SBL one looks for thin resistive layers in conductive sediments by using an electric dipole source that emits low-frequency signals into the surroundings (Eidesmo et al., 2002). Although SBL has been used to describe applications of marine CSEM where one seeks to directly detect thin resistive layers such as hydrocarbons, both naming conventions are nowadays used to describe the same exploration technique. I will in the following refer to both applications as marine CSEM. In realistic geological scenarios one needs 3-D modelling tools in order to accurately predict how electromagnetic fields from an electric dipole in seawater will propagate. However, the modelling routines for layered media are often well suited to predict the electromagnetic response from the subsurface since geological structures in a typical CSEM setting in many cases can be represented as stratified layers (Constable and Weiss, 2006; Hoversten et al., 2006). A simple 1-D model should include the interface between the seawater and sediments, a thin layer, and the interface between seawater and air (cf. Figure 4.1).

Even if 1-D modelling provides information about the resulting response, it does not clarify which interfaces and layers that contribute what to the modelled signal response. In order to clarify this matter it might be interesting to perform a direct evaluation of the so-called Sommerfeld integrals, i.e., the integrals that describe the electromagnetic field components in a stratified medium. A well-known evaluation technique of integrals is the method of steepest descents (cf. Morse and Feshbach, 1953; Brekhovskikh, 1960; Felsen and Marcuvitz, 2003). The basic idea is to deform the integration path in the complex plane of the integration variable so that the imaginary part of the function in the exponential of the integrand is constant along the deformed path. A function which is analytic in the complex domain has its most rapid changes for the real part along the curves of constant imaginary part (Bender and Orszag, 1999). The main contribution from the integration will

then *normally* be from a saddle point. However, during the deformation of the integration path, poles and branch cuts might be encountered and in this case they contribute to the resulting integral value. These contributions can sometimes be far more significant than the saddle-point contribution.

The evaluation of wave propagation by the method of steepest descents dates back to the early attempts to describe radio-wave propagation in terms of a ground wave (Zenneck, 1907; Sommerfeld, 1909). In a recent paper Wait (1998) reviewed the history of ground-wave investigations related to radio-wave transmission. The method of steepest descents is obviously used for evaluating types of wave propagation other than radio waves; e.g., Brekhovskikh (1960) has a thorough treatment of spherical acoustic and electromagnetic wave propagation in layered media, and Baños (1966) considers dipole radiation in presence of a conducting halfspace.

The asymptotic evaluation of an integral that describes reflection or transmission of a spherical wave or dipole wave in a medium with one interface may give a lateral wave which can be ascribed to a branch point in the complex integration domain. Branch points are always associated with the outermost halfspaces in integrals that describe propagation in layered models (Chew, 1995). In seismology the term head wave is used for the lateral wave (DeSanto, 1992). The description of electromagnetic signal propagation in terms of a lateral wave along the interface between sea and air has been – and still is – important when considering e.g., communication (with submarines) and measurement techniques with submerged electric and magnetic dipoles. Baños (1966) calculated the electromagnetic potentials, due to a source either above or below the surface, by using asymptotic expansions that are valid near the interface, near the vertical axis, and in the entire hemisphere. For all the cases he used the method of steepest descents, but with different expansion parameters. He furthermore reported that the so-called double saddle-point method, where the asymptotic expansion of the Hankel function is performed along with the expansion of the rest of the integral kernel, is more efficient than the normal way of expanding the Hankel function *before* one expands the integration kernel. Baños (1966) then simplified the asymptotic expressions for three separate distances which were referred to as the near-field zone, intermediate zone, and far-field zone. In the near-field case, of importance for low frequencies, he also considered the quasi-static approach which means that the wavenumber in air is set to zero. In fact, Wait (1961) stated that only in the quasi-static analysis does the exponential factor in the resulting field expressions appear in an appropriate manner, and from his analysis, Wait (1961) obtained exact expressions for the lateral wave between the sea and air. Bannister (1984) derived simplified formulas by using the work of Wait (1961). The effect of the sphericity of the earth on lateral waves was investigated by Bremmer (1949) and Hill and Wait (1980). An investigation of lateral waves in general was presented in King et al. (1992).

The saddle point gives a contribution to the asymptotic expansion which may be inter-

preted as a reflected or transmitted ray which propagates from the source to the observation point (Brekhovskikh, 1960). In the deformation of the integration path into the steepest descent path, singularities of the functions in the integration kernels may be encountered. These singularities (or poles) must be taken into account by adding the residue of the function at these points. Poles represent surface waves, leaky waves, or guided waves (Felsen and Marcuvitz, 2003). Wait (1966) examined the possibility of a resistive layer in the earth's crust to support guided waves.

Although asymptotic expansions of integrals that describe field propagation find their most widespread use in cases where one seeks far-field responses for wave propagation with low attenuation, it might be worthwhile to apply asymptotic analysis to dipole radiation in conductive media. This is not a new idea and has, as already mentioned, been done by e.g., Baños (1966) and Wait (1966). However, in this paper I consider the marine CSEM field integrals expressed in terms of their TE and TM modes directly, and the integrals are evaluated for the following three simple models: a conductive halfspace (seawater) in presence of a resistive halfspace (air), seawater in presence of a less conductive halfspace (sediments), and a thin resistive layer within a conductive background medium. In addition, models that consist of different combinations of the simple scenarios are looked into. For the different models, explicit spatial expressions for the field propagation in terms of lateral-wave, guided-wave and ray-reflection contributions are derived. The major motivation of the analysis is to obtain a better physical understanding of the signal propagation in marine CSEM.

The paper starts by reviewing the method of steepest descents. The contributions from a saddle point, branch point, and a simple pole are presented along with a method for calculating the saddle- or branch-point contribution when a pole is located close to the respective point. Next, integrals that describe the horizontal electric field from a horizontal electric dipole, found in e.g., Løseth et al. (2006a) and Løseth and Ursin (2007), are presented. The asymptotic evaluation of these field integrals is sufficient for the investigation of the TE- and TM-mode propagation in a layered model. The evaluation is performed by writing the integrals in terms of Hankel functions and the appropriate reflection-response functions. The single-interface model is studied first. In this case the integrals are considered in the complex wavenumber domain before a method from Baños (1966) is used. This implies a transformation of the branch-point contribution into a saddle-point contribution. However, the double saddle-point method that Baños (1966) used in his investigations has not been found to be of any advantage here. The method for properly handling the presence of a pole in vicinity of a branch point is applied for the TM mode. The next model considered is a thin resistive layer within a conductive background medium. The deformation of the integration path is done in the angular-spectrum domain. This transformation of the integration variable was first done by Ott (1942) for nonconductive media. The influence of the poles (in the reflection response) on the field integrals is determined by their location in the complex

angular-spectrum domain. The corresponding residue contributions are calculated. Having considered the simple models, different combinations of them are looked into. First, the case with a seabed and a thin layer is studied. Next, the case of having a model with a seawater column is considered, and eventually a full model which includes both the water column and the thin layer is discussed. In an appendix the separation of measured data into the TE and TM modes is discussed.

4.2 Method of steepest descents

Consider an integral with the functions $\phi(\zeta)$ and $f(\zeta)$:

$$\mathcal{I}(\chi) = \int_C d\zeta f(\zeta)\, \mathrm{e}^{\chi\phi(\zeta)}, \tag{4.1}$$

where the integration path C originally goes from minus infinity to infinity along the real axis in the complex ζ-plane. Assume that the parameter χ is large. Then a good approximation to the integral can be found by using the method of steepest descents (which is also referred to as the saddle-point method). The method of steepest descents implies a deformation of the original integration path into a path with a constant phase contour. If the function in the exponent is written as $\phi(\zeta) = \phi_r(\zeta) + i\phi_i(\zeta)$, where ϕ_r is the real part and ϕ_i is the imaginary part, the constant phase contours are found where ϕ_i is constant. From complex function theory it is evident that when ϕ_i is constant, ϕ_r must have its most rapid increase or decrease (Bender and Orszag, 1999). Assume in the following that the integrand has one saddle point in the interior of the complex integration domain. Then the saddle point is found at the point on the constant phase curve where $\phi'(\zeta) = 0$. The phase contour that passes through the saddle point is either a steepest descent path (SDP) or a steepest ascent path. The deformation of the integration path into the SDP, assuming that the functions in equation 4.1 are analytic, does not alter the value of the integral. Moreover, along the deformed path, the dominating contribution to the integral comes from a short path segment around the saddle point. Thus, a good approximation to the integral can be found by replacing the function $f(\zeta)$ with a simpler function that equals the original function along the short path segment through the saddle point. The accuracy of the resulting asymptotic approximation usually improves with increasing value of the large parameter χ. However, it is rather the radius of convergence of a power-series expansion of the part of the integrand that is multiplied with the exponential behaviour, that determines how well the asymptotic approximation works [Watson's Lemma (Baños, 1966)]. This usually implies that χ is large.

During the deformation of the integration path one must account for the following: At infinity the deformation from the real axis to the steepest descent curve is justified as long as the value of the integral approaches zero sufficiently fast as the integration variable approaches infinity (Jordan's Lemma). Next, if the functions in the integrand are not analytic,

one must account for possible crossings of poles or branch cuts as the path is deformed. In addition, possible nearby poles must be carefully handled in the calculation of the saddle- and/or branch-point contributions.

In the next sections, general expressions for contributions to the integral in equation 4.1 from saddle points, possible branch points, and possible poles are reviewed.

4.2.1 Contribution from the saddle point

Both the functions $\phi(\zeta)$ and $f(\zeta)$ in equation 4.1 can be Taylor expanded around the saddle point ζ_s:

$$\phi(\zeta) = \phi(\zeta_s) + \phi'(\zeta_s)(\zeta - \zeta_s) + \frac{1}{2}\phi''(\zeta_s)(\zeta - \zeta_s)^2 + .. , \tag{4.2a}$$

$$f(\zeta) = f(\zeta_s) + f'(\zeta_s)(\zeta - \zeta_s) + \frac{1}{2}f''(\zeta_s)(\zeta - \zeta_s)^2 + .. . \tag{4.2b}$$

The notation is simplified when using $\zeta - \zeta_s = s$, $\phi_n = \phi^{(n)}(\zeta_s)/n!$, and $f_n = f^{(n)}(\zeta_s)/n!$. At the saddle point $\phi'(\zeta_s) = 0$, and along the path of steepest descents the imaginary part of $\phi(\zeta)$ is constant. Thus, the variable s is real. Now, by inserting the Taylor expansions from equation 4.2 into the integral in equation 4.1, and by rewriting the expression in the exponential function in terms of its series expansion after the ϕ_2-term, one obtains the contribution from the saddle point (Stamnes, 1986):

$$\begin{aligned}\mathcal{I}_s(\chi) \sim \mathrm{e}^{\chi\phi_0} \int_{-\infty}^{\infty} ds\ \mathrm{e}^{\chi\phi_2 s^2} \left[f_0 + f_1 s + f_2 s^2 + ..\right] \\ \left[1 + \chi\left(\phi_3 s^3 + \phi_4 s^4 + ..\right) + \tfrac{1}{2}\chi^2\left(\phi_3 s^3 + ..\right)^2 + ..\right].\end{aligned} \tag{4.3}$$

Using equation 4.A-5 in Appendix 4.A, this leads to:

$$\mathcal{I}_s(\chi) \sim \mathrm{e}^{\chi\phi(\zeta_s)} \sqrt{\frac{-2\pi}{\chi\phi''(\zeta_s)}} f(\zeta_s) \left[1 + \frac{1}{2\chi\phi''(\zeta_s)}\psi(\zeta_s) + ..\right], \tag{4.4}$$

where

$$\psi(\zeta_s) = \frac{\phi'''(\zeta_s)}{\phi''(\zeta_s)}\frac{f'(\zeta_s)}{f(\zeta_s)} - \frac{f''(\zeta_s)}{f(\zeta_s)} + \frac{1}{4}\frac{\phi^{IV}(\zeta_s)}{\phi''(\zeta_s)} - \frac{5}{12}\frac{[\phi'''(\zeta_s)]^2}{[\phi''(\zeta_s)]^2}. \tag{4.5}$$

The value of the square-root term in equation 4.4 is made unique by requiring that the sign of its argument is equal to the sign of the inclination of the steepest descent path through the saddle point (cf. Felsen and Marcuvitz, 2003).

The expression in equation 4.4 can also be derived by using the substitution

$$\phi(\zeta) = \phi(\zeta_s) - u^2. \tag{4.6}$$

Note furthermore that a series expansion of the integration kernel f in terms of the small variable u followed by an integration of each term, might save laborious work on differentiations that follows from equation 4.4 and 4.5.

4.2.2 Contribution from a branch point

Branch points with appropriate cuts originate from multivalued functions in the integration kernel in equation 4.1. In the problems encountered in this paper, branch points are due to square-root functions in the integrals. The two solutions of the square-root function are on two different Riemann sheets which are glued together at the branch cuts in the complex plane. If the deformation from the original integration path to the SDP leads to a crossing of a branch cut, one must enter another Riemann sheet in order for the function to be continuous. However, the integration path should be kept on the same Riemann sheet all along the path. Thus, the sign of the square root is chosen so that the integrand is not exponentially growing towards infinity, and this also determines the Riemann sheet on which the integration should be performed (in order to satisfy the radiation condition). It furthermore implies that the function $f(\zeta)$ is discontinuous along a branch cut. Thus, the integration path should be deformed to encircle possible cuts.

In order to obtain the contribution to the integral in equation 4.1 from a branch point at ζ_b, the function $f(\zeta)$ can be expanded in terms of the variable $t = \sqrt{\zeta - \zeta_b}$:

$$f(\zeta) = f(\zeta_b) + b_1(\zeta_b)\, t + b_2(\zeta_b)\, t^2 + b_3(\zeta_b)\, t^3 + .. \,, \tag{4.7}$$

where

$$b_1(\zeta) = 2\sqrt{\zeta - \zeta_b}\frac{df(\zeta)}{d\zeta}, \quad b_2(\zeta) = \sqrt{\zeta - \zeta_b}\frac{db_1(\zeta)}{d\zeta}, \quad \text{and} \quad b_3(\zeta) = \frac{1}{3}\sqrt{\zeta - \zeta_b}\frac{db_2(\zeta)}{d\zeta}. \tag{4.8}$$

By expanding ϕ in terms of $t^2 = \zeta - \zeta_b$, i.e., $\phi(\zeta) = \phi(\zeta_b) + \phi_1 t^2 + ..$, one gets:

$$\mathcal{I}_b(\chi) \sim \mathrm{e}^{\chi\phi(\zeta_b)} \int_{-\infty}^{\infty} dt \;\; 2t \;\; \mathrm{e}^{\chi\phi_1 t^2} \left[f(\zeta_b) + b_1 t + b_2 t^2 + b_3 t^3 + ..\right] \\ \left[1 + \chi\left(\phi_2 t^4 + \phi_3 t^6 + ..\right) + \tfrac{1}{2}\chi^2\left(\phi_2 t^4 + ..\right)^2 + ..\right], \tag{4.9}$$

which leads to the following contribution:

$$\mathcal{I}_b(\chi) \sim \mathrm{e}^{\chi\phi(\zeta_b)} \frac{\sqrt{\pi} b_1}{[-\chi\phi'(\zeta_b)]^{3/2}} \left[1 + \frac{3}{2\chi\phi'}\left(\frac{5}{4}\frac{\phi''}{\phi'} - \frac{b_3}{b_1}\right) + ..\right]. \tag{4.10}$$

The functions in equation 4.10 must be evaluated at the branch point. Note that an implicit assumption in equation 4.9 is that the integral is evaluated along a constant phase contour.

The expression for the branch-point contribution can also be obtained by writing $\phi(\zeta)$ as in equation 4.6 (with ζ_s replaced by ζ_b). Instead of doing the differentiations that follow from equation 4.10, the integration kernel can be expanded in terms of the small variable u, and then integrated for each power of u. It might furthermore be advantageous to map the portion of the integration path around the branch point into a steepest descent path.

4.2.3 Contribution from poles

If a simple pole of the function $f(\zeta)$ is crossed when the integration path in equation 4.1 is deformed, the contribution from the pole must be added to the integral. This contribution is found by considering the residue of the kernel function at the singularity:

$$\mathcal{I}_p(\chi) = \oint_C d\zeta\, f(\zeta)\, \mathrm{e}^{\chi\phi(\zeta)} = 2\pi i\, \mathrm{e}^{\chi\phi(\zeta_p)} \operatorname*{Res}_{\zeta=\zeta_p} f(\zeta). \tag{4.11}$$

In cases where $f(\zeta)$ can be written as a rational function $f(\zeta) = f_N(\zeta)/f_D(\zeta)$, the expression for the residue is simplified by performing a Taylor expansion of the denominator:

$$\operatorname*{Res}_{\zeta=\zeta_p} f(\zeta) = \lim_{\zeta\to\zeta_p} [(\zeta-\zeta_p)f(\zeta_p)] = \lim_{\zeta\to\zeta_p} \left[\frac{(\zeta-\zeta_p)f_N(\zeta)}{f_D(\zeta_p) + f_D'(\zeta_p)(\zeta-\zeta_p) + ..}\right] = \frac{f_N(\zeta_p)}{f_D'(\zeta_p)}, \tag{4.12}$$

since $f_D(\zeta_p) = 0$. The contribution from the pole to the overall response in equation 4.1 must in principle not be taken into account before the argument χ is of such a value that the deformation of the path (which is dependent on χ) crosses the pole. However, if the pole is close to a saddle or branch point it will affect the saddle- or branch-point contribution to the integral. Thus, in this case the effect of the pole must also be taken into consideration for values of χ that do not lead to a crossing of the pole as the path is deformed.

4.2.4 Pole in the vicinity of a branch or saddle point

When a pole is close to a saddle point or branch point the expressions for the contribution from a saddle (equation 4.4) or branch point (equation 4.10) might become worthless. This is due to the radius of convergence for the power-series expansion of the integrand becoming small because of the nearby located pole. In such cases one attempts to remove the pole from the integral kernel. Consider the integral

$$\mathcal{I}_v(\chi) = \mathrm{e}^{\chi\phi_0} \int_{-\infty}^{\infty} du\, q(u)\, \mathrm{e}^{-\chi u^2}, \tag{4.13}$$

which is obtained from equation 4.1 after a substitution as in equation 4.6. This way of evaluating the integral can be used for a saddle point as well as a branch point; the subscript v may represent one or the other, and the constant ϕ_0 is either $\phi(\zeta_s)$ or $\phi(\zeta_b)$. The integral is approximated for large χ by expanding $q(u) = f(\zeta)d\zeta/du$ in a Taylor series for small u. Note that u is real on a constant phase contour.

A pole in $f(\zeta)$ at ζ_p results in a corresponding pole in $q(u)$ at u_p which might be complex and is given by:

$$u_p = \sqrt{\phi_0 - \phi(\zeta_p)}, \tag{4.14}$$

where the sign of the double-valued root is selected so that the position of u_p is in accordance with the relative position of the pole compared to the SDP in the original complex domain.

The evaluation of the saddle- or branch-point contribution when a pair of poles at $u = \pm u_p$ have an effect on the contributions can be handled by separating the singularity from the rest of the integrand:

$$q(u) = q_c(u) + \frac{2\Gamma u_p}{u^2 - u_p^2}, \quad \text{where} \quad \Gamma = \lim_{u \to u_p} \left[\frac{u^2 - u_p^2}{2u_p} q(u) \right] = \operatorname*{Res}_{\zeta = \zeta_p} f(\zeta), \tag{4.15}$$

where the last relation holds for the substitutions used in the current analysis, cf. equation 4.6. The method for explicitly calculating the contribution from a pair of poles in a saddle- or branch-point evaluation is presented in e.g., Baños (1966) and Kong (2000). The calculation is reviewed in Appendix 4.B for completeness. The results in equation 4.B-15 means that the integral in equation 4.13, when $q(u)$ has singularities at $u = \pm u_p$, can be written as

$$\mathcal{I}_v(\chi) = \mathcal{I}_{vc} + \mathcal{I}_{vp}, \quad \text{where} \tag{4.16a}$$

$$\mathcal{I}_{vc}(\chi) = \mathrm{e}^{\chi\phi_0} \int_{-\infty}^{\infty} du\, q_c(u)\, \mathrm{e}^{-\chi u^2}, \quad \text{and} \tag{4.16b}$$

$$\mathcal{I}_{vp}(\chi) = \pm 2\pi i\, \Gamma\, \mathrm{e}^{\chi\phi_0} \left[1 - \operatorname{erf}\left(\mp i\sqrt{\chi} u_p\right)\right]\, \mathrm{e}^{-\chi u_p^2}. \tag{4.16c}$$

The sign in front of equation 4.16c and corresponding opposite sign in the argument of the error function are determined according to the location of the pole u_p compared to the deformed integration path. Thus, when $\mathrm{Im}(u_p) > 0$ the positive sign in front of the expression and negative sign in the argument of the error function must be selected. When $\mathrm{Im}(u_p) < 0$ the signs must be switched. This corresponds to the discontinuity that is encountered when crossing the pole.

When considering one pole at $u = u_p$, the expression in equation 4.15 can be written as $q(u) = q_c(u) + \Gamma/(u - u_p)$. This means that the contribution from the pole is half of the value given in equation 4.16c (cf. Felsen and Marcuvitz, 2003).

The integral in equation 4.16b can be calculated by subtracting the series expansion of the $\mathcal{I}_{vp}$-integral from the series expansion of the $\mathcal{I}_v$-integral. Thus, the expansion of the error function times the exponential function for small arguments is needed (Abramowitz and Stegun, 1962, equation 7.2.14):

$$\mathrm{e}^{\zeta^2} \left[1 - \operatorname{erf}(\zeta)\right] \sim \frac{1}{\sqrt{\pi}\zeta} \left[1 - \frac{1}{2\zeta^2} + \frac{3}{4\zeta^4} - \frac{15}{8\zeta^6} + ..\right]. \tag{4.17}$$

When the argument in the error function is small, the pole is close to the saddle or branch point in the complex plane and the effect of the pole is large. When its argument is large, the error function approaches unity which means that the effect of the pole becomes negligible.

4.3 Electric field from a horizontal electric dipole

In Figure 4.1 a sketch of a layered structure for a typical marine CSEM-exploration case is presented. The electromagnetic field in such a model is easily calculated by a standard modelling tool. However, it is not obvious how the signals propagate in the model. In order to enlighten this matter, it is found illustrative to consider the signal propagation for 5 different versions of the model: The first case consists of the presence of only a single interface as sketched in Figure 4.2. This case embodies the two very different situations of a conductive and a nonconductive halfspace (sea-surface), and two conductive halfspaces (seabed) where the source is within the more conducting medium. Next, the case of a thin layer contained within a more conductive background medium (Figure 4.1 without the seawater layer and air) is considered. Having studied the relatively simple single-interface and thin-layer cases, the signal propagation in models where these cases are combined is looked into. The combinations that have been considered are: a seabed interface with a thin layer in the subsurface, a sea-surface and seabed interface (water column), and finally a complete model as shown in Figure 4.1.

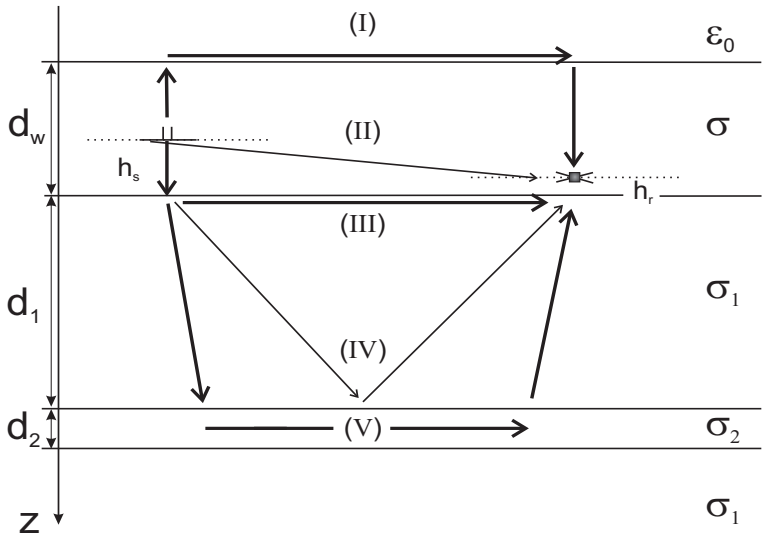

Figure 4.1: Sketch of the signal propagation in a stratified model. The permittivity in air is ε_0, the conductivity is σ in the seawater (thickness d_w) , σ_1 in the sediments (thickness d_1), and σ_2 in the thin resistive layer (thickness d_2). In the water column the source (receiver) is at height h_s (h_r) above the seabed. The signal paths sketched are (the most important ones): the lateral wave on the sea-surface interface (I), the direct wave between the source and receiver (II), the lateral wave on the seabed interface (III), the reflected wave from the thin layer (IV), and the guided wave in the thin layer (V).

The signal propagation is studied by using asymptotic evaluations of the field integrals with the method of steepest descents. Thus, general expressions for the field integrals in stratified media are needed. In the following the horizontal electric field components will be considered since they contain both the transverse electric polarization components (TE mode) and the transverse magnetic polarization components (TM mode). The expressions that describe the vertical electric field component (E_z) are given in Appendix 4.C, and the magnetic field can be obtained from the electric field components by differentiations that follow from Faraday's law.

The polarization modes behave differently when reflected from or transmitted through an interface. Thus, a field needs to be separated into its polarization modes in order to calculate the reflection and transmission responses for the spectrum of plane waves that constitutes the field integral. The TE mode has no electric field component vertical to the interface and the TM mode has no magnetic field component vertical to the interface (Kong, 2000). The E_z-component is a pure TM mode, and its behaviour is similar to the behaviour of the TM mode considered for the horizontal electric field.

In the frequency domain the radial and azimuthal electric field components from a horizontal electric dipole (HED) within the source layer are (Løseth and Ursin, 2007):

$$E_\rho = -\frac{Il_x}{4\pi}\cos\beta\left[\mathcal{I}_{A0}^{TM} + \frac{1}{\rho}\left(\mathcal{I}_{A1}^{TE} - \mathcal{I}_{A1}^{TM}\right)\right], \tag{4.18a}$$

$$E_\beta = -\frac{Il_x}{4\pi}\sin\beta\left[-\mathcal{I}_{A0}^{TE} + \frac{1}{\rho}\left(\mathcal{I}_{A1}^{TE} - \mathcal{I}_{A1}^{TM}\right)\right], \tag{4.18b}$$

where Il_x is the electric dipole current moment, ρ is the radial distance in the horizontal plane, and β is the azimuthal angle. The contributions from the TE and TM modes are:

$$\mathcal{I}_{A0}^{TE} = \int_0^\infty d\lambda\, \lambda\, J_0(\lambda\rho)\, g_A^{TE}(\lambda), \qquad \mathcal{I}_{A1}^{TE} = \int_0^\infty d\lambda\, J_1(\lambda\rho)\, g_A^{TE}(\lambda), \tag{4.19a}$$

$$\mathcal{I}_{A0}^{TM} = \int_0^\infty d\lambda\, \lambda\, J_0(\lambda\rho)\, g_A^{TM}(\lambda), \qquad \mathcal{I}_{A1}^{TM} = \int_0^\infty d\lambda\, J_1(\lambda\rho)\, g_A^{TM}(\lambda), \tag{4.19b}$$

where λ is the horizontal wavenumber, and J_0 and J_1 are the Bessel functions of order zero and one, respectively. The functions in the integral expressions are

$$g_A^{TE}(\lambda) = \frac{\omega\mu}{\gamma}\left[\mathrm{e}^{i\gamma h_{rs}} + R_A^{TE}(\lambda)\right], \tag{4.20a}$$

$$g_A^{TM}(\lambda) = \frac{\gamma}{\omega\tilde{\varepsilon}}\left[\mathrm{e}^{i\gamma h_{rs}} + R_A^{TM}(\lambda)\right], \tag{4.20b}$$

where the first terms on the right hand side describe a direct field (the contribution in a homogeneous medium), h_{rs} is the vertical distance between the source and the receiver, and the second terms are the reflection responses. The parameter ω is the source frequency, μ is the magnetic permeability, and $\tilde{\varepsilon} = \varepsilon + i\sigma/\omega$ is a complex permittivity that includes both the electric permittivity ε and the conductivity σ. The vertical wavenumber is denoted γ and

given by $\gamma = \sqrt{k^2 - \lambda^2}$, where k is the total wavenumber. The sign of the square root must be chosen so that $\mathrm{Im}(\gamma) > 0$ in order to satisfy the radiation condition. The wavenumber in terms of electromagnetic properties and frequency is

$$k = \sqrt{\omega^2 \mu\varepsilon + i\omega\mu\sigma}. \tag{4.21}$$

Assume that the z-axis is pointing downwards and that the receiver position is below the source position. Then the reflection response can be written as (Løseth and Ursin, 2007):

$$R_A = \frac{\grave{R}_b(1 + \acute{R}_s) + \acute{R}_s(1 + \grave{R}_s)}{1 - \acute{R}_s\grave{R}_s} \mathrm{e}^{i\gamma h_{rs}}, \tag{4.22}$$

where $\grave{R}_b$ is the reflection response from a lower stack up to the level of the receiver, $\grave{R}_s$ is the response from a lower stack up to the level of the source [i.e., $\grave{R}_b = \grave{R}_s \exp(-2i\gamma h_{rs})$], $\acute{R}_s$ is the reflection response from an upper stack down to the level of the source, and $\exp(i\gamma h_{rs})$ is the phase-propagation factor from the source to the receiver.

The reflection coefficient from a stack of layers for both the TE and TM mode is:

$$R_m = \frac{r_m + R_{m+1}}{1 + r_m R_{m+1}} \mathrm{e}^{2i\gamma_m h_m}, \quad m = 0, 1, 2, .., \tag{4.23}$$

where γ_m is the vertical wavenumber in the m'th layer. The initial condition at the start of the stack is that $R_M = 0$. The expressions can be used for both upgoing and downgoing reflection coefficients. In both cases R_{m+1} is the reflection response just behind the m'th interface, r_m is the reflection coefficient at the m'th interface, and h_m is the distance from the m'th interface to the z-level of R_m.

The TE- and TM-mode reflection coefficients at an interface are for the horizontal electric field components (cf. Løseth et al., 2006b):

$$r_{TE} = \frac{\mu_2\gamma_1 - \mu_1\gamma_2}{\mu_2\gamma_1 + \mu_1\gamma_2} \quad \text{and} \quad r_{TM} = \frac{\tilde{\varepsilon}_1\gamma_2 - \tilde{\varepsilon}_2\gamma_1}{\tilde{\varepsilon}_2\gamma_1 + \tilde{\varepsilon}_1\gamma_2}, \tag{4.24}$$

where the subscript 1 refers to material parameters in the region that contains the incident field, and the subscript 2 denotes material parameters on the opposite side of the interface. The transmission coefficients can be written as

$$t_{TE} = \frac{2\mu_2\gamma_1}{\mu_2\gamma_1 + \mu_1\gamma_2} \quad \text{and} \quad t_{TM} = \frac{2\tilde{\varepsilon}_1\gamma_2}{\tilde{\varepsilon}_2\gamma_1 + \tilde{\varepsilon}_1\gamma_2}, \tag{4.25}$$

which gives the relations $1 + r_{TE} = t_{TE}$ and $1 + r_{TM} = t_{TM}$.

In order to simplify the calculations in the following it will be assumed that the magnetic permeability is constant in all the layers in Figure 4.1. For simplicity it will be referred to as μ. In air the wavenumber in equation 4.21 reduces to

$$k_0 = \omega\sqrt{\mu\varepsilon_0}, \tag{4.26}$$

where the subscript 0 is used to denote the air halfspace, and ε_0 is the free-space permittivity. For all other layers the low-frequency wavenumber approximation for conductive media is used. This means that equation 4.21 reduces to

$$k = \frac{1+i}{\sqrt{2}}\sqrt{\omega\mu\sigma}. \tag{4.27}$$

The wavenumber in seawater will be referred to without subscript, in the sediment layer (or overburden) the subscript 1 is used, and the subscript 2 represents the thin layer. Thus, the only electromagnetic properties that will be considered in the following, in addition to the free-space permittivity and permeability, are the conductivities in the seawater, sediments, and thin layer; denoted σ, σ_1, and σ_2, respectively.

4.3.1 Direct and reflected field integrals

The integrals in equation 4.19 can be written as a sum of a direct field and a reflected field ($\mathcal{I} = \mathcal{I}_d + \mathcal{I}_r$). In the integrals that describe the reflection response, the Bessel functions can be replaced by the Hankel functions using equation 4.D-29 from Appendix 4.D. It furthermore simplifies the notation if the function H_ν^- is introduced as the Hankel function without the exponential term $\exp(i\zeta)$:

$$H_0^-(\zeta) = H_0^{(1)}(\zeta)\mathrm{e}^{-i\zeta} \quad \text{and} \quad H_1^-(\zeta) = H_1^{(1)}(\zeta)\mathrm{e}^{-i\zeta}. \tag{4.28}$$

If the reflection response is written as the response at an appropriate interface times the factor that describes the vertical propagation distance h between the source, interface, and receiver, one gets the following expressions for the reflected field integrals:

$$\mathcal{I}^{TE}_{A0,r} = \frac{\omega\mu}{2}\int_{-\infty}^{\infty} d\lambda\, \frac{\lambda}{\gamma}\, H_0^-(\lambda\rho)\, R_{TE}(\lambda)\, \mathrm{e}^{i\lambda\rho+i\gamma h}, \tag{4.29a}$$

$$\mathcal{I}^{TE}_{A1,r} = \frac{\omega\mu}{2}\int_{-\infty}^{\infty} d\lambda\, \frac{1}{\gamma}\, H_1^-(\lambda\rho)\, R_{TE}(\lambda)\, \mathrm{e}^{i\lambda\rho+i\gamma h}, \tag{4.29b}$$

$$\mathcal{I}^{TM}_{A0,r} = \frac{\omega\mu}{2k^2}\int_{-\infty}^{\infty} d\lambda\, \lambda\gamma\, H_0^-(\lambda\rho)\, R_{TM}(\lambda)\, \mathrm{e}^{i\lambda\rho+i\gamma h}, \tag{4.29c}$$

$$\mathcal{I}^{TM}_{A1,r} = \frac{\omega\mu}{2k^2}\int_{-\infty}^{\infty} d\lambda\, \gamma\, H_1^-(\lambda\rho)\, R_{TM}(\lambda)\, \mathrm{e}^{i\lambda\rho+i\gamma h}. \tag{4.29d}$$

The relation $1/\omega\tilde{\varepsilon} = \omega\mu/k^2$ has been used in equation 4.20b when deriving equations 4.29c and 4.29d. The introduction of the Hankel function leads to an integration path from minus to plus infinity which is convenient in order to deform the integration path into a steepest descent path. The direct field integrals can be calculated as shown in Appendix 4.E. This

results in:

$$\mathcal{I}^{TE}_{A0,d} = -i\omega\mu\frac{\mathrm{e}^{ikr}}{r}, \tag{4.30a}$$

$$\mathcal{I}^{TE}_{A1,d} = -i\omega\mu\frac{\mathrm{e}^{ikr} - \mathrm{e}^{ikh_{rs}}}{ik\rho}, \tag{4.30b}$$

$$\mathcal{I}^{TM}_{A0,d} = -i\omega\mu\frac{\mathrm{e}^{ikr}}{r}\left[\left(1 - \frac{2}{ikr} - \frac{2}{k^2r^2}\right) + \frac{\rho^2}{r^2}\left(-1 + \frac{3}{ikr} + \frac{3}{k^2r^2}\right)\right], \tag{4.30c}$$

$$\mathcal{I}^{TM}_{A1,d} = -i\omega\mu\left[\frac{\mathrm{e}^{ikr}}{r}\left(-\frac{1}{ikr} - \frac{1}{k^2r^2}\right)\rho + \frac{\mathrm{e}^{ikr} - \mathrm{e}^{ikh_{rs}}}{ik\rho}\right], \tag{4.30d}$$

where r here is the distance from the source to the receiver $r = \sqrt{\rho^2 + h_{rs}^2}$. Note that when separated into the TE and TM modes, the homogeneous field contributions from the first order integrals ($\mathcal{I}_{A1}$) have a plane-wave contribution. These vertically propagating plane-wave components cancel each other in the final field expressions (equation 4.18) since they depend on the difference of $\mathcal{I}^{TE}_{A1}$ and $\mathcal{I}^{TM}_{A1}$, and since the reflection coefficients in equation 4.24 are equal for normal incidence.

4.4 Single interface

In this section, asymptotic expansions of the field integrals in equation 4.29 for a stratified model with one interface are derived. The objective is to obtain explicit spatial expressions in terms of the TE and TM modes for a source in seawater in presence of a seabed or sea-surface interface. The resulting expressions can in all cases be pictured as a sum of a lateral and ray-reflected contribution. Consider the model depicted in Figure 4.2. The model may represent both a seabed and a sea-surface interface. The source and receiver are situated in seawater, and the interface is close to the antennas. The vertical propagation distance in the seabed case is $h = h_s + h_r$. In the sea-surface case, Figure 4.2 can be thought of as upside/down, and the source (receiver) is at depth d_s (d_r) below the interface. In accordance with the expressions in equation 4.29, the wavenumber in seawater is denoted k and the vertical wavenumber is denoted γ. The corresponding total wavenumber and vertical wavenumber in the other medium are denoted k_a and γ_a, respectively.

4.4.1 Reflection coefficients

The reflection coefficients in equation 4.29 are obtained from equation 4.24 with the assumption of constant permeability across the interface:

$$R^{TE}_{si}(\lambda) = \frac{\gamma - \gamma_a}{\gamma + \gamma_a}, \tag{4.31a}$$

$$R^{TM}_{si}(\lambda) = \frac{k^2\gamma_a - k_a^2\gamma}{k^2\gamma_a + k_a^2\gamma} = \frac{\gamma_a - n^2\gamma}{\gamma_a + n^2\gamma}, \tag{4.31b}$$

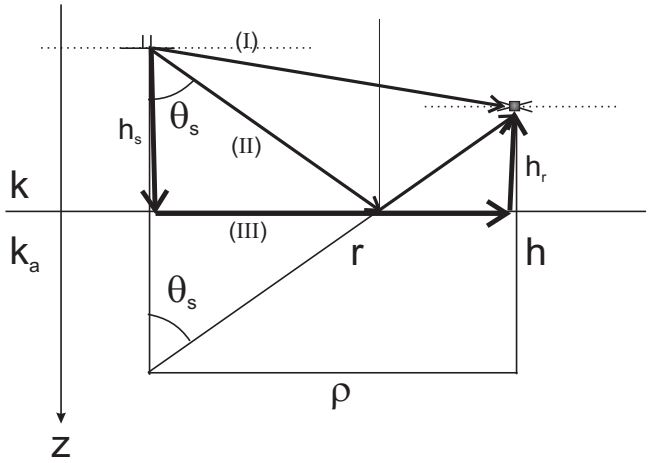

Figure 4.2: Sketch of the signal propagation between the source and receiver in case of a single-interface model. The wavenumber in the source medium is k and in the other medium it is k_a. The height of the source (receiver) is h_s (h_r). The main contributions to the signal at the receiver are: the direct wave (I), the "ray"-reflected wave (II), and the lateral wave (III). The reflected ray with angle θ_s propagates a distance $r = \sqrt{\rho^2 + h^2}$, where ρ is the horizontal distance and h the vertical distance.

where the subscript si denotes single interface, and the reflection coefficient for the TM mode has been written in terms of the refraction index $n = k_a/k$. It is useful to rewrite the reflection coefficients as

$$R_{si}^{TE}(\lambda) = \frac{k^2\left(1+n^2\right) - 2\gamma\gamma_a - 2\lambda^2}{k^2\left(1-n^2\right)}, \tag{4.32a}$$

$$R_{si}^{TM}(\lambda) = \frac{1}{1-n^4}\frac{\gamma_a^2 - 2n^2\gamma\gamma_a + n^4\gamma}{k_p^2 - \lambda^2}, \tag{4.32b}$$

where the pole in the TM coefficient is given as

$$k_p = \pm\frac{k_a}{\sqrt{1+n^2}}. \tag{4.33}$$

This is the famous Sommerfeld pole (Sommerfeld, 1909; Baños, 1966).

4.4.2 Integration in the horizontal wavenumber domain

The integrals in equation 4.29 are given in terms of the horizontal wavenumber variable from minus to plus infinity. In order to use the saddle-point method, λ is considered complex:

$$\lambda = \lambda_r + i\lambda_i, \tag{4.34}$$

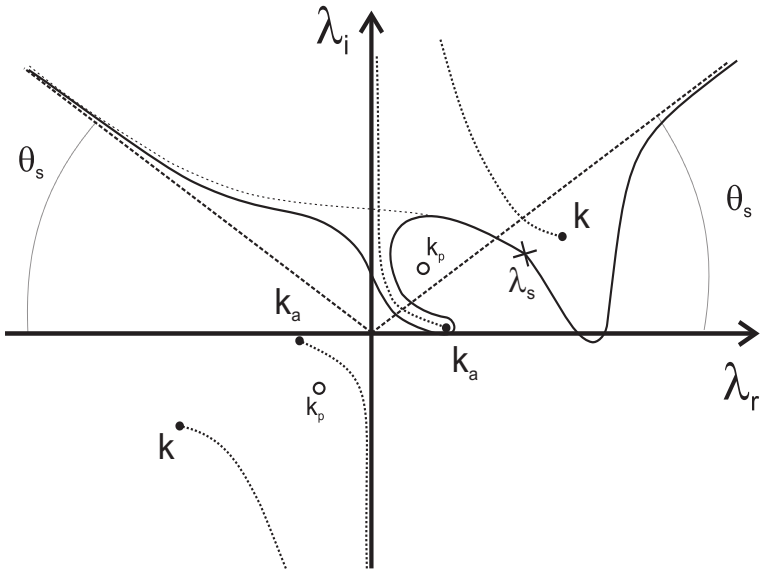

Figure 4.3: Sketch of the original path, steepest descent path (SDP), branch cuts, and pole in the complex horizontal wavenumber domain when the integrals are evaluated in the case of having a single interface. The TM-mode poles are located at $\pm k_p$, and the branch points at $\pm k_a$ and $\pm k$. The saddle point is at $\lambda_s = k \sin\theta_s$. The asymptotes of the SDP are given by $\tan\theta_s = \lambda_i/|\lambda_r|$, and the SDP furthermore crosses the λ_i-axis at $\lambda_i \approx \mathrm{Re}(k)/\cos\theta_s$, and the λ_r-axis twice at $\lambda_r \approx \mathrm{Re}(k)/\sin\theta_s$.

where λ_r is the real part and λ_i is the imaginary part. By comparing the integrals in equation 4.29 with the integral in equation 4.1, an obvious choice of the large parameter χ is the distance travelled by the signals between the source and receiver $r = \sqrt{\rho^2 + h^2}$. The function in the exponent in equation 4.29 then takes the form:

$$\phi(\lambda) = i\lambda\frac{\rho}{r} + i\sqrt{k^2 - \lambda^2}\frac{h}{r}. \tag{4.35}$$

The saddle point λ_s is given by $\phi'(\lambda_s) = 0$:

$$\lambda_s = \pm k\frac{\rho}{r} = \pm k\sin\theta_s, \tag{4.36}$$

where the parameterization $\sin\theta_s = \rho/r$ has been introduced. This means that $\cos\theta_s = h/r$. The deformation of the original integration path is performed in the upper halfplane. Thus, the positive sign in equation 4.36 must be selected. The inclination of the SDP through the saddle point is found to be $\Delta\lambda_i/\Delta\lambda_r = -1$ by inserting $\lambda_s + \Delta\lambda$, where $\Delta\lambda = \Delta\lambda_r + i\Delta\lambda_i$, into equation 4.35. The asymptotes of the SDP are found from equation 4.35 by letting $\lambda_r \to \pm\infty$ along the constant phase contour that passes through the saddle point in the

upper halfplane:

$$\lambda_i \sim |\lambda_r| \frac{\rho}{h} = |\lambda_r| \tan\theta_s. \tag{4.37}$$

Possible branch points and poles in the complex λ-plane are found by considering the analyticity of the integration kernel in equation 4.29. From the reflection coefficients in equation 4.31 it is clear that there are branch points at $\pm k$ and $\pm k_a$ for all the integrals in equation 4.29. In addition, the TM integrals have simple poles at $\pm k_p$. Note also that the Hankel function has a singularity at zero which will not lead to complications in the current considerations.

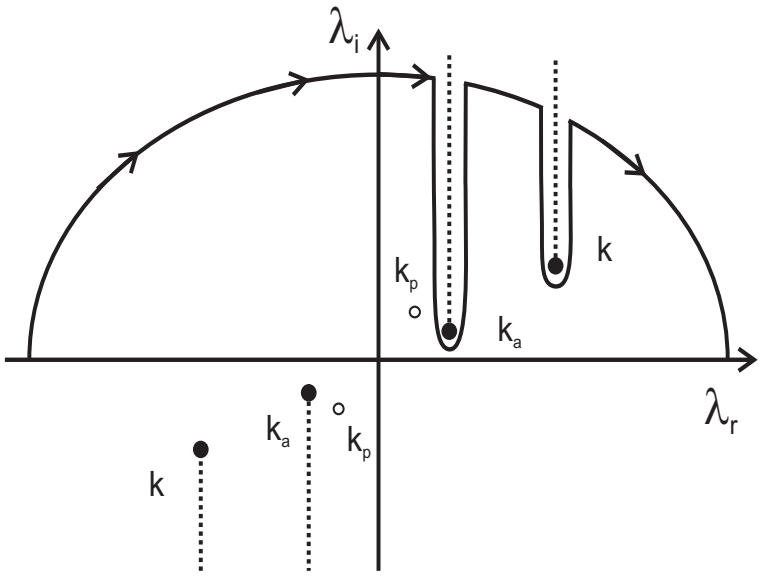

Figure 4.4: Sketch of the branch cuts and integration path when the source and receiver are close to the interface ($\theta_s \to \pi/2$ in Figure 4.3). The curve around k_a gives the branch-point contribution whereas the curve around k gives the saddle-point contribution.

A deformation from the original integration path along the λ_r-axis into the SDP is sketched in Figure 4.3. The figure is meant to illustrate both the seabed and sea-surface cases since when k_a is real, a small artificial imaginary part should be added during the calculations in order for the integrals to converge. The angle θ_s from the λ_r-axis to the SDP is seen from Figure 4.2 to be the reflection angle of a ray between the source and receiver. Observe furthermore that the branch cut from k_a is crossed when the angle θ_s becomes larger than a certain (small) value. The integration path should then be deformed so that it encircles the branch point in order to be on the physical Riemann sheet. For the TM integrals, Figure 4.3 shows that the pole is crossed and that it is close to the branch point. Moreover, the source medium is more conductive than the medium on the opposite interface. Since the

imaginary part of k is larger than the imaginary part of k_a, the contribution from the branch point will dominate the saddle-point contribution as ρ gets large.

In the models considered in Figure 4.2, the antennas are close to the interface. As the angle of incidence approaches 90°, i.e., $\rho >> h$, the SDP in Figure 4.3 approaches the integration path in Figure 4.4 where the integration path around k_a yields the branch-point contribution and integration path around k yields the saddle-point contribution. In Figures 4.3 and 4.4 the branch cuts have been chosen in two different ways. The branch cuts can be chosen at will as long as they imply that $\mathrm{Im}(\gamma) > 0$ and $\mathrm{Im}(\gamma_a) > 0$ on the original path of integration (Baños, 1966). Thus, both the cuts sketched in Figure 4.3 (Sommerfeld cuts) and Figure 4.4 (Baños cuts) are valid. However, on which Riemann sheet the poles are situated is dependent on the choice of cuts. If the Sommerfeld cuts are chosen, the pole k_p lies on the physical sheet which means that the pole must be accounted for explicitly. If however the Baños cuts are chosen, as will be done in the calculations here, the pole is not on the physical Riemann sheet. Then it contributes to the expressions only through limiting the convergence radius of the power-series expansion of the integrand that is used for the branch-point evaluation. The determination of which Riemann sheet the pole is on is done by considering the denominator in equation 4.31b: The vertical wavenumbers γ and γ_a must have opposite signs in order for the pole to be on the physical sheet. This happens when the pole is to the right of the cut as in Figure 4.3, but not when the pole is to the left as in Figure 4.4 (cf. Kong, 2000). The choice of cuts must eventually lead to the same overall contribution to the integral which is thoroughly discussed by Baños (1966).

4.4.3 Branch-point contribution

The branch-point contribution to the asymptotic expansions of the integrals in equation 4.29 can be found by using equation 4.10. However, when h is much smaller than ρ, a method suggested by Baños (1966) simplifies the calculation of higher-order terms. The substitution

$$\lambda = k_a \cos\alpha, \tag{4.38}$$

transforms the branch cut through k_a into a steepest descent path through k_a. The integrals to evaluate can be written on the same form as in equation 4.1 with α as the integration variable. The function $\phi(\alpha)$ and its derivatives are then

$$\phi(\alpha) = ik_a\rho\cos\alpha, \quad \phi'(\alpha) = -ik_a\rho\sin\alpha, \quad \text{and} \quad \phi''(\alpha) = -ik_a\rho\cos\alpha. \tag{4.39}$$

The part of the exponential function that contains the vertical propagation distance h is contained in the function $f(\alpha)$, and the large parameter (the horizontal distance ρ) has been kept within $\phi(\alpha)$ for simplicity. The saddle point is found at $\alpha_s = 0$. Another transformation

$$\tau^2 = \phi(\alpha_s) - \phi(\alpha), \tag{4.40}$$

now implies that the integration kernel can be expressed as a series expansion in terms of the small parameter τ. Baños (1966) uses this method with success, but he uses integrals that come from a description of the fields in terms of potentials and a double saddle-point method required by using integral expressions for the Hankel functions. In this work, asymptotic expressions for the Hankel functions are used (equation 4.D-30) which means that double integrals are avoided.

The calculations of the branch-point contribution to the integrals in equation 4.29 are shown in Appendix 4.F. For the TE integrals, equations 4.F-45 and 4.F-46 give:

$$\mathcal{I}^{TE}_{A0,b} \sim -\frac{2\mathrm{e}^{ik_a\rho+ikh\sqrt{1-n^2}}}{\sigma\rho^2(1-n^2)}\left[ink+\tfrac{1}{\rho}\left(-1+\tfrac{3}{2}ikh\tfrac{n^2}{\sqrt{1-n^2}}\right)+..\right], \tag{4.41a}$$

$$\mathcal{I}^{TE}_{A1,b} \sim -\frac{2\mathrm{e}^{ik_a\rho+ikh\sqrt{1-n^2}}}{\sigma\rho^2(1-n^2)}\left[1+\tfrac{3nh}{2\rho\sqrt{1-n^2}}+..\right]. \tag{4.41b}$$

In the TM case the expressions in equation 4.F-53 and 4.F-54 give:

$$\mathcal{I}^{TM}_{A0,b} \sim -\frac{2\omega\mu}{k_a\rho^2}\mathrm{e}^{ik_a\rho+ikh\sqrt{1-n^2}}\left[1-\tfrac{1}{ik_a\rho}\left(1-\tfrac{3n^2}{1-n^2}-\tfrac{3(1+n^2)}{n^2}-\tfrac{3}{2}ikh\tfrac{n^2}{\sqrt{1-n^2}}\right)+..\right], \tag{4.42a}$$

$$\mathcal{I}^{TM}_{A1,b} \sim -\frac{2\omega\mu}{ik_a^2\rho^2}\mathrm{e}^{ik_a\rho+ikh\sqrt{1-n^2}}\left[1+\tfrac{1}{ik_a\rho}\left(\tfrac{3n^2}{1-n^2}+\tfrac{3(1+n^2)}{n^2}+\tfrac{3}{2}ikh\tfrac{n^2}{\sqrt{1-n^2}}\right)+..\right]. \tag{4.42b}$$

With a choice of branch cuts as in Figure 4.4, the residue due to the pole in equation 4.33 is not to be included in the asymptotic expansion of the integral. However, as can be observed from equation 4.42, the TM-mode expressions are useless when n is small. This is due to the presence of the pole in close vicinity to the branch point for small n. Thus, the effect of the pole must be subtracted from the integrands and considered separately. The branch-point contribution due to the pole is denoted $\mathcal{I}^{TM}_{bp}$. The series expansion of this expression can be termwise subtracted from the appropriate expression in equation 4.42 in order to obtain the contribution $\mathcal{I}^{TM}_{bc}$ where the presence of the pole has been removed. The total branch-point contribution is thus written as:

$$\mathcal{I}^{TM}_{b} = \mathcal{I}^{TM}_{bc} + \mathcal{I}^{TM}_{bp}. \tag{4.43}$$

The branch-point pole contribution is given by equation 4.16c:

$$\mathcal{I}^{TM}_{A,bp} = -2\pi i\,\Gamma\,\mathrm{e}^{ik_a\rho}\left[1-\mathrm{erf}\,(i\tau_p)\right]\,\mathrm{e}^{-\tau_p^2}, \tag{4.44}$$

where the locations of the pair of poles in the τ-domain are derived from equations 4.40, 4.39, 4.38, and 4.33:

$$\tau_p^2 = ik_a\rho(1-1/\sqrt{1+n^2}). \tag{4.45}$$

The negative sign must be chosen when taking the square root of this expression according to the selected integration path in Figure 4.4 and the transformations in equations 4.38 and 4.40. The choice of signs in equation 4.44 follows from the same reasoning. The residues,

Γ_0 for the zeroth- and Γ_1 for the first-order integral, are found by using the procedure in equation 4.15. The calculations shown in Appendix 4.F, cf. equation 4.F-55, give:

$$\Gamma_0 = \frac{\omega\mu k n^4}{2(1-n^4)(1+n^2)^{3/2}}\ H_0^-\left(\tfrac{k_a\rho}{\sqrt{1+n^2}}\right)\ \mathrm{e}^{ikh\left(1+n^2\right)^{-1/2}}, \tag{4.46a}$$

$$\Gamma_1 = \frac{\omega\mu n^3}{2(1-n^4)(1+n^2)}\ H_1^-\left(\tfrac{k_a\rho}{\sqrt{1+n^2}}\right)\ \mathrm{e}^{ikh\left(1+n^2\right)^{-1/2}}. \tag{4.46b}$$

The first term in the contribution from equation 4.44 can be referred to as a surface wave (cf. Baños, 1966). The surface wave can be of importance for certain medium configurations and offsets. However, in the present analysis, the surface-wave term is of minor significance.

The expressions where the effect of the pole has been removed are derived in Appendix 4.F, and the results in equations 4.F-62 and 4.F-65 can be written as:

$$\mathcal{I}^{TM}_{A0,bc} \sim \frac{i\omega\mu}{\rho}\mathrm{e}^{ik_a\rho+ikh\left(1+n^2\right)^{-1/2}}\left(u_1+\tfrac{1}{ik\rho}u_2+..\right), \tag{4.47a}$$

$$\mathcal{I}^{TM}_{A1,bc} \sim \frac{\omega\mu}{k\rho}\mathrm{e}^{ik_a\rho+ikh\left(1+n^2\right)^{-1/2}}\left(v_1+\tfrac{1}{ik\rho}v_2+..\right), \tag{4.47b}$$

$$u_1 = 2n^2\left[1-\tfrac{7}{8}n^2+\tfrac{235}{128}n^4-..\right], \quad u_2 = n^3\left[\left(\tfrac{137}{64}+ikh\right)-\left(\tfrac{35}{256}+\tfrac{1}{2}ikh\right)n^2+..\right], \tag{4.48a}$$

$$v_1 = 2n\left[1-\tfrac{3}{8}n^2+\tfrac{163}{128}n^4-..\right], \quad v_2 = n^2\left[\left(\tfrac{113}{64}+ikh\right)+\left(\tfrac{25}{256}-\tfrac{1}{2}ikh\right)n^2+..\right]. \tag{4.48b}$$

In an asymptotic series, the first few terms normally converge. The series starts to diverge for higher-order terms. The series should be broken off just before the smallest term. This term can then be used as an error estimate for the expansion (Bender and Orszag, 1999). In the expansions in equations 4.41 and 4.47, it has been found sufficient to consider the first two terms. The third term can then be used as an error estimate.

4.4.4 Saddle-point contribution

Even if the branch-point contribution dominates for both the seabed and sea-surface interface, the saddle-point contribution is of some importance at the shorter horizontal separation distances. It will become evident in the next section that it is least laborious to obtain the contribution from the saddle point in the angular-spectrum domain. The calculations are presented in Appendix 4.G, the final relations can be found in equation 4.G-71, and they are

$$\mathcal{I}^{TE}_{A0,s} \sim -i\omega\mu\frac{\mathrm{e}^{ikr}}{r}R^{TE}_{si}(\theta_s)\left[1+\frac{1}{ikr}\Psi^{TE}_0(\theta_s)+..\right], \tag{4.49a}$$

$$\mathcal{I}^{TE}_{A1,s} \sim -i\omega\mu\frac{\mathrm{e}^{ikr}}{r}R^{TE}_{si}(\theta_s)\frac{1}{ik\sin\theta_s}\left[1+\frac{1}{ikr}\Psi^{TE}_1(\theta_s)+..\right], \tag{4.49b}$$

$$\mathcal{I}^{TM}_{A0,s} \sim -i\omega\mu\frac{\mathrm{e}^{ikr}}{r}R^{TM}_{si}(\theta_s)\cos^2\theta_s\left[1+\frac{1}{ikr}\Psi^{TM}_0(\theta_s)+..\right], \tag{4.49c}$$

$$\mathcal{I}^{TM}_{A1,s} \sim -i\omega\mu\frac{\mathrm{e}^{ikr}}{r}R^{TM}_{si}(\theta_s)\frac{\cos^2\theta_s}{ik\sin\theta_s}\left[1+\frac{1}{ikr}\Psi^{TM}_1(\theta_s)+..\right], \tag{4.49d}$$

where $\theta_s = \sin^{-1}(\rho/r)$ and the reflection coefficients are given by equation 4.G-73. The second-order terms represented by the Ψ-variables are given by equations 4.G-72 and 4.G-74 for the TM mode and equation 4.G-75 for the TE mode. The first term in the expressions in equation 4.49 is the well-known geometrical optics contribution. The next term gives the first correction to the raypath contribution.

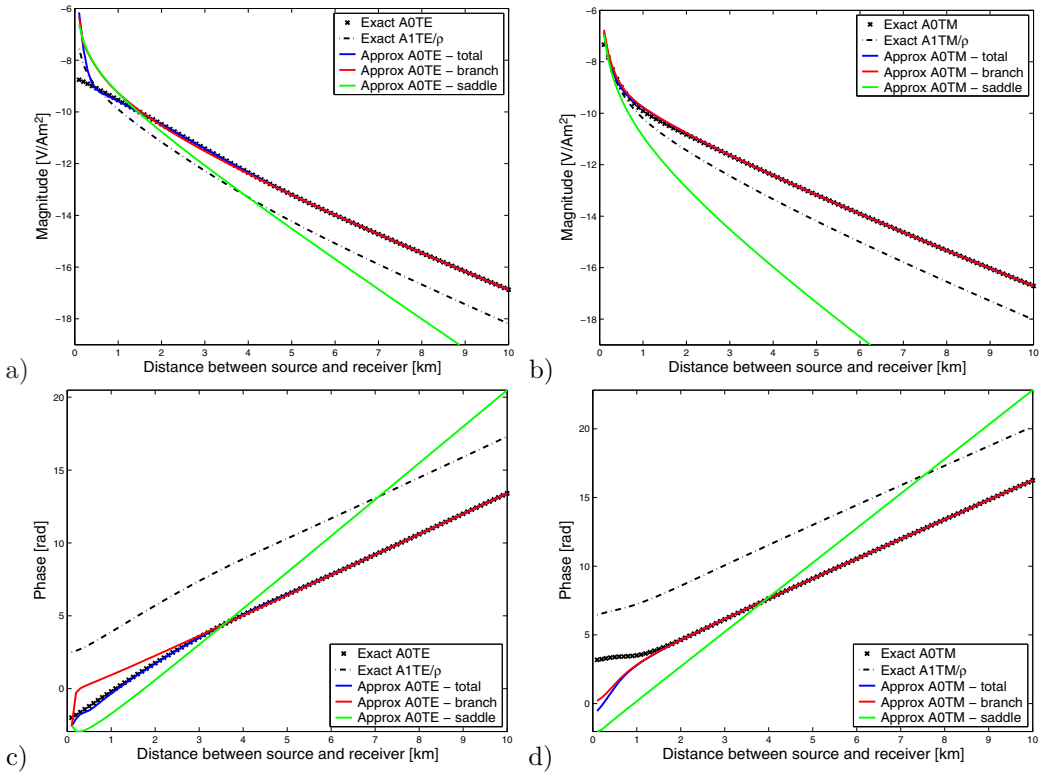

Figure 4.5: Plots of the asymptotic expressions with corresponding exact numerical evaluation of the integrals for the single-interface seabed case. Figures a and c show the TE magnitudes and phases, respectively. In the same manner the TM mode is presented in Figures b and d. The receiver is situated on the seabed whereas the source is elevated by 30 m. The source frequency is 0.5 Hz, the conductivity in seawater $\sigma = 3.2$ S/m, and the conductivity in the overburden $\sigma_1 = 1.0$ S/m. The notation "A0TE" refers to the $\mathcal{I}_{A0}^{TE}$-integral, "A1TM" refers to the $\mathcal{I}_{A1}^{TM}$-integral, and so on.

4.4.5 The seabed interface

Consider Figure 4.5 where the asymptotic expressions for the TE mode (equation 4.41) and TM mode (equations 4.44 and 4.47) are compared to exact numerical evaluations of the field

integrals. In the seabed case, $k_a = k_1$, $n = k_1/k$, and $h = h_s + h_r$. The receivers are situated on the seabed and the source is elevated by 30 m. The source frequency is 0.5 Hz and the conductivity is $\sigma = 3.2$ S/m in seawater and $\sigma_1 = 1.0$ S/m in the sediments. In the plots the exact numerical calculations of the zeroth-order integrals are shown with the thick "sawtooth" black line, and the first-order integrals with the dash-dot black line. The contributions from the asymptotic branch-point expansions are plotted with the red curves, the saddle-point contributions with the green curves, and the combination of the contributions with the blue curves. It can be observed that the branch point accounts for the response almost entirely. The saddle-point contribution improves the match for distances up to 3-4 km in the TE case. In the TM case, the saddle-point contribution is insignificant compared to the branch-point contribution. The dominance of the lateral-wave contribution can be explained using Figure 4.2: The rays that travel down to the seabed, into the sediments, and then along the interface within the sediments are damped less than the reflected rays in seawater.

4.4.6 The sea-surface interface

When the interface under consideration is the sea-surface, $k_a = k_0$, $n = k_0/k$, and $h = d_s + d_r$ in the branch-point expressions in equations 4.41, 4.44, and 4.47. Since $|k| >> k_0$ which implies that $n \approx 0$, the expressions for the TE mode can be simplified into

$$\mathcal{I}^{TE}_{A0} \sim \frac{2\mathrm{e}^{ikh}}{\sigma\rho^3} \quad \text{and} \quad \mathcal{I}^{TE}_{A1} \sim -\frac{2\mathrm{e}^{ikh}}{\sigma\rho^2}, \tag{4.50}$$

where the propagation factor in air can be neglected because k_0 is small. Equations 4.44 and 4.47 show that the main branch-point contribution for the TM mode is proportional to n^2 for the zeroth-order integral and n for the first-order integral. Thus, the sea-surface response from the TM mode becomes negligible compared to the TE-mode response. When the expressions in equation 4.50 are inserted into equation 4.18, the well-known expressions for the electric field from a submerged dipole close to a sea-surface are obtained [compare with e.g., Wait (1961), Baños (1966), and Bannister (1984)]. Here, I have shown that these expressions are TE-polarized field components.

A comparison to numerical modelling for the asymptotic expressions in the sea-surface case has been performed in Figure 4.6. The source frequency is 0.5 Hz, and the depth below the interface is 50 m (100 m) for the source (receiver). The approximate expressions for the TE mode fit the curves from the modelling program well, and the branch-point contribution accounts almost entirely for the response. The addition of the saddle-point contribution gives a slight improvement for small distances. The contributions to the field components from the zeroth- and first-order integrals are equal in magnitude (except at small distances) as is evident from equations 4.18 and 4.50. For the TM response, which is much weaker than the TE response, the comparisons in Figure 4.6 are made for the first-order integral

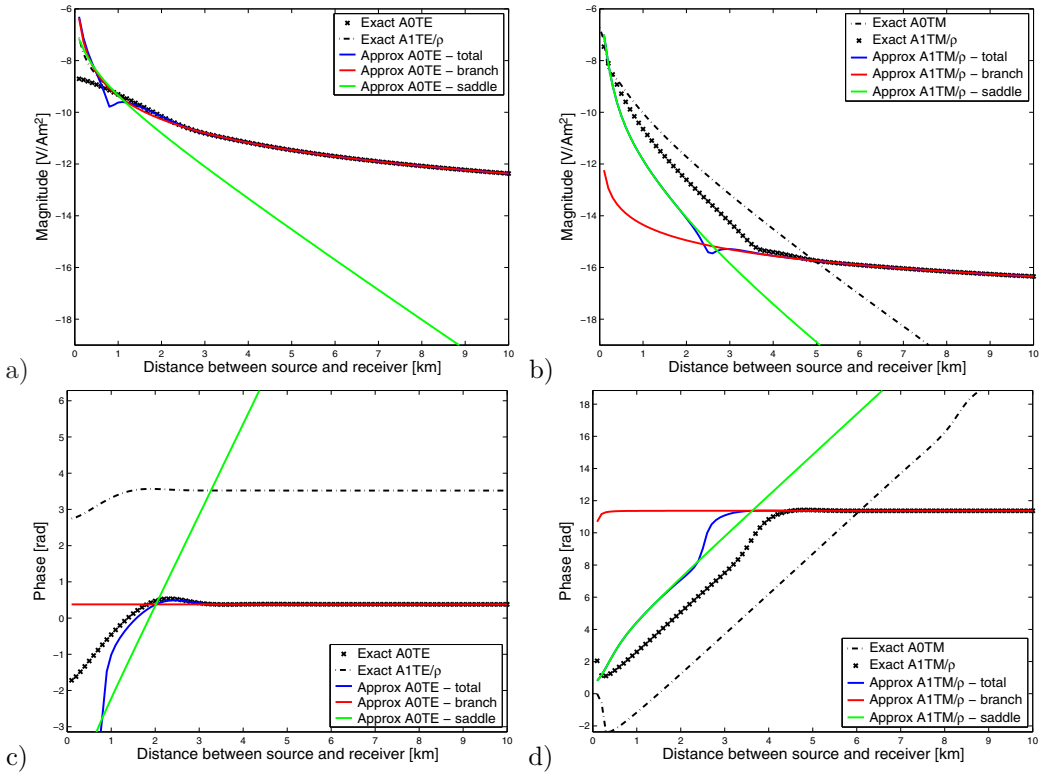

Figure 4.6: Plots of the asymptotic expressions and the exact values from numerical modelling in case of an interface between sea and air. The depth below the interface is 50 m for the source and 100 m for the receiver. The subfigures show the TE- and TM-mode responses in the same way as in Figure 4.5.

since the zeroth-order integral is smaller in magnitude (see equations 4.47 and 4.48). The TM-mode branch-point contribution explains the curves well at large distances. In order to improve the asymptotic expansion of the TM-mode integral for short offsets, more terms in the saddle-point evaluation could be considered, but since the response is small, this is not pursued further here.

4.5 Thin resistive layer

In this section, asymptotic expansions of the field integrals in equation 4.29 for a stratified model that consists of a thin resistive layer within a conductive background medium are derived. The resulting explicit spatial expressions are for the TM mode a sum of a residue contribution and a saddle-point contribution. For the TE mode, the contribution is accounted

for by the ray reflection due to the saddle point. The model in Figure 4.1 without the seawater layer and the air halfspace describes a thin layer with thickness d_2 within a conductive background medium. Assume that the antennas are situated in the background medium (wavenumber k_1). In order to perform the asymptotic evaluation of the field integrals, the reflection response from the thin layer is needed. It will be shown that the response contains poles for both the TE and TM mode, but that only the TM pole has an explicit contribution to the expansion. However, for certain values of the expansion parameter, both the TE- and TM-mode poles will affect the saddle-point contributions. To determine how the poles and saddle point contribute to the asymptotic expansions, it is found convenient to perform the integration in the angular-spectrum domain. The residues are however calculated in terms of the horizontal wavenumber variable.

4.5.1 Reflection response

The reflection response R_y from a layer is derived from equation 4.23. When assuming that the medium below the layer is different from the medium above the layer, one gets

$$R_y = \frac{r_{12} + r_{23}\mathrm{e}^{2i\gamma_2 d_2}}{1 + r_{12}r_{23}\mathrm{e}^{2i\gamma_2 d_2}}, \tag{4.51}$$

where r_{12} and r_{23} are the reflection coefficients for the upper and lower interfaces, respectively. The distance between the two interfaces is expressed by d_2, and γ_2 is the vertical wavenumber within the layer. By writing the reflection coefficient from one interface in terms of impedances

$$r_{jk} = \frac{\eta_k - \eta_j}{\eta_k + \eta_j} \quad \text{where} \quad k = j + 1 \quad \text{and} \quad j = 1, 2, 3.., \tag{4.52}$$

the following expression is obtained:

$$R_y = \frac{\left(\eta_2^2 - \eta_1\eta_3\right) + \eta_2\left(\eta_3 - \eta_1\right) i\cot\left(\gamma_2 d_2\right)}{\left(\eta_2^2 + \eta_1\eta_3\right) + \eta_2\left(\eta_3 + \eta_1\right) i\cot\left(\gamma_2 d_2\right)}. \tag{4.53}$$

The series expansion of the cotangent function in equation 4.A-7 can be used in order to obtain the reflection response R_{tl} for a thin layer since $|\gamma_2|d_2 << 1$ in this case. In fact, keeping only the first term will be sufficient. The expression in equation 4.53 is further simplified by assuming that the impedance in medium 3 is the same as in medium 1 ($\eta_3 = \eta_1$):

$$R_{tl} = \frac{\left(\eta_2^2 - \eta_1^2\right)\gamma_2 d_2}{2i\eta_1\eta_2 + \left(\eta_1^2 + \eta_2^2\right)\gamma_2 d_2}. \tag{4.54}$$

When inserting for the appropriate impedances (compare equation 4.52 to 4.24), this leads to the following reflection responses for the TE and TM mode:

$$R_{tl}^{TE}(\lambda) = \frac{k_1^2\left(1-n_1^2\right)d_2}{2i\gamma_1 + \left[k_1^2\left(1+n_1^2\right) - 2\lambda^2\right]d_2}, \tag{4.55a}$$

$$R_{tl}^{TM}(\lambda) = \frac{\left[n_1^2k_1^2\left(1-n_1^2\right) - \lambda^2\left(1-n_1^4\right)\right]d_2}{2in_1^2\gamma_1 + \left[n_1^2k_1^2\left(1+n_1^2\right) - \lambda^2\left(1+n_1^4\right)\right]d_2}, \tag{4.55b}$$

where $n_1 = k_2/k_1$.

4.5.2 Angular-spectrum representation

The evaluation of the integrals in equation 4.29 for the thin-layer case simplifies if the integration variable is transformed from the complex horizontal wavenumber domain into the angular-spectrum domain. Let θ represent the complex angle between a "ray" with wavenumber k_1 and the z-axis. Then

$$\lambda = k_1\sin\theta \quad \text{and} \quad \gamma = k_1\cos\theta, \quad \text{where} \quad \theta = \theta_r + i\theta_i. \tag{4.56}$$

The function in the exponent of the integrand in equation 4.29 can now be written as

$$\phi(\lambda) = i\lambda\frac{\rho}{r} + i\gamma_1\frac{h}{r} = ik_1\cos\left(\theta-\theta_s\right), \tag{4.57}$$

where θ_s is the saddle point, $h = r\cos\theta_s$, and $\rho = r\sin\theta_s$. The large parameter is given by the propagation distance between the source, upper interface, and receiver: $r = \sqrt{\rho^2+h^2}$. The real and imaginary parts of the horizontal wavenumber in terms of θ are obtained from equation 4.56 by writing $k_1 = \mathrm{Re}(k_1) + i\,\mathrm{Im}(k_1)$ and using the relation from equation 4.A-6a in Appendix 4.A:

$$\lambda_r = \mathrm{Re}(k_1)\sin\theta_r\cosh\theta_i - \mathrm{Im}(k_1)\cos\theta_r\sinh\theta_i, \tag{4.58a}$$

$$\lambda_i = \mathrm{Im}(k_1)\sin\theta_r\cosh\theta_i + \mathrm{Re}(k_1)\cos\theta_r\sinh\theta_i. \tag{4.58b}$$

The original integration path is found by requiring that $\lambda_i = 0$. In the conductive source medium, $\mathrm{Re}(k_1) = \mathrm{Im}(k_1)$ which follows from equation 4.27. Thus, the original path goes as

$$\theta_i = \tfrac{1}{2}\ln\frac{\cos\left(\theta_r+\frac{\pi}{4}\right)}{\cos\left(\theta_r-\frac{\pi}{4}\right)}. \tag{4.59}$$

Note that when the source medium is lossless, one obtains the well-known path in the complex θ-plane that goes from $-\pi/2 + i\infty$ down to $-\pi/2$, then along the θ_r-axis to $\pi/2$, and finally from $\pi/2$ to $\pi/2 - i\infty$ (Ott, 1942).

The steepest descent path is found where the imaginary part of ϕ is constant. Since the path passes through the saddle point:

$$\mathrm{Im}[ik_1\cos\left(\theta-\theta_s\right)] = \mathrm{Re}(k_1). \tag{4.60}$$

By using the relations from equation 4.A-6 in Appendix 4.A, this gives:

$$\theta_i = \ln \frac{\sin\left[\frac{\pi}{8} - \frac{1}{2}(\theta_r - \theta_s)\right]}{\sin\left[\frac{\pi}{8} + \frac{1}{2}(\theta_r - \theta_s)\right]}. \tag{4.61}$$

The original path and steepest descent path are sketched in Figure 4.7. Note that the inclination of the SDP through the saddle point is negative. There are no branch cuts in Figure 4.7, and it can be seen from equation 4.55 that there are no branch points related to the thin layer. This is as expected since branch points and lateral waves are affiliated with halfspaces at the ends of a layered stack. The branch point for the source medium in the wavenumber domain is removed with the mapping into the angular-spectrum domain in equation 4.56. Thus, the contributions to the field integrals in the thin-layer case come from the saddle point and possibly the poles in the reflection coefficients.

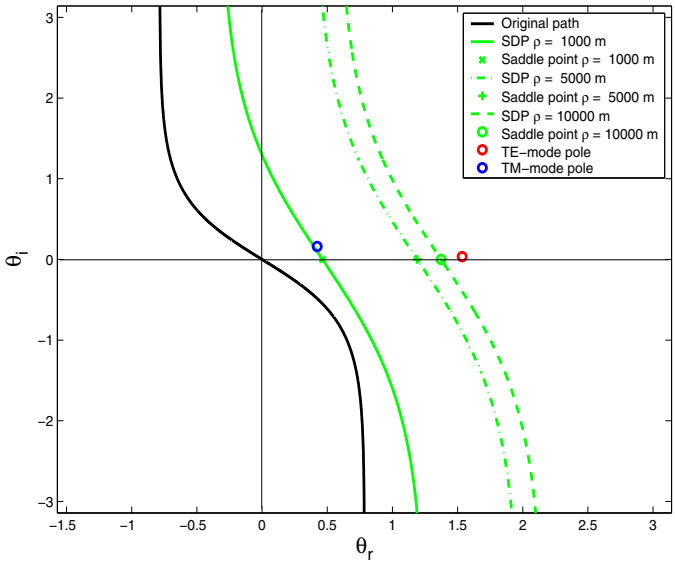

Figure 4.7: Angular-spectrum domain for a scenario where a thin resistive layer is contained within a conductive background medium. The plot shows the original path, steepest descent path (SDP), TM pole (blue), and TE pole (red). The SDP is plotted for three distinct horizontal separation distances ρ. The conductivity in the background medium is $\sigma_1 = 1.0$ S/m and in the resistive layer $\sigma_2 = 0.01$ S/m. The thickness of the thin layer is 50 m. The source frequency is 0.5 Hz and the source and receiver height above the thin layer is $h_s = h_r = 1000$ m. The SDP crosses the TM pole at $\rho \approx 1000$ m. As $\rho \to \infty$ the SDP moves towards the TE pole, but this pole is not crossed.

4.5.3 Location of the poles

The reflection response from equation 4.55 in terms of the angle variable θ is:

$$R_{tl}^{TE}(\theta) = \frac{\left(1-n_1^2\right) k_1 d_2}{2i\cos\theta + \left[\left(1+n_1^2\right) - 2\sin^2\theta\right] k_1 d_2}, \tag{4.62a}$$

$$R_{tl}^{TM}(\theta) = \frac{\left[n_1^2\left(1-n_1^2\right) - \sin^2\theta\left(1-n_1^4\right)\right] k_1 d_2}{2in_1^2\cos\theta + \left[n_1^2\left(1+n_1^2\right) - \left(1+n_1^4\right)\sin^2\theta\right] k_1 d_2}. \tag{4.62b}$$

The poles are found at the values of θ which make the denominator of the expressions in equation 4.62 zero:

$$\cos\theta_p^{TE} = \pm\sqrt{\frac{1}{2}\left(1-n_1^2\right) + \left(\frac{i}{2k_1 d_2}\right)^2} - \frac{i}{2k_1 d_2}, \tag{4.63a}$$

$$\cos\theta_p^{TM} = \pm\sqrt{\frac{1-n_1^2}{1+n_1^4} + \left(\frac{in_1^2}{1+n_1^4}\frac{1}{k_1 d_2}\right)^2} - \frac{in_1^2}{1+n_1^4}\frac{1}{k_1 d_2}. \tag{4.63b}$$

In the wavenumber domain, the poles are given by the relations:

$$\lambda_p^{TE} = k_1\sin\theta_p^{TE} \quad \text{and} \quad \lambda_p^{TM} = k_1\sin\theta_p^{TM}. \tag{4.64}$$

Note that $n_1 = k_2/k_1$ is small since $\sigma_1 >> \sigma_2$. The locations of the poles, when the positive signs in front of the square roots in equation 4.63 are used, are plotted in the angular-spectrum domain in Figure 4.7. The TM pole is passed when deforming the integration path. This happens when the horizontal distance ρ gets larger than the depth of the thin layer, and implies that the contribution from the TM pole must be taken into account in the evaluation of the field integrals. The TE pole is not crossed, but it can be expected to influence the saddle-point contribution for large horizontal distances.

4.5.4 Contribution from the TM pole

Consider the $\mathcal{I}_{A0}^{TM}$-integral in equation 4.29c with reflection response given by equation 4.55b. The response function contains a simple pole, and the contribution from this TM pole can be obtained by using equation 4.11. The derivative of the denominator in equation 4.55b is

$$\frac{df_D^{TM}}{d\lambda} = -2\lambda\gamma_1^{-1}\left[\left(1+n_1^4\right)\gamma_1 d_2 + in_1^2\right], \tag{4.65}$$

and the residue is obtained using equation 4.12 when the nominator of the reflection-response function and the rest of the integrand in equation 4.29c except for the exponential factor, are accounted for:

$$\Gamma_{0,tl}^{TM} = \frac{\omega\mu}{4k_1^2} H_0^-\left(\lambda_p\rho\right) \frac{\left(k_1^2-\lambda_p^2\right)\left[\lambda_p^2(1-n_1^4) - n_1^2k_1^2(1-n_1^2)\right] d_2}{\left(1+n_1^4\right) d_2\sqrt{k_1^2-\lambda_p^2} + in_1^2}. \tag{4.66}$$

It is implicit in this expression that λ_p is the TM pole (i.e., λ_p^{TM} from equation 4.64). The residue for the first-order integral is obtained from equation 4.66 by a division with the factor λ_p and a replacement of the zeroth-order Hankel function by the first-order function.

The pole contribution is obtained by inserting the residue and the propagation factor [with $\phi(\lambda_p)$ from equation 4.57] into the expression in equation 4.11:

$$\mathcal{I}_{A0,p}^{TM} = \frac{\pi}{2\sigma_1} H_0^-(\lambda_p\rho)\, \frac{\left(k_1^2-\lambda_p^2\right)\left[\lambda_p^2(1-n_1^4)-n_1^2k_1^2(1-n_1^2)\right] d_2}{\left(1+n_1^4\right) d_2\sqrt{k_1^2-\lambda_p^2}+in_1^2}\, \mathrm{e}^{i\lambda_p\rho+i\sqrt{k_1^2-\lambda_p^2}h}, \quad (4.67a)$$

$$\mathcal{I}_{A1,p}^{TM} = \frac{\pi}{2\sigma_1} H_1^-(\lambda_p\rho)\, \frac{\left(k_1^2-\lambda_p^2\right)\left[\lambda_p^2(1-n_1^4)-n_1^2k_1^2(1-n_1^2)\right] d_2}{\lambda_p\left[\left(1+n_1^4\right) d_2\sqrt{k_1^2-\lambda_p^2}+in_1^2\right]}\, \mathrm{e}^{i\lambda_p\rho+i\sqrt{k_1^2-\lambda_p^2}h}. \quad (4.67b)$$

4.5.5 Saddle-point contributions

The calculation of the saddle-point contributions is presented in Appendix 4.G. The expressions are on the same form as in equation 4.49, but now the wavenumber is k_1 rather than k, and the reflection response functions are as in equation 4.62. This means that the expressions in equations 4.G-76 and 4.G-77 must be inserted into the second-order terms Ψ_0^{TE}, Ψ_1^{TE}, Ψ_0^{TM}, and Ψ_1^{TM} in equation 4.G-72.

From Figure 4.7 it can be observed that the presence of the TE pole may affect the saddle-point contribution. The effect is stronger for large distances since the SDP moves closer to the pole with increasing horizontal separation between the source and receiver. Thus, the residue due to the TE pole also needs to be calculated. The derivative of the denominator in the reflection-response function in equation 4.55a is

$$\frac{df_D^{TE}}{d\lambda} = -2\lambda\gamma_1^{-1}\left[i+2\gamma_1 d_2\right]. \quad (4.68)$$

The residue for the integral in equation 4.29a is then found using equation 4.12:

$$\Gamma_{0,tl}^{TE} = -\frac{\omega\mu}{4} H_0^-(\lambda_p\rho)\frac{k_1^2 d_2(1-n_1^2)}{i+2d_2\sqrt{k_1^2-\lambda_p^2}}, \quad (4.69)$$

where it is implicit that the TE pole (λ_p^{TE} from equation 4.64) must be used. For the first-order integral, the residue is obtained by a division of the factor λ_p and the replacement of the zeroth-order by the first-order Hankel function. The contribution from the TE pole (if it were to be crossed during the deformation of the path) would be:

$$\mathcal{I}_{A0,p}^{TE} = -\frac{\pi}{2}\, i\omega\mu\, H_0^-(\lambda_p\rho)\, \frac{k_1^2 d_2(1-n_1^2)}{i+2d_2\sqrt{k_1^2-\lambda_p^2}}\, \mathrm{e}^{i\lambda_p\rho+i\sqrt{k_1^2-\lambda_p^2}h}, \quad (4.70a)$$

$$\mathcal{I}_{A1,p}^{TE} = -\frac{\pi}{2}\, i\omega\mu\, H_1^-(\lambda_p\rho)\, \frac{k_1^2 d_2(1-n_1^2)}{\lambda_p\left(i+2d_2\sqrt{k_1^2-\lambda_p^2}\right)}\, \mathrm{e}^{i\lambda_p\rho+i\sqrt{k_1^2-\lambda_p^2}h}. \quad (4.70b)$$

The TM pole also has an effect on the saddle-point calculation in addition to its explicit contribution. Thus, the method in section 4.2.4 is applied to account for the presence of the pole in both the TE and TM case. Now, let $\mathcal{I}_{A,p}$ represent the pole contributions in equations 4.67 and 4.70. As seen from equation 4.11 and 4.16c, the pole effect $\mathcal{I}_{A,sp}$ on the saddle-point contribution is obtained by a multiplication with the error function complement:

$$\mathcal{I}_{A,sp} = \pm\frac{1}{2}\,\mathcal{I}_{A,p}\,\left[1 - \operatorname{erf}\left(\mp iu_p\sqrt{r}\right)\right], \tag{4.71}$$

where the "distance" from the pole to the saddle point is given by equation 4.14:

$$u_p = \left[ik_1 - i\left(\lambda_p \sin\theta_s + \sqrt{k_1^2 - \lambda_p^2}\,\cos\theta_s\right)\right]^{1/2}. \tag{4.72}$$

The division by the factor 2 in equation 4.71 is required because of the presence of a single pole rather than a pair of poles (cf. equation 4.16c). Equation 4.71 can be interpreted as the SDP picking up the effect of the pole presence by encircling half the residue. If the deformation of the integration path implies that the pole is crossed, the minus sign in front of equation 4.71 must be selected since the SDP picks up the residue contribution clockwise. In addition, since $\mathrm{Im}(u_p) < 0$ in this case, the sign of the argument in the error function must be positive. If the pole location is not picked up by the deformation, $\mathcal{I}_{A,sp}$ takes the plus sign since the pole is encountered in the counterclockwise direction. In this case $\mathrm{Im}(u_p) > 0$, and the sign of the argument in the error function must be negative.

The removed pole presence $\mathcal{I}_{A,sc}$ in the saddle-point contribution is found by subtracting the pole contribution $\mathcal{I}_{A,sp}$ from the original saddle-point contribution $\mathcal{I}_{A,s}$. When using the expansion in equation 4.17, this gives:

$$\mathcal{I}_{A,sc} \sim \mathcal{I}_{A,s} + \sqrt{\frac{\pi}{r}}\frac{\Gamma_{tl}}{u_p}\left(1 + \frac{1}{2ru_p^2} + ..\right)\,\mathrm{e}^{ik_1 r}, \tag{4.73}$$

where the expressions for Γ_{tl} for the zeroth-order TE and TM integrals are found in equation 4.66 and 4.69, respectively. The first-order integrals are obtained by a division of λ_p and by using the first-order instead of the zeroth-order Hankel function.

4.5.6 Discussion

For the thin-layer response, the results of the asymptotic evaluation of the integrals are compared to exact numerical calculations in Figure 4.8. The comparisons are presented for the zeroth-order integrals whereas the exact first-order integrals are shown as a reference. The source frequency is 0.5 Hz, the conductivity in the background medium is $\sigma_1 = 1.0$ S/m, and the source and receiver are 1 km above the thin layer. The thickness of the thin layer is $d_2 = 50$ m and the conductivity is $\sigma_2 = 0.01$ S/m. The green curve shows the saddle-point contribution and the yellow curve shows the pole contribution (only the TM mode). The

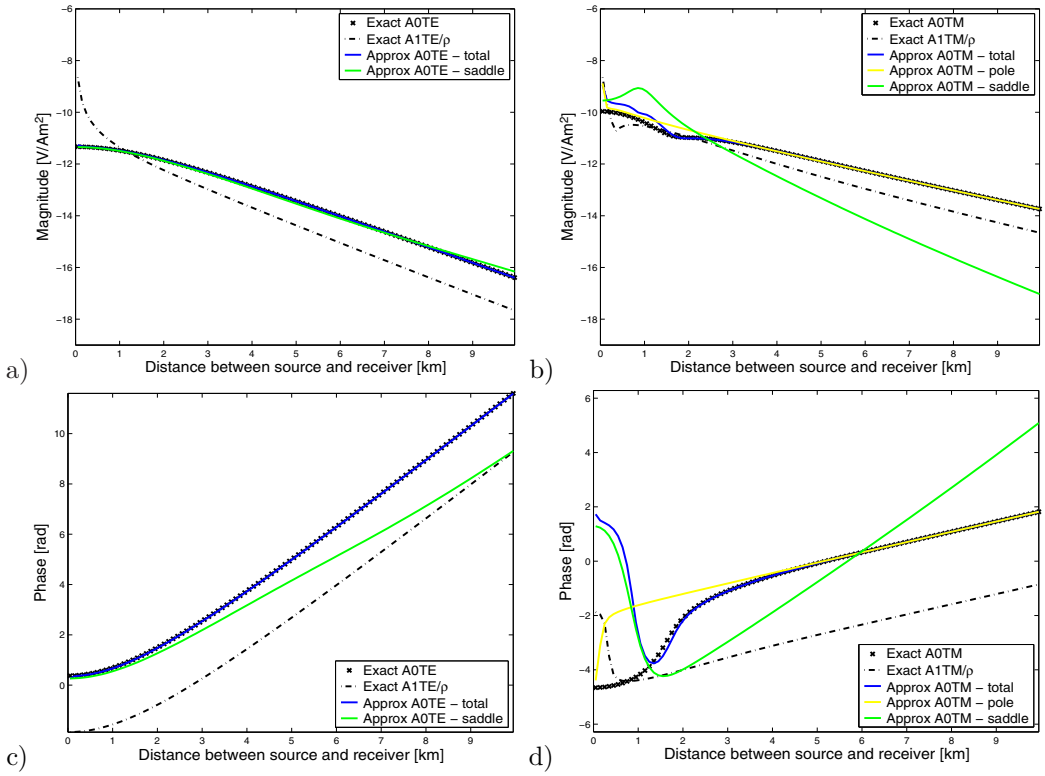

Figure 4.8: Comparison of asymptotic expressions and numerical modelling in case of a thin resistive layer contained in a more conductive background medium. The TE-mode plots are shown on the left hand side, and the TM-mode plots to the right. The model parameters are the same as in Figure 4.7.

TE plot is made better for large distances (from 2-3 km) by accounting for the pole influence on the saddle point (blue curve based on expressions in equations 4.71 and 4.73). In the same manner the TM plot is improved at short distances (up to 3 km) by accounting for the pole in the saddle-point calculations (blue curve includes the saddle-point contributions from equations 4.71 and 4.73 *and* the pole contribution). For the TM response, it can be seen that the saddle-point calculations could be improved some more at short distances. This would involve taking more terms into account. However, the important points to make about the thin-layer response are already evident in the plots: The TE response can be pictured as a ray reflection as sketched in Figure 4.1 (path IV) whereas the TM response is a guided mode due to the pole contribution in equation 4.67a (path V in Figure 4.1).

4.6 Combined models

Having obtained asymptotic expressions for the simple seabed, sea-surface, and thin-layer case, the resulting asymptotic expansions for different combinations of these cases can be studied. First, a model which consists of a thin layer and a seabed interface is investigated. Next, a model with a seabed and sea-surface interface is considered (water column). Finally the complete model including the thin layer, seabed, and sea-surface is discussed. In all the cases the vertical distances are kept constant, e.g., the distance from the source to the thin layer is the same for both the simple thin-layer case and the full model. In Figure 4.1 the source depth is 70 m, the thickness of the water column is 100 m, the receiver is situated on the seabed, the thickness of the overburden is 1000 m, and the thin resistive layer has a thickness of 50 m. As in the simple cases, the source frequency is 0.5 Hz, and the conductivities are: $\sigma = 3.2$ S/m for the seawater, $\sigma_1 = 1.0$ S/m for the overburden, and $\sigma_2 = 0.01$ S/m for the resistor.

In Figures 4.9, 4.10, and 4.11, only the $\mathcal{I}_{A0}$-integrals are plotted since they always dominate the $\mathcal{I}_{A1}$-integrals (except for the sea-surface case). Moreover, the $\mathcal{I}_{A1}$-integrals repeat the same trends as can be found in the $\mathcal{I}_{A0}$-integrals since they normally compare to the second term in the expansion of the $\mathcal{I}_{A0}$-integrals. The direct field contributions from equation 4.30 are shown in the seawater-layer case for reference.

4.6.1 Seabed interface and thin layer

When the seabed interface is introduced into the thin-layer model, the reflection responses in equation 4.55 change, and the expressions for the pole locations in equation 4.63 are modified accordingly. However, since the thickness d_1 of the overburden is fairly large (so that it can be assumed to suppress the effects of multiples), one can approximate the reflection response from the seabed and thin layer R_d by using the reflection series from equation 4.23 in terms of the reflection coefficient R_{tl} from the thin layer and r_1 from the seabed:

$$R_d = \frac{r_1 + R_{tl}\mathrm{e}^{2i\gamma_1 d_1}}{1 + r_1 R_{tl}\mathrm{e}^{2i\gamma_1 d_1}} = r_1 + \grave{t}_1\acute{t}_1\left[R_{tl}\mathrm{e}^{2i\gamma_1 d_1} - r_1 R_{tl}^2\mathrm{e}^{4i\gamma_1 d_1} + ..\right]. \tag{4.74}$$

The second term in the expansion describes the downward ($\grave{t}_1$) and upward ($\acute{t}_1$) transmission through the seabed ($1 - r_1^2 = \grave{t}_1\acute{t}_1$), the propagation through the sediments ($\mathrm{e}^{2i\gamma_1 d_1}$), and the reflection response from the thin layer. The third term accounts for the first multiple between the seabed and the thin layer.

From Figure 4.9 it can be observed that the TE response is nearly the same no matter if the thin layer is present or not. Thus, the first term on the right hand side in equation 4.74 dominates in the TE case. For the TM mode on the other hand, the response in the seabed and thin-layer case resembles the response in the simple thin-layer case. Thus, the second

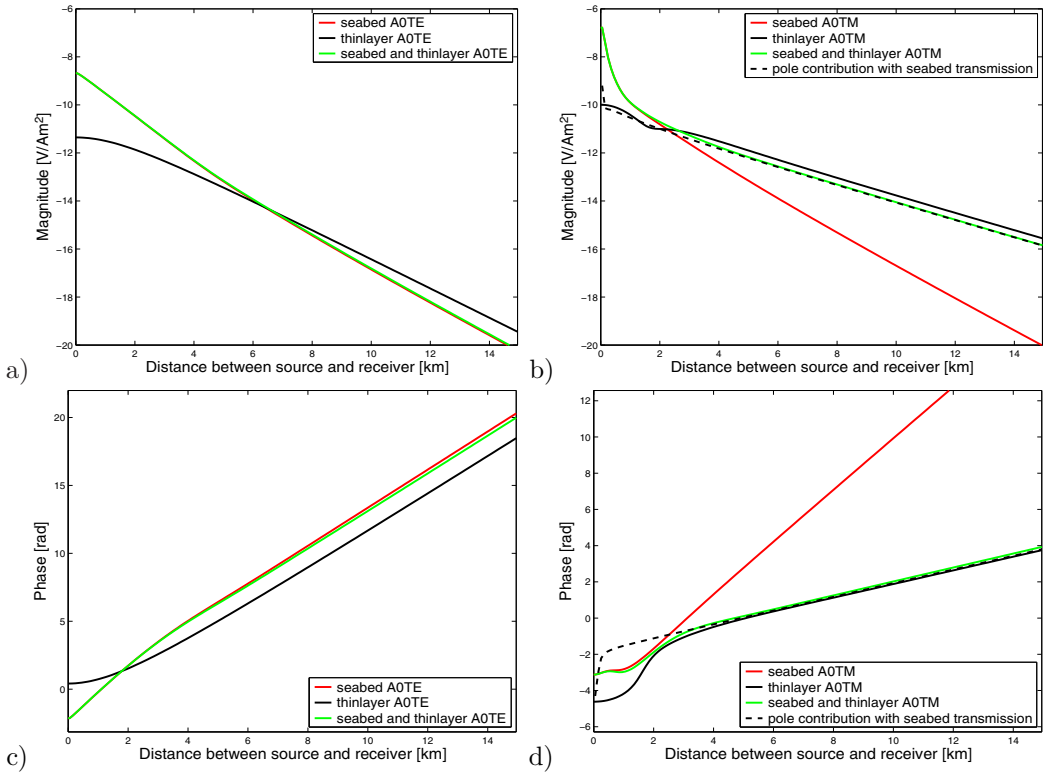

Figure 4.9: Comparison of the responses from a thin layer, a single seabed interface, and a combination of the seabed interface and a thin resistive layer; TE modes to the left and TM modes to the right. It can be observed that the TE mode only "sees" the seabed interface (green curve overlying the red curve), whereas the response in the TM case is shifted in amplitude due to the transmission through the seabed.

term must dominate both the first term and the third term. An approximate expression for the TM response when the seabed interface is introduced into the thin-layer model can then be obtained by using the relations for the transmitted field integrals in Appendix 4.H. Consider equations 4.H-85 and 4.H-86: With the assumption that the signals are transmitted almost normal to the seabed interface, the approximation $\cos^2\theta_s/\cos^2\theta_s' \approx 1$ can be made. The propagation distance in the sediment layer is moreover much larger than in the seawater. Thus, for the downward propagation $r_2 >> r_1$. The transmitted source signal should thus be multiplied with the transmission coefficient and the refraction index n. The guided signal is transmitted up through the seabed interface, but in this case $r_1 >> r_2$. An approximation to the TM response is then obtained from multiplying equation 4.67a by the factor $n\grave{t}_1\acute{t}_1$,

and moreover accounting for the propagation through seawater:

$$\mathcal{I}^{TM}_{A0,d} \sim \frac{\pi}{\sqrt{\sigma_1\sigma}}\, \grave{t}_1 \acute{t}_1\, \Gamma^{TM}_{0,d}\, \mathrm{e}^{i\lambda_p\rho + i\sqrt{k_1^2-\lambda_p^2}\,2d_1 + ikh}, \tag{4.75}$$

where $\Gamma^{TM}_{0,d}$ is the residue from equation 4.66 without the factor $\omega\mu/2k_1^2$ and h is the vertical propagation distance in the source layer. The transmission coefficients are obtained using equation 4.25:

$$\grave{t}_1\acute{t}_1 \approx \frac{4\sigma_1\sigma\sqrt{k^2-\lambda_p^2}\sqrt{k_1^2-\lambda_p^2}}{\left[\sigma\sqrt{k_1^2-\lambda_p^2}+\sigma_1\sqrt{k^2-\lambda_p^2}\right]^2} \approx \left[\frac{1}{2}+\frac{1}{4}\left(\sqrt{\frac{\sigma}{\sigma_1}}+\sqrt{\frac{\sigma_1}{\sigma}}\right)\right]^{-1}, \tag{4.76}$$

where normal incidence for the transmission through the seabed is a fairly good approximation when λ_p^{TM} is smaller than k_1 and k.

As seen in Figure 4.9, the thin-layer response is only slightly altered for the TM mode when the seabed is introduced into the model. The smaller amplitude is accounted for when adding the effect of the transmission through the seabed. The extra damping from the propagation in seawater has little influence on the amplitude due to the short distance travelled. From the TE plots in Figure 4.9, it is observed that the TE mode does not "see" the thin layer when the seabed is present. However, it should be noted that the overburden in the case study presented here has a thickness that suppresses the multiples that are generated between the seabed and the thin layer. If the overburden gets thinner, these multiples lead to more complicated deviations from the TE-mode seabed response and the TM-mode transmitted thin-layer response.

4.6.2 Seawater layer

From equation 4.22, the reflection response R_w in a region between two interfaces can be formulated as

$$R_w = \frac{r_1\mathrm{e}^{i\gamma(h_s+h_r)} + r_0\mathrm{e}^{i\gamma(2d_w-h_s-h_r)} + r_0r_1\mathrm{e}^{i\gamma(2d_w-h_s+h_r)} + r_0r_1\mathrm{e}^{i\gamma(2d_w+h_s-h_r)}}{1-r_0r_1\mathrm{e}^{2i\gamma d_w}}, \tag{4.77}$$

where r_0 and r_1 in the case considered here are the reflection coefficients from the sea-surface and seabed, respectively. The propagation factors are determined from the thickness of the water column d_w and the height of the source h_s (receiver h_r) above the seabed. From the geometric series expansion of the denominator in equation 4.77, the following expressions can be derived:

$$R_w = r_0\mathrm{e}^{i\gamma(d_s+d_r)}\left[1+r_1\mathrm{e}^{2i\gamma h_r}\right]\left[1+r_1\mathrm{e}^{2i\gamma h_s}\right]\left[1+r_0r_1\mathrm{e}^{2i\gamma d_w}+..\right] + r_1\mathrm{e}^{i\gamma(h_s+h_r)}, \tag{4.78a}$$

$$= r_1\mathrm{e}^{i\gamma(h_s+h_r)}\left[1+r_0\mathrm{e}^{2i\gamma d_r}\right]\left[1+r_0\mathrm{e}^{2i\gamma d_s}\right]\left[1+r_0r_1\mathrm{e}^{2i\gamma d_w}+..\right] + r_0\mathrm{e}^{i\gamma(d_s+d_r)}, \tag{4.78b}$$

where the expression in equation 4.78a (4.78b) has been obtained by considering the multiples in terms of r_0 (r_1). The source depth (below the sea-surface) $d_s = d_w - h_s$ and receiver depth

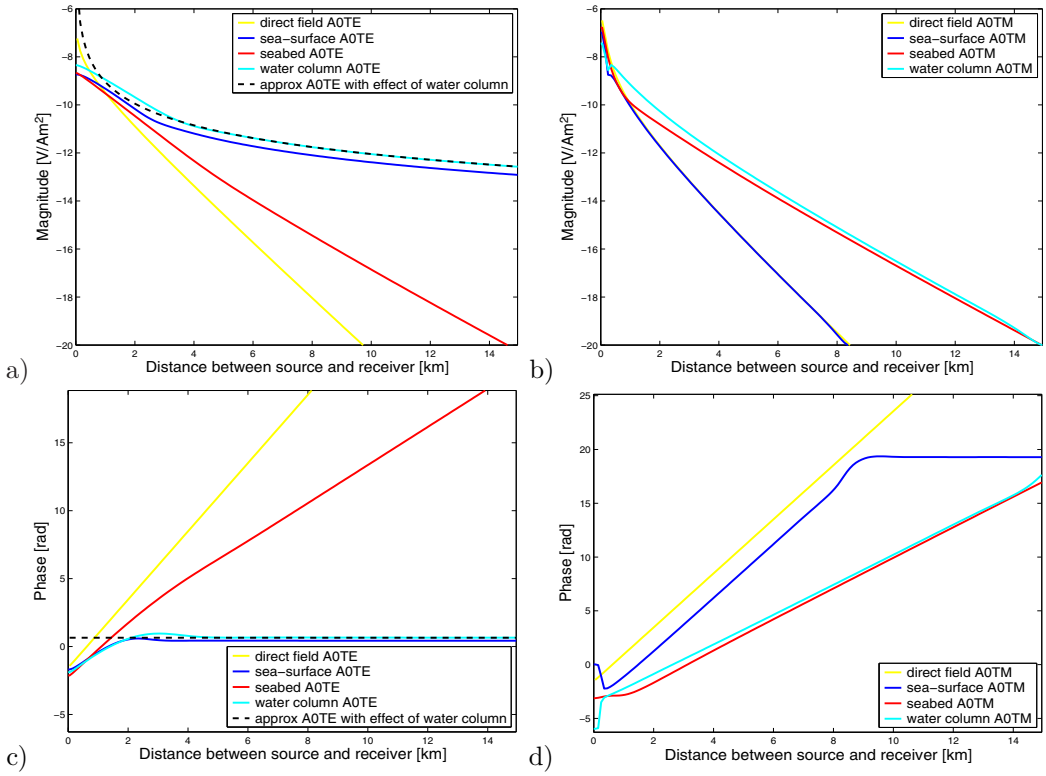

Figure 4.10: Comparison of the responses from a sea-surface, a seabed interface, and a combination of the seabed and sea-surface interface; TE modes to the left and TM modes to the right. The TE mode is dominated by the sea-surface response which is larger for the water-column model than for the model with the single sea-surface interface. The TM mode has a water-column response that is similar to the seabed response.

$d_r = d_w - h_r$ have been introduced into equation 4.78b for simplicity. Note that in both equations, the reflection response is a sum of two terms where all the multiples are accounted for in the first term.

Figure 4.10 shows that the TM response from the seabed is slightly increased when the sea-surface is added to the model. Of the two modes, the TE mode has by far the largest response in the water column. This is due to the sea-surface response being increased by the presence of the seabed. Equation 4.78a can be used in order to explain the increase in the TE response: The reflection coefficient at the sea-surface r_0 is multiplied by the term $1+r_1 e^{2i\gamma h_s}$ which can be pictured as an amplification of the source signal. The next term, $1 + r_1 e^{2i\gamma h_r}$, can be considered as an added strength to the signal at the receiver. The geometric series that follows these terms accounts for additional multiples in the water column, and the last

term in equation 4.78a is small and can be ignored. Now, for the lateral wave along the sea-surface, the seabed reflection r_1 and vertical wavenumber γ can be approximated by assuming vertical propagation ($\gamma = k$). For the multiples, the consequence of the reflection coefficient squared, cubed, quadrupled, etc., in the branch-point contribution must be evaluated. This is done in Appendix 4.F where equation 4.F-48 implies that $r_0^2 \approx 2r_0$ when $n \approx 0$. For the higher-order terms, $r_0^3 \approx 3r_0$, $r_0^4 \approx 4r_0$, and so on, as shown in Appendix 4.F. When the water-column effects are added to the sea-surface response in equation 4.50, one thus gets:

$$\mathcal{I}^{TE}_{A0,f} \sim \frac{2\mathrm{e}^{ikh}}{\sigma\rho^3}\left[1 + r_1\mathrm{e}^{2ikh_r}\right]\left[1 + r_1\mathrm{e}^{2ikh_s}\right]\left[1 + 2r_1\mathrm{e}^{2ikd_w} + 3r_1^2\mathrm{e}^{4ikd_w} + ..\right], \tag{4.79}$$

where $h = d_s + d_r$. The expression in the last bracket can be written as $\left[1 - r_1\mathrm{e}^{2ikd_w}\right]^{-2}$, but because of the attenuation in the water column, only the first few terms in the corresponding series expansion are needed. The relation in equation 4.79 gives a good approximation to the water-column TE response as can be seen in Figure 4.10. The increased TM response can in principle be calculated by using the same approach (cf. equation 4.F-48). However, since the TM response is "governed" by the seabed interaction, and thus is small compared to the water-column TE response, the calculation is not pursued further here.

4.6.3 Full model

For the TE-mode response, the asymptotic expression for the field integral that is given in equation 4.79 will still be a good approximation when the thin layer is introduced into the water-column model. This is evident from Figure 4.9 where it can be seen that the seabed TE response is almost not altered at all by the introduction of the thin layer. The TM response in the water-column model is much weaker than the TE response. However, when the thin resistive layer is introduced into the model, the TM response increases substantially. An approximation to the TM response in the full model can be found by considering equation 4.78b if the seabed reflection coefficient r_1 is replaced by the seabed/thin-layer response R_d from equation 4.74. The transmitted guide response described in equation 4.75 increases when a sea-surface is present in the model. This is due to the amplifications of emitted as well as received signal introduced by the water column. In order to quantitatively account for the increase, the powers of R_d in the geometric series that describes the reflection response (cf. equation 4.78b with r_1 replaced by R_d) must be evaluated. If the reflection response from the seabed and thin layer is denoted as $R_d \approx r_1 + R_{tt}$ where R_{tt} is the transmitted thin-layer response (second term in equation 4.74), one gets

$$R_d^2 \approx (r_1 + R_{tt})^2 \approx 2r_1R_{tt} \quad \text{and} \quad R_d^3 \approx (r_1 + R_{tt})^3 \approx 3r_1^2R_{tt}, \tag{4.80}$$

because terms with pure seabed reflections are much weaker than the terms that contain the thin-layer response, and because the higher-order terms of R_{tt} are negligible due to the

substantial thickness of the overburden.

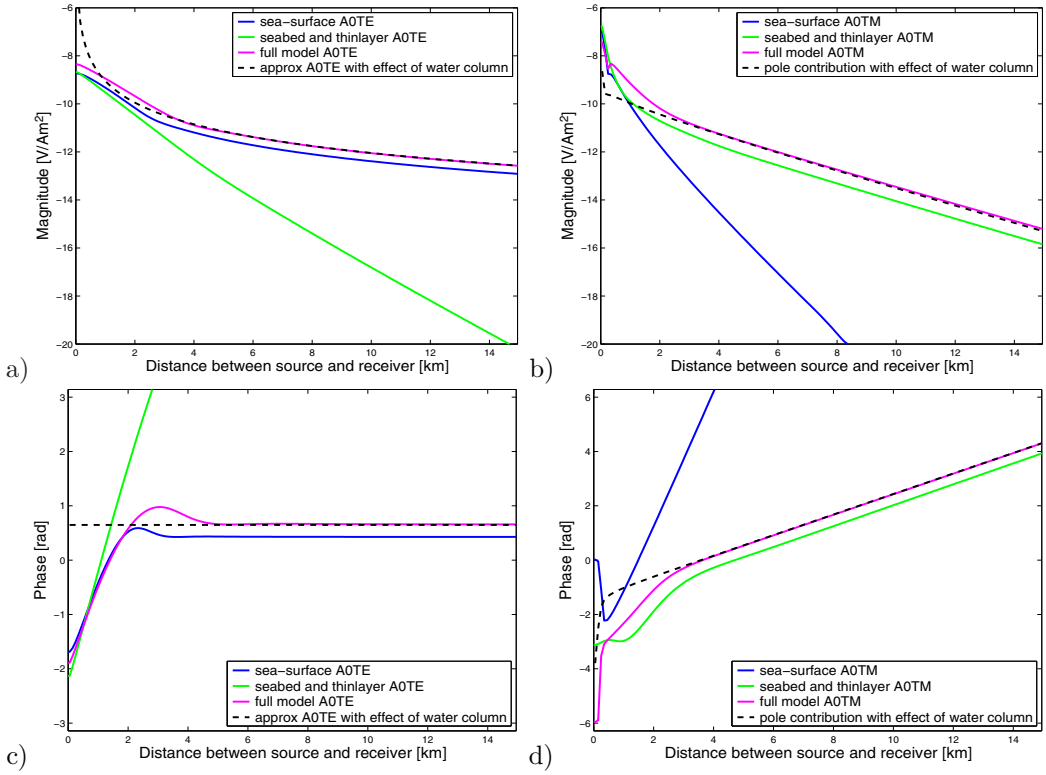

Figure 4.11: Plots of the responses from the full model described in Figure 4.1 along with the responses from a single sea-surface interface and a model with infinite water depth. The TE mode has an increased sea-surface response due to the presence of the seabed. The TM mode has an increased thin-layer response due to the presence of the sea-surface. The explicit spatial expressions from the asymptotic evaluations fit the exact modelled data well.

Now, when assuming vertical propagation in the water column ($\gamma \approx k$), the combination of the reflection series in equation 4.78b, with R_d instead of r_1, and the expression in equation 4.75 leads to the approximate expression:

$$\mathcal{I}^{TM}_{A0,f} \sim \mathcal{I}^{TM}_{A0,d} \left[1 + \mathrm{e}^{2ikd_s}\right] \left[1 + \mathrm{e}^{2ikd_r}\right] \left[1 + 2r_1\mathrm{e}^{2ikd_w} + 3r_1^2\mathrm{e}^{4ikd_w} + ..\right], \tag{4.81}$$

where it has been used that $r_0 \approx 1$. In Figure 4.11 it is shown that this expression is a quite good approximation to the TM response in the complete model. It can furthermore be observed from Figure 4.11 that the lateral response from the sea-surface for the TE mode, and the guided response in the thin layer for the TM mode, are the strongest contributors to the overall response in the complete model. Thus, the asymptotic expressions in equation 4.79

for the TE mode and equation 4.81 for the TM mode account well for the total contributions from the corresponding field integrals. The thin-layer TM response, which looses strength due to the seabed transmission, is amplified by the presence of the sea-surface. Even if the multiples in the water column are rapidly attenuated, the first few terms cannot be neglected in shallow water. From equation 4.79 and 4.81 it is seen that the effect of the water column is similar for the seabed-transmitted thin-layer TM response and the sea-surface TE response.

4.7 Conclusions

Propagation of horizontal electric field components in layered media in terms of their TE- and TM-polarization parts has been studied. Asymptotic evaluations of the field integrals using the method of steepest descents give expressions that describe the signal propagation in conductive media well. The expressions have been verified by exact numerical modelling. The large parameter that justifies the asymptotic expansion is the propagation distance between the source and receiver.

The asymptotic expansions of the CSEM field integrals have been obtained in order to contribute to the understanding of the physics of marine CSEM. The considerations have been made for propagation in ideal models that simulate the typical settings in conventional marine CSEM surveying for hydrocarbons.

It has been verified that the sea-surface response is due to a lateral wave, and that the propagation term in air is negligible. The notion of the signal propagation along the sea-surface as instantaneous might be appropriate. It has moreover been shown that the response is dominated by the TE mode. The responses in a simple model with only a seabed interface are also due to lateral waves, and in this case the magnitudes of the TE and TM responses are similar. At the seabed interface, the propagation term cannot be neglected. In a model with a thin resistive layer contained in a conductive background medium, the response is accounted for by the pole in the reflection response for the TM mode. Hence, the thin-layer response can be pictured as a guided TM mode. The TE response from the thin-layer model is moderate compared to the TM response, and it is accounted for by a ray reflection from the thin resistor.

The main point that follows from the accurate asymptotic expressions that describe field propagation in the simple models, is that the sea-surface response is a TE mode, whereas the thin-layer response is a TM mode.

In the more complicated models this conclusion still holds. In presence of a seabed, the thin-layer TM response for the electric field is only slightly more damped due to the transmission through the seabed. The TE-mode response from the seabed/thin-layer model on the other hand, is due to the seabed interaction even with the thin layer present in the subsurface.

For the complete model described in Figure 4.1, i.e., when the sea-surface interface is added to the seabed/thin-layer model, the TM response from the thin resistive layer increases due to the first few multiple reflections in the seawater layer. The multiples can be interpreted in terms of amplifications of the signals at both the source and receiver sides. The response is explained quite well by the spatial expression in equation 4.81. The TE response is accounted for by the lateral sea-surface response and the additional "boost" of the emitted and received signal due to the seabed interaction. The expression in equation 4.79 is a good approximation to the TE response.

An interpretation of marine CSEM data in terms of the TE and TM modes requires that the modes can be separated in acquisition or data processing. A brief discussion on how this can be done is provided in Appendix 4.I.

4.8 Acknowledgments

The author would like to thank VISTA for financial support and Bjørn Ursin and Lasse Amundsen for useful discussions and suggestions.

4.A Useful relations

From Abramowitz and Stegun (1962) the following relations are obtained for a small parameter x:

$$\frac{1}{1+x} = 1 - x + x^2 - x^3 + x^4 - .. , \tag{4.A-1a}$$

$$\sqrt{1+x} = 1 + \tfrac{1}{2}x - \tfrac{1}{8}x^2 + \tfrac{1}{16}x^3 - \tfrac{5}{128}x^4 + .. , \tag{4.A-1b}$$

$$\frac{1}{\sqrt{1+x}} = 1 - \tfrac{1}{2}x + \tfrac{3}{8}x^2 - \tfrac{5}{16}x^3 + \tfrac{35}{128}x^4 - .. , \tag{4.A-1c}$$

$$\mathrm{e}^x = 1 + x + \tfrac{1}{2}x^2 + \tfrac{1}{6}x^3 + \tfrac{1}{24}x^4 + .. , \tag{4.A-1d}$$

$$\mathrm{e}^{a(1+x)} = \mathrm{e}^a \left[1 + ax + \tfrac{1}{2}(ax)^2 + \tfrac{1}{6}(ax)^3 + \tfrac{1}{24}(ax)^4 + ..\right]. \tag{4.A-1e}$$

In the calculations the following relations involving complex numbers are used:

$$\sqrt{i} = \pm\frac{1+i}{\sqrt{2}} = \pm\mathrm{e}^{i\pi/4}, \quad \sqrt{-i} = \pm i^{3/2} = \pm\mathrm{e}^{i3\pi/4}. \tag{4.A-2}$$

The square root of a complex number can be written as:

$$\sqrt{a \pm ib} = \alpha \pm i\beta, \quad \alpha = \left[\tfrac{1}{2}\left(\sqrt{a^2+b^2}+a\right)\right]^{1/2}, \quad \beta = \left[\tfrac{1}{2}\left(\sqrt{a^2+b^2}-a\right)\right]^{1/2}. \tag{4.A-3}$$

From Gradshteyn and Ryzhik (1980), equation 3.461, one gets:

$$\int_{-\infty}^{\infty} ds\, \mathrm{e}^{-as^2} s^{2n} = \frac{(2n)!}{2^n n!(2a)^n}\sqrt{\frac{\pi}{a}}, \tag{4.A-4}$$

which gives:

$$\int_{-\infty}^{\infty} ds\, \mathrm{e}^{-as^2} = \sqrt{\frac{\pi}{a}}, \qquad \int_{-\infty}^{\infty} ds\, \mathrm{e}^{-as^2} s^2 = \frac{1}{2a}\sqrt{\frac{\pi}{a}}, \tag{4.A-5a}$$

$$\int_{-\infty}^{\infty} ds\, \mathrm{e}^{-as^2} s^4 = \frac{3}{4a^2}\sqrt{\frac{\pi}{a}}, \qquad \int_{-\infty}^{\infty} ds\, \mathrm{e}^{-as^2} s^6 = \frac{15}{8a^3}\sqrt{\frac{\pi}{a}}. \tag{4.A-5b}$$

The sine and cosine of a complex angle $\theta = \theta_r + i\theta_i$ can be written as:

$$\sin\theta = \sin\theta_r \cosh\theta_i + i\cos\theta_r \sinh\theta_i, \tag{4.A-6a}$$

$$\cos\theta = \cos\theta_r \cosh\theta_i - i\sin\theta_r \sinh\theta_i. \tag{4.A-6b}$$

The series expansion of the cotangent function is:

$$\cot\zeta = \frac{1}{\zeta} - \frac{1}{3}\zeta - \frac{1}{45}\zeta^3 - \ldots. \tag{4.A-7}$$

4.B Pole near a saddle or branch point

In order to derive an expression for the contribution from the pole, the same approach as in Baños (1966) and Kong (2000) is used. Define the integral:

$$\mathcal{I}_y(y) = \int_{-\infty}^{\infty} du \frac{2u_p\Gamma}{u^2 - u_p^2}\, \mathrm{e}^{-yu^2}, \tag{4.B-8}$$

which leads to the relation

$$\frac{d\mathcal{I}_y(y)}{dy} + u_p^2\, \mathcal{I}_y(y) = -2u_p\Gamma \int_{-\infty}^{\infty} du\, \mathrm{e}^{-yu^2} = -2u_p\Gamma\sqrt{\frac{\pi}{y}}. \tag{4.B-9}$$

The homogeneous solution to this equation is $\mathcal{I}_y^h(y) = p_0 \exp(-yu_p^2)$ where p_0 is a constant. A particular solution is on the form $\mathcal{I}_y(y) = p(y)\exp(-yu_p^2)$. Inserted into equation 4.B-9 this yields

$$p'(y) = -2u_p\Gamma\sqrt{\frac{\pi}{y}}\, \mathrm{e}^{yu_p^2}. \tag{4.B-10}$$

An integration from y = 0 to y = 1 leads to

$$p(1) - p(0) = -2u_p\Gamma\sqrt{\pi}\int_0^1 dy \sqrt{\frac{1}{y}}\, \mathrm{e}^{yu_p^2}, \tag{4.B-11}$$

where the substitution $v = -iu_p\sqrt{y}$, assuming that $\mathrm{Im}(u_p) > 0$, gives

$$\int_0^1 dy \sqrt{\frac{1}{y}}\, \mathrm{e}^{yu_p^2} = \frac{2i}{u_p}\int_0^{-iu_p} dv\, \mathrm{e}^{-v^2} = \frac{\sqrt{\pi}i}{u_p}\mathrm{erf}(-iu_p). \tag{4.B-12}$$

The integral has been expressed in terms of the error function:

$$\mathrm{erf}(\zeta) = 1 - \mathrm{erfc}(\zeta) = \frac{2}{\sqrt{\pi}}\int_0^{\zeta} dv\, \mathrm{e}^{-v^2}, \tag{4.B-13}$$

where erfc(ζ) is the complementary error function. An expression for $\mathcal{I}_y(0)$ is furthermore needed. When $\mathrm{Im}(u_p) > 0$:

$$\mathcal{I}_y(0) = \Gamma \int_{-\infty}^{\infty} du\, \frac{2u_p}{u^2 - u_p^2} = \Gamma \int_{-\infty}^{\infty} du\, \left(\frac{1}{u - u_p} - \frac{1}{u + u_p} \right) = 2\pi i \Gamma. \tag{4.B-14}$$

This leads to the expression:

$$\mathcal{I}_y(1) = p(1) \mathrm{e}^{-u_p^2} = 2\pi i \Gamma \left[1 - \mathrm{erf}\left(-i u_p \right) \right] \mathrm{e}^{-u_p^2}. \tag{4.B-15}$$

4.C The magnetic and vertical electric field

In the main text the horizontal electric field has been considered in order to show how the TE and TM modes propagate in a layered model. The derivations of the lateral, guided, and ray-reflected responses for the E_z-component are found using the same procedures as for the TM-mode integrals in the main text. The E_z-integral is (Løseth and Ursin, 2007):

$$E_z = \frac{I l_x}{4\pi} \cos\beta \; \mathcal{I}_{D2}^{TM}, \quad \text{where} \quad \mathcal{I}_{D2}^{TM} = \frac{i}{\omega \tilde{\varepsilon}} \int_0^{\infty} d\lambda \, \lambda^2 J_1(\lambda\rho) \, g_D^{TM}(\lambda). \tag{4.C-16}$$

The function g_D is given by:

$$g_D(\lambda) = \mathrm{e}^{i\gamma h_{rs}} + R_D(\lambda), \quad \text{where} \quad R_D = \frac{-\grave{R}_b(1 + \acute{R}_s) + \acute{R}_s(1 + \grave{R}_s)}{1 - \acute{R}_s \grave{R}_s} \mathrm{e}^{i\gamma h_{rs}}. \tag{4.C-17}$$

An explanation of the different reflection-response contributions to the total response R_D is given following equation 4.22 in the main text.

In the single-interface case (cf. section 4.4), the branch-point contribution is:

$$\mathcal{I}_{D2,b}^{TM} \sim \frac{2\omega\mu \, \mathrm{e}^{ik_a\rho + ikh\sqrt{1-n^2}}}{k\rho^2\sqrt{1-n^2}} \left[1 + \tfrac{1}{ik_a\rho} \left(-3 + \tfrac{3n^2}{2(1-n^2)} + \tfrac{3(1+n^2)}{n^2} + \tfrac{3}{2} ikh \tfrac{n^2}{\sqrt{1-n^2}} \right) + .. \right], \tag{4.C-18}$$

which for small n must be separated into an explicit pole contribution and an asymptotic expansion with the pole contribution removed:

$$\mathcal{I}_{D2,bp}^{TM} = -2\pi i \, \Gamma_{D2} \, \mathrm{e}^{ik_a\rho} \left[1 - \mathrm{erf}\left(i\tau_p \right) \right] \mathrm{e}^{-\tau_p^2}, \tag{4.C-19a}$$

where τ_p is given in equation 4.45,

$$\Gamma_{D2} = \frac{-i\omega\mu k n^5}{2(1-n^4)\left(1+n^2\right)^{3/2}} \, H_1^- \left(\tfrac{k_a\rho}{\sqrt{1+n^2}} \right) \mathrm{e}^{ikh\left(1+n^2\right)^{-1/2}}, \tag{4.C-19b}$$

and

$$\mathcal{I}_{D2,bc}^{TM} \sim \frac{-i\omega\mu}{\rho} \, \mathrm{e}^{ik_a\rho + ikh\left(1+n^2\right)^{-1/2}} \left(w_1 + \tfrac{1}{ik\rho} w_2 + .. \right), \tag{4.C-20a}$$

where

$$w_1 = 2n^3\left[1 - \tfrac{7}{8}n^2 + \tfrac{235}{128}n^4 - ..\right], \quad w_2 = n^2\left[-2 + \left(\tfrac{113}{64} + ikh\right)n^2 - \tfrac{521}{256}n^4 + ..\right]. \quad \text{(4.C-20b)}$$

The thin-layer response is (cf. section 4.5):

$$\mathcal{I}^{TM}_{D2,p} = -\frac{\pi i}{2\sigma_1} H_1^-(\lambda_p\rho)\,\frac{\lambda_p\sqrt{k_1^2-\lambda_p^2}\left[\lambda_p^2(1-n_1^4) - n_1^2k_1^2(1-n_1^2)\right]d_2}{(1+n_1^4)\,d_2\sqrt{k_1^2-\lambda_p^2} + in_1^2}\,\mathrm{e}^{i\lambda_p\rho + i\sqrt{k_1^2-\lambda_p^2}h}. \quad \text{(4.C-21)}$$

The saddle-point contribution is:

$$\mathcal{I}^{TM}_{D2,s} \sim i\omega\mu\frac{\mathrm{e}^{ikr}}{r}\,\sin\theta_s\cos\theta_s\,R^{TM}_{si}(\theta_s), \quad \text{(4.C-22)}$$

where the positive sign in front of equation 4.C-22 is due to the negative sign in equation 4.C-17. The saddle-point contribution in case of transmission through an interface (cf. section 4.H) takes a similar form:

$$\mathcal{I}^{TM}_{D2,t} \sim -i\omega\mu\frac{\mathrm{e}^{ikr_1 + ik_a r_2}}{r_t}\,\sin\theta_s\cos\theta_s\,t'_{TM}(\theta_s), \quad \text{(4.C-23)}$$

where $t'_{TM} = 1 - r_{TM}$ in terms of the definitions in equation 4.24. From equation 4.C-23 and an analogous argumentation as in section 4.6.1, the corresponding expression to equation 4.75 can be derived:

$$\mathcal{I}^{TM}_{D2,d} \sim n^2\,\grave{t}_1\acute{t}_1\,\mathcal{I}^{TM}_{D2,p}\,\mathrm{e}^{ikh}, \quad \text{(4.C-24)}$$

where $\grave{t}_1\acute{t}_1$ is given in equation 4.76, and where h in equation 4.C-21 now is $2d_1$. In the full model, the expression for the multiple reflections in the water column described by equation 4.78b for R_A is modified due to the difference between R_D (equation 4.C-17) and R_A (equation 4.22). Accounting for this difference, the expression for the $\mathcal{I}^{TM}_{D2}$-integral in the full model becomes:

$$\mathcal{I}^{TM}_{D2,f} \sim \mathcal{I}^{TM}_{D2,d}\left[1 - \mathrm{e}^{2ikd_s}\right]\left[1 + \mathrm{e}^{2ikd_r}\right]\left[1 + 2r_1\mathrm{e}^{2ikd_w} + 3r_1^2\mathrm{e}^{4ikd_w} + ..\right]. \quad \text{(4.C-25)}$$

The derivation of the asymptotic expressions for the integral in equation 4.C-16 does not add substantial new insight into the behaviour of the signal propagation for the TM mode in a stratified medium. However, it should be noted that there is a sign difference in the expression that describes water-layer reflection effects in equation 4.C-25 (for the E_z-component) compared to the corresponding relation in equation 4.81 (TM mode for the horizontal electric field), and that the effect of the transmission of the thin-layer response through the seabed interface is different (factor n^2 instead of n).

When the asymptotic expressions for the electric field components are known, expressions for the magnetic field components can be obtained using Faraday's law:

$$H_\rho = \frac{1}{i\omega\mu}\left[\frac{1}{\rho}\frac{\partial E_z}{\partial \beta} - \frac{\partial E_\beta}{\partial z}\right], \tag{4.C-26a}$$

$$H_\beta = \frac{1}{i\omega\mu}\left[\frac{\partial E_\rho}{\partial z} - \frac{\partial E_z}{\partial \rho}\right], \tag{4.C-26b}$$

$$H_z = \frac{1}{i\omega\mu}\frac{1}{\rho}\left[\frac{\partial(\rho E_\beta)}{\partial \rho} - \frac{\partial E_\rho}{\partial \beta}\right]. \tag{4.C-26c}$$

4.D Hankel functions

The Hankel functions of the first and second kind are defined as (Abramowitz and Stegun, 1962):

$$H_\nu^{(1)}(\zeta) = J_\nu(\zeta) + iY_\nu(\zeta) \quad \text{and} \quad H_\nu^{(2)}(\zeta) = J_\nu(\zeta) - iY_\nu(\zeta), \tag{4.D-27}$$

where ζ is a complex variable, J_ν is the Bessel function of the first kind, and Y_ν is the Bessel function of the second kind (or Weber's function). The Hankel functions in equation 4.D-27 are related as (Abramowitz and Stegun, 1962, equation 9.1.39)

$$H_\nu^{(2)}(\zeta) = -\mathrm{e}^{\nu\pi i} H_\nu^{(1)}\left(\zeta \mathrm{e}^{\pi i}\right), \tag{4.D-28}$$

and by using equation 4.D-27 and 4.D-28, the Bessel functions J_0 and J_1 can be expressed as

$$J_0(\zeta) = \frac{1}{2}\left[H_0^{(1)}(\zeta) - H_0^{(1)}(-\zeta)\right], \tag{4.D-29a}$$

$$J_1(\zeta) = \frac{1}{2}\left[H_1^{(1)}(\zeta) + H_1^{(1)}(-\zeta)\right]. \tag{4.D-29b}$$

In the main text the Hankel function of the first kind (sometimes referred to as the Bessel function of the third kind) is referred to as the Hankel function.

For large arguments the Hankel functions of the zeroth and first order can be written as (Abramowitz and Stegun, 1962):

$$H_0^{(1)}(\zeta) = \sqrt{\frac{2}{\pi\zeta}}\left[1 + \frac{1}{8i\zeta} + \frac{9}{128(i\zeta)^2} + ..\right]\mathrm{e}^{i\zeta - \frac{\pi}{4}i}, \tag{4.D-30a}$$

$$H_1^{(1)}(\zeta) = \sqrt{\frac{2}{\pi\zeta}}\left[1 - \frac{3}{8i\zeta} - \frac{15}{128(i\zeta)^2} - ..\right]\mathrm{e}^{i\zeta - \frac{3\pi}{4}i}. \tag{4.D-30b}$$

Because the Hankel functions involve Weber's function, both $H_0^{(1)}(\zeta)$ and $H_1^{(1)}(\zeta)$ have a logarithmic branch-point singularity at $\zeta = 0$. The asymptotic expansions have a multiple-valued singularity at $\zeta = 0$.

The following relations between the zeroth- and first-order Hankel functions and their derivatives are useful (with $\zeta = \lambda\rho$):

$$\frac{d}{d\rho}H_0^{(1)}(\lambda\rho) = -\lambda H_1^{(1)}(\lambda\rho), \tag{4.D-31a}$$

$$\frac{d}{d\rho}H_1^{(1)}(\lambda\rho) = \lambda H_0^{(1)}(\lambda\rho) - \frac{1}{\rho}H_1^{(1)}(\lambda\rho). \tag{4.D-31b}$$

The relations in equation 4.D-31 are valid for the Bessel functions of the first kind as well.

4.E Field integrals in a homogeneous medium

The first terms on the right hand side in equation 4.20 can be integrated analytically. The solution to the first integral in equation 4.E-32 is found in Gradshteyn and Ryzhik (1980), and the solution for the other integrals follow, unless otherwise noted, by a differentiation of the integral above the one that is considered in terms of the variable z:

$$\mathcal{I}_1 = \int_0^\infty d\lambda \frac{1}{\gamma} J_1(\lambda\rho)\, \mathrm{e}^{iz\gamma} = -\frac{1}{k\rho}\left(\mathrm{e}^{ikr} - \mathrm{e}^{ikz}\right), \tag{4.E-32a}$$

$$\mathcal{I}_2 = \int_0^\infty d\lambda\, J_1(\lambda\rho)\, \mathrm{e}^{iz\gamma} = -\frac{1}{\rho}\left(\frac{z}{r}\mathrm{e}^{ikr} - \mathrm{e}^{ikz}\right), \tag{4.E-32b}$$

$$\mathcal{I}_3 = \int_0^\infty d\lambda\, \gamma\, J_1(\lambda\rho)\, \mathrm{e}^{iz\gamma} = \left(-\frac{kz^2}{\rho r^2} + \frac{i\rho}{r^3}\right)\mathrm{e}^{ikr} + \frac{k}{\rho}\mathrm{e}^{ikz}, \tag{4.E-32c}$$

$$\mathcal{I}_4 = \int_0^\infty d\lambda \frac{\lambda}{\gamma} J_0(\lambda\rho)\, \mathrm{e}^{iz\gamma} = \frac{d\mathcal{I}_1}{d\rho} + \frac{1}{\rho}\mathcal{I}_1 = -i\frac{\mathrm{e}^{ikr}}{r}, \tag{4.E-32d}$$

$$\mathcal{I}_5 = \int_0^\infty d\lambda\, \lambda\, J_0(\lambda\rho)\, \mathrm{e}^{iz\gamma} = \left(-\frac{ikz}{r^2} + \frac{z}{r^3}\right)\mathrm{e}^{ikr}, \tag{4.E-32e}$$

$$\mathcal{I}_6 = \int_0^\infty d\lambda\, \lambda\gamma\, J_0(\lambda\rho)\, \mathrm{e}^{iz\gamma} = \left(-\frac{k}{r^2} - \frac{i + ik^2z^2}{r^3} + \frac{3kz^2}{r^4} + \frac{3iz^2}{r^5}\right)\mathrm{e}^{ikr}. \tag{4.E-32f}$$

where $\gamma = \sqrt{k^2 - \lambda^2}$ and $r = \sqrt{z^2 + \rho^2}$. The expressions for $\mathcal{I}^{TE}_{A0,d}$, $\mathcal{I}^{TE}_{A1,d}$, $\mathcal{I}^{TM}_{A0,d}$, and $\mathcal{I}^{TM}_{A1,d}$ are found using equations 4.E-32d, 4.E-32a, 4.E-32f, and 4.E-32c, respectively.

4.F Single-interface branch-point contributions

The calculations of the branch-point contributions for the single-interface case are presented in this section. First, a simple relation between integrals that contain zeroth- and first-order Hankel functions is derived. Next, the TE- and TM-mode branch-point contributions are calculated. The asymptotic expansions are obtained with the horizontal source and receiver offset (ρ) as the large variable. Finally, an asymptotic evaluation of the TM-mode branch-point contribution is performed where the effect of the pole is removed from the asymptotic expression and considered separately.

4.F.1 Relation between the zeroth- and first-order integrals

If the $\mathcal{I}_{A0}$-integrals can be written on the form

$$\mathcal{I}_{A0}(\rho) = \left(\frac{a_0}{\rho} + \frac{a_1}{\rho^2} + \frac{a_2}{\rho^3} + \frac{a_3}{\rho^4} + ..\right) \mathrm{e}^{b\rho}, \tag{4.F-33a}$$

the corresponding $\mathcal{I}_{A1}$-integrals are given as

$$\mathcal{I}_{A1}(\rho) = \frac{1}{b}\left[\frac{a_0}{\rho} + \frac{a_1}{\rho^2} + \left(a_2 + \frac{a_1}{b}\right)\frac{1}{\rho^3} + \left(a_3 + \frac{2a_2}{b} + \frac{2a_1}{b^2}\right)\frac{1}{\rho^4} + ..\right] \mathrm{e}^{b\rho}. \tag{4.F-33b}$$

This can be derived by noting that the integrals in equation 4.19 are related as follows (cf. equation 4.D-31):

$$\left(\frac{d}{d\rho} + \frac{1}{\rho}\right)\mathcal{I}_{A1} = \mathcal{I}_{A0}. \tag{4.F-34}$$

The homogeneous solution is $\mathcal{I}^h_{A1} = q_0/\rho$ where q_0 is a constant. A particular solution is found by taking $\mathcal{I}_{A1} = q(\rho)/\rho$ where $q(\rho)$ is a function of ρ. Using equation 4.F-34 one gets $q(\rho) = \int d\rho' \rho' \mathcal{I}_{A0}(\rho')$. When $\mathcal{I}_{A0}$ is on a form which includes an inverse power series times an exponential function of ρ, the resulting relation between $\mathcal{I}_{A0}$ and $\mathcal{I}_{A1}$ is as given in equation 4.F-33.

4.F.2 Transformation of the integrals

The following relations derived from equation 4.38 ($\lambda = k_a \cos\alpha$) are needed:

$$d\lambda = -k_a \sin\alpha \, d\alpha, \tag{4.F-35a}$$

$$\gamma_a = -k_a \sin\alpha, \tag{4.F-35b}$$

$$\gamma = k\sqrt{1 - n^2\cos^2\alpha}, \tag{4.F-35c}$$

where $n = k_a/k$ is the refractive index. As seen from the transformation in equation 4.38, $\alpha = \pm\pi/2$ when $\lambda = 0$. Since the branch point is transformed into a saddle point at $\alpha = 0$, α should be $-\pi/2$ when $\lambda = 0$. The negative sign must then be chosen in equation 4.F-35b because γ_a must be equal to $+k_a$ when $\lambda = 0$.

The variable τ from equation 4.40 can be expressed in terms of a new variable ξ as

$$\xi = \kappa\tau \quad \text{where} \quad \kappa = (ik_a\rho)^{-1/2}. \tag{4.F-36}$$

The relations in equation 4.38 and 4.F-35 expressed in terms of ξ then become:

$$\cos\alpha = 1 - \xi^2, \tag{4.F-37a}$$

$$\sin\alpha = \sqrt{2}\xi\sqrt{1 - \tfrac{1}{2}\xi^2}, \tag{4.F-37b}$$

$$\sin\alpha d\alpha = 2\xi d\xi, \tag{4.F-37c}$$

$$\sqrt{1 - n^2\cos^2\alpha} = \sqrt{1 - n^2}\sqrt{1 + \tfrac{n^2}{1-n^2}\xi^2(2 - \xi^2)}. \tag{4.F-37d}$$

The integral in equation 4.1 is rewritten in terms of α by using equation 4.38 and 4.39. From the transformations in equation 4.40 and 4.F-36, the integral in terms of ξ can be written as

$$\mathcal{I}_b(\rho) = \mathrm{e}^{ik_a\rho} \int_{-\infty}^{\infty} d\xi f_\xi(\xi)\, \mathrm{e}^{-\xi^2/\kappa^2}, \tag{4.F-38}$$

where $f_\xi(\xi)$ can be expanded in a power series in terms of the small parameter ξ. From equation 4.A-4 it is observed that only even powers of ξ will contribute to the integral.

4.F.3 TE mode

Consider the expression in equation 4.29a with a reflection response as given in equation 4.32a. Since $\phi(\lambda) = i\lambda\rho$, the function $f_{TE}(\lambda)$, cf. equation 4.1, is:

$$f_{TE}(\lambda) = \frac{\omega\mu}{2}\,\frac{\lambda}{\gamma}\,\frac{k^2\left(1+n^2\right) - 2\gamma\gamma_a - 2\lambda^2}{k^2\left(1-n^2\right)}\, H_0^-(\lambda\rho)\, \mathrm{e}^{i\gamma h}. \tag{4.F-39a}$$

From equation 4.F-37c (4.F-35a) comes an odd-order term in ξ. Since the only other odd-order term in the expressions is in equation 4.F-37b (4.F-35b), the branch-point contribution in equation 4.F-39a is:

$$f_{TE}(\lambda)|_b = \frac{-\omega\mu}{k^2\left(1-n^2\right)}\, \lambda\gamma_a\, H_0^-(\lambda\rho)\, \mathrm{e}^{i\gamma h}. \tag{4.F-39b}$$

The part of the reflection coefficient from equation 4.32a that contributes to the branch-point response is then:

$$R_{si}^{TE}(\lambda)|_b = \frac{-2\gamma\gamma_a}{k^2\left(1-n^2\right)}. \tag{4.F-39c}$$

When the asymptotic expansion of the Hankel function in equation 4.D-30 is inserted into equation 4.F-39b, one gets:

$$f_{TE}(\lambda)|_b = \frac{-\omega\mu}{k^2\left(1-n^2\right)}\sqrt{\frac{2}{\pi\rho}}\mathrm{e}^{-i\frac{\pi}{4}}\,\sqrt{\lambda}\gamma_a\,\left[1 + \tfrac{1}{8i\lambda\rho} + \tfrac{9}{128(i\lambda\rho)^2} + ..\right]\,\mathrm{e}^{i\gamma h}. \tag{4.F-39d}$$

Now, $f(\lambda)$ is transformed into $f_\xi(\xi)$ by using the relations in equation 4.F-35 and 4.F-37. The series expansions in powers of ξ are furthermore worked out using the relations in equation 4.A-1. The exponential term becomes:

$$\mathrm{e}^{i\gamma h} = \mathrm{e}^{c_e}\left[1 + e_1\xi^2 + e_2\xi^4 + ..\right], \tag{4.F-40a}$$

where the shorthand notation

$$c_e = ikh\sqrt{1-n^2}, \quad e_1 = c_e\tfrac{n^2}{1-n^2}, \quad e_2 = -\tfrac{1}{2}c_e\tfrac{n^2}{(1-n^2)^2}(1-c_e n^2), \tag{4.F-40b}$$

has been used. The second- and third-order terms in the Hankel function are:

$$\frac{1}{8i\lambda\rho} = h_1\left(1+\xi^2+\xi^4+..\right), \quad \text{where} \quad h_1 = \frac{1}{8ik_a\rho}, \tag{4.F-41a}$$

$$\frac{9}{128(i\lambda\rho)^2} = h_2\left(1+2\xi^2+3\xi^4+..\right), \quad \text{where} \quad h_2 = \frac{9}{128(ik_a\rho)^2}, \tag{4.F-41b}$$

and in addition, the expansion of the following variables is needed:

$$\sqrt{\lambda}\gamma_a = -\sqrt{2}k_a^{3/2}\,\xi\,\left(1 - \tfrac{3}{4}\xi^2 - \tfrac{1}{32}\xi^4 - ..\right). \tag{4.F-42}$$

The relation between the differentials is given by equation 4.F-35a and 4.F-37c:

$$d\lambda = -2k_a\xi d\xi, \tag{4.F-43}$$

and the function f_ξ^{TE} then becomes:

$$f_\xi^{TE}(\xi) = A_b^{TE}\,\xi^2\left[1 + h_1 + h_2 + \left(e_1 - \tfrac{3}{4} + e_1h_1 + \tfrac{1}{4}h_1\right)\xi^2 + \left(e_2 - \tfrac{3}{4}e_1 - \tfrac{1}{32}\right)\xi^4 + ..\right], \tag{4.F-44a}$$

where

$$A_b^{TE} = -\omega\mu\frac{4k_a^{5/2}}{k^2\,(1-n^2)}\sqrt{\frac{1}{\pi\rho}}\mathrm{e}^{-i\frac{\pi}{4}}\mathrm{e}^{ikh\sqrt{1-n^2}}. \tag{4.F-44b}$$

An asymptotic series for the TE integral is now obtained using equation 4.F-38, 4.F-44, and the relations in equation 4.A-2 and 4.A-4:

$$\mathcal{I}_{A0,b}^{TE} \sim -\frac{2\,i\omega\mu\,ik_a\,\mathrm{e}^{ik_a\rho+ikh\sqrt{1-n^2}}}{k^2\rho^2\,(1-n^2)}\left[1 + \tfrac{1}{ik_a\rho}\left(-1 + \tfrac{3}{2}e_1\right) + \tfrac{1}{(ik_a\rho)^2}\left(\tfrac{15}{4}e_2 - \tfrac{21}{8}e_1\right) + ..\right]. \tag{4.F-45}$$

The sign has been chosen in accordance with the slope of the steepest descent curve in the α-plane. Note that the third-order term only contains factors from the expansion of the exponential function in equation 4.F-40. Note moreover that each successive term in ξ^2 in the integral corresponds to a multiplication with $1/ik_1\rho$ in the asymptotic series. Terms from the Hankel function in equation 4.F-44 that give higher-order terms than those considered in the expansion can thus be ignored when deriving equation 4.F-44. An expression for $\mathcal{I}_{A1,b}^{TE}$ is obtained by using equation 4.F-33:

$$\mathcal{I}_{A1,b}^{TE} \sim -\frac{2\,i\omega\mu\,\mathrm{e}^{ik_a\rho+ikh\sqrt{1-n^2}}}{k^2\rho^2\,(1-n^2)}\left[1 + \tfrac{1}{ik_a\rho}\tfrac{3}{2}e_1 + \tfrac{1}{(ik_a\rho)^2}\left(\tfrac{15}{4}e_2 + \tfrac{3}{8}e_1\right) + ..\right]. \tag{4.F-46}$$

In the considerations for the combined models in section 4.6, the multiples in the water column are expressed as a power series in terms of the sea-surface reflection coefficient. From equation 4.31a and 4.32a it is found that

$$[R_{si}^{TE}(\lambda)]^2 = \left(\frac{\gamma - \gamma_a}{\gamma + \gamma_a}\right)^2 = \frac{\gamma^4 - 4\gamma^3\gamma_a + 6\gamma^2\gamma_a^2 - 4\gamma\gamma_a^3 + \gamma_a^4}{k^4(1-n^2)^2}. \tag{4.F-47}$$

The part that contributes to the branch-point integral becomes

$$R^{TE}|_b^2 = \frac{-2\gamma\gamma_a}{k^2(1-n^2)}\,2\left[1 + \frac{2n^2}{1-n^2}\left(2\xi^2 - \xi^4\right)\right], \tag{4.F-48}$$

which follows from equation 4.F-39c and the substitutions in equation 4.F-35 and 4.F-37. For the interface between air and seawater, the refraction index is $n_0 \approx 0$. Thus the approximation $R^2 \approx 2R$ (where the TE superscript and b subscript have been omitted for simplicity), can be used for the branch-point contribution that describes the first multiple of the sea-surface reflection. By repeating the above procedure for higher powers of the reflection coefficients, one readily obtains that $R^3 \approx 3R$, $R^4 \approx 4R$, and so on.

4.F.4 TM mode

Consider the expression in equation 4.29c with a reflection response as given in equation 4.32b. The function $f_{TM}(\lambda)$ for the TM mode is, cf. equation 4.1:

$$f_{TM}(\lambda) = \frac{\omega\mu}{2k^2(1-n^4)}\,\lambda\gamma\,\frac{\gamma_a^2 - 2n^2\gamma\gamma_a + n^4\gamma}{k_p^2-\lambda^2}\,H_0^-(\lambda\rho)\,\mathrm{e}^{i\gamma h}, \tag{4.F-49a}$$

where k_p is as given in equation 4.33. Since only even-order terms contribute to the integral, this expression reduces to

$$f_{TM}(\lambda)|_b = \frac{-n^2\omega\mu}{k^2(1-n^4)}\,\lambda\,\frac{\gamma_a\gamma^2}{k_p^2-\lambda^2}\,H_0^-(\lambda\rho)\,\mathrm{e}^{i\gamma h}. \tag{4.F-49b}$$

When the asymptotic expansion of the Hankel function in equation 4.D-30 is inserted into equation 4.F-49b, one gets:

$$f_{TM}(\lambda)|_b = \frac{-n^2\omega\mu}{k^2(1-n^4)}\sqrt{\frac{2}{\pi\rho}}\mathrm{e}^{-i\pi/4}\,\sqrt{\lambda}\gamma_a\,\frac{\gamma^2}{k_p^2-\lambda^2}\,\left[1+\tfrac{1}{8i\lambda\rho}+\tfrac{9}{128(i\lambda\rho)^2}+..\right]\mathrm{e}^{i\gamma h}. \tag{4.F-49c}$$

The series expansion of $1/(k_p^2-\lambda^2)$ is

$$\frac{1}{\lambda^2-k_p^2} = \frac{1+n^2}{n^2k_a^2}\left[1+p_1\xi^2+p_2\xi^4+..\right], \tag{4.F-50a}$$

where the shorthand notation

$$p_1 = \frac{2(1+n^2)}{n^2} \quad \text{and} \quad p_2 = \frac{4+7n^2+3n^4}{n^4}, \tag{4.F-50b}$$

has been used. The vertical wavenumber squared is

$$\gamma^2 = k^2(1-n^2)\left[1+c_1\xi^2+c_2\xi^4\right], \quad \text{where} \quad c_1 = \frac{2n^2}{1-n^2} \quad \text{and} \quad c_2 = -\frac{1}{2}c_1. \tag{4.F-51}$$

Series representations of the exponential factor, the terms in the Hankel function, and the term $\sqrt{\lambda}\gamma_a$, have been obtained in equation 4.F-40, 4.F-41, and 4.F-42, respectively. Inserted into equation 4.F-49c, the above expansions and the relation between the differentials in equation 4.F-43 imply that the function $f_\xi^{TM}(\xi)$ becomes:

$$f_\xi^{TM}(\xi) = A_b^{TM}\,\xi^2\left[1+h_1+h_2+\left(q_1-\tfrac{3}{4}+q_1h_1+\tfrac{1}{4}h_1\right)\xi^2+\left(q_2-\tfrac{3}{4}q_1-\tfrac{1}{32}\right)\xi^4+..\right], \tag{4.F-52a}$$

where

$$q_1 = e_1 + c_1 + p_1 \quad \text{and} \quad q_2 = e_2 + c_2 + p_2 + c_1p_1 + e_1c_1 + e_1p_1, \tag{4.F-52b}$$

and the amplitude factor is

$$A_b^{TM} = 4\omega\mu\sqrt{\frac{k_a}{\pi\rho}}\mathrm{e}^{-i\frac{\pi}{4}}\mathrm{e}^{ikh\sqrt{1-n^2}}. \tag{4.F-52c}$$

The integral is then calculated by inserting the expression for $f_\xi^{TM}(\xi)$ into equation 4.F-38:

$$\mathcal{I}_{A0,b}^{TM} \sim -\frac{2\omega\mu}{k_a\rho^2}\mathrm{e}^{ik_a\rho+ikh\sqrt{1-n^2}}\left[1 + \tfrac{1}{ik_a\rho}\left(-1+\tfrac{3}{2}q_1\right) + \tfrac{1}{(ik_a\rho)^2}\left(\tfrac{15}{4}q_2 - \tfrac{21}{8}q_1\right) + ..\right]. \tag{4.F-53}$$

The first-order integral $\mathcal{I}_{A1,b}^{TM}$ is obtained from equation 4.F-53 by using equation 4.F-33:

$$\mathcal{I}_{A1,b}^{TM} \sim -\frac{2\omega\mu}{ik_a^2\rho^2}\mathrm{e}^{ik_a\rho+ikh\sqrt{1-n^2}}\left[1 + \tfrac{1}{ik_a\rho}\tfrac{3}{2}q_1 + \tfrac{1}{(ik_a\rho)^2}\left(\tfrac{15}{4}q_2 + \tfrac{3}{8}q_1\right) + ..\right]. \tag{4.F-54}$$

4.F.5 Accounting for the influence of the TM pole

The asymptotic expansions in equation 4.F-53 and 4.F-54 are useless for small n. This is due to the pole in close vicinity to the branch point for this case as observed in Figure 4.4. The procedure in section 4.2.4 is applied to obtain a separate expression for the branch-point contribution due to the pole. This contribution is given by equation 4.44 for both the zeroth- (residue Γ_0) and first-order (residue Γ_1) integrals. The residue Γ_0 is found from equation 4.F-49b and the relation in equation 4.15:

$$\Gamma_0 = \lim_{\lambda\to k_p}\left[\tfrac{\lambda^2-k_p^2}{2k_p}f(\lambda)\right] = \frac{\omega\mu n^2}{2k^2(1-n^4)}\sqrt{k_a^2-k_p^2}\,(k^2-k_p^2)\,H_0^-(k_p\rho)\,\mathrm{e}^{i\sqrt{k^2-k_p^2}\,h}, \tag{4.F-55}$$

where $k_p = k_a/\sqrt{1+n^2}$.

In order to obtain an expression for $\mathcal{I}_{A0,bc}^{TM}$, a series expansion of equation 4.44 is performed. The terms in this expansion are subtracted from the corresponding terms in the expression given by equation 4.F-53. The locations of the pair of poles in the ξ-domain are given by (cf. equation 4.40 and 4.F-36):

$$\xi_p^2 = 1 - \frac{1}{\sqrt{1+n^2}}\,, \tag{4.F-56}$$

and thus, the residue in equation 4.F-55 can be written as

$$\Gamma_0 = \frac{\omega\mu\sqrt{k_a}\,n^2\mathrm{e}^{-i\pi/4}}{\sqrt{2\pi\rho}(1-n^4)}\xi_p\frac{\sqrt{1+\sqrt{1+n^2}}}{1+n^2}\left[1 + \tfrac{\sqrt{1+n^2}}{8ik_a\rho} + \tfrac{9(1+n^2)}{128(ik_a\rho)^2} + ..\right]\mathrm{e}^{ikh\left(1+n^2\right)^{-1/2}}. \tag{4.F-57}$$

4.F Single-interface branch-point contributions

The series expansion of the error function times the Gaussian function in equation 4.44 is given in equation 4.17, and in terms of τ_p it becomes ($\xi = \kappa\tau$):

$$\mathrm{e}^{-\tau_p^2}\mathrm{erfc}(-i\tau_p) \sim \frac{i}{\sqrt{\pi}\tau_p}\left[1 + \frac{1}{2\tau_p^2} + \frac{3}{4\tau_p^4} + ..\right]. \tag{4.F-58}$$

From equation 4.45 one gets

$$\frac{1}{\tau_p^2} = \frac{\kappa^2\sqrt{1+n^2}}{\sqrt{1+n^2}-1}\,, \tag{4.F-59}$$

and the series expansion of the contribution from the pole then becomes:

$$\mathcal{I}^{TM}_{A0,bp} \sim -\frac{i\omega\mu}{\rho}\frac{\sqrt{2}n^2\sqrt{1+\sqrt{1+n^2}}}{(1+n^2)(1-n^4)}\mathrm{e}^{ik_a\rho+ikh\left(1+n^2\right)^{-1/2}}\left[1 + \tfrac{1}{ik_a\rho}\mathcal{U}_1 + \tfrac{1}{(ik_a\rho)^2}\mathcal{U}_2 + ..\right], \tag{4.F-60a}$$

where

$$\mathcal{U}_1 = \tfrac{1}{2}\sqrt{1+n^2}\left(\tfrac{1}{\sqrt{1+n^2}-1} + \tfrac{1}{4}\right), \tag{4.F-60b}$$

$$\mathcal{U}_2 = \tfrac{1}{4}(1+n^2)\left(\tfrac{3}{(\sqrt{1+n^2}-1)^2} + \tfrac{1}{4(\sqrt{1+n^2}-1)} + \tfrac{9}{32}\right). \tag{4.F-60c}$$

In addition the exponent in equation 4.F-53 must be modified in order to compare terms with the expression in equation 4.F-60:

$$\mathrm{e}^{ikh\sqrt{1-n^2}} = \mathrm{e}^{ikh\left(1+n^2\right)^{-1/2}}\left[1 - \tfrac{1}{2}ikhn^4 + \tfrac{1}{4}ikhn^6 - \tfrac{1}{8}ikh\left(\tfrac{5}{2} - ikh\right)n^8 + ..\right]. \tag{4.F-61}$$

Now, the contribution from the branch point when the pole contribution is separated out becomes:

$$\mathcal{I}^{TM}_{A0,bc} = \mathcal{I}^{TM}_{A0,b} - \mathcal{I}^{TM}_{A0,bp} \sim \frac{i\omega\mu}{\rho}\mathrm{e}^{ik_a\rho+ikh\left(1+n^2\right)^{-1/2}}\left[U_0 + \tfrac{1}{ik_a\rho}U_1 + \tfrac{1}{(ik_a\rho)^2}U_2 + ..\right], \tag{4.F-62a}$$

where:

$$U_0 = 2n^2\left[1 - \tfrac{7}{8}n^2 + \tfrac{235}{128}n^4 - \tfrac{1731}{1024}n^6 + \tfrac{86451}{32768}n^8 + ..\right], \tag{4.F-62b}$$

$$U_1 = n^4\left[\left(\tfrac{137}{64} + ikh\right) - \left(\tfrac{35}{256} + \tfrac{1}{2}ikh\right)n^2 + \left(\tfrac{37151}{16384} + \tfrac{1}{4}ikh\left\{\tfrac{5}{2} - ikh\right\}\right)n^4 + ..\right], \tag{4.F-62c}$$

$$U_2 = -n^4\left[\left(\tfrac{949}{512} + ikh\right) + \left(\tfrac{1525}{16384} - \tfrac{1}{4}ikh\left\{11 + 3ikh\right\}\right)n^2 + ..\right]. \tag{4.F-62d}$$

The contribution from the pole in $\mathcal{I}^{TM}_{A1,b}$ is found in the same manner as for $\mathcal{I}^{TM}_{A0,b}$. The only difference is an extra division of k_p and that the residue consists of the Hankel function of first order:

$$\Gamma_1 = \frac{\omega\mu n^2\mathrm{e}^{-i3\pi/4}}{\sqrt{2\pi k_a\rho}\,(1-n^4)}\xi_p\sqrt{\frac{1+\sqrt{1+n^2}}{1+n^2}}\left[1 - \tfrac{3\sqrt{1+n^2}}{8ik_a\rho} - \tfrac{15(1+n^2)}{128(ik_a\rho)^2} - ..\right]\mathrm{e}^{ikh\left(1+n^2\right)^{-1/2}}. \tag{4.F-63}$$

The pole contribution is given in equation 4.44. A series expansion of this expression leads to

$$\mathcal{I}^{TM}_{A1,bp} \sim -\frac{\omega\mu}{k_a\rho}\frac{\sqrt{2}n^2}{(1-n^4)}\sqrt{\frac{1+\sqrt{1+n^2}}{1+n^2}}\mathrm{e}^{ik_a\rho+\frac{ikh}{\sqrt{1+n^2}}}\left[1+\tfrac{1}{ik_a\rho}\mathcal{V}_1+\tfrac{1}{(ik_a\rho)^2}\mathcal{V}_2+..\right], \tag{4.F-64a}$$

where

$$\mathcal{V}_1 = \tfrac{1}{2}\sqrt{1+n^2}\left(\tfrac{1}{\sqrt{1+n^2}-1}-\tfrac{3}{4}\right), \tag{4.F-64b}$$

$$\mathcal{V}_2 = \tfrac{1}{4}(1+n^2)\left(\tfrac{3}{(\sqrt{1+n^2}-1)^2}-\tfrac{3}{4(\sqrt{1+n^2}-1)}-\tfrac{15}{32}\right). \tag{4.F-64c}$$

The branch-point contribution to the integral $\mathcal{I}^{TM}_{A1}$ when the pole contribution is separated out then becomes:

$$\mathcal{I}^{TM}_{A1,bc} = \mathcal{I}^{TM}_{A1,b} - \mathcal{I}^{TM}_{A1,bp} \sim \frac{\omega\mu}{k_a\rho}\mathrm{e}^{ik_a\rho+ikh\left(1+n^2\right)^{-1/2}}\left[V_0+\tfrac{1}{ik_a\rho}V_1+\tfrac{1}{(ik_a\rho)^2}V_2+..\right], \tag{4.F-65a}$$

where

$$V_0 = 2n^2\left[1-\tfrac{3}{8}n^2+\tfrac{163}{128}n^4-\tfrac{615}{1024}n^6+\tfrac{48163}{32768}n^8+..\right], \tag{4.F-65b}$$

$$V_1 = n^4\left[\left(\tfrac{113}{64}+ikh\right)+\left(\tfrac{25}{256}-\tfrac{1}{2}ikh\right)n^2+\left(\tfrac{27983}{16384}+\tfrac{1}{4}ikh\left\{\tfrac{5}{2}-ikh\right\}\right)n^4+..\right], \tag{4.F-65c}$$

$$V_2 = n^4\left[-\tfrac{105}{512}+\left(\tfrac{315}{16384}+\tfrac{3}{4}ikh\left\{3+ikh\right\}\right)n^2+..\right]. \tag{4.F-65d}$$

4.G Saddle-point contributions

In this section, expressions with two terms for the saddle-point contributions are derived. Consider the integral in equation 4.1 in terms of the angle variable θ where the function $f(\theta)$ is in angular coordinates after the transformation in equation 4.56. The function ϕ is given by equation 4.57, and at the saddle point:

$$\phi(\theta_s) = ik, \quad \phi'(\theta_s) = 0, \quad \phi''(\theta_s) = -ik, \quad \phi'''(\theta_s) = 0, \quad \text{and} \quad \phi^{IV}(\theta_s) = ik, \tag{4.G-66}$$

where the subscript 1 on the wavenumber has been ignored since the derivations that follow can be used for saddle-point contributions in both the single-interface and thin-layer case. The saddle-point contribution is given by equation 4.4. The second term in the expansion is given by equation 4.5 which reduces to

$$\psi(\theta_s) = -\frac{f''(\theta_s)}{f(\theta_s)} - \frac{1}{4}, \tag{4.G-67}$$

for the angular-spectrum representation when inserting the relations in equation 4.G-66. From writing $f(\theta) = h(\theta)R(\theta)$ and expressing the derivative of the reflection coefficient as

$$R'(\theta) = R(\theta)y(\theta), \tag{4.G-68}$$

the derivatives of $f(\theta)$ become

$$\frac{f'}{f} = \frac{h'}{h} + y \quad \text{and} \quad \frac{f''}{f} = \frac{h''}{h} + \left(2\frac{h'}{h} + y\right) y + y'. \tag{4.G-69}$$

4.G.1 TE-mode functions

The function h_0^{TE} in the integral $\mathcal{I}_{A0}^{TE}$ is derived from equation 4.29a and the transformation in equation 4.56:

$$h_0^{TE}(\theta) = \frac{\omega\mu}{2}\sqrt{\frac{2k}{\pi\rho}}\mathrm{e}^{-i\pi/4}\,\sqrt{\sin\theta}\left(1 + \frac{1}{8ik\rho\sin\theta} + ..\right). \tag{4.G-70a}$$

Since the derivatives of the second-order term of h contribute to the third-order term, the second-order term is ignored in the calculation of the derivatives:

$$\left(\frac{1}{h_0}\frac{dh_0}{d\theta}\right)_1^{TE} = \frac{\cos\theta}{2\sin\theta} \quad \text{and} \quad \left(\frac{1}{h_0}\frac{d^2h_0}{d\theta^2}\right)_1^{TE} = -\frac{1}{4} - \frac{1}{4\sin^2\theta}, \tag{4.G-70b}$$

where the subscript 1 denotes that only the first-order term of h_0^{TE} is taken into account.

The integral $\mathcal{I}_{A1}^{TE}$ differs from $\mathcal{I}_{A0}^{TE}$ by a factor $1/ik\sin\theta$ and different weights in the asymptotic Hankel-function series (i.e., the factor 1/8 in the second term of equation 4.G-70a must be substituted by $-3/8$). The function h_1^{TE} then becomes

$$h_1^{TE}(\theta) = \frac{\omega\mu}{2ik}\sqrt{\frac{2k}{\pi\rho}}\mathrm{e}^{-i\pi/4}\,\frac{1}{\sqrt{\sin\theta}}\left(1 - \frac{3}{8ik\rho\sin\theta} + ..\right), \tag{4.G-70c}$$

and the derivatives of the first-order term are:

$$\left(\frac{1}{h_1}\frac{dh_1}{d\theta}\right)_1^{TE} = -\frac{\cos\theta}{2\sin\theta} \quad \text{and} \quad \left(\frac{1}{h_1}\frac{d^2h_1}{d\theta^2}\right)_1^{TE} = -\frac{1}{4} + \frac{3}{4\sin^2\theta}. \tag{4.G-70d}$$

4.G.2 TM-mode functions

As seen from equation 4.29 after applying the transformation in equation 4.56, the TM-mode h-functions differ from those of the TE mode by an extra factor $\cos^2\theta$:

$$h_0^{TM}(\theta) = \frac{\omega\mu}{2}\sqrt{\frac{2k}{\pi\rho}}\mathrm{e}^{-i\pi/4}\,\sqrt{\sin\theta}\cos^2\theta\left(1 + \frac{1}{8ik\rho\sin\theta} + ..\right). \tag{4.G-70e}$$

When ignoring the second-order term in h_0^{TM}, one gets

$$\left(\frac{1}{h_0}\frac{dh_0}{d\theta}\right)_1^{TM} = \frac{1 - 5\sin^2\theta}{2\sin\theta\cos\theta} \quad \text{and} \quad \left(\frac{1}{h_0}\frac{d^2h_0}{d\theta^2}\right)_1^{TM} = -\frac{17}{4} - \frac{1}{4\sin^2\theta} + 2\frac{\sin^2\theta}{\cos^2\theta}. \tag{4.G-70f}$$

The first-order TM integral differs from the zeroth-order integral by the factor $1/ik\sin\theta$ and different weights in the Hankel function. Accounting for this, h_1^{TM} becomes

$$h_1^{TM}(\theta) = \frac{\omega\mu}{2ik}\sqrt{\frac{2k}{\pi\rho}}\mathrm{e}^{-i\pi/4}\,\frac{\cos^2\theta}{\sqrt{\sin\theta}}\left(1 - \frac{3}{8ik\rho\sin\theta} + ..\right), \tag{4.G-70g}$$

and the derivatives of the first-order term are:

$$\left(\frac{1}{h_1}\frac{dh_1}{d\theta}\right)_1^{TM} = -\frac{1+3\sin^2\theta}{2\sin\theta\cos\theta} \quad \text{and} \quad \left(\frac{1}{h_1}\frac{d^2h_1}{d\theta^2}\right)_1^{TM} = -\frac{1}{4} + \frac{3}{4\sin^2\theta} + 2\frac{\sin^2\theta}{\cos^2\theta}. \tag{4.G-70h}$$

4.G.3 General expressions

The saddle-point contributions are found using equation 4.4 with the appropriate functions in the integrand, i.e., $f(\theta_s) = h(\theta_s)R(\theta_s)$ where R is the reflection response and where the various h-functions are given in equation 4.G-70, and $\phi(\theta_s)$ is as given in equation 4.G-66. Then:

$$\mathcal{I}_{A0,s}^{TE} \sim -i\omega\mu\,\frac{e^{ikr}}{r}\,R_{TE}(\theta_s)\,\left[1+\frac{1}{ikr}\Psi_0^{TE}(\theta_s)+..\right], \tag{4.G-71a}$$

$$\mathcal{I}_{A1,s}^{TE} \sim -i\omega\mu\,\frac{e^{ikr}}{r}\,R_{TE}(\theta_s)\,\frac{1}{ik\sin\theta_s}\,\left[1+\frac{1}{ikr}\Psi_1^{TE}(\theta_s)+..\right], \tag{4.G-71b}$$

$$\mathcal{I}_{A0,s}^{TM} \sim -i\omega\mu\,\frac{e^{ikr}}{r}\,R_{TM}(\theta_s)\,\cos^2\theta_s\,\left[1+\frac{1}{ikr}\Psi_0^{TM}(\theta_s)+..\right], \tag{4.G-71c}$$

$$\mathcal{I}_{A1,s}^{TM} \sim -i\omega\mu\,\frac{e^{ikr}}{r}\,R_{TM}(\theta_s)\,\frac{\cos^2\theta_s}{ik\sin\theta_s}\,\left[1+\frac{1}{ikr}\Psi_1^{TM}(\theta_s)+..\right]. \tag{4.G-71d}$$

By inserting the derivatives of the h-functions (equation 4.G-70) into equations 4.G-69 and 4.G-67, and accounting for the second-order Hankel-function term ($1/8ik\rho\sin\theta_s$ for H_0 and $-3/8ik\rho\sin\theta_s$ for H_1), the following expressions for the Ψ-variables are obtained:

$$\Psi_0^{TE}(\theta_s) = \frac{1}{2}\left[\frac{\cos\theta_s}{\sin\theta_s} + y_{TE}(\theta_s)\right]y_{TE}(\theta_s) + \frac{1}{2}y'_{TE}(\theta_s), \tag{4.G-72a}$$

$$\Psi_1^{TE}(\theta_s) = \frac{1}{2}\left[-\frac{\cos\theta_s}{\sin\theta_s} + y_{TE}(\theta_s)\right]y_{TE}(\theta_s) + \frac{1}{2}y'_{TE}(\theta_s), \tag{4.G-72b}$$

$$\Psi_0^{TM}(\theta_s) = -2 + \frac{\sin^2\theta_s}{\cos^2\theta_s} + \frac{1}{2}\left[\frac{1-5\sin^2\theta_s}{\sin\theta_s\cos\theta_s} + y_{TM}(\theta_s)\right]y_{TM}(\theta_s) + \frac{1}{2}y'_{TM}(\theta_s), \tag{4.G-72c}$$

$$\Psi_1^{TM}(\theta_s) = \frac{\sin^2\theta_s}{\cos^2\theta_s} + \frac{1}{2}\left[-\frac{1+3\sin^2\theta_s}{\sin\theta_s\cos\theta_s} + y_{TM}(\theta_s)\right]y_{TM}(\theta_s) + \frac{1}{2}y'_{TM}(\theta_s). \tag{4.G-72d}$$

The expressions for the y-functions are found from the reflection coefficients (cf. equation 4.G-68). Note that the first-order term of the TM mode gets small as $\theta_s \to \pi/2$, and that the second-order term gets large. However, the squared cosine factor in the denominator of the second term is cancelled by the squared cosine term in the overall expression. Thus, the second-order term is still bounded.

4.G.4 Single interface

The reflection coefficients in case of a single interface are rewritten into angular coordinates by using the transformation in equation 4.56 on the expressions in equation 4.31:

$$R_{si}^{TE}(\theta) = \frac{\cos\theta - \sqrt{n^2 - \sin^2\theta}}{\cos\theta + \sqrt{n^2 - \sin^2\theta}}, \tag{4.G-73a}$$

$$R_{si}^{TM}(\theta) = \frac{-n^2\cos\theta + \sqrt{n^2 - \sin^2\theta}}{n^2\cos\theta + \sqrt{n^2 - \sin^2\theta}}. \tag{4.G-73b}$$

The saddle-point contribution in the single-interface case is then obtained by inserting the values of these reflection coefficients at the saddle point into equation 4.G-71. The functions y_{TE} and y_{TM} that are needed in equation 4.G-72 to compute the second-order term of the saddle-point expansion then become:

$$y_{TE} = \tfrac{2\sin\theta}{\sqrt{n^2-\sin^2\theta}}, \qquad y_{TM} = \tfrac{2n^2\sin\theta}{\sqrt{n^2-\sin^2\theta}}\tfrac{1}{(1+n^2)\sin^2\theta - n^2}, \tag{4.G-74a}$$

$$y'_{TE} = \tfrac{2n^2\cos\theta}{(n^2-\sin^2\theta)^{3/2}}, \qquad y'_{TM} = y_{TM}\,\tfrac{\cos\theta}{\sin\theta}\left[\tfrac{n^2}{n^2-\sin^2\theta} - \tfrac{2\left(n^2+1\right)\sin^2\theta}{(1+n^2)\sin^2\theta - n^2}\right]. \tag{4.G-74b}$$

The second-order terms in the asymptotic expansion are obtained by inserting the expressions in equation 4.G-74 into equation 4.G-72. For the TE mode the resulting expressions simplify to

$$\Psi_0^{TE}(\theta_s) = \tfrac{\cos\theta_s}{\sqrt{n^2-\sin^2\theta_s}} + \tfrac{2\sin^2\theta_s}{n^2-\sin^2\theta_s} + \tfrac{n^2\cos\theta_s}{(n^2-\sin^2\theta_s)^{3/2}}, \tag{4.G-75a}$$

$$\Psi_1^{TE}(\theta_s) = -\tfrac{\cos\theta_s}{\sqrt{n^2-\sin^2\theta_s}} + \tfrac{2\sin^2\theta_s}{n^2-\sin^2\theta_s} + \tfrac{n^2\cos\theta_s}{(n^2-\sin^2\theta_s)^{3/2}}. \tag{4.G-75b}$$

4.G.5 Thin layer

The reflection coefficients in the thin-layer case in angular coordinates are given by equation 4.62. The functions $y_{TE}(\theta)$ and $y_{TM}(\theta)$ in equation 4.G-68 are:

$$y_{TE}(\theta) = \frac{2i\sin\theta + 4k_1d_2\sin\theta\cos\theta}{2i\cos\theta + k_1d_2\left[(1+n_1^2) - 2\sin^2\theta\right]}, \tag{4.G-76a}$$

$$y_{TM}(\theta) = \frac{2\sin\theta\cos\theta}{\sin^2\theta - n_1^2\left(1+n_1^2\right)^{-1}} + \frac{2in_1^2\sin\theta + 2k_1d_2(1+n_1^4)\sin\theta\cos\theta}{2in_1^2\cos\theta + k_1d_2\left[n_1^2(1+n_1^2) - (1+n_1^4)\sin^2\theta\right]}. \tag{4.G-76b}$$

The saddle-point contributions are on the same form as in equation 4.G-71, but the wavenumber is now k_1 and the reflection coefficients are those in equation 4.62. In addition the second-order terms are found using equation 4.G-76. By writing the y-functions in terms of their fractions

$$y_{TE} = \frac{y_{N0}}{y_{D0}} \quad \text{and} \quad y_{TM} = y_{TM,1} + y_{TM,2} = \frac{y_{N1}}{y_{D1}} + \frac{y_{N2}}{y_{D2}}, \tag{4.G-76c}$$

their derivatives can be expressed as

$$y'_{TE} = y_{TE}\left[\frac{y'_{N0}}{y_{N0}} - \frac{y'_{D0}}{y_{D0}}\right] \quad \text{and} \quad y'_{TM} = \sum_{j=1}^{2} y_{TM,j}\left[\frac{y'_{Nj}}{y_{Nj}} - \frac{y'_{Dj}}{y_{Dj}}\right], \tag{4.G-77a}$$

where the values at the saddle point are needed:

$$y'_{N0}(\theta_s) = 2i\cos\theta_s + 4k_1d_2\left(\cos^2\theta_s - \sin^2\theta_s\right), \tag{4.G-77b}$$
$$y'_{D0}(\theta_s) = -2i\sin\theta_s - 4k_1d_2\sin\theta_s\cos\theta_s, \tag{4.G-77c}$$
$$y'_{N1}(\theta_s) = 2\left(\cos^2\theta_s - \sin^2\theta_s\right), \tag{4.G-77d}$$
$$y'_{D1}(\theta_s) = 2\sin\theta_s\cos\theta_s, \tag{4.G-77e}$$
$$y'_{N2}(\theta_s) = 2in_1^2\cos\theta_s + 2k_1d_2(1+n_1^4)\left(\cos^2\theta_s - \sin^2\theta_s\right), \tag{4.G-77f}$$
$$y'_{D2}(\theta_s) = -2in_1^2\sin\theta_s - 2k_1d_2(1+n_1^4)\sin\theta_s\cos\theta_s. \tag{4.G-77g}$$

4.H The transmitted field through one interface

The integrals that describe the transmitted fields through one interface can be written as (cf. equation 4.29)

$$\mathcal{I}^{TE}_{A0,t} = \frac{\omega\mu}{2}\int_{-\infty}^{\infty} d\lambda\,\frac{\lambda}{\gamma}\,H_0^-(\lambda\rho)\,t_{TE}(\lambda)\,\mathrm{e}^{i\lambda\rho+i\gamma h_s+i\gamma_a h_a}, \tag{4.H-78a}$$
$$\mathcal{I}^{TE}_{A1,t} = \frac{\omega\mu}{2}\int_{-\infty}^{\infty} d\lambda\,\frac{1}{\gamma}\,H_1^-(\lambda\rho)\,t_{TE}(\lambda)\,\mathrm{e}^{i\lambda\rho+i\gamma h_s+i\gamma_a h_a}, \tag{4.H-78b}$$
$$\mathcal{I}^{TM}_{A0,t} = \frac{\omega\mu}{2k^2}\int_{-\infty}^{\infty} d\lambda\,\lambda\gamma\,H_0^-(\lambda\rho)\,t_{TM}(\lambda)\,\mathrm{e}^{i\lambda\rho+i\gamma h_s+i\gamma_a h_a}, \tag{4.H-78c}$$
$$\mathcal{I}^{TM}_{A1,t} = \frac{\omega\mu}{2k^2}\int_{-\infty}^{\infty} d\lambda\,\gamma\,H_1^-(\lambda\rho)\,t_{TM}(\lambda)\,\mathrm{e}^{i\lambda\rho+i\gamma h_s+i\gamma_a h_a}, \tag{4.H-78d}$$

where h_s is the vertical distance from the interface to the source and h_a is the vertical distance from the interface to the receiver. The transmission coefficients are given by the expressions in equation 4.25. The function $\phi(\lambda)$, cf. equation 4.1, and its derivatives now become:

$$\phi(\lambda) = \frac{i}{r}\left(\lambda\rho + \gamma h_s + \gamma_a h_a\right), \tag{4.H-79a}$$
$$\phi'(\lambda) = \frac{i}{r}\left(\rho - \frac{\lambda}{\gamma}h_s - \frac{\lambda}{\gamma_a}h_a\right), \tag{4.H-79b}$$
$$\phi''(\lambda) = \frac{i}{r}\left(-\frac{k^2}{\gamma^3}h_s - \frac{k_a^2}{\gamma_a^3}h_a\right). \tag{4.H-79c}$$

The saddle point is then given by the equation

$$\rho - \frac{\lambda}{\gamma}h_s - \frac{\lambda}{\gamma_a}h_a = 0. \tag{4.H-80}$$

The horizontal and vertical wavenumbers can be parameterized as (DeSanto, 1992)

$$\lambda_s = k\sin\theta_s, \quad \gamma_s = k\cos\theta_s, \quad \text{and} \quad \gamma_a = k_a\cos\theta'_s, \tag{4.H-81}$$

since the distances in the triangles; h_s, ρ_1, and r_1 on the source side and h_a, ρ_2, and r_2 on the opposite side of the interface, are related as

$$h_s = r_1\cos\theta_s, \;\; \rho_1 = r_1\sin\theta_s, \;\; h_a = r_2\cos\theta'_s, \;\; \rho_2 = r_2\sin\theta'_s. \tag{4.H-82}$$

Note that r_1 is the distance travelled by a ray on the source side of the interface whereas r_2 is the distance travelled after the ray has been transmitted. From equation 4.H-80 the relation

$$\lambda_s = k\sin\theta_s = k\frac{\rho}{r_1 + \frac{1}{n}r_2} \tag{4.H-83}$$

where $n = k_a/k$ is obtained. By using Snell's law, $k\sin\theta = k_a\sin\theta'$, the following relations are obtained from equation 4.H-79:

$$r\phi(\lambda_s) = ikr_1 + ik_a r_2 \quad \text{and} \quad r\phi''(\lambda_s) = -i\left[\frac{r_1}{k}\frac{1}{\cos^2\theta_s} + \frac{r_2}{k_a}\frac{1}{\cos^2\theta'_s}\right]. \tag{4.H-84}$$

By plugging into the formula in equation 4.4 the first term in the saddle-point expansion is found to be

$$\mathcal{I}^{TE}_{A0,t} \sim -i\omega\mu\,\frac{\mathrm{e}^{ikr_1+ik_a r_2}}{r_t}\,t_{TE}(\theta_s), \tag{4.H-85a}$$

$$\mathcal{I}^{TE}_{A1,t} \sim -\frac{i\omega\mu}{ik}\,\frac{\mathrm{e}^{ikr_1+ik_a r_2}}{r_t}\,t_{TE}(\theta_s)\,\frac{1}{\sin\theta_s}, \tag{4.H-85b}$$

$$\mathcal{I}^{TM}_{A0,t} \sim -i\omega\mu\,\frac{\mathrm{e}^{ikr_1+ik_a r_2}}{r_t}\,t_{TM}(\theta_s)\,\cos^2\theta_s, \tag{4.H-85c}$$

$$\mathcal{I}^{TM}_{A1,t} \sim -\frac{i\omega\mu}{ik}\,\frac{\mathrm{e}^{ikr_1+ik_a r_2}}{r_t}\,t_{TM}(\theta_s)\,\frac{\cos^2\theta_s}{\sin\theta_s}, \tag{4.H-85d}$$

where

$$r_t = \sqrt{\left(r_1 + \tfrac{1}{n}r_2\right)\left[r_1 + \left(\frac{\cos\theta_s}{\cos\theta'_s}\right)^2\tfrac{1}{n}r_2\right]}. \tag{4.H-86}$$

4.I Separation of the TE and TM modes

From equation 4.18 it is seen that if the fields are measured at an azimuth angle (with the source direction) other than 0° and 90°, the field integrals can be obtained from measured data if one has access to the TE and TM parts separately:

$$\mathcal{I}^{TM}_{A0} + \mathcal{I}^{TE}_{A0} = \frac{1}{c_h}\left(\frac{E_\rho}{\cos\beta} - \frac{E_\beta}{\sin\beta}\right), \quad \text{where} \quad c_h = -\frac{Il_x}{4\pi}. \tag{4.I-87a}$$

This furthermore implies that

$$\mathcal{I}_{A1}^{TM} = -\frac{\rho E_\beta^{TM}}{c_h \sin\beta} \quad \text{and} \quad \mathcal{I}_{A1}^{TE} = \frac{\rho E_\rho^{TE}}{c_h \cos\beta}. \tag{4.I-87b}$$

The TE and TM part of the measured horizontal electric field components can be separated by using the procedure described in Løseth and Ursin (2007). In order to do this, the horizontal electric field components must be known in a 2-D plane on the seabed. If this is the case, the data can be transformed into the wavenumber domain and rotated using the eigenvector matrix described in Løseth and Ursin (2007). The resulting upgoing and downgoing TE- and TM-field quantities can be transformed back to the space domain separately. Hence the TE and TM modes are separated.

In marine CSEM the interesting mode to measure is often the TM mode since this mode can detect a possible thin resistive layer. The presence of a sea-surface interface normally increases the thin-layer response. Since the vertical electric field (E_z) is a pure TM mode (Kong, 2000), an alternative to measuring the horizontal fields in a 2-D manner on the seabed is to measure the E_z-component.

The E_z-response can also be derived by measuring the horizontal derivatives of the horizontal magnetic field components. By using Ampère's law:

$$E_z = \frac{i}{\omega\tilde{\varepsilon}} \frac{1}{\rho} \left[\frac{\partial(\rho H_\beta)}{\partial\rho} - \frac{\partial H_\rho}{\partial\beta} \right]. \tag{4.I-88}$$

TM responses are furthermore obtained by measuring quantities that when combined correspond to derivatives of the E_z-response. In this case one can measure horizontal magnetic field components and vertical changes in the horizontal electric field components or horizontal derivatives of the horizontal electric field components. This follows directly from Faraday's law or Gauss' law, respectively:

$$\frac{\partial E_z}{\partial\beta} = \rho \left[i\omega\mu H_\rho + \frac{\partial E_\beta}{\partial z} \right], \tag{4.I-89a}$$

$$\frac{\partial E_z}{\partial\rho} = \left[-i\omega\mu H_\beta + \frac{\partial E_\rho}{\partial z} \right], \tag{4.I-89b}$$

$$\frac{\partial E_z}{\partial z} = -\frac{1}{\rho} \left[\frac{\partial(\rho E_\rho)}{\partial\rho} + \frac{\partial E_\beta}{\partial\beta} \right]. \tag{4.I-89c}$$

Similar relations can also be obtained for the TE response in terms of the vertical magnetic field component and its derivatives.

Chapter 5

Electromagnetic fields in planarly layered anisotropic media

L. O. Løseth and B. Ursin
Accepted for publication in Geophysical Journal International

Summary

This paper presents a method for calculating the electromagnetic field from a dipole source in stratified media with general anisotropy. The formulation can be applied to geophysical applications such as ground penetrating radar (GPR) and marine controlled source electromagnetic (CSEM) methods. In stratified media, the propagation of fields can be considered in the frequency-wavenumber domain. The resulting set of ordinary differential equations consists of a field vector, a system matrix, and a source vector. In each piecewise homogeneous region, the system matrix is given by the material properties and the horizontal slownesses. The vertical slownesses are the eigenvalues of the system matrix. A diagonalization of the system matrix transforms the field vector into a mode-field that contains upgoing and downgoing field constituents. For system matrices that account for general anisotropy, it is shown how the electromagnetic field from any of the four basic dipole types can be calculated at any desired position in the stratified medium. It is furthermore shown how the reflection and transmission response from a stack can be calculated by a recursive scheme. Potential numerical instabilities due to using propagators are avoided by using this recursion method. Due to an energy-flux normalization of the eigenvector matrices, the reciprocity relations for reflection and transmission of electromagnetic fields in general anisotropic media can be derived. Several other useful relations between the reflection and transmission matrices are obtained as well. The propagator method is dependent on the ability to calculate eigenvalues and eigenvectors of the system matrix for all layers. In simple cases with isotropy or trans-

verse isotropy in the direction of medium variation, the eigenvalue problem can be solved explicitly. These eigenvector matrices have useful properties, e.g., when processing data. The possibility to remove layers above or below the receiver layer follows from the decomposition of a field into upgoing and downgoing modes. The propagator theory was implemented in order to model anisotropy in marine CSEM. A modelling study shows that responses are affected by horizontal, vertical, and dipping anisotropy in different manners. This suggests that when anisotropy is present at a survey site, careful planning and interpretation are required in order to correctly account for the responses.

5.1 Introduction

Anisotropy is a phenomenon that occurs on various scales, and it is a concern or an advantage (depending on how it can be exploited), in a variety of geophysical applications such as ground penetrating radar (GPR), which is towards the high-frequency end of applications, and marine controlled source electromagnetic (CSEM) methods or SeaBed Logging (SBL), which are applications that use very low frequencies.

In electromagnetic surveying of the subsurface, anisotropy effects will almost certainly be encountered to some extent. Thus, it is important to have an understanding of how various forms of anisotropy will affect the measurements. In elastic theory, a lot of work on anisotropy has been performed. Helbig and Thomsen (2005) review its history in elastic wave propagation. One of their main points is that anisotropy in many cases can be exploited in the exploration. Anisotropic effects when measuring electromagnetic fields in geophysical applications have also been studied for quite some time. Much of this work has been for media with stratification and transverse isotropy in the same direction, e.g., Maillet (1947), O'Brien and Morrison (1967), Sinha and Bhattacharyya (1967), Kong (1972), Chlamtac and Abramovici (1981), and Edwards et al. (1984). Another type of anisotropy configuration that has been studied, is transverse isotropy in a direction normal to a layered structure, e.g., Li and Pedersen (1991) and Yu and Edwards (1992). Everett and Constable (1999) studied the effects of such anisotropy on CSEM data, and Yu et al. (1997) considered triaxial (orthorhombic) anisotropy. For the modelling of GPR, Carcione and Schoenberg (2000) and Carcione and Cavallini (2001) treated anisotropy with orthorhombic symmetry in 3-D structures. Arbitrary anisotropy was considered for the DC-resistivity method in layered media by Yin and Weidelt (1999). Their solution approach, in terms of potentials, was extended to the controlled source audio-magnetotelluric (CSAMT) method by Yin and Maurer (2001). Moreover, Yin (2006) considered the marine magnetotellurics (MT) forward problem formulated for stratified media with arbitrary anisotropy.

There are many material configurations in the subsurface that might lead to anisotropy (Negi and Saraf, 1989). It might be that there are some preferred directions in the subsurface

rocks, or some preferred orientation of grains in the sediments. Fine layering or a pronounced strike direction might lead to an effective anisotropy. Alternations of sandstone and shales may give reservoir anisotropies. Kennedy and Herrick (2004) examined the consequences of anisotropy in reservoir rocks.

Anisotropic material properties can often be described in terms of different parameters along three orthogonal coordinate axes in a principal coordinate system for each property. Anisotropic media are furthermore often classified as triclinic, meaning that the various material properties have no principal axes in common, monoclinic meaning that they have one principal axis in common, or orthorhombic, which means that the principal axes coincide for all the medium properties (Carcione and Schoenberg, 2000). When two parameters in the principal coordinate frame for an orthorhombic medium are equal, the medium can be referred to as transversely isotropic. In this case, we will refer to the axis with the distinct parameter as the axis of anisotropy. In optics, one often works with anisotropy related to crystal classes. It is in this case common to consider uniaxial and biaxial media meaning either one or two anisotropy axes, respectively (Born and Wolf, 1999; Huard, 1997; Stamnes and Sithambaranathan, 2001).

In the following we study stratified media with arbitrary anisotropy by using a matrix propagator method. There are several reasons for studying plane-layered media. The calculation of electromagnetic fields in such media is often useful in order to simplify a problem for interpretational purposes. In case of anisotropy, the added complication to the interpretation makes it worthwhile to study the effects of anisotropy in 1-D models. In addition, plane-layer modelling codes are fast and useful in e.g., more complicated modelling schemes and inversion. Plane-layer modelling is also important as a verification tool for numerical algorithms that handle 2-D or 3-D structures.

The matrix propagator methods are well known techniques for treating wave propagation in stratified media cf. Berremann (1972) in optics, Suchy and Altman (1975) in plasma physics, Kong (1972) for the geophysical electromagnetic problem in stratified media with transverse isotropy in the direction of medium changes, Griffiths and Steinke (2000) for wave propagation in locally periodic media, Kennett (1983) for seismic wave propagation, Ursin (1983) reviewing elastic and electromagnetic wave propagation, and White and Zhou (2006) for electroseismic prospecting in layered media.

However, to our knowledge, there has not been many applications of propagator techniques to electromagnetic problems in stratified media with general anisotropy and loss. In the following we derive equations that describe electromagnetic field propagation from any of the basic dipole sources in general anisotropic media. An implementation and application of the theory will be presented after the theory sections. During the derivation of the formalism, several useful relations for reflection and transmission in anisotropic media are derived.

The constitutive relations between the field variables are considered in terms of dyadic

material parameters (second rank tensors). It will be assumed that these dyads can be given in an orthogonal principal frame where they have only diagonal elements. This means that a rotation into another (e.g., the main) coordinate frame will preserve the symmetry of the dyads (Onsager, 1931). In geophysical applications where one uses low frequencies, the important material parameter will be the dyadic conductivity. In applications such as GPR, the electric permittivity is also important. Even if the magnetic permeability in many applications is assumed to be that of free space, all the material parameters are taken to be dyads for completeness. Nonlinear effects are however not considered, and the entries in the material dyads are assumed to be frequency-domain scalars, meaning that they are local parameters in space. It should also be noted that cross-coupling between electric and magnetic fields in the constitutive relations, so-called bianisotropy, is not considered since we expect these effects to be minimal in geophysical applications.

Since the medium varies in one direction, the electromagnetic fields are Fourier transformed into the frequency-wavenumber domain. This leads to a set of ordinary differential equations for the horizontal field components that can be written as in Ursin (1983). The set of equations involves a field vector that contains the horizontal electromagnetic field components, a system matrix (4×4) that describes the medium seen by one frequency-wavenumber component, and a source vector that can either be an infinitesimal electric or magnetic dipole. The system matrix will in the general anisotropic case have no nonzero elements, but because of the assumption of symmetric material parameters, it will contain symplectic symmetries (Chapman, 1994). The eigenvalues of the system matrix can be obtained by solving a quartic equation, and they correspond to vertical wavenumbers or slownesses (wavenumber divided by frequency). An alternative to solving the quartic equation, is solving the eigenvalue problem with standard routines from linear algebra libraries. To this end it should be noted that the structure of the matrix resembles the structure found in Hamiltonian systems (Bunse-Gerstner et al., 1992; Faßbender et al., 2001).

By introducing an ad-hoc field, we show that the eigenvector matrix, which is used for the similarity transform of the system matrix, should be chosen to be flux normalized. In lossless media this is straightforward, but in lossy media, a general "energy-invariant" which corresponds to the Poynting vector in the vertical direction for lossless media is introduced. A discussion of adjoint and conjugate fields for these purposes can be found in Altman and Suchy (1998).

In a homogeneous region the transformed physical field, using the flux-normalized eigenvectors, will be referred to as the upgoing and downgoing mode-field. From considering propagation of the mode-field in a homogeneous region, across a source, across an interface or a stack of layers, expressions for the electromagnetic field anywhere in the layered system are obtained. In homogeneous regions the differential equation is decoupled, and from the boundary conditions a description of reflection and transmission in terms of the eigenvector

matrices (2×2) at each side can be obtained. The reflection and transmission in a stack of layers can be described by a recursive scheme similar to that found in Kennett (1983), Chapman (2004), Ursin and Stovas (2002), and Stovas and Ursin (2003). By using the recursive expressions, one avoids the problem with exponentially large terms.

In order to handle a stack of layers that can contain general anisotropy as well as isotropy, various special cases of anisotropy configurations are considered. In addition to arbitrary anisotropy which normally leads to four different magnitudes of the system matrix' eigenvalues, up/down-symmetric media, meaning that the eigenvalues for the upgoing and downgoing mode-fields are equal in magnitude, are treated. A medium with transverse isotropy in the horizontal direction (TIH) is an example of an up/down-symmetric configuration. With transverse isotropy in the vertical direction (TIV), the eigenvalues and eigenvectors reduce to simple expressions. The polarization modes of the field vector do not couple at the interfaces in this case. Even if this might happen for some wavenumbers in more complicated anisotropic structures, it is only for TIV media and isotropic media that the eigenvalues of the system matrix correspond to pure polarization modes which are decoupled at interfaces between homogeneous regions for the entire wavenumber spectrum. The decoupling means that the 2×2-matrix problem reduces to a scalar problem.

In most of the realistic problems in geophysics, the source medium will be TIV or isotropic. Assuming that the receiver (the position where the field is calculated) layer has the same characteristics, but not necessarily is the same layer as that of the source, we derive explicit expressions for the electromagnetic fields. In these formulas, other layers than the source and receiver layers may have general anisotropy. It should be noted that the derived field components correspond to Green's functions when normalized properly. The expressions have been implemented in FORTRAN 90, and a modelling study of some scenarios from CSEM/SBL has been performed.

In the last appendix, an application of the separation into upgoing and downgoing field constituents is demonstrated. Depending on the choice of eigenvector matrix, it is possible to remove the effect of a stack of layers above the source in the measured electromagnetic field. In order to do this "free-surface" removal, the horizontal field components should be known throughout a 2-D plane.

5.2 Maxwell's equations

Maxwell's equations in the frequency domain are (cf. Stratton, 1941; Jackson, 1998; Kong, 2000)

$$\nabla \cdot \mathbf{D} = \rho, \tag{5.1a}$$

$$\nabla \cdot \mathbf{B} = 0, \tag{5.1b}$$

$$\nabla \times \mathbf{E} - i\omega\mathbf{B} = \mathbf{0}, \tag{5.1c}$$

$$\nabla \times \mathbf{H} + i\omega\mathbf{D} = \mathbf{J}, \tag{5.1d}$$

where $\mathbf{E}$ is the complex electric field intensity and $\mathbf{H}$ is the complex magnetic field intensity. The fields vary with position $\mathbf{x} = [x, y, z]$ and frequency ω. In the equations there are two more field quantities which are normally referred to as the electric displacement $\mathbf{D}$ and the magnetic induction $\mathbf{B}$. The density of free charges is described by ρ, and $\mathbf{J}$ is the current density. The charge conservation is described by the relation $-i\omega\rho = \nabla \cdot \mathbf{J}$. In conductive media it is convenient to split the current density $\mathbf{J}$ into a source term $\mathbf{J}_0$ and a conduction-current density $\mathbf{J}_c$. For macroscopic media it might furthermore be advantageous to introduce a magnetic source term $\mathbf{J}_{0M}$ into Faraday's law (equation 5.1c) which in this case is modified to $\nabla \times \mathbf{E} - i\omega\mathbf{B} = -\mathbf{J}_{0M}$. Charge conservation then leads to the modification $\nabla \cdot \mathbf{B} = \rho_M$ where ρ_M is the magnetic source-charge density. Although magnetic sources have not yet been found to exist, their introduction into the equations is justified by the equivalence principle (Kong, 2000). Since magnetic sources have been introduced, we will in the following refer to the source term $\mathbf{J}_0$ as the electric source.

In macroscopic media the constitutive relations between the field quantities might be very complicated (Nabighian, 1987; Jackson, 1998; Kong, 2000). In the following, nonlinear effects found in ferroelectric and ferromagnetic materials are not taken into account. Unless otherwise noted, only (piecewise) homogeneous regions are considered, and possible nonlocal effects in space of the material parameters are ignored. The constitutive relations may then be written as

$$\mathbf{D} = \boldsymbol{\varepsilon}(\omega)\mathbf{E}, \tag{5.2a}$$

$$\mathbf{B} = \boldsymbol{\mu}(\omega)\mathbf{H}, \tag{5.2b}$$

and in conductive media the relation between the conduction-current density $\mathbf{J}_c$ and the electric field (Ohm's law) is

$$\mathbf{J}_c = \boldsymbol{\sigma}(\omega)\mathbf{E}, \tag{5.2c}$$

where $\boldsymbol{\sigma}$ is the electric conductivity. The material parameters $\boldsymbol{\varepsilon}$, $\boldsymbol{\mu}$, and $\boldsymbol{\sigma}$ are dyads. The principal axes of the medium-property dyads can be illustrated using Figure 5.1, where the

main coordinate system xyz is sketched along with a rotated system $x'y'z'$. This rotated system may represent the principal axes of one of the material dyads, e.g., conductivity. The dyads, which are diagonal in the principal coordinate frame, will be symmetric after a rotation into a new coordinate frame when the principal axes are orthogonal (Onsager, 1931).

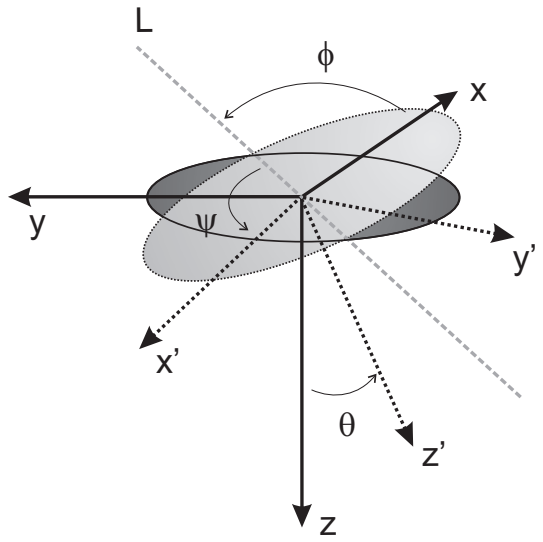

Figure 5.1: The main coordinate frame xyz and a principal system $x'y'z'$. Rotation from the main frame to the principal system (and vice versa) can be performed in terms of the Euler angles ϕ, θ, and ψ. L represents the line of nodes.

In the following it will be assumed that the material dyads have been rotated from their principal system into the main coordinate system. A procedure for doing so is presented in Appendix 5.A. To simplify notation, the permittivity and conductivity can be written as a complex electric permittivity

$$\tilde{\boldsymbol{\varepsilon}} = \boldsymbol{\varepsilon} + i\boldsymbol{\sigma}/\omega \tag{5.3}$$

in the main coordinate frame. Note that by doing this, the meaning of the electric flux density changes. The charge density in Gauss' law now describes source charges instead of free charges.

As sources of the electromagnetic field in the stratified medium, electric and magnetic dipoles with general orientation are considered. An infinitesimal electric dipole antenna can be represented by a periodic line current of length $\mathbf{l} = l_x\hat{\mathbf{x}} + l_y\hat{\mathbf{y}} + l_z\hat{\mathbf{z}}$ with current amplitude $I(\omega)$. The frequency-domain source-current density can then be written as:

$$\mathbf{J}_0 = I(\omega)\left[l_x\hat{\mathbf{x}} + l_y\hat{\mathbf{y}} + l_z\hat{\mathbf{z}}\right]\delta(\mathbf{r}), \tag{5.4}$$

where $\mathbf{r}$ is the distance from the source, i.e., the radial vector is described in terms of Cartesian coordinates as $\mathbf{r} = \mathbf{x} - \mathbf{x}_s$, where the source position is given as $\mathbf{x}_s = [x_s, y_s, z_s]$. If the electric dipole moment is represented by $\mathbf{P}$ (polarization), the dipole current moment becomes $-i\omega\mathbf{P}$. The magnetic dipole moment is given by $\mathbf{m} = \boldsymbol{\mu} I(\omega)\mathbf{a}$, where $\mathbf{a}$ is the area of a current carrying loop with direction normal to the loop. Analogous to the source-current density for the electric dipole in equation 5.4, an infinitesimal magnetic dipole source can be introduced as

$$\mathbf{J}_{0M} = -i\omega\boldsymbol{\mu} I(\omega)\mathbf{a}\delta(\mathbf{r}) = \begin{pmatrix} -i\omega I(\omega)\left[\mu_{xx}a_x + \mu_{xy}a_y + \mu_{xz}a_z\right]\delta(\mathbf{r}) \\ -i\omega I(\omega)\left[\mu_{yx}a_x + \mu_{yy}a_y + \mu_{yz}a_z\right]\delta(\mathbf{r}) \\ -i\omega I(\omega)\left[\mu_{zx}a_x + \mu_{zy}a_y + \mu_{zz}a_z\right]\delta(\mathbf{r}) \end{pmatrix}, \tag{5.5}$$

where possible anisotropic effects have been taken into account.

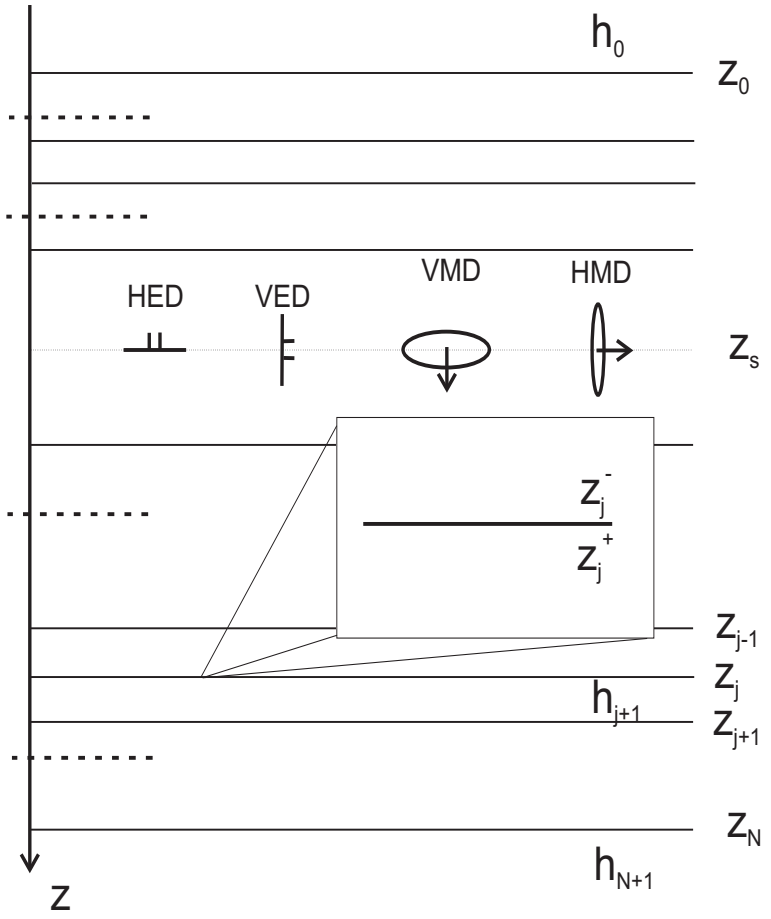

Figure 5.2: A sketch of the multilayer system. Four types of sources are considered: the horizontal electric dipole (HED), vertical electric dipole (VED), vertical magnetic dipole (VMD), and horizontal magnetic dipole (HMD).

In planarly stratified media the electromagnetic properties vary in one direction only. Consider a layered medium as depicted in Figure 5.2, and assume that the medium properties vary in the z-direction. The Fourier transform pair

$$\Phi(k_x, k_y, z, \omega) = \int_{-\infty}^{\infty} dxdydt\, \phi(x, y, z, t) \exp\left[-i(k_x x + k_y y - \omega t)\right], \tag{5.6a}$$

$$\phi(x, y, z, t) = \frac{1}{(2\pi)^3} \int_{-\infty}^{\infty} dk_x dk_y d\omega\, \Phi(k_x, k_y, z, \omega) \exp\left[i(k_x x + k_y y - \omega t)\right], \tag{5.6b}$$

where k_x and k_y are the wavenumbers in the x- and y-directions, respectively, describe transformations between the space-time and frequency-wavenumber domains. Equation 5.6a transforms Maxwell's equations in the time domain into the frequency-wavenumber domain and implies the following operations: $\partial_t \rightarrow -i\omega$, $\partial_x \rightarrow ik_x$, and $\partial_y \rightarrow ik_y$. The time and frequency part of equation 5.6a has already been applied in order to obtain equation 5.1 from the time-domain Maxwell's equations. In the time domain, the variables in Maxwell's equations are real, whereas in both the frequency and frequency-wavenumber domains the variables might be complex. From Faraday's law (equation 5.1c) with source term and Ampère's law (equation 5.1d), a set of ordinary differential equations is obtained after using the wavenumber part of the transformation in equation 5.6a:

$$\frac{dE_x}{dz} = \quad i\omega B_y + ik_x E_z - J_y^M, \tag{5.7a}$$

$$\frac{dE_y}{dz} = -i\omega B_x + ik_y E_z + J_x^M, \tag{5.7b}$$

$$-\frac{dH_y}{dz} = -i\omega D_x - ik_y H_z + J_x, \tag{5.7c}$$

$$\frac{dH_x}{dz} = -i\omega D_y + ik_x H_z + J_y. \tag{5.7d}$$

The components in the z-direction are related to the horizontal components as

$$D_z = \frac{1}{i\omega}\left(-ik_x H_y + ik_y H_x + J_z\right), \tag{5.8a}$$

$$B_z = \frac{1}{i\omega}\left(ik_x E_y - ik_y E_x + J_z^M\right). \tag{5.8b}$$

The variables J_n and J_n^M $(n = x, y, z)$ denote the Cartesian components of the frequency-wavenumber domain appearance of the electric and magnetic source, respectively. Likewise the field components E_n, D_n, H_n, and B_n are frequency-wavenumber domain quantities. In order to simplify notation it is convenient to introduce the slowness variables $p_x = k_x/\omega$ and $p_y = k_y/\omega$. With the constitutive relations $D_n = \tilde{\varepsilon}_{nm} E_m$ and $B_n = \mu_{nm} H_m$ $(m = x, y, z)$, the system of equations can be written as

$$\left(\boldsymbol{I}\frac{d}{dz} + i\omega\boldsymbol{A}\right)\boldsymbol{b} = \boldsymbol{\mathcal{L}}\boldsymbol{b} = \boldsymbol{s}, \tag{5.9}$$

with field vector

$$\boldsymbol{b} = \begin{pmatrix} \boldsymbol{b}_E \\ \boldsymbol{b}_H \end{pmatrix}, \quad \boldsymbol{b}_E = \begin{pmatrix} E_x \\ E_y \end{pmatrix}, \quad \boldsymbol{b}_H = \begin{pmatrix} -H_y \\ H_x \end{pmatrix}, \tag{5.10}$$

identity matrix $\boldsymbol{I}$, system matrix $\boldsymbol{A}$, and source vector $\boldsymbol{s}$. In addition the operator $\boldsymbol{\mathcal{L}}$ has been introduced. The system matrix is

$$\boldsymbol{A} = \begin{pmatrix} \boldsymbol{A}_0 & \boldsymbol{A}_1 \\ \boldsymbol{A}_2 & \boldsymbol{A}_3 \end{pmatrix} = \begin{pmatrix} a_{11} & a_{12} & a_{13} & a_{14} \\ a_{21} & a_{22} & a_{23} & a_{24} \\ a_{31} & a_{32} & a_{33} & a_{34} \\ a_{41} & a_{42} & a_{43} & a_{44} \end{pmatrix}, \tag{5.11}$$

where

$$a_{11} = \tfrac{\tilde{\varepsilon}_{zx}}{\tilde{\varepsilon}_{zz}} p_x + \tfrac{\mu_{yz}}{\mu_{zz}} p_y, \qquad a_{12} = \tfrac{\tilde{\varepsilon}_{zy}}{\tilde{\varepsilon}_{zz}} p_x - \tfrac{\mu_{yz}}{\mu_{zz}} p_x, \tag{5.12a}$$

$$a_{13} = \mu_{yy} - \tfrac{\mu_{yz}\mu_{zy}}{\mu_{zz}} - \tfrac{p_x^2}{\tilde{\varepsilon}_{zz}}, \qquad a_{14} = -\mu_{yx} + \tfrac{\mu_{yz}\mu_{zx}}{\mu_{zz}} - \tfrac{p_x p_y}{\tilde{\varepsilon}_{zz}}, \tag{5.12b}$$

$$a_{21} = \tfrac{\tilde{\varepsilon}_{zx}}{\tilde{\varepsilon}_{zz}} p_y - \tfrac{\mu_{xz}}{\mu_{zz}} p_y, \qquad a_{22} = \tfrac{\tilde{\varepsilon}_{zy}}{\tilde{\varepsilon}_{zz}} p_y + \tfrac{\mu_{xz}}{\mu_{zz}} p_x, \tag{5.12c}$$

$$a_{23} = -\mu_{xy} + \tfrac{\mu_{xz}\mu_{zy}}{\mu_{zz}} - \tfrac{p_x p_y}{\tilde{\varepsilon}_{zz}}, \qquad a_{24} = \mu_{xx} - \tfrac{\mu_{xz}\mu_{zx}}{\mu_{zz}} - \tfrac{p_y^2}{\tilde{\varepsilon}_{zz}}, \tag{5.12d}$$

$$a_{31} = \tilde{\varepsilon}_{xx} - \tfrac{\tilde{\varepsilon}_{xz}\tilde{\varepsilon}_{zx}}{\tilde{\varepsilon}_{zz}} - \tfrac{p_y^2}{\mu_{zz}}, \qquad a_{32} = \tilde{\varepsilon}_{xy} - \tfrac{\tilde{\varepsilon}_{xz}\tilde{\varepsilon}_{zy}}{\tilde{\varepsilon}_{zz}} + \tfrac{p_x p_y}{\mu_{zz}}, \tag{5.12e}$$

$$a_{33} = \tfrac{\tilde{\varepsilon}_{xz}}{\tilde{\varepsilon}_{zz}} p_x + \tfrac{\mu_{zy}}{\mu_{zz}} p_y, \qquad a_{34} = \tfrac{\tilde{\varepsilon}_{xz}}{\tilde{\varepsilon}_{zz}} p_y - \tfrac{\mu_{zx}}{\mu_{zz}} p_y, \tag{5.12f}$$

$$a_{41} = \tilde{\varepsilon}_{yx} - \tfrac{\tilde{\varepsilon}_{yz}\tilde{\varepsilon}_{zx}}{\tilde{\varepsilon}_{zz}} + \tfrac{p_x p_y}{\mu_{zz}}, \qquad a_{42} = \tilde{\varepsilon}_{yy} - \tfrac{\tilde{\varepsilon}_{yz}\tilde{\varepsilon}_{zy}}{\tilde{\varepsilon}_{zz}} - \tfrac{p_x^2}{\mu_{zz}}, \tag{5.12g}$$

$$a_{43} = \tfrac{\tilde{\varepsilon}_{yz}}{\tilde{\varepsilon}_{zz}} p_x - \tfrac{\mu_{zy}}{\mu_{zz}} p_x, \qquad a_{44} = \tfrac{\tilde{\varepsilon}_{yz}}{\tilde{\varepsilon}_{zz}} p_y + \tfrac{\mu_{zx}}{\mu_{zz}} p_x. \tag{5.12h}$$

In the following it will be assumed that all the material dyads have a set of orthogonal principal axes. Thus, the material parameters are symmetric, and because of this reciprocity, 6 of the 16 entries in $\boldsymbol{A}$ are equal:

$$\begin{aligned} &a_{23} = a_{14}, \quad a_{33} = a_{11}, \quad a_{34} = a_{21}, \\ &a_{41} = a_{32}, \quad a_{43} = a_{12}, \quad a_{44} = a_{22}. \end{aligned} \tag{5.13}$$

This implies that the system matrix is on the form

$$\boldsymbol{A} = \begin{pmatrix} \boldsymbol{A}_0 & \boldsymbol{A}_1 \\ \boldsymbol{A}_2 & \boldsymbol{A}_0^T \end{pmatrix}, \tag{5.14}$$

with $\boldsymbol{A}_1^T = \boldsymbol{A}_1$ and $\boldsymbol{A}_2^T = \boldsymbol{A}_2$.

The vertical components of the electromagnetic field are given in terms of the horizontal components as

$$E_z = \frac{1}{\tilde{\varepsilon}_{zz}} \left(p_y H_x - p_x H_y - \tilde{\varepsilon}_{zx} E_x - \tilde{\varepsilon}_{zy} E_y + \frac{1}{i\omega} J_z \right), \tag{5.15a}$$

$$H_z = \frac{1}{\mu_{zz}} \left(-p_y E_x + p_x E_y - \mu_{zx} H_x - \mu_{zy} H_y + \frac{1}{i\omega} J_z^M \right). \tag{5.15b}$$

The source vector consists of an electric source vector $\boldsymbol{s}_E$ and a magnetic source vector $\boldsymbol{s}_M$ ($\boldsymbol{s} = \boldsymbol{s}_E + \boldsymbol{s}_M$):

$$\boldsymbol{s}_E = \begin{pmatrix} p_x J_z/\tilde{\varepsilon}_{zz} \\ p_y J_z/\tilde{\varepsilon}_{zz} \\ J_x - \frac{\tilde{\varepsilon}_{xz}}{\tilde{\varepsilon}_{zz}} J_z \\ J_y - \frac{\tilde{\varepsilon}_{yz}}{\tilde{\varepsilon}_{zz}} J_z \end{pmatrix} \quad \text{and} \quad \boldsymbol{s}_M = \begin{pmatrix} -J_y^M + \frac{\mu_{yz}}{\mu_{zz}} J_z^M \\ J_x^M - \frac{\mu_{xz}}{\mu_{zz}} J_z^M \\ -p_y J_z^M/\mu_{zz} \\ p_x J_z^M/\mu_{zz} \end{pmatrix}. \tag{5.16}$$

The x- and y-components of the electric and magnetic sources will be referred to as the horizontal electric dipole (HED) and horizontal magnetic dipole (HMD), respectively. In a plane-layered model the coordinate system may be rotated so that the horizontal component of the electric or magnetic dipoles points in the x-direction, but it is sometimes advantageous to let the HED and HMD have components in both the x- and y-direction. The vertical components of the electric and magnetic dipoles are referred to as the VED and VMD, respectively. In the frequency-wavenumber domain the HED components are

$$J_x = I(\omega) l_x \delta(z - z_s), \tag{5.17a}$$

$$J_y = I(\omega) l_y \delta(z - z_s), \tag{5.17b}$$

where $x_s = y_s = 0$, and the VED component is

$$J_z = I(\omega) l_z \delta(z - z_s). \tag{5.17c}$$

The HMD components become

$$J_x^M = -i\omega I(\omega) \left(\mu_{xx} a_x + \mu_{xy} a_y + \mu_{xz} a_z\right) \delta(z - z_s), \tag{5.17d}$$

$$J_y^M = -i\omega I(\omega) \left(\mu_{yx} a_x + \mu_{yy} a_y + \mu_{yz} a_z\right) \delta(z - z_s), \tag{5.17e}$$

and the VMD component is

$$J_z^M = -i\omega I(\omega) \left(\mu_{zx} a_x + \mu_{zy} a_y + \mu_{zz} a_z\right) \delta(z - z_s). \tag{5.17f}$$

The infinitesimal or Hertzian dipoles are good approximations for any physical dipole source with finite length or size when the wavelength of the radiated signal, or distances at which the fields are considered, are larger than the dimensions of the dipole (length of the electric dipole and diameter of the magnetic dipole).

5.3 Symmetry relations and energy flux

From equation 5.14 it can be seen that $\boldsymbol{A}$ has a symplectic symmetry (Goldstein, 1980; Chapman, 1994) which can be exploited in order to find invariants and reciprocity relations.

Consider equation 5.9 in source-free regions ($\boldsymbol{\mathcal{L}b} = \mathbf{0}$). Introduce an operator $\tilde{\boldsymbol{\mathcal{L}}}$ in order to construct a new set of equations for a field vector $\tilde{\boldsymbol{b}}$:

$$\tilde{\boldsymbol{\mathcal{L}}}\tilde{\boldsymbol{b}} = \left(\boldsymbol{I}\frac{d}{dz} - i\omega\boldsymbol{A}\right)\tilde{\boldsymbol{b}} = \mathbf{0}. \tag{5.18}$$

By using the property $\boldsymbol{KA} = (\boldsymbol{KA})^T$ with

$$\boldsymbol{K} = \boldsymbol{K}^{-1} = \boldsymbol{K}^T = \begin{pmatrix} \mathbf{0} & \boldsymbol{I} \\ \boldsymbol{I} & \mathbf{0} \end{pmatrix}, \tag{5.19}$$

one obtains the invariant

$$\frac{d}{dz}\left(\tilde{\boldsymbol{b}}^T\boldsymbol{K}\boldsymbol{b}\right) = 0. \tag{5.20}$$

The time-averaged Poynting vector in the z-direction is $< S_z >= \frac{1}{2}\mathrm{Re}(\mathbf{E}\times\mathbf{H}^*)_z$ which can be written as:

$$< S_z >= \frac{1}{4}\left(E_xH_y^* - E_yH_x^* + E_x^*H_y - E_y^*H_x\right) = -\frac{1}{4}\boldsymbol{b}^\dagger\boldsymbol{K}\boldsymbol{b}. \tag{5.21}$$

The superscript † denotes complex conjugate transpose. In *lossless* media $\boldsymbol{A}$ is real, and from equation 5.9 and 5.18 it can be seen that $\tilde{\boldsymbol{b}} = \boldsymbol{b}^*$ *in this case*. The consequence is that $\tilde{\boldsymbol{b}}^T\boldsymbol{K}\boldsymbol{b} = -4 < S_z >$, meaning that the time-averaged energy flux in the z-direction is constant for lossless media.

Next, introduce an operator $\bar{\boldsymbol{\mathcal{L}}}$ which is obtained from $\boldsymbol{\mathcal{L}}$ by reversing the directions of the horizontal slowness components $p_x, p_y \rightarrow -p_x, -p_y$. The set of equations for the field vector $\bar{\boldsymbol{b}}$ is then:

$$\bar{\boldsymbol{\mathcal{L}}}\bar{\boldsymbol{b}} = \left(\boldsymbol{I}\frac{d}{dz} + i\omega\boldsymbol{A}'\right)\bar{\boldsymbol{b}} = \mathbf{0}, \tag{5.22}$$

where $\boldsymbol{A}'$ is obtained from $\boldsymbol{A}$ by changing the signs of $\boldsymbol{A}_0$ and $\boldsymbol{A}_0^T$:

$$\boldsymbol{A}' = \begin{pmatrix} -\boldsymbol{A}_0 & \boldsymbol{A}_1 \\ \boldsymbol{A}_2 & -\boldsymbol{A}_0^T \end{pmatrix}. \tag{5.23}$$

By using that $\left(\boldsymbol{K}'\boldsymbol{A}'\right)^T = \boldsymbol{K}'\boldsymbol{A}$ where

$$\boldsymbol{K}' = -\boldsymbol{K}'^{-1} = -\boldsymbol{K}'^T = \begin{pmatrix} \mathbf{0} & \boldsymbol{I} \\ -\boldsymbol{I} & \mathbf{0} \end{pmatrix}, \tag{5.24}$$

one obtains the invariant

$$\frac{d}{dz}\left(\bar{\boldsymbol{b}}^T\boldsymbol{K}'\boldsymbol{b}\right) = 0. \tag{5.25}$$

5.4 Decomposition into upgoing and downgoing fields

The system matrix $\boldsymbol{A}$ is diagonalizable when there is a set of four linearly independent eigenvectors of $\boldsymbol{A}$ (Horn and Johnson, 1985). Then the similarity transformation

$$\boldsymbol{A}\boldsymbol{N} = \boldsymbol{N}\boldsymbol{\Lambda}, \tag{5.26}$$

where the eigenvector matrix $\boldsymbol{N}$ is formed by the set of eigenvectors as columns, implies that the diagonal matrix $\boldsymbol{\Lambda}$ contains the four eigenvalues of $\boldsymbol{A}$ along its diagonal. By using equation 5.26, the differential equation 5.9 can be written as

$$\frac{d\boldsymbol{w}}{dz} = -i\omega\boldsymbol{\Lambda}\boldsymbol{w} - \boldsymbol{N}^{-1}\frac{d\boldsymbol{N}}{dz}\boldsymbol{w} + \boldsymbol{N}^{-1}\boldsymbol{s}, \tag{5.27}$$

where the physical field vector $\boldsymbol{b}$ has been transformed into a mode-field vector $\boldsymbol{w}$:

$$\boldsymbol{b} = \boldsymbol{N}\boldsymbol{w} \quad \text{and} \quad \boldsymbol{w} = \boldsymbol{N}^{-1}\boldsymbol{b} = \begin{pmatrix} \boldsymbol{u} \\ \boldsymbol{d} \end{pmatrix}. \tag{5.28}$$

Since $\boldsymbol{\Lambda}$ is diagonal, the solution of equation 5.27 in a source-free and homogeneous region

$$\boldsymbol{w}(z) = \exp\left[-i\omega\boldsymbol{\Lambda}(z - z_0)\right]\boldsymbol{w}_0(z_0), \tag{5.29}$$

reveals that the mode-field vector $\boldsymbol{w}$ consists of upgoing ($\boldsymbol{u}$) and downgoing ($\boldsymbol{d}$) field constituents. Thus, the eigenvalues of $\boldsymbol{A}$ are the vertical slownesses, and it is convenient to write $\boldsymbol{\Lambda}$ as

$$\boldsymbol{\Lambda} = \begin{pmatrix} \acute{\mathbf{p}}_{\mathbf{z}} & \mathbf{0} \\ \mathbf{0} & -\grave{\mathbf{p}}_{\mathbf{z}} \end{pmatrix} = \mathrm{diag}\{p_{z\mathrm{I}}, p_{z\mathrm{II}}, p_{z\mathrm{III}}, p_{z\mathrm{IV}}\}, \tag{5.30}$$

where $\acute{\mathbf{p}}_{\mathbf{z}} = \mathrm{diag}\{p_{z\mathrm{I}}, p_{z\mathrm{II}}\}$ and $\grave{\mathbf{p}}_{\mathbf{z}} = \mathrm{diag}\{-p_{z\mathrm{III}}, -p_{z\mathrm{IV}}\}$. The two eigenvalues in $\acute{\mathbf{p}}_{\mathbf{z}}$ are related to the upgoing field, and the two eigenvalues in $\grave{\mathbf{p}}_{\mathbf{z}}$ are related to the downgoing field.

Since it will simplify many derivations and relations at later stages, the eigenvector matrix $\boldsymbol{N}$ and its inverse should be normalized with respect to vertical energy flux. In order to achieve this, consider source-free and homogeneous media and use the invariant in equation 5.20. A decomposition of the ad-hoc field vector $\tilde{\boldsymbol{b}}$ into $\tilde{\boldsymbol{b}} = \tilde{\boldsymbol{N}}\tilde{\boldsymbol{w}}$ then leads to

$$\frac{d\tilde{\boldsymbol{w}}}{dz} = i\omega\tilde{\boldsymbol{\Lambda}}\tilde{\boldsymbol{w}}, \tag{5.31}$$

by using the similarity transform

$$\boldsymbol{A}\tilde{\boldsymbol{N}} = \tilde{\boldsymbol{N}}\tilde{\boldsymbol{\Lambda}}. \tag{5.32}$$

Now, $\tilde{\boldsymbol{\Lambda}}$ must contain the same eigenvalues as $\boldsymbol{\Lambda}$. From

$$\tilde{\boldsymbol{\Lambda}} = \begin{pmatrix} -\grave{\mathbf{p}}_{\mathbf{z}} & \mathbf{0} \\ \mathbf{0} & \acute{\mathbf{p}}_{\mathbf{z}} \end{pmatrix}, \tag{5.33}$$

the invariant

$$\frac{d}{dz}\left(\tilde{\boldsymbol{w}}^T\boldsymbol{K}\boldsymbol{w}\right)=0 \tag{5.34}$$

is obtained by using that $\boldsymbol{K}\tilde{\boldsymbol{\Lambda}}=\boldsymbol{K}\boldsymbol{\Lambda}$. In order for $\boldsymbol{N}$ to be energy normalized, the following relation must hold:

$$\tilde{\boldsymbol{w}}^T\boldsymbol{K}\boldsymbol{w}=\tilde{\boldsymbol{b}}^T\boldsymbol{K}\boldsymbol{b}. \tag{5.35}$$

By using that $\boldsymbol{b}=\boldsymbol{N}\boldsymbol{w}$ and $\tilde{\boldsymbol{b}}=\tilde{\boldsymbol{N}}\tilde{\boldsymbol{w}}$ this means that

$$\tilde{\boldsymbol{N}}^T\boldsymbol{K}\boldsymbol{N}=\boldsymbol{K}. \tag{5.36}$$

A relation between $\tilde{\boldsymbol{N}}$ and $\boldsymbol{N}$ can now be obtained by multiplying equation 5.26 by $\boldsymbol{K}'$ from the right and using that $\boldsymbol{\Lambda}\boldsymbol{K}'=\boldsymbol{K}'\tilde{\boldsymbol{\Lambda}}$. This leads to $\boldsymbol{A}\boldsymbol{N}\boldsymbol{K}'=\boldsymbol{N}\boldsymbol{K}'\tilde{\boldsymbol{\Lambda}}$ which is consistent with equation 5.32 if $\tilde{\boldsymbol{N}}=\boldsymbol{N}\boldsymbol{K}'$. The latter result combined with equation 5.36 yields

$$\boldsymbol{N}^{-1}=\boldsymbol{J}\boldsymbol{N}^T\boldsymbol{K}, \tag{5.37}$$

where

$$\boldsymbol{J}=\boldsymbol{J}^{-1}=\boldsymbol{J}^T=\begin{pmatrix}\boldsymbol{I} & \boldsymbol{0}\\ \boldsymbol{0} & -\boldsymbol{I}\end{pmatrix}. \tag{5.38}$$

The choice of sign in the derivation of $\tilde{\boldsymbol{N}}=\boldsymbol{N}\boldsymbol{K}'$ is justified by considering the lossless case. The energy contained in the mode-field in the vertical direction for lossless media is:

$$<S_z>=\frac{1}{4}\left(\boldsymbol{d}^\dagger\boldsymbol{d}-\boldsymbol{u}^\dagger\boldsymbol{u}\right)=-\frac{1}{4}\boldsymbol{w}^\dagger\boldsymbol{J}\boldsymbol{w}. \tag{5.39}$$

Equation 5.39 must be equal to the energy expression in equation 5.21. This yields equation 5.37 in the lossless case by using that the energy-normalized eigenvector matrix in the lossless medium is real.

The eigenvector matrix $\boldsymbol{N}$ can be written in terms of submatrices as

$$\boldsymbol{N}=\frac{1}{\sqrt{2}}\begin{pmatrix}\acute{\boldsymbol{N}}_E & \grave{\boldsymbol{N}}_E\\ \acute{\boldsymbol{N}}_H & -\grave{\boldsymbol{N}}_H\end{pmatrix}. \tag{5.40a}$$

Equation 5.37 then implies that the inverse eigenvector matrix is given in terms of the submatrices transposed:

$$\boldsymbol{N}^{-1}=\frac{1}{\sqrt{2}}\begin{pmatrix}\acute{\boldsymbol{N}}_H^T & \acute{\boldsymbol{N}}_E^T\\ \grave{\boldsymbol{N}}_H^T & -\grave{\boldsymbol{N}}_E^T\end{pmatrix}, \tag{5.40b}$$

which means that the electromagnetic energy in the field vector $\boldsymbol{b}$ is preserved within the mode-field vector $\boldsymbol{w}$ after the transformation $\boldsymbol{w}=\boldsymbol{N}^{-1}\boldsymbol{b}$.

5.5 Propagation of upgoing and downgoing fields

The mode-field vector $\boldsymbol{w}$ can be used to describe propagation of electromagnetic fields in homogeneous regions, across interfaces, and in a system of layers. Now, represent propagation of $\boldsymbol{w}$ downwards in the positive z-direction in terms of the propagator $\grave{\boldsymbol{Q}}$, and propagation upwards in the negative z-direction by $\acute{\boldsymbol{Q}}$. Since the z-axis is pointing downwards, this means that if $z > z_0$:

$$\boldsymbol{w}(z) = \grave{\boldsymbol{Q}}(z, z_0)\boldsymbol{w}(z_0), \tag{5.41a}$$

$$\boldsymbol{w}(z_0) = \acute{\boldsymbol{Q}}(z_0, z)\boldsymbol{w}(z). \tag{5.41b}$$

The relation between a propagator and its inverse is thus

$$\acute{\boldsymbol{Q}}(z_0, z) = \grave{\boldsymbol{Q}}^{-1}(z, z_0). \tag{5.42}$$

5.5.1 Source-free homogeneous regions

In a source-free homogeneous region, equation 5.27 simplifies to $d\boldsymbol{w}/dz = -i\omega\boldsymbol{\Lambda}\boldsymbol{w}$ with solution $\boldsymbol{w}(z) = \exp\left[-i\omega\boldsymbol{\Lambda}(z - z_0)\right]\boldsymbol{w}_0(z_0)$. Thus, propagation downwards within a homogeneous region from z_0 to z is described in terms of the propagator matrix $\grave{\boldsymbol{Q}}$ in equation 5.41a where

$$\grave{\boldsymbol{Q}}(z, z_0) = \begin{pmatrix} \mathrm{e}^{-i\omega\acute{\mathbf{p}}_{\mathbf{z}}(z-z_0)} & \mathbf{0} \\ \mathbf{0} & \mathrm{e}^{i\omega\grave{\mathbf{p}}_{\mathbf{z}}(z-z_0)} \end{pmatrix}. \tag{5.43}$$

The propagation upwards is related to the propagation downwards as described in equation 5.42.

5.5.2 Propagation across a source

A *point source* causes a discontinuity in the mode-field vector $\boldsymbol{w}$. The transformation of the source in equation 5.27 is denoted as

$$\boldsymbol{\Sigma} = \boldsymbol{N}^{-1}\boldsymbol{s}. \tag{5.44}$$

Propagation across a source can be described by

$$\boldsymbol{w}(z_s^+) = \boldsymbol{\Sigma}(z_s) + \boldsymbol{w}(z_s^-), \tag{5.45}$$

where z_s denotes the source position and z_s^- and z_s^+ are the positions just above and just below the source, respectively. The mode-domain source can furthermore be written as $\boldsymbol{\Sigma} = \left(\acute{\boldsymbol{\Sigma}}^T \;\; \grave{\boldsymbol{\Sigma}}^T\right)^T$, where $\acute{\boldsymbol{\Sigma}}$ describes the upgoing radiation and $\grave{\boldsymbol{\Sigma}}$ describes the downgoing radiation.

5.5.3 Propagation in continuously varying media

In equation 5.27 the term that contains the derivative of the eigenvector matrix describes possible medium variations. In homogeneous regions this term is zero, and the medium variations are discretized into piecewise homogeneous regions which are connected by applying the appropriate boundary conditions. In several occasions it can be useful to consider medium variations by using the entire differential equation 5.27. Write the product of $\boldsymbol{N}^{-1}$ and the derivative of $\boldsymbol{N}$ as:

$$\boldsymbol{N}^{-1}\frac{d\boldsymbol{N}}{dz} = -\begin{pmatrix} \acute{\boldsymbol{F}} & \hat{\boldsymbol{G}} \\ \check{\boldsymbol{G}} & \grave{\boldsymbol{F}} \end{pmatrix}, \tag{5.46}$$

where

$$\acute{\boldsymbol{F}} = -\frac{1}{2}\left(\acute{\boldsymbol{N}}_H^T\frac{d\acute{\boldsymbol{N}}_E}{dz} + \acute{\boldsymbol{N}}_E^T\frac{d\acute{\boldsymbol{N}}_H}{dz}\right), \tag{5.47a}$$

$$\grave{\boldsymbol{F}} = -\frac{1}{2}\left(\grave{\boldsymbol{N}}_H^T\frac{d\grave{\boldsymbol{N}}_E}{dz} + \grave{\boldsymbol{N}}_E^T\frac{d\grave{\boldsymbol{N}}_H}{dz}\right), \tag{5.47b}$$

$$\hat{\boldsymbol{G}} = -\frac{1}{2}\left(\acute{\boldsymbol{N}}_H^T\frac{d\grave{\boldsymbol{N}}_E}{dz} - \acute{\boldsymbol{N}}_E^T\frac{d\grave{\boldsymbol{N}}_H}{dz}\right), \tag{5.47c}$$

$$\check{\boldsymbol{G}} = -\frac{1}{2}\left(\grave{\boldsymbol{N}}_H^T\frac{d\acute{\boldsymbol{N}}_E}{dz} - \grave{\boldsymbol{N}}_E^T\frac{d\acute{\boldsymbol{N}}_H}{dz}\right). \tag{5.47d}$$

Then equation 5.27 in terms of the upgoing and downgoing fields can be written as

$$\frac{d\boldsymbol{u}}{dz} = -i\omega\acute{\mathbf{p}}_{\mathbf{z}}\boldsymbol{u} + \acute{\boldsymbol{F}}\boldsymbol{u} + \hat{\boldsymbol{G}}\boldsymbol{d} + \acute{\boldsymbol{\Sigma}}, \tag{5.48a}$$

$$\frac{d\boldsymbol{d}}{dz} = \; i\omega\grave{\mathbf{p}}_{\mathbf{z}}\boldsymbol{d} + \grave{\boldsymbol{F}}\boldsymbol{d} + \check{\boldsymbol{G}}\boldsymbol{u} + \grave{\boldsymbol{\Sigma}}. \tag{5.48b}$$

Considerations of the symmetries in $\boldsymbol{N}$ and $\boldsymbol{N}^{-1}$ lead to $\hat{\boldsymbol{G}} = \check{\boldsymbol{G}}^T$, $\acute{\boldsymbol{F}} = -\acute{\boldsymbol{F}}^T$, and $\grave{\boldsymbol{F}} = -\grave{\boldsymbol{F}}^T$. Thus,

$$\acute{\boldsymbol{F}} = \begin{pmatrix} 0 & \acute{f}_{12} \\ -\acute{f}_{12} & 0 \end{pmatrix} \quad \text{and} \quad \grave{\boldsymbol{F}} = \begin{pmatrix} 0 & \grave{f}_{12} \\ -\grave{f}_{12} & 0 \end{pmatrix}. \tag{5.49}$$

These relations are useful e.g., when considering slow and continuous medium variations in for instance the WKB approximation, and in the calculation of approximate expressions for the reflection and transmission matrices at interfaces with weak contrasts as will be shown in the next section.

5.6 Reflection and transmission responses

Figure 5.3 describes reflection and transmission of a unit incident field in a region between the coordinates z^- and z^+. This region might contain an arbitrary number of layers or just a

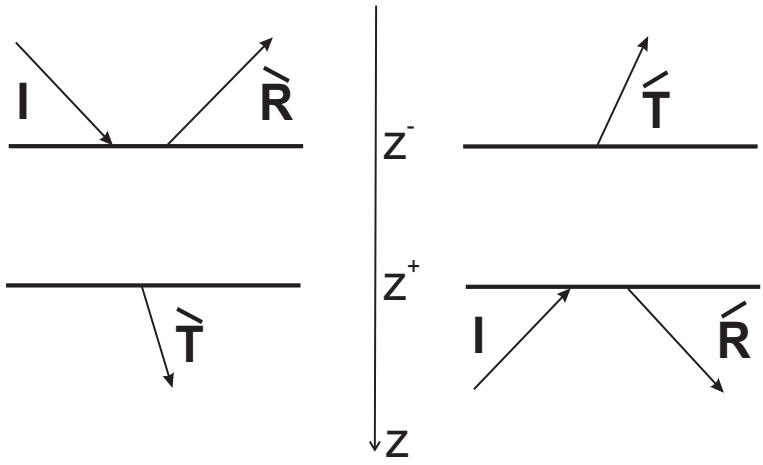

Figure 5.3: Reflection and transmission for an upgoing and downgoing incident plane wave through a stack of layers.

single interface. The reflection and transmission at an interface when propagating downwards in the positive z-direction can be written in terms of a propagator matrix $\grave{\boldsymbol{Q}}(z^+, z^-)$:

$$\begin{pmatrix} \boldsymbol{0} \\ \grave{\boldsymbol{T}} \end{pmatrix} = \begin{pmatrix} \grave{\boldsymbol{Q}}_{11} & \grave{\boldsymbol{Q}}_{12} \\ \grave{\boldsymbol{Q}}_{21} & \grave{\boldsymbol{Q}}_{22} \end{pmatrix} \begin{pmatrix} \grave{\boldsymbol{R}} \\ \boldsymbol{I} \end{pmatrix} \quad \text{and} \quad \begin{pmatrix} \boldsymbol{I} \\ \acute{\boldsymbol{R}} \end{pmatrix} = \begin{pmatrix} \grave{\boldsymbol{Q}}_{11} & \grave{\boldsymbol{Q}}_{12} \\ \grave{\boldsymbol{Q}}_{21} & \grave{\boldsymbol{Q}}_{22} \end{pmatrix} \begin{pmatrix} \acute{\boldsymbol{T}} \\ \boldsymbol{0} \end{pmatrix}, \tag{5.50}$$

where $\grave{\boldsymbol{R}}$ and $\grave{\boldsymbol{T}}$ denote reflection and transmission of a downgoing field, respectively; and $\acute{\boldsymbol{R}}$ and $\acute{\boldsymbol{T}}$ denote reflection and transmission of an upgoing field, respectively. The reflection and transmission coefficients can be written in terms of the elements of $\grave{\boldsymbol{Q}}$:

$$\acute{\boldsymbol{T}} = \grave{\boldsymbol{Q}}_{11}^{-1}, \tag{5.51a}$$

$$\acute{\boldsymbol{R}} = \grave{\boldsymbol{Q}}_{21}\grave{\boldsymbol{Q}}_{11}^{-1}, \tag{5.51b}$$

$$\grave{\boldsymbol{R}} = -\grave{\boldsymbol{Q}}_{11}^{-1}\grave{\boldsymbol{Q}}_{12}, \tag{5.51c}$$

$$\grave{\boldsymbol{T}} = \grave{\boldsymbol{Q}}_{22} - \grave{\boldsymbol{Q}}_{21}\grave{\boldsymbol{Q}}_{11}^{-1}\grave{\boldsymbol{Q}}_{12}. \tag{5.51d}$$

When propagating upwards in the negative z-direction, the relations between the incoming reflected and transmitted fields in terms of the propagator $\acute{\boldsymbol{Q}}(z^-, z^+)$ are:

$$\begin{pmatrix} \grave{\boldsymbol{R}} \\ \boldsymbol{I} \end{pmatrix} = \begin{pmatrix} \acute{\boldsymbol{Q}}_{11} & \acute{\boldsymbol{Q}}_{12} \\ \acute{\boldsymbol{Q}}_{21} & \acute{\boldsymbol{Q}}_{22} \end{pmatrix} \begin{pmatrix} \boldsymbol{0} \\ \grave{\boldsymbol{T}} \end{pmatrix} \quad \text{and} \quad \begin{pmatrix} \acute{\boldsymbol{T}} \\ \boldsymbol{0} \end{pmatrix} = \begin{pmatrix} \acute{\boldsymbol{Q}}_{11} & \acute{\boldsymbol{Q}}_{12} \\ \acute{\boldsymbol{Q}}_{21} & \acute{\boldsymbol{Q}}_{22} \end{pmatrix} \begin{pmatrix} \boldsymbol{I} \\ \acute{\boldsymbol{R}} \end{pmatrix}, \tag{5.52}$$

and in terms of $\acute{\boldsymbol{Q}}$, the reflection and transmission coefficients are:

$$\grave{\boldsymbol{T}} = \acute{\boldsymbol{Q}}_{22}^{-1}, \tag{5.53a}$$

$$\grave{\boldsymbol{R}} = \acute{\boldsymbol{Q}}_{12}\acute{\boldsymbol{Q}}_{22}^{-1}, \tag{5.53b}$$

$$\acute{\boldsymbol{R}} = -\acute{\boldsymbol{Q}}_{22}^{-1}\acute{\boldsymbol{Q}}_{21}, \tag{5.53c}$$

$$\acute{\boldsymbol{T}} = \acute{\boldsymbol{Q}}_{11} - \acute{\boldsymbol{Q}}_{12}\acute{\boldsymbol{Q}}_{22}^{-1}\acute{\boldsymbol{Q}}_{21}. \tag{5.53d}$$

The propagators written in terms of the reflection and transmission coefficients become

$$\grave{\boldsymbol{Q}}(z^+, z^-) = \begin{pmatrix} \acute{\boldsymbol{T}}^{-1} & -\acute{\boldsymbol{T}}^{-1}\grave{\boldsymbol{R}} \\ \acute{\boldsymbol{R}}\acute{\boldsymbol{T}}^{-1} & \grave{\boldsymbol{T}} - \acute{\boldsymbol{R}}\acute{\boldsymbol{T}}^{-1}\grave{\boldsymbol{R}} \end{pmatrix}, \tag{5.54a}$$

$$\acute{\boldsymbol{Q}}(z^-, z^+) = \begin{pmatrix} \acute{\boldsymbol{T}} - \grave{\boldsymbol{R}}\grave{\boldsymbol{T}}^{-1}\acute{\boldsymbol{R}} & \grave{\boldsymbol{R}}\grave{\boldsymbol{T}}^{-1} \\ -\grave{\boldsymbol{T}}^{-1}\acute{\boldsymbol{R}} & \grave{\boldsymbol{T}}^{-1} \end{pmatrix}, \tag{5.54b}$$

where $\grave{\boldsymbol{Q}}(z^+, z^-) = \acute{\boldsymbol{Q}}^{-1}(z^-, z^+)$.

5.6.1 Reciprocity relations

Consider the field vector $\bar{\boldsymbol{b}}$ in equation 5.22. In this system the direction of the slowness vectors are reversed. Thus, the similarity transform of the system matrix $\boldsymbol{A}'$ becomes

$$\boldsymbol{A}'\bar{\boldsymbol{N}} = -\bar{\boldsymbol{N}}\boldsymbol{\Lambda}. \tag{5.55}$$

By using the diagonal matrix $\boldsymbol{J}$ from equation 5.38, the relationship $\boldsymbol{A}'\boldsymbol{J} + \boldsymbol{J}\boldsymbol{A} = \boldsymbol{0}$ is obtained. The use of this property when comparing the expressions in equation 5.55 and equation 5.26, gives that $\bar{\boldsymbol{N}} = \boldsymbol{J}\boldsymbol{N}$. Inserted into equation 5.37 this means that

$$\bar{\boldsymbol{N}}^T\boldsymbol{K}'\boldsymbol{N} = \boldsymbol{J}. \tag{5.56}$$

Equation 5.25 with the mode-field transformations ($\bar{\boldsymbol{w}} = \bar{\boldsymbol{N}}\bar{\boldsymbol{b}}$ and $\boldsymbol{w} = \boldsymbol{N}\boldsymbol{b}$) and equation 5.56 now lead to

$$\bar{\boldsymbol{w}}^T\boldsymbol{J}\boldsymbol{w} = \text{constant}. \tag{5.57}$$

Consider the preservation of the quantity in equation 5.57 between e.g., the interfaces z^+ and z^- (propagation upwards cf. equation 5.52). For simplicity a matrix where the left column represents the mode-field vector with incidence from above (left side of Figure 5.3) and the right column represents the mode-field with incidence from below (right side of Figure 5.3) can be formed. Then equation 5.57 leads to

$$\begin{pmatrix} \boldsymbol{I} & \grave{\boldsymbol{R}}'^T \\ \boldsymbol{0} & \acute{\boldsymbol{T}}'^T \end{pmatrix} \boldsymbol{J} \begin{pmatrix} \grave{\boldsymbol{R}} & \acute{\boldsymbol{T}} \\ \boldsymbol{I} & \boldsymbol{0} \end{pmatrix} = \begin{pmatrix} \grave{\boldsymbol{T}}'^T & \boldsymbol{0} \\ \acute{\boldsymbol{R}}'^T & \boldsymbol{I} \end{pmatrix} \boldsymbol{J} \begin{pmatrix} \boldsymbol{0} & \boldsymbol{I} \\ \grave{\boldsymbol{T}} & \acute{\boldsymbol{R}} \end{pmatrix}, \tag{5.58}$$

where the reflection and transmission in the slowness-reversed system are denoted $\boldsymbol{R}'$ and $\boldsymbol{T}'$, respectively. The upgoing and downgoing incident, reflected, and transmitted fields have furthermore been swapped for the slowness reversed mode-field since there is a reversal of the propagation direction in this system. This also implies that the reflection and transmission coefficients have opposite signs for the horizontal slowness parameters in the slowness reversed and "normal" systems. Thus, the following reciprocity relations for the transmission and reflection coefficients become evident:

$$\grave{\boldsymbol{R}}(p_x, p_y) = \grave{\boldsymbol{R}}^T(-p_x, -p_y), \tag{5.59a}$$

$$\acute{\boldsymbol{R}}(p_x, p_y) = \acute{\boldsymbol{R}}^T(-p_x, -p_y), \tag{5.59b}$$

$$\grave{\boldsymbol{T}}(p_x, p_y) = \acute{\boldsymbol{T}}^T(-p_x, -p_y). \tag{5.59c}$$

These expressions are equivalent to the expressions found in Chapman (1994) for elastic anisotropic media.

5.6.2 Reflection and transmission at a single interface

Explicit expressions for the reflection and transmission coefficients at a single interface can be derived by using the boundary conditions. The horizontal electromagnetic field components represented by $\boldsymbol{b} = \boldsymbol{N}\boldsymbol{w}$ are continuous across an interface. This leads to $\boldsymbol{N}(z_j^-)\boldsymbol{w}(z_j^-) = \boldsymbol{N}(z_j^+)\boldsymbol{w}(z_j^+)$, where z_j^- and z_j^+ are the z-coordinates on each side of the interface at z_j as illustrated in Figure 5.2. Thus, the propagators across the interface become

$$\acute{\boldsymbol{Q}}(z_j^-, z_j^+) = \boldsymbol{N}^{-1}(z_j^-)\boldsymbol{N}(z_j^+) \quad \text{and} \quad \grave{\boldsymbol{Q}}(z_j^+, z_j^-) = \boldsymbol{N}^{-1}(z_j^+)\boldsymbol{N}(z_j^-). \tag{5.60}$$

In order to derive the 2×2 reflection and transmission matrices at an interface, it is convenient to introduce the matrices

$$\acute{\boldsymbol{C}} = \left[\acute{\boldsymbol{N}}_H^-\right]^T \acute{\boldsymbol{N}}_E^+, \qquad \acute{\boldsymbol{D}} = \left[\acute{\boldsymbol{N}}_E^-\right]^T \acute{\boldsymbol{N}}_H^+, \tag{5.61a}$$

$$\hat{\boldsymbol{C}} = \left[\acute{\boldsymbol{N}}_H^-\right]^T \grave{\boldsymbol{N}}_E^+, \qquad \hat{\boldsymbol{D}} = \left[\acute{\boldsymbol{N}}_E^-\right]^T \grave{\boldsymbol{N}}_H^+, \tag{5.61b}$$

$$\check{\boldsymbol{C}} = \left[\grave{\boldsymbol{N}}_H^-\right]^T \acute{\boldsymbol{N}}_E^+, \qquad \check{\boldsymbol{D}} = \left[\grave{\boldsymbol{N}}_E^-\right]^T \acute{\boldsymbol{N}}_H^+, \tag{5.61c}$$

$$\grave{\boldsymbol{C}} = \left[\grave{\boldsymbol{N}}_H^-\right]^T \grave{\boldsymbol{N}}_E^+, \qquad \grave{\boldsymbol{D}} = \left[\grave{\boldsymbol{N}}_E^-\right]^T \grave{\boldsymbol{N}}_H^+, \tag{5.61d}$$

where the superscripts "−" and "+" denote eigenvector matrices in the upper and lower homogeneous regions, respectively. The propagators in both directions across the interface can now be written (using equations 5.60 and 5.40) as:

$$\acute{\boldsymbol{Q}} = \frac{1}{2}\begin{pmatrix} \acute{\boldsymbol{C}} + \acute{\boldsymbol{D}} & \hat{\boldsymbol{C}} - \hat{\boldsymbol{D}} \\ \check{\boldsymbol{C}} - \check{\boldsymbol{D}} & \grave{\boldsymbol{C}} + \grave{\boldsymbol{D}} \end{pmatrix} \quad \text{and} \quad \grave{\boldsymbol{Q}} = \frac{1}{2}\begin{pmatrix} \acute{\boldsymbol{D}}^T + \acute{\boldsymbol{C}}^T & \check{\boldsymbol{D}}^T - \check{\boldsymbol{C}}^T \\ \hat{\boldsymbol{D}}^T - \hat{\boldsymbol{C}}^T & \grave{\boldsymbol{D}}^T + \grave{\boldsymbol{C}}^T \end{pmatrix}. \tag{5.62}$$

The propagator elements are related to the reflection and transmission coefficients as described in equations 5.51 and 5.53, and from this the reflection and transmission matrices can be derived in terms of the $\boldsymbol{C}$ and $\boldsymbol{D}$ matrices:

$$\acute{\boldsymbol{t}} = 2\left(\acute{\boldsymbol{C}} + \acute{\boldsymbol{D}}\right)^{-T}, \tag{5.63a}$$

$$\acute{\boldsymbol{r}} = -\left(\hat{\boldsymbol{C}} - \hat{\boldsymbol{D}}\right)^{T}\left(\acute{\boldsymbol{C}} + \acute{\boldsymbol{D}}\right)^{-T} = -\left(\grave{\boldsymbol{C}} + \grave{\boldsymbol{D}}\right)^{-1}\left(\check{\boldsymbol{C}} - \check{\boldsymbol{D}}\right), \tag{5.63b}$$

$$\grave{\boldsymbol{r}} = \left(\hat{\boldsymbol{C}} - \hat{\boldsymbol{D}}\right)\left(\grave{\boldsymbol{C}} + \grave{\boldsymbol{D}}\right)^{-1} = \left(\acute{\boldsymbol{C}} + \acute{\boldsymbol{D}}\right)^{-T}\left(\check{\boldsymbol{C}} - \check{\boldsymbol{D}}\right)^{T}, \tag{5.63c}$$

$$\grave{\boldsymbol{t}} = 2\left(\grave{\boldsymbol{C}} + \grave{\boldsymbol{D}}\right)^{-1}. \tag{5.63d}$$

Note the use of small boldface letters to denote reflection $\boldsymbol{r}$ and transmission $\boldsymbol{t}$ from a *single* interface.

5.6.3 Single-interface weak-contrast approximation

In case of weak contrasts at an interface, equation 5.48 can be used to derive approximate expressions for the reflection and transmission matrices in terms of $\boldsymbol{F}$ and $\boldsymbol{G}$ as in Ursin and Stovas (2002) and Stovas and Ursin (2003). In a source-free region a Taylor expansion of $\boldsymbol{u}$ leads to

$$\boldsymbol{u}(z-\Delta z) \approx \boldsymbol{u}(z) - \frac{d\boldsymbol{u}}{dz}\Delta z = \left(\boldsymbol{I} + i\omega\acute{\mathbf{p}}_{\mathbf{z}}\Delta z - \acute{\boldsymbol{F}}\Delta z\right)\boldsymbol{u}(z) - \hat{\boldsymbol{G}}\boldsymbol{d}(z). \tag{5.64}$$

When $\Delta z \to 0$ this becomes

$$\boldsymbol{u}^{\text{out}} = (\boldsymbol{I} - \acute{\boldsymbol{\mathcal{F}}})\boldsymbol{u}^{\text{in}} - \hat{\boldsymbol{\mathcal{G}}}\boldsymbol{d}^{\text{in}}, \tag{5.65}$$

where $\boldsymbol{u}^{\text{out}}$ is the resulting upgoing field after transmission of $\boldsymbol{u}^{\text{in}}$ and reflection of $\boldsymbol{d}^{\text{in}}$. The propagation is in the negative z-direction and $\boldsymbol{u}^{\text{out}}$ and $\boldsymbol{d}^{\text{in}}$ are on the upper side of the interface (z_j^-) whereas $\boldsymbol{u}^{\text{in}}$ is on the lower side (z_j^+). The matrices $\boldsymbol{\mathcal{F}}$ and $\boldsymbol{\mathcal{G}}$ refer to $\boldsymbol{F}$ and $\boldsymbol{G}$ with the derivatives replaced by the discontinuity in the parameters, and the parameters replaced by their average values. A Taylor expansion for $\boldsymbol{d}$ leads to

$$\boldsymbol{d}(z+\Delta z) \approx \boldsymbol{d}(z) + \frac{d\boldsymbol{d}}{dz}\Delta z = \left(\boldsymbol{I} + i\omega\grave{\mathbf{p}}_{\mathbf{z}}\Delta z + \grave{\boldsymbol{F}}\Delta z\right)\boldsymbol{d}(z) + \check{\boldsymbol{G}}\boldsymbol{u}(z), \tag{5.66}$$

which when $\Delta z \to 0$ leads to

$$\boldsymbol{d}^{\text{out}} = (\boldsymbol{I} + \grave{\boldsymbol{\mathcal{F}}})\boldsymbol{d}^{\text{in}} + \check{\boldsymbol{\mathcal{G}}}\boldsymbol{u}^{\text{in}}. \tag{5.67}$$

Thus, from equation 5.65 it can be seen that

$$\acute{\boldsymbol{t}} \approx \boldsymbol{I} - \acute{\boldsymbol{\mathcal{F}}} \quad \text{and} \quad \grave{\boldsymbol{r}} \approx -\hat{\boldsymbol{\mathcal{G}}}, \tag{5.68a}$$

whereas equation 5.67 gives

$$\grave{\boldsymbol{t}} \approx \boldsymbol{I} + \grave{\boldsymbol{\mathcal{F}}} \quad \text{and} \quad \acute{\boldsymbol{r}} \approx \check{\boldsymbol{\mathcal{G}}}. \tag{5.68b}$$

5.6.4 Recursive reflection and transmission responses

The eigenvalues in $\boldsymbol{\Lambda}$ will in general be complex and have a spectrum that contains evanescent waves and attenuation for both upgoing and downgoing waves. A calculation of reflection and transmission responses from a stack of layers can be done by matrix multiplication of all the propagator elements involved. However, in numerical simulations this procedure may lead to numerical instabilities. It might be better to obtain the overall reflection and transmission matrices from a recursive calculation. Consider a propagator through a stack of layers from z_{N+1} to z_j^+, and furthermore propagation through the interface z_j and the homogeneous region up to z_{j-1}^+ (cf. Figure 5.2):

$$\acute{\boldsymbol{Q}}(z_{j-1}^+, z_{N+1}) = \acute{\boldsymbol{Q}}(z_{j-1}^+, z_j^-)\acute{\boldsymbol{Q}}(z_j^-, z_j^+)\acute{\boldsymbol{Q}}(z_j^+, z_{N+1}). \tag{5.69}$$

In the 4×4 propagator $\acute{\boldsymbol{Q}}(z_j^+, z_{N+1})$, the 2×2 reflection and transmission matrices in the right column of equation 5.54b are denoted as $\acute{\boldsymbol{R}}_{j+1}$ and $\acute{\boldsymbol{T}}_{j+1}$. In the propagator $\acute{\boldsymbol{Q}}(z_{j-1}^+, z_{N+1})$, the corresponding reflection and transmission matrices are denoted $\acute{\boldsymbol{R}}_j$ and $\acute{\boldsymbol{T}}_j$. The propagation across the single interface z_j is described by equation 5.54b as well, and in this case the reflection and transmission matrices are written in lowercase letters ($\boldsymbol{r}$ and $\boldsymbol{t}$) with subscript j. For propagation upwards in the homogeneous region, the inverse of the matrix expression in equation 5.43 is used. The following recursion formulas for the downward reflection and transmission matrices are then obtained:

$$\grave{\boldsymbol{R}}_j = \mathrm{e}^{i\omega\hat{\mathbf{p}}_\mathbf{z}h_j}\left[\grave{\boldsymbol{r}}_j + \grave{\boldsymbol{t}}_j\grave{\boldsymbol{R}}_{j+1}\left(\boldsymbol{I} - \acute{\boldsymbol{r}}_j\grave{\boldsymbol{R}}_{j+1}\right)^{-1}\grave{\boldsymbol{t}}_j\right]\mathrm{e}^{i\omega\hat{\mathbf{p}}_\mathbf{z}h_j}, \tag{5.70a}$$

$$\grave{\boldsymbol{T}}_j = \grave{\boldsymbol{T}}_{j+1}\left(\boldsymbol{I} - \acute{\boldsymbol{r}}_j\grave{\boldsymbol{R}}_{j+1}\right)^{-1}\grave{\boldsymbol{t}}_j\mathrm{e}^{i\omega\hat{\mathbf{p}}_\mathbf{z}h_j}, \tag{5.70b}$$

where $h_j = z_j - z_{j-1}$, and where $\hat{\mathbf{p}}_\mathbf{z}$ and $\grave{\mathbf{p}}_\mathbf{z}$ are the eigenvalue submatrices in layer j. The initial values are $\grave{\boldsymbol{R}}_{N+1} = \mathbf{0}$ and $\grave{\boldsymbol{T}}_{N+1} = \mathrm{e}^{i\omega\grave{\mathbf{p}}_\mathbf{z}h_{N+1}}$.

The same procedure can be used for the downgoing propagators to find recursive relations for $\acute{\boldsymbol{R}}_j$ and $\acute{\boldsymbol{T}}_j$:

$$\acute{\boldsymbol{R}}_j = \mathrm{e}^{i\omega\grave{\mathbf{p}}_\mathbf{z}h_{j+1}}\left[\acute{\boldsymbol{r}}_j + \grave{\boldsymbol{t}}_j\acute{\boldsymbol{R}}_{j-1}\left(\boldsymbol{I} - \grave{\boldsymbol{r}}_j\acute{\boldsymbol{R}}_{j-1}\right)^{-1}\acute{\boldsymbol{t}}_j\right]\mathrm{e}^{i\omega\hat{\mathbf{p}}_\mathbf{z}h_{j+1}}, \tag{5.71a}$$

$$\acute{\boldsymbol{T}}_j = \acute{\boldsymbol{T}}_{j-1}\left(\boldsymbol{I} - \grave{\boldsymbol{r}}_j\acute{\boldsymbol{R}}_{j-1}\right)^{-1}\acute{\boldsymbol{t}}_j\mathrm{e}^{i\omega\hat{\mathbf{p}}_\mathbf{z}h_{j+1}}. \tag{5.71b}$$

Here, $\acute{\boldsymbol{R}}_{j-1}$ and $\acute{\boldsymbol{T}}_{j-1}$ describe reflection and transmission at z_j^- whereas $\acute{\boldsymbol{R}}_j$ and $\acute{\boldsymbol{T}}_j$ describe reflection and transmission at z_{j+1}^-. The initial values are $\acute{\boldsymbol{R}}_0 = \mathbf{0}$ and $\acute{\boldsymbol{T}}_0 = \mathrm{e}^{i\omega\hat{\mathbf{p}}_\mathbf{z}h_0}$, and the eigenvalue submatrices are those of layer $j+1$. The initial conditions are not necessarily related to the "top" and "bottom" of the stack as the interpretation of Figure 5.2 might suggest; the recursion formulas can be applied to substacks anywhere in the medium, but not across a source (cf. Figure 5.4). Note that the structure of the formulas is the same for both the upward and downward reflection and transmission matrices.

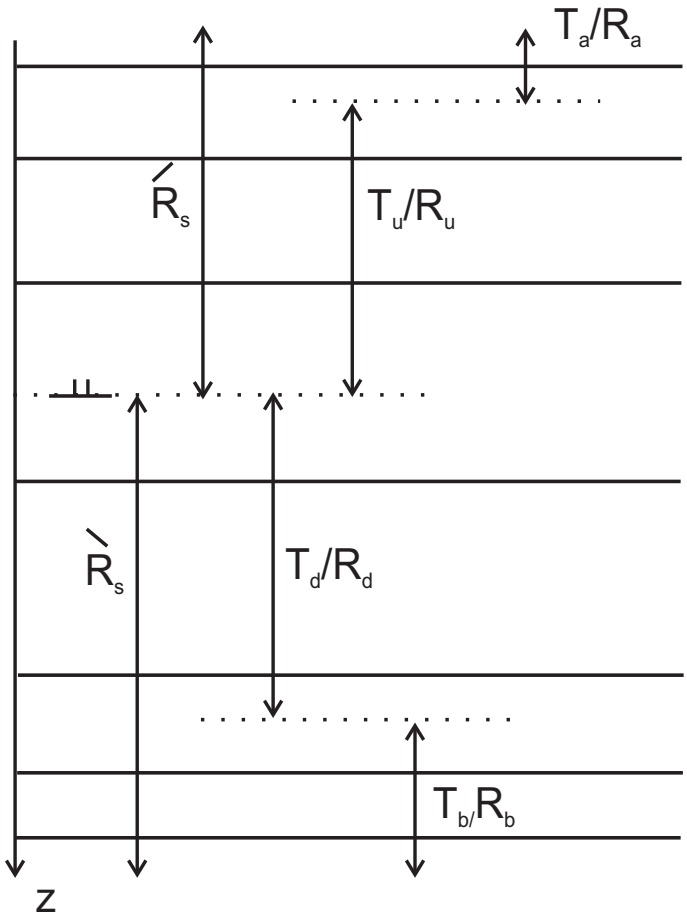

Figure 5.4: A sketch of the multilayered medium with reflection and transmission responses that must be calculated in order to obtain the field anywhere above or below the source in any layer.

5.7 System of layers containing a source

A system of homogeneous layers containing a source is shown in Figure 5.2. The interfaces are denoted as $0, ...j, ...N$ along the positive z-direction from the topmost interface to the bottommost interface. Now, consider propagation downwards from the source through the stack below:

$$\boldsymbol{w}(z_N) = \grave{\boldsymbol{Q}}(z_N, z_s^+)\boldsymbol{w}(z_s^+) = \grave{\boldsymbol{Q}}(z_N, z_s^-)\left[\boldsymbol{w}(z_s^-) + \boldsymbol{\Sigma}(z_s)\right]. \tag{5.72}$$

In the lower halfspace, that is, in the region below the interface z_N, there are only downgoing fields. Furthermore, the downgoing field above the source is the reflected upgoing field;

$\boldsymbol{d}(z_s^-) = \acute{\boldsymbol{R}}_s \boldsymbol{u}(z_s^-)$, where $\acute{\boldsymbol{R}}_s$ is the reflection response from a stack above z_s. Thus, equation 5.72 can be written as

$$\begin{pmatrix} \boldsymbol{0} \\ \boldsymbol{d}(z_N) \end{pmatrix} = \grave{\boldsymbol{Q}}_{11} \begin{pmatrix} \boldsymbol{I} & -\grave{\boldsymbol{R}}_s \\ \grave{\boldsymbol{Q}}_{11}^{-1}\grave{\boldsymbol{Q}}_{21} & \grave{\boldsymbol{Q}}_{11}^{-1}\grave{\boldsymbol{Q}}_{22} \end{pmatrix} \left\{ \begin{pmatrix} \boldsymbol{u}(z_s^-) \\ \acute{\boldsymbol{R}}_s \boldsymbol{u}(z_s^-) \end{pmatrix} + \begin{pmatrix} \acute{\boldsymbol{\Sigma}}(z_s) \\ \grave{\boldsymbol{\Sigma}}(z_s) \end{pmatrix} \right\}, \tag{5.73}$$

where the relation $\grave{\boldsymbol{R}}_s = -\grave{\boldsymbol{Q}}_{11}^{-1}\grave{\boldsymbol{Q}}_{12}$ from equation 5.51c has been used. The matrix $\grave{\boldsymbol{R}}_s$ represents the reflection response from the stack below z_s. The mode-field vector just above the source now becomes:

$$\boldsymbol{w}(z_s^-) = \begin{pmatrix} \boldsymbol{I} \\ \acute{\boldsymbol{R}}_s \end{pmatrix} \left(\boldsymbol{I} - \grave{\boldsymbol{R}}_s \acute{\boldsymbol{R}}_s \right)^{-1} \left(-\acute{\boldsymbol{\Sigma}} + \grave{\boldsymbol{R}}_s \grave{\boldsymbol{\Sigma}} \right). \tag{5.74}$$

In order to obtain an expression for the mode-field vector anywhere above the source, downward propagation of $\boldsymbol{w}(z)$ to $\boldsymbol{w}(z_s^-)$, where $z < z_s$, is considered by using equation 5.54a. The relation between the upgoing mode-fields now gives

$$\boldsymbol{u}(z < z_s) = \left(\boldsymbol{I} - \grave{\boldsymbol{R}}_u \acute{\boldsymbol{R}}_a \right)^{-1} \acute{\boldsymbol{T}}_u \boldsymbol{u}(z_s^-), \tag{5.75}$$

when the relation $\boldsymbol{d}(z) = \acute{\boldsymbol{R}}_a \boldsymbol{u}(z)$ is used. The notation follows from Figure 5.4: The reflection and transmission between $z < z_s$ and z_s is denoted $\acute{\boldsymbol{T}}_u$ and $\grave{\boldsymbol{R}}_u$, respectively; whereas the reflection from the above layers is denoted $\acute{\boldsymbol{R}}_a$. The total mode-field vector is thus

$$\boldsymbol{w}(z < z_s) = \begin{pmatrix} \boldsymbol{I} \\ \acute{\boldsymbol{R}}_a \end{pmatrix} \left(\boldsymbol{I} - \grave{\boldsymbol{R}}_u \acute{\boldsymbol{R}}_a \right)^{-1} \acute{\boldsymbol{T}}_u \left(\boldsymbol{I} - \grave{\boldsymbol{R}}_s \acute{\boldsymbol{R}}_s \right)^{-1} \left(-\acute{\boldsymbol{\Sigma}} + \grave{\boldsymbol{R}}_s \grave{\boldsymbol{\Sigma}} \right). \tag{5.76}$$

Written in this way the mode-field expression contains multiple reflections in the source layer and in the receiver layer. In addition there is a transmission matrix between these two layers.

An expression for the mode-field vector below the source can be found by considering propagation from the source through the upper stack:

$$\boldsymbol{w}(z_0) = \acute{\boldsymbol{Q}}(z_0, z_s^-)\boldsymbol{w}(z_s^-) = \acute{\boldsymbol{Q}}(z_0, z_s^+) \left[\boldsymbol{w}(z_s^+) - \boldsymbol{\Sigma}(z_s) \right]. \tag{5.77}$$

The radiation condition for the upper halfspace implies that there are only upgoing waves in this region. The upgoing field below the source equals the reflection response from the downgoing field, $\boldsymbol{u}(z_s^+) = \grave{\boldsymbol{R}}_s \boldsymbol{d}(z_s^+)$. This leads to a corresponding relation to equation 5.73:

$$\begin{pmatrix} \boldsymbol{u}(z_0) \\ \boldsymbol{0} \end{pmatrix} = \acute{\boldsymbol{Q}}_{22} \begin{pmatrix} \acute{\boldsymbol{Q}}_{22}^{-1}\acute{\boldsymbol{Q}}_{11} & \acute{\boldsymbol{Q}}_{22}^{-1}\acute{\boldsymbol{Q}}_{12} \\ -\acute{\boldsymbol{R}}_s & \boldsymbol{I} \end{pmatrix} \left\{ \begin{pmatrix} \grave{\boldsymbol{R}}_s \boldsymbol{d}(z_s^+) \\ \boldsymbol{d}(z_s^+) \end{pmatrix} - \begin{pmatrix} \acute{\boldsymbol{\Sigma}}(z_s) \\ \grave{\boldsymbol{\Sigma}}(z_s) \end{pmatrix} \right\}, \tag{5.78}$$

where $\acute{\boldsymbol{R}}_s = -\acute{\boldsymbol{Q}}_{22}^{-1}\acute{\boldsymbol{Q}}_{21}$ from equation 5.53c, and $\acute{\boldsymbol{R}}_s$ is the reflection response from the stack above z_s. The mode-field vector just below the source now becomes

$$\boldsymbol{w}(z_s^+) = \begin{pmatrix} \grave{\boldsymbol{R}}_s \\ \boldsymbol{I} \end{pmatrix} \left(\boldsymbol{I} - \acute{\boldsymbol{R}}_s \grave{\boldsymbol{R}}_s \right)^{-1} \left(\grave{\boldsymbol{\Sigma}} - \acute{\boldsymbol{R}}_s \acute{\boldsymbol{\Sigma}} \right), \tag{5.79}$$

and the mode-field vector anywhere below the source, $z > z_s$, is found by propagating $\boldsymbol{w}(z)$ up to $\boldsymbol{w}(z_s^+)$ with the propagator in equation 5.54b. By using that $\boldsymbol{u}(z) = \grave{\boldsymbol{R}}_b \boldsymbol{d}(z)$, a relation between the downgoing fields can be derived:

$$\boldsymbol{d}(z > z_s) = \left(\boldsymbol{I} - \acute{\boldsymbol{R}}_d \grave{\boldsymbol{R}}_b\right)^{-1} \grave{\boldsymbol{T}}_d \boldsymbol{d}(z_s^+). \tag{5.80}$$

The reflection and transmission between $z > z_s$ and z_s are denoted $\grave{\boldsymbol{T}}_d$ and $\acute{\boldsymbol{R}}_d$, respectively; whereas the reflection from the bottom layers is denoted $\grave{\boldsymbol{R}}_b$ as shown in Figure 5.4. The total mode-field vector then becomes

$$\boldsymbol{w}(z > z_s) = \begin{pmatrix} \grave{\boldsymbol{R}}_b \\ \boldsymbol{I} \end{pmatrix} \left(\boldsymbol{I} - \acute{\boldsymbol{R}}_d \grave{\boldsymbol{R}}_b\right)^{-1} \grave{\boldsymbol{T}}_d \left(\boldsymbol{I} - \acute{\boldsymbol{R}}_s \grave{\boldsymbol{R}}_s\right)^{-1} \left(\grave{\boldsymbol{\Sigma}} - \acute{\boldsymbol{R}}_s \acute{\boldsymbol{\Sigma}}\right). \tag{5.81}$$

Note that equation 5.76 can be obtained from equation 5.81 and vice versa by switching the roles of upgoing and downgoing mode-fields, reflection, transmission, and radiation. In addition, the signs of the mode-fields must be switched.

Within the source layer equations 5.76 and 5.81 reduce to

$$\boldsymbol{w}_s(z < z_s) = \begin{pmatrix} \mathrm{e}^{-i\omega \acute{\mathbf{p}}_{\mathbf{z}}(z - z_s)} \\ \acute{\boldsymbol{R}}_a \mathrm{e}^{-i\omega \acute{\mathbf{p}}_{\mathbf{z}}(z - z_s)} \end{pmatrix} \left(\boldsymbol{I} - \grave{\boldsymbol{R}}_s \acute{\boldsymbol{R}}_s\right)^{-1} \left(-\acute{\boldsymbol{\Sigma}} + \grave{\boldsymbol{R}}_s \grave{\boldsymbol{\Sigma}}\right), \tag{5.82a}$$

$$\boldsymbol{w}_s(z > z_s) = \begin{pmatrix} \grave{\boldsymbol{R}}_b \mathrm{e}^{i\omega \grave{\mathbf{p}}_{\mathbf{z}}(z - z_s)} \\ \mathrm{e}^{i\omega \grave{\mathbf{p}}_{\mathbf{z}}(z - z_s)} \end{pmatrix} \left(\boldsymbol{I} - \acute{\boldsymbol{R}}_s \grave{\boldsymbol{R}}_s\right)^{-1} \left(\grave{\boldsymbol{\Sigma}} - \acute{\boldsymbol{R}}_s \acute{\boldsymbol{\Sigma}}\right), \tag{5.82b}$$

where $\acute{\boldsymbol{R}}_a$ in this case differs from $\acute{\boldsymbol{R}}_s$ by a phase factor that corresponds to propagation down and up between the receiver and source, and likewise $\grave{\boldsymbol{R}}_b$ equals $\grave{\boldsymbol{R}}_s$ when the receiver is at the same z-level as the source. The eigenvalue submatrices in equation 5.82 are those of the source medium.

5.8 Eigenvalues and eigenvectors

In the previous section, expressions for the mode-field from an infinitesimal dipole source have been derived. The physical field follows from the transformation $\boldsymbol{b} = \boldsymbol{N}\boldsymbol{w}$ (equation 5.28). In order to calculate the mode-field, the reflection and transmission from a stack of layers are needed. These are provided by the relations in equation 5.70 and 5.71. The reflection and transmission from a single interface are described by equation 5.63. Finally, the expression for the source vector in the mode-domain as given by equation 5.44 is required.

In all of the derivations, the relations are obtained from the eigenvalues and eigenvectors of the system matrix $\boldsymbol{A}$. Thus, the calculation of the electromagnetic field is dependent on solving the eigenvalue problem for the system matrix in each homogeneous region. The eigenvalues and eigenvectors of $\boldsymbol{A}$ are dependent on the material parameters in the specified region and the horizontal slownesses p_x and p_y.

5.8.1 Eigenvalues

The eigenvalues of $\boldsymbol{A}$ are determined by solving $\det(\boldsymbol{A} - p_z \boldsymbol{I}) = 0$. This leads to the quartic equation

$$p_z^4 + b_3\, p_z^3 + b_2\, p_z^2 + b_1\, p_z + b_0 = 0, \tag{5.83}$$

where

$$b_3 = -2(a_{11} + a_{22}), \tag{5.84a}$$

$$b_2 = (a_{11} + a_{22})^2 + 2a_{11}a_{22} - 2a_{12}a_{21} - 2a_{14}a_{32} - a_{13}a_{31} - a_{24}a_{42}, \tag{5.84b}$$

$$\begin{aligned} b_1 = {} & 2a_{11}[a_{12}a_{21} + a_{14}a_{32} + a_{24}a_{42} - a_{22}(a_{11} + a_{22})] + 2a_{12}(a_{21}a_{22} - a_{24}a_{32} - a_{14}a_{31}), \\ & + 2a_{13}(a_{31}a_{22} - a_{21}a_{32}) + 2a_{14}(a_{22}a_{32} - a_{21}a_{42}), \end{aligned} \tag{5.84c}$$

$$\begin{aligned} b_0 = {} & a_{11}[a_{11}(a_{22}^2 - a_{24}a_{42}) + 2a_{12}(a_{24}a_{32} - a_{21}a_{22}) + 2a_{14}(a_{21}a_{42} - a_{22}a_{32})], \\ & + a_{12}[a_{12}(a_{21}^2 - a_{24}a_{31}) + 2a_{14}(a_{22}a_{31} - a_{21}a_{32})], \\ & + a_{13}[a_{21}(a_{22}a_{32} - a_{21}a_{42}) + a_{22}(a_{21}a_{32} - a_{22}a_{31}) + a_{24}(a_{31}a_{42} - a_{32}^2)], \\ & + a_{14}[a_{14}(a_{32}^2 - a_{31}a_{42})]. \end{aligned} \tag{5.84d}$$

The solution of equation 5.83 can be found using the approach in Abramowitz and Stegun (1962), page 17. This implies to determine one solution, e.g., u_1 of the cubic equation

$$u^3 - b_2 u^2 + (b_3 b_1 - 4b_0)u - [b_1^2 + b_0(b_3^2 - 4b_2)] = 0, \tag{5.85}$$

and then determining the four roots from the two quadratic equations:

$$p_z^2 + \left(\frac{b_3}{2} \mp \sqrt{\frac{b_3^2}{4} + u_1 - b_2}\right) p_z + \left(\frac{u_1}{2} \mp \sqrt{\frac{u_1^2}{4} - b_0}\right) = 0. \tag{5.86}$$

The derived set of roots p_{zj} (where $j = \{I, II, III, IV\}$) must satisfy the following relations

$$\sum p_{zj} = -b_3, \quad \sum p_{zj}p_{zk}p_{zl} = -b_1, \quad \sum p_{zj}p_{zk} = b_2, \quad \text{and} \quad p_{z\mathrm{I}}p_{z\mathrm{II}}p_{z\mathrm{III}}p_{z\mathrm{IV}} = b_0. \tag{5.87}$$

The eigenvalues represent slownesses in the vertical direction, and in general, these are all complex parameters. In order for the iterative reflectivity method to work properly (cf. equation 5.70 and 5.71), it is important that the eigenvalues that have positive (negative) imaginary parts are sorted into the upgoing (downgoing) submatrix in equation 5.30. Since the horizontal slownesses are real, this requirement (i.e., the radiation condition) corresponds to the requirement that the direction of the energy flow should determine which eigenvalue that relates to upgoing and downgoing constituents (cf. Chapman, 1994; Carcione and Schoenberg, 2000). In case of real eigenvalues, the determination of an eigenvalue being upgoing or downgoing relies on the energy-flow condition. In Appendix 5.C, a method for calculating the energy velocity in a homogeneous region in terms of the slowness and material parameters is presented.

Within each eigenvalue submatrix for upgoing and downgoing constituents, the sorting of the eigenvalues does not matter as shown in Appendix 5.D. If it is desirable to derive the correct physical reflection and transmission matrices at an interface, the eigenvalues must however have the same sorting on each side of the interface. This can be obtained by accounting for signs throughout the solution of the quartic equation. Another method for sorting the eigenvalues is provided through the calculation of the energy velocity in Appendix 5.C.

5.8.2 Eigenvectors

The eigenvector matrix $\boldsymbol{N}$ can be written in terms of the eigenvectors, matrix elements, and submatrices as

$$\sqrt{2}\boldsymbol{N} = \begin{pmatrix} \boldsymbol{n}_{\mathrm{I}} & \boldsymbol{n}_{\mathrm{II}} & \boldsymbol{n}_{\mathrm{III}} & \boldsymbol{n}_{\mathrm{IV}} \end{pmatrix} = \begin{pmatrix} n_{11} & n_{12} & n_{13} & n_{14} \\ n_{21} & n_{22} & n_{23} & n_{24} \\ n_{31} & n_{32} & -n_{33} & -n_{34} \\ n_{41} & n_{42} & -n_{43} & -n_{44} \end{pmatrix} = \begin{pmatrix} \acute{\boldsymbol{N}}_E & \grave{\boldsymbol{N}}_E \\ \acute{\boldsymbol{N}}_H & -\grave{\boldsymbol{N}}_H \end{pmatrix}. \quad (5.88)$$

Thus, $j = \{I,II,III,IV\}$ in the eigenvectors and corresponding eigenvalues, appear as $j = \{1,2,3,4\}$ in the second number in the subscript of the eigenvector-matrix elements. The eigenvectors that correspond to the eigenvalues are found from solving

$$\boldsymbol{A}\boldsymbol{n}_j = p_{zj}\boldsymbol{n}_j, \quad (5.89)$$

and for each eigenvalue p_{zj}, the following relations between the entries in an eigenvector can be obtained:

$$n_{2j} = \frac{\beta_{2j}}{\beta_{1j}} n_{1j}, \quad n_{3j} = \pm\frac{\beta_{3j}}{\beta_{1j}} n_{1j}, \quad \text{and} \quad n_{4j} = \pm\frac{\beta_{4j}}{\beta_{1j}} n_{1j}, \quad (5.90)$$

where the plus sign is applied when $j = \{1,2\}$ and minus sign when $j = \{3,4\}$, and where

$$\begin{aligned} \beta_{1j} = \quad & (a_{11}-p_{zj})(a_{22}-p_{zj})a_{14} - (a_{11}-p_{zj})a_{12}a_{24} \\ & - (a_{22}-p_{zj})a_{13}a_{21} - a_{14}^2 a_{32} + a_{12}a_{14}a_{21} + a_{13}a_{24}a_{32}, \quad (5.91a) \\ \beta_{2j} = \quad & a_{24}(a_{11}-p_{zj})^2 - 2a_{14}a_{21}(a_{11}-p_{zj}) + a_{13}(a_{21}^2 - a_{24}a_{31}) + a_{14}^2 a_{31}, \quad (5.91b) \\ \beta_{3j} = \quad & a_{21}(a_{11}-p_{zj})(a_{22}-p_{zj}) - a_{24}a_{32}(a_{11}-p_{zj}) \\ & - a_{14}a_{31}(a_{22}-p_{zj}) - a_{12}(a_{21}^2 - a_{24}a_{31}) + a_{14}a_{21}a_{32}, \quad (5.91c) \\ \beta_{4j} = \quad & -(a_{11}-p_{zj})^2(a_{22}-p_{zj}) + (a_{12}a_{21}+a_{14}a_{32})(a_{11}-p_{zj}) \\ & + a_{13}a_{31}(a_{22}-p_{zj}) - a_{12}a_{14}a_{31} - a_{13}a_{21}a_{32}. \quad (5.91d) \end{aligned}$$

The n_{1j}-entries are obtained from the flux-normalization criterion. The relation $\boldsymbol{N}\boldsymbol{N}^{-1} = \boldsymbol{I}$ in terms of the eigenvector submatrices from equation 5.40 implies that

$$\begin{aligned} \acute{\boldsymbol{N}}_E\acute{\boldsymbol{N}}_H^T + \grave{\boldsymbol{N}}_E\grave{\boldsymbol{N}}_H^T = 2\boldsymbol{I}, \quad \acute{\boldsymbol{N}}_H\acute{\boldsymbol{N}}_H^T = \grave{\boldsymbol{N}}_H\grave{\boldsymbol{N}}_H^T, \\ \acute{\boldsymbol{N}}_H\acute{\boldsymbol{N}}_E^T + \grave{\boldsymbol{N}}_H\grave{\boldsymbol{N}}_E^T = 2\boldsymbol{I}, \quad \acute{\boldsymbol{N}}_E\acute{\boldsymbol{N}}_E^T = \grave{\boldsymbol{N}}_E\grave{\boldsymbol{N}}_E^T, \end{aligned} \quad (5.92)$$

and these equations provide the set of equations:

$$n_{11}^2 + n_{12}^2 - n_{13}^2 - n_{14}^2 = 0, \tag{5.93a}$$

$$n_{11}n_{21} + n_{12}n_{22} - n_{13}n_{23} - n_{14}n_{24} = 0, \tag{5.93b}$$

$$n_{11}n_{31} + n_{12}n_{32} + n_{13}n_{33} + n_{14}n_{34} = 2, \tag{5.93c}$$

$$n_{11}n_{41} + n_{12}n_{42} + n_{13}n_{43} + n_{14}n_{44} = 0, \tag{5.93d}$$

where n_{11}, n_{12}, n_{13}, and n_{14} are the unknowns. The solution is

$$n_{11}^2 = 2(\alpha_{12}\alpha_{23} - \alpha_{13}\alpha_{22})D_\alpha^{-1}, \qquad n_{12}^2 = 2(\alpha_{13}\alpha_{21} - \alpha_{11}\alpha_{23})D_\alpha^{-1}, \tag{5.94a}$$

$$n_{13}^2 = 2(\alpha_{11}\alpha_{22} - \alpha_{12}\alpha_{21})D_\alpha^{-1}, \qquad n_{14}^2 = n_{11}^2 + n_{12}^2 - n_{13}^2, \tag{5.94b}$$

$$\alpha_{11} = \beta'_{24} - \beta'_{21}, \qquad \alpha_{12} = \beta'_{24} - \beta'_{22}, \qquad \alpha_{13} = \beta'_{23} - \beta'_{24}, \tag{5.94c}$$

$$\alpha_{21} = \beta'_{41} - \beta'_{44}, \qquad \alpha_{22} = \beta'_{42} - \beta'_{44}, \qquad \alpha_{23} = \beta'_{44} - \beta'_{43}, \tag{5.94d}$$

$$\alpha_{31} = \beta'_{31} - \beta'_{34}, \qquad \alpha_{32} = \beta'_{32} - \beta'_{34}, \qquad \alpha_{33} = \beta'_{34} - \beta'_{33}, \tag{5.94e}$$

where the quotient $\beta'_{ij} = \beta_{ij}/\beta_{1j}$ has been introduced, and

$$D_\alpha = \alpha_{11}(\alpha_{22}\alpha_{33} - \alpha_{23}\alpha_{32}) + \alpha_{12}(\alpha_{23}\alpha_{31} - \alpha_{21}\alpha_{33}) + \alpha_{13}(\alpha_{21}\alpha_{32} - \alpha_{22}\alpha_{31}). \tag{5.94f}$$

The sign of the square root in the solutions for n_{11} and n_{12} can be chosen at will, but the sign of n_{13} and n_{14} must correspond to the selected sign for n_{11} and n_{12}, respectively.

5.9 Up/down-symmetric media

When one of the principal axes in the anisotropic medium coincides with the vertical axis of the main coordinate system, the relation between the principal and main coordinate systems is given in terms of one rotation in the horizontal plane (cf. Appendix 5.A). This corresponds to a monoclinic medium with the horizontal plane as a mirror plane of symmetry. Then the system matrix reduces to:

$$\boldsymbol{A} = \begin{pmatrix} \boldsymbol{0} & \boldsymbol{A}_1 \\ \boldsymbol{A}_2 & \boldsymbol{0} \end{pmatrix}. \tag{5.95}$$

In this case the entries in the submatrices are denoted

$$\boldsymbol{A}_1 = \begin{pmatrix} a'_{13} & a'_{14} \\ a'_{14} & a'_{24} \end{pmatrix} \quad \text{and} \quad \boldsymbol{A}_2 = \begin{pmatrix} a'_{31} & a'_{32} \\ a'_{32} & a'_{42} \end{pmatrix}, \tag{5.96}$$

where the same indices as in the general case are used. However, the expressions in the entries simplify compared to the general case and become:

$$a'_{13} = \mu_{yy} - \tfrac{p_x^2}{\tilde{\varepsilon}_v}, \qquad a'_{14} = -\mu_{xy} - \tfrac{p_x p_y}{\tilde{\varepsilon}_v}, \tag{5.97a}$$

$$a'_{24} = \mu_{xx} - \tfrac{p_y^2}{\tilde{\varepsilon}_v}, \qquad a'_{31} = \tilde{\varepsilon}_{xx} - \tfrac{p_y^2}{\mu_v}, \tag{5.97b}$$

$$a'_{32} = \tilde{\varepsilon}_{xy} + \tfrac{p_x p_y}{\mu_v}, \qquad a'_{42} = \tilde{\varepsilon}_{yy} - \tfrac{p_x^2}{\mu_v}. \tag{5.97c}$$

Now, because of the symmetry in the original 4×4-matrices, the eigenvalues and eigenvectors can be obtained from 2×2-matrices. The product of the submatrices will become useful:

$$\boldsymbol{A}_1\boldsymbol{A}_2 = \begin{pmatrix} \alpha'_{11} & \alpha'_{12} \\ \alpha'_{21} & \alpha'_{22} \end{pmatrix}, \tag{5.98}$$

where

$$\begin{aligned} \alpha'_{11} &= a'_{13}a'_{31} + a'_{14}a'_{32}, \quad \alpha'_{12} = a'_{13}a'_{32} + a'_{14}a'_{42}, \\ \alpha'_{21} &= a'_{14}a'_{31} + a'_{24}a'_{32}, \quad \alpha'_{22} = a'_{14}a'_{32} + a'_{24}a'_{42}. \end{aligned} \tag{5.99}$$

The eigenvalues can be derived from the expression in equation 5.83 where the terms b_3 and b_1 are zero for the up/down-symmetric (u/d-symmetric) case. This means that the quartic equation reduces to a quadratic equation for the squared eigenvalues, which can be written in terms of the submatrix product as:

$$p_z = \pm\left\{\frac{1}{2}\left[\mathrm{tr}(\boldsymbol{A}_1\boldsymbol{A}_2) \pm \sqrt{\mathrm{tr}^2\left(\boldsymbol{A}_1\boldsymbol{A}_2\right) - 4\mathrm{det}(\boldsymbol{A}_1\boldsymbol{A}_2)}\right]\right\}^{1/2}. \tag{5.100}$$

The two eigenvalues that correspond to the positive sign in front of the square root are $p_{z\mathrm{I}}$ and $p_{z\mathrm{II}}$. These two quantities are furthermore obtained by using the positive and negative sign inside the square root, respectively. Then $p_{z\mathrm{III}} = -p_{z\mathrm{I}}$ and $p_{z\mathrm{IV}} = -p_{z\mathrm{II}}$, which means that the eigenvalue submatrices in equation 5.30 are equal due to the u/d-symmetry: $\acute{\mathbf{p}}_\mathbf{z} = \grave{\mathbf{p}}_\mathbf{z} = \mathbf{p}_\mathbf{z}$.

Because of the symmetry in the upgoing and downgoing field constituents, the submatrices in equation 5.88 become pairwise equal:

$$\boldsymbol{N} = \frac{1}{\sqrt{2}}\begin{pmatrix} \boldsymbol{N}_E & \boldsymbol{N}_E \\ \boldsymbol{N}_H & -\boldsymbol{N}_H \end{pmatrix}, \tag{5.101}$$

where the block inverse and relation from the general expression for the eigenvector matrix (equation 5.40) give:

$$\boldsymbol{N}^{-1} = \frac{1}{\sqrt{2}}\begin{pmatrix} \boldsymbol{N}_E^{-1} & \boldsymbol{N}_H^{-1} \\ \boldsymbol{N}_E^{-1} & -\boldsymbol{N}_H^{-1} \end{pmatrix} = \frac{1}{\sqrt{2}}\begin{pmatrix} \boldsymbol{N}_H^{T} & \boldsymbol{N}_E^{T} \\ \boldsymbol{N}_H^{T} & -\boldsymbol{N}_E^{T} \end{pmatrix}. \tag{5.102}$$

The following symmetry-relations thus appear:

$$\boldsymbol{N}_E^{-1} = \boldsymbol{N}_H^{T}, \quad \boldsymbol{N}_H^{-1} = \boldsymbol{N}_E^{T}. \tag{5.103}$$

The similarity transform $\boldsymbol{A}\boldsymbol{N} = \boldsymbol{N}\boldsymbol{\Lambda}$, where $\boldsymbol{\Lambda} = \mathrm{diag}\{\mathbf{p}_\mathbf{z}, -\mathbf{p}_\mathbf{z}\}$ then gives the equations:

$$\boldsymbol{A}_1 = \boldsymbol{N}_E\mathbf{p}_\mathbf{z}\boldsymbol{N}_E^{T} \quad \text{and} \quad \boldsymbol{A}_2 = \boldsymbol{N}_H\mathbf{p}_\mathbf{z}\boldsymbol{N}_H^{T}. \tag{5.104}$$

Complex symmetric matrices as $\boldsymbol{A}_1$ and $\boldsymbol{A}_2$ can always be diagonalized as in equation 5.104 (Horn and Johnson, 1985). It has previously been shown that this choice of eigenvectors corresponds to a flux normalization.

By writing $\boldsymbol{N}_E = \begin{pmatrix} \boldsymbol{n}_{\text{I}} & \boldsymbol{n}_{\text{II}} \end{pmatrix}$, the multiplication of $\boldsymbol{A}_2$ by $\boldsymbol{A}_1$ from the left in equation 5.104 leads to:

$$\boldsymbol{A}_1\boldsymbol{A}_2\boldsymbol{n}_j = p_{zj}^2\boldsymbol{n}_j, \tag{5.105}$$

where $j = \{I,II\}$. Using the relations in equation 5.103, the eigenvector submatrices $\boldsymbol{N}_E$ and $\boldsymbol{N}_H$ can be written as:

$$\boldsymbol{N}_E = \begin{pmatrix} n_{11} & n_{12} \\ n_{21} & n_{22} \end{pmatrix}, \quad \boldsymbol{N}_H = \frac{1}{n_{11}n_{22} - n_{12}n_{21}} \begin{pmatrix} n_{22} & -n_{21} \\ -n_{12} & n_{11} \end{pmatrix}. \tag{5.106}$$

The elements in the eigenvector matrices can now be calculated in terms of the eigenvalues $p_{z\text{I}}$ and $p_{z\text{II}}$ from equation 5.100 as follows: Find a relation between the entries in the eigenvectors from equation 5.105, and use equation 5.104 to obtain a scaling between the eigenvectors that satisfies the flux-normalization condition. It is useful to derive two sets of solutions. The following expressions can be used as long as the anisotropy is not uniaxial and in the y-direction:

$$n_{21} = \left[\frac{a'_{14}\alpha'_{21} + a'_{24}\left(\alpha'_{22} - p_{z\text{II}}^2\right)}{p_{z\text{I}}\left(p_{z\text{I}}^2 - p_{z\text{II}}^2\right)}\right]^{1/2}, \quad n_{22} = \left[\frac{a'_{14}\alpha'_{21} + a'_{24}\left(\alpha'_{22} - p_{z\text{I}}^2\right)}{p_{z\text{II}}\left(p_{z\text{II}}^2 - p_{z\text{I}}^2\right)}\right]^{1/2}, \tag{5.107a}$$

$$n_{11} = \frac{p_{z\text{I}}^2 - \alpha'_{22}}{\alpha'_{21}}n_{21}, \qquad n_{12} = \frac{p_{z\text{II}}^2 - \alpha'_{22}}{\alpha'_{21}}n_{22}. \tag{5.107b}$$

Equivalently, the following set of eigenvectors can be used, except for uniaxial anisotropy with a direction that coincides with the x-direction:

$$n_{11} = \left[\frac{a'_{14}\alpha'_{12} + a'_{13}\left(\alpha'_{11} - p_{z\text{II}}^2\right)}{p_{z\text{I}}\left(p_{z\text{I}}^2 - p_{z\text{II}}^2\right)}\right]^{1/2}, \quad n_{12} = \left[\frac{a'_{14}\alpha'_{12} + a'_{13}\left(\alpha'_{11} - p_{z\text{I}}^2\right)}{p_{z\text{II}}\left(p_{z\text{II}}^2 - p_{z\text{I}}^2\right)}\right]^{1/2}, \tag{5.108a}$$

$$n_{21} = \frac{p_{z\text{I}}^2 - \alpha'_{11}}{\alpha'_{12}}n_{11}, \qquad n_{22} = \frac{p_{z\text{II}}^2 - \alpha'_{11}}{\alpha'_{12}}n_{12}. \tag{5.108b}$$

5.9.1 Common principal and coordinate axes

The case where the principal axes of anisotropy coincide with the coordinate axes will be denoted as nonrotated orthorhombic. Since the Fourier expansion of dipole radiation in stratified media gives a spectrum of slownesses in terms of p_x and p_y, this orthorhombic case does not in general lead to any simplifications compared to an u/d-symmetric case where the principal axes are rotated with respect to the horizontal coordinate axes. However, the expressions for the eigenvalues simplify for uniaxial nonrotated orthorhombic media. Thus, it might be enlightening to calculate the eigenvalues for biaxial orthorhombic media explicitly. To this end, note that it is possible to always choose the coordinate system to coincide with the principal axes of anisotropy for u/d-symmetric media by decomposing the antenna into x- and y-components that coincide with the principal axes.

For nonrotated orthorhombic media, the material parameters are $\tilde{\boldsymbol{\varepsilon}} = \mathrm{diag}\{\tilde{\varepsilon}_1, \tilde{\varepsilon}_2, \tilde{\varepsilon}_3\}$ and $\boldsymbol{\mu} = \mathrm{diag}\{\mu_1, \mu_2, \mu_3\}$. The eigenvalues of $\boldsymbol{A}$ become:

$$p_{z\mathrm{I}} = \left[\tfrac{1+f(p_x)}{2}\left(\mu_2\tilde{\varepsilon}_1 - \tfrac{\mu_1}{\mu_3}p_x^2 - \tfrac{\mu_2}{\mu_3}p_y^2\right) + \tfrac{1-f(p_x)}{2}\left(\mu_1\tilde{\varepsilon}_2 - \tfrac{\tilde{\varepsilon}_1}{\tilde{\varepsilon}_3}p_x^2 - \tfrac{\tilde{\varepsilon}_2}{\tilde{\varepsilon}_3}p_y^2\right)\right]^{1/2}, \tag{5.109a}$$

$$p_{z\mathrm{II}} = \left[\tfrac{1+f(p_x)}{2}\left(\mu_1\tilde{\varepsilon}_2 - \tfrac{\tilde{\varepsilon}_1}{\tilde{\varepsilon}_3}p_x^2 - \tfrac{\tilde{\varepsilon}_2}{\tilde{\varepsilon}_3}p_y^2\right) + \tfrac{1-f(p_x)}{2}\left(\mu_2\tilde{\varepsilon}_1 - \tfrac{\mu_1}{\mu_3}p_x^2 - \tfrac{\mu_2}{\mu_3}p_y^2\right)\right]^{1/2}, \tag{5.109b}$$

where

$$f(p_x) = \sqrt{1 + \tfrac{4(\mu_1\tilde{\varepsilon}_2 - \mu_2\tilde{\varepsilon}_1)q_1p_x^2}{\left(\mu_1\tilde{\varepsilon}_2 - \mu_2\tilde{\varepsilon}_1 + q_1p_x^2 + q_2p_y^2\right)^2}}\,, \tag{5.109c}$$

with $q_1 = \tilde{\varepsilon}_1/\tilde{\varepsilon}_3 - \mu_1/\mu_3$ and $q_2 = \tilde{\varepsilon}_2/\tilde{\varepsilon}_3 - \mu_2/\mu_3$. The eigenvalues can also be written as

$$p_{z\mathrm{I}} = \left[\tfrac{1+f(p_y)}{2}\left(\mu_1\tilde{\varepsilon}_2 - \tfrac{\mu_1}{\mu_3}p_x^2 - \tfrac{\mu_2}{\mu_3}p_y^2\right) + \tfrac{1-f(p_y)}{2}\left(\mu_2\tilde{\varepsilon}_1 - \tfrac{\tilde{\varepsilon}_1}{\tilde{\varepsilon}_3}p_x^2 - \tfrac{\tilde{\varepsilon}_2}{\tilde{\varepsilon}_3}p_y^2\right)\right]^{1/2}, \tag{5.110a}$$

$$p_{z\mathrm{II}} = \left[\tfrac{1+f(p_y)}{2}\left(\mu_2\tilde{\varepsilon}_1 - \tfrac{\tilde{\varepsilon}_1}{\tilde{\varepsilon}_3}p_x^2 - \tfrac{\tilde{\varepsilon}_2}{\tilde{\varepsilon}_3}p_y^2\right) + \tfrac{1-f(p_y)}{2}\left(\mu_1\tilde{\varepsilon}_2 - \tfrac{\mu_1}{\mu_3}p_x^2 - \tfrac{\mu_2}{\mu_3}p_y^2\right)\right]^{1/2}, \tag{5.110b}$$

where

$$f(p_y) = \sqrt{1 - \tfrac{4(\mu_1\tilde{\varepsilon}_2 - \mu_2\tilde{\varepsilon}_1)q_2p_y^2}{\left(\mu_1\tilde{\varepsilon}_2 - \mu_2\tilde{\varepsilon}_1 + q_1p_x^2 + q_2p_y^2\right)^2}}\,. \tag{5.110c}$$

Note that the quantity $f(p_x)$ is equal to one when p_x is zero, and similarly that $f(p_y)$ is equal to one when p_y is zero.

When the anisotropy is uniaxial and in the x-direction, the expressions for the eigenvalues simplify since $q_2 = 0$ which means that $f(p_y) = 1$. Thus,

$$p_{z\mathrm{I}} = \sqrt{\mu_1\tilde{\varepsilon}_2 - \tfrac{\mu_1}{\mu_3}p_x^2 - p_y^2} \quad \text{and} \quad p_{z\mathrm{II}} = \sqrt{\mu_2\tilde{\varepsilon}_1 - \tfrac{\tilde{\varepsilon}_1}{\tilde{\varepsilon}_3}p_x^2 - p_y^2}\,. \tag{5.111}$$

Similarly, when the anisotropy direction is along the y-axis only, $q_1 = 0$ and $f(p_x) = 1$. Then

$$p_{z\mathrm{I}} = \sqrt{\mu_2\tilde{\varepsilon}_1 - p_x^2 - \tfrac{\mu_2}{\mu_3}p_y^2} \quad \text{and} \quad p_{z\mathrm{II}} = \sqrt{\mu_1\tilde{\varepsilon}_2 - p_x^2 - \tfrac{\tilde{\varepsilon}_2}{\tilde{\varepsilon}_3}p_y^2}\,. \tag{5.112}$$

5.9.2 Reflection and transmission coefficients

In u/d-symmetric stratified layers the relations in equation 5.59 reduce to

$$\acute{\boldsymbol{R}} = \acute{\boldsymbol{R}}^T, \quad \grave{\boldsymbol{R}} = \grave{\boldsymbol{R}}^T, \quad \text{and} \quad \acute{\boldsymbol{T}} = \grave{\boldsymbol{T}}^T. \tag{5.113}$$

At an interface between two u/d-symmetric media, the relations in equation 5.63 reduce to:

$$\acute{\boldsymbol{t}} = 2\left(\boldsymbol{C} + \boldsymbol{D}\right)^{-T}, \tag{5.114a}$$

$$\acute{\boldsymbol{r}} = -\left(\boldsymbol{C} - \boldsymbol{D}\right)^T\left(\boldsymbol{C} + \boldsymbol{D}\right)^{-T} = -\left(\boldsymbol{C} + \boldsymbol{D}\right)^{-1}\left(\boldsymbol{C} - \boldsymbol{D}\right), \tag{5.114b}$$

$$\grave{\boldsymbol{r}} = \left(\boldsymbol{C} - \boldsymbol{D}\right)\left(\boldsymbol{C} + \boldsymbol{D}\right)^{-1} = \left(\boldsymbol{C} + \boldsymbol{D}\right)^{-T}\left(\boldsymbol{C} - \boldsymbol{D}\right)^T, \tag{5.114c}$$

$$\grave{\boldsymbol{t}} = 2\left(\boldsymbol{C} + \boldsymbol{D}\right)^{-1}, \tag{5.114d}$$

since the relations in equation 5.61 now are

$$\boldsymbol{C} = \left[\boldsymbol{N}_H^-\right]^T \boldsymbol{N}_E^+ \quad \text{and} \quad \boldsymbol{D} = \left[\boldsymbol{N}_E^-\right]^T \boldsymbol{N}_H^+, \tag{5.115}$$

because of the symmetries in the eigenvector submatrices in equation 5.103. The superscripts "−" and "+" denote upper and lower homogeneous regions, respectively; and the matrices $\boldsymbol{C}$ and $\boldsymbol{D}$ have the property $\boldsymbol{C}\boldsymbol{D}^T = \boldsymbol{I}$. This way of writing reflection and transmission matrices for u/d-symmetric media was introduced by Ursin and Stovas (2002). From equation 5.114 it can be verified that the upgoing and downgoing reflection matrices are related as

$$\acute{\boldsymbol{r}} = -\grave{\boldsymbol{t}}\hat{\boldsymbol{r}}\grave{\boldsymbol{t}}^{-1} \quad \text{and} \quad \hat{\boldsymbol{r}} = -\acute{\boldsymbol{t}}\acute{\boldsymbol{r}}\acute{\boldsymbol{t}}^{-1}, \tag{5.116}$$

and that the reflection matrices are related to the transmission matrices as

$$\acute{\boldsymbol{r}}^2 = \boldsymbol{I} - \grave{\boldsymbol{t}}\acute{\boldsymbol{t}} \quad \text{and} \quad \hat{\boldsymbol{r}}^2 = \boldsymbol{I} - \acute{\boldsymbol{t}}\grave{\boldsymbol{t}}. \tag{5.117}$$

The relations in continuously varying media also simplify with u/d-symmetry since $\acute{\boldsymbol{F}} = \grave{\boldsymbol{F}} = \boldsymbol{F}$ and $\check{\boldsymbol{G}} = \hat{\boldsymbol{G}} = \boldsymbol{G}$. For *weak contrasts*, the approximations in equation 5.68 then imply that $\acute{\boldsymbol{r}} \approx -\hat{\boldsymbol{r}}$.

5.10 Transverse isotropy in the vertical direction

Transverse isotropy in the vertical direction (TIV) means that the electromagnetic properties of a medium are rotationally symmetric about the z-axis. In this case the constitutive relations simplify to $\tilde{\boldsymbol{\varepsilon}} = \operatorname{diag}\{\tilde{\varepsilon}_h, \tilde{\varepsilon}_h, \tilde{\varepsilon}_v\}$ and $\boldsymbol{\mu} = \operatorname{diag}\{\mu_h, \mu_h, \mu_v\}$, and the system matrix has the same form as in equation 5.95 with

$$\boldsymbol{A}_1 = \frac{1}{\tilde{\varepsilon}_v}\begin{pmatrix} \mu_h\tilde{\varepsilon}_v - p_x^2 & -p_x p_y \\ -p_x p_y & \mu_h\tilde{\varepsilon}_v - p_y^2 \end{pmatrix}, \quad \boldsymbol{A}_2 = \frac{1}{\mu_v}\begin{pmatrix} \mu_v\tilde{\varepsilon}_h - p_y^2 & p_x p_y \\ p_x p_y & \mu_v\tilde{\varepsilon}_h - p_x^2 \end{pmatrix}. \tag{5.118}$$

The eigenvalues of $\boldsymbol{A}$ now become

$$p_{z\mathrm{I}} = -p_{z\mathrm{III}} = \sqrt{\mu_h\tilde{\varepsilon}_h - \tfrac{\mu_h}{\mu_v}\left(p_x^2 + p_y^2\right)}\,, \tag{5.119a}$$

$$p_{z\mathrm{II}} = -p_{z\mathrm{IV}} = \sqrt{\mu_h\tilde{\varepsilon}_h - \tfrac{\tilde{\varepsilon}_h}{\tilde{\varepsilon}_v}\left(p_x^2 + p_y^2\right)}\,. \tag{5.119b}$$

The eigenvector matrix and its inverse from equation 5.101 and 5.102 have the submatrices:

$$\boldsymbol{N}_E = \frac{1}{p_\rho}\begin{pmatrix} p_y\sqrt{\frac{\mu_h}{p_{z\mathrm{I}}}} & p_x\sqrt{\frac{p_{z\mathrm{II}}}{\tilde{\varepsilon}_h}} \\ -p_x\sqrt{\frac{\mu_h}{p_{z\mathrm{I}}}} & p_y\sqrt{\frac{p_{z\mathrm{II}}}{\tilde{\varepsilon}_h}} \end{pmatrix} \quad \text{and} \quad \boldsymbol{N}_H = \frac{1}{p_\rho}\begin{pmatrix} p_y\sqrt{\frac{p_{z\mathrm{I}}}{\mu_h}} & p_x\sqrt{\frac{\tilde{\varepsilon}_h}{p_{z\mathrm{II}}}} \\ -p_x\sqrt{\frac{p_{z\mathrm{I}}}{\mu_h}} & p_y\sqrt{\frac{\tilde{\varepsilon}_h}{p_{z\mathrm{II}}}} \end{pmatrix}, \tag{5.120}$$

where $p_\rho = \sqrt{p_x^2 + p_y^2}$.

5.10.1 Reflection and transmission matrices

In the TIV case, explicit expressions for the reflection and transmission matrices can be derived by inserting equation 5.120 into 5.115 and using equation 5.114:

$$\grave{\boldsymbol{t}} = \begin{pmatrix} \frac{2\sqrt{\mu_h^-\,\mu_h^+\,p_{z\mathrm{I}}^-\,p_{z\mathrm{I}}^+}}{\mu_h^+\,p_{z\mathrm{I}}^- + \mu_h^-\,p_{z\mathrm{I}}^+} & 0 \\ 0 & \frac{2\sqrt{\tilde{\varepsilon}_h^-\,\tilde{\varepsilon}_h^+\,p_{z\mathrm{II}}^-\,p_{z\mathrm{II}}^+}}{\tilde{\varepsilon}_h^-\,p_{z\mathrm{II}}^+ + \tilde{\varepsilon}_h^+\,p_{z\mathrm{II}}^-} \end{pmatrix} \quad \grave{\boldsymbol{r}} = \begin{pmatrix} \frac{\mu_h^+\,p_{z\mathrm{I}}^- - \mu_h^-\,p_{z\mathrm{I}}^+}{\mu_h^+\,p_{z\mathrm{I}}^- + \mu_h^-\,p_{z\mathrm{I}}^+} & 0 \\ 0 & \frac{\tilde{\varepsilon}_h^-\,p_{z\mathrm{II}}^+ - \tilde{\varepsilon}_h^+\,p_{z\mathrm{II}}^-}{\tilde{\varepsilon}_h^-\,p_{z\mathrm{II}}^+ + \tilde{\varepsilon}_h^+\,p_{z\mathrm{II}}^-} \end{pmatrix}. \quad (5.121)$$

Since these matrices are diagonal, the relations in equation 5.113 and 5.116 lead to

$$\acute{\boldsymbol{t}} = \grave{\boldsymbol{t}} \quad \text{and} \quad \acute{\boldsymbol{r}} = -\grave{\boldsymbol{r}}. \quad (5.122)$$

In equation 5.121 the reflection coefficients are recognized as the Fresnel coefficients for transverse electric (TE) and transverse magnetic (TM) polarization (cf. Stratton, 1941; Jackson, 1998). Thus, in the TIV case, the eigenvalue $p_{z\mathrm{I}}$ corresponds to a TE mode, and the eigenvalue $p_{z\mathrm{II}}$ corresponds to a TM mode. The transmission coefficients are symmetric across the interface. In order to obtain the Fresnel transmission coefficients, another normalization of the eigenvectors can be chosen as shown in Appendix 5.E.

5.10.2 Recursive reflection and transmission responses

When the transmission and reflection matrices describing propagation through one interface are diagonal, the expressions in equations 5.70 and 5.71 simplify. The result is scalar recursive reflection and transmission responses valid for both modes. By using the relations in equation 5.117 and 5.122, one gets:

$$R_m = \frac{r_m + R_{m+1}}{1 + r_m R_{m+1}} \mathrm{e}^{2i\omega p_z h_m}, \quad (5.123a)$$

$$T_m = \frac{t_m T_{m+1}}{1 + r_m R_{m+1}} \mathrm{e}^{i\omega p_z h_m}, \quad (5.123b)$$

where $p_z = p_{z\mathrm{I}}$ for the TE mode and $p_z = p_{z\mathrm{II}}$ for the TM mode. It is implicit that the eigenvalues take their respective values in the m'th layer. The initial conditions at the start of the stack are $R_{M+1} = 0$ and $T_{M+1} = \mathrm{e}^{i\omega p_z h_{M+1}}$. The expressions can be used for both upgoing and downgoing reflection and transmission coefficients. In both cases h_m describes the thickness from the m'th interface, where r_m and t_m are evaluated, to the z-level of R_m and T_m.

5.11 Isotropic media

In isotropic media the system matrix has the same form as in equation 5.95, but now

$$\boldsymbol{A}_1 = \frac{1}{\tilde{\varepsilon}} \begin{pmatrix} \mu\tilde{\varepsilon} - p_x^2 & -p_x p_y \\ -p_x p_y & \mu\tilde{\varepsilon} - p_y^2 \end{pmatrix}, \quad \boldsymbol{A}_2 = \frac{1}{\mu} \begin{pmatrix} \mu\tilde{\varepsilon} - p_y^2 & p_x p_y \\ p_x p_y & \mu\tilde{\varepsilon} - p_x^2 \end{pmatrix}, \quad (5.124)$$

and the eigenvalues are

$$p_z = p_{z\mathrm{I}} = p_{z\mathrm{II}} = -p_{z\mathrm{III}} = -p_{z\mathrm{IV}} = \sqrt{\mu\tilde{\varepsilon} - p_x^2 - p_y^2}. \tag{5.125}$$

Because of the degeneracy of the eigenvalues there are several possibilities for choosing a linear independent set of 4 eigenvectors that satisfy the flux-normalization condition. It will however be convenient to choose the same form of the eigenvector matrix as in the TIV case. Thus, the same eigenvector matrices as in equation 5.120 can be used with $\mu_h = \mu_v = \mu$, $\tilde{\varepsilon}_h = \tilde{\varepsilon}_v = \tilde{\varepsilon}$ and $p_{z\mathrm{I}} = p_{z\mathrm{II}} = p_z$. All the relations that have been derived and will be derived for TIV media are hence valid for isotropic media.

5.12 Explicit expressions for the electromagnetic fields

By using equations 5.76 and 5.81 the electromagnetic field in a stratified medium with general anisotropy in *all* the layers can be obtained. However, in many applications in geophysics the source medium is isotropic or transversely isotropic in the vertical direction (TIV). The purpose in this section is to derive explicit expressions for the electromagnetic fields from sources that are either a horizontal electric dipole (HED), vertical electric dipole (VED), horizontal magnetic dipole (HMD), or vertical magnetic dipole (VMD) when the source and receiver are situated in TIV or isotropic media. The infinitesimal dipole source is contained in one of the layers as shown in Figure 5.2, and the resulting electromagnetic field can be obtained in any TIV or isotropic layer from the explicit expressions that will be derived. In all layers other than the source and receiver layer(s), the anisotropy may be arbitrary.

The field expressions are given in the frequency-wavenumber domain, and a 2-D Fourier transform is required in order to get to the spatial domain. It is only in the case of TIV or isotropy in all the layers that the transformation to the spatial domain can be reduced to a single integral by using cylindrical coordinates. The field expressions for such cases are given in Appendix 5.F.

5.12.1 Up/down-symmetry in the source and receiver layer(s)

If the source and receiver layers have u/d-symmetry, the expressions for the mode-field vectors in equations 5.76 and 5.81, and the corresponding physical field vectors $\boldsymbol{b} = (\boldsymbol{b}_E\,;\ \boldsymbol{b}_H)$, simplify. The resulting fields from the four types of sources (HED, HMD, VED, and VMD) are considered. The source vectors from equation 5.16 are split into $\boldsymbol{s}_E = \left(\boldsymbol{s}_E^v\,;\ \boldsymbol{s}_E^h\right)$ and $\boldsymbol{s}_M = \left(\boldsymbol{s}_M^h\,;\ \boldsymbol{s}_M^v\right)$. The different source types in the mode-field domain then become

$$\begin{aligned}
&\text{HED:}\ \grave{\boldsymbol{\Sigma}} = -\acute{\boldsymbol{\Sigma}} = -\boldsymbol{N}_E^T\boldsymbol{s}_E^h/\sqrt{2}, \qquad &&\text{VED:}\ \grave{\boldsymbol{\Sigma}} = \acute{\boldsymbol{\Sigma}} = \boldsymbol{N}_H^T\boldsymbol{s}_E^v/\sqrt{2},\\
&\text{HMD:}\ \grave{\boldsymbol{\Sigma}} = \acute{\boldsymbol{\Sigma}} = \boldsymbol{N}_H^T\boldsymbol{s}_M^h/\sqrt{2}, \qquad &&\text{VMD:}\ \grave{\boldsymbol{\Sigma}} = -\acute{\boldsymbol{\Sigma}} = -\boldsymbol{N}_E^T\boldsymbol{s}_M^v/\sqrt{2},
\end{aligned} \tag{5.126}$$

where equation 5.44 with the eigenvector matrices from equation 5.101 has been used. The electromagnetic field due to any of these sources is then given by the expression

$$\boldsymbol{b}_E = \boldsymbol{N}_E \, \boldsymbol{\mathcal{R}} \, \grave{\boldsymbol{\Sigma}}/\sqrt{2} \quad \text{and} \quad \boldsymbol{b}_H = \boldsymbol{N}_H \, \boldsymbol{\mathcal{R}} \, \grave{\boldsymbol{\Sigma}}/\sqrt{2}, \tag{5.127}$$

where the coefficient matrices $\boldsymbol{\mathcal{R}}$ (RT-amplitudes) are, respectively, $\boldsymbol{\mathcal{R}}^A$ and $\boldsymbol{\mathcal{R}}^D$ for the electric and magnetic field components in case of a HED and VMD. When the source is a HMD or a VED, the coefficient matrices for the electric and magnetic fields are $\boldsymbol{\mathcal{R}}^B$ and $\boldsymbol{\mathcal{R}}^C$, respectively. The RT-amplitudes above the source, $z < z_s$, are:

$$\acute{\boldsymbol{\mathcal{R}}}^A = \left(\boldsymbol{I} + \acute{\boldsymbol{R}}_a\right)\left(\boldsymbol{I} - \grave{\boldsymbol{R}}_u\acute{\boldsymbol{R}}_a\right)^{-1}\acute{\boldsymbol{T}}_u\left(\boldsymbol{I} - \grave{\boldsymbol{R}}_s\acute{\boldsymbol{R}}_s\right)^{-1}\left(\grave{\boldsymbol{R}}_s + \boldsymbol{I}\right), \tag{5.128a}$$

$$\acute{\boldsymbol{\mathcal{R}}}^B = \left(\boldsymbol{I} + \acute{\boldsymbol{R}}_a\right)\left(\boldsymbol{I} - \grave{\boldsymbol{R}}_u\acute{\boldsymbol{R}}_a\right)^{-1}\acute{\boldsymbol{T}}_u\left(\boldsymbol{I} - \grave{\boldsymbol{R}}_s\acute{\boldsymbol{R}}_s\right)^{-1}\left(\grave{\boldsymbol{R}}_s - \boldsymbol{I}\right), \tag{5.128b}$$

$$\acute{\boldsymbol{\mathcal{R}}}^C = \left(\boldsymbol{I} - \acute{\boldsymbol{R}}_a\right)\left(\boldsymbol{I} - \grave{\boldsymbol{R}}_u\acute{\boldsymbol{R}}_a\right)^{-1}\acute{\boldsymbol{T}}_u\left(\boldsymbol{I} - \grave{\boldsymbol{R}}_s\acute{\boldsymbol{R}}_s\right)^{-1}\left(\grave{\boldsymbol{R}}_s - \boldsymbol{I}\right), \tag{5.128c}$$

$$\acute{\boldsymbol{\mathcal{R}}}^D = \left(\boldsymbol{I} - \acute{\boldsymbol{R}}_a\right)\left(\boldsymbol{I} - \grave{\boldsymbol{R}}_u\acute{\boldsymbol{R}}_a\right)^{-1}\acute{\boldsymbol{T}}_u\left(\boldsymbol{I} - \grave{\boldsymbol{R}}_s\acute{\boldsymbol{R}}_s\right)^{-1}\left(\grave{\boldsymbol{R}}_s + \boldsymbol{I}\right), \tag{5.128d}$$

and the RT-amplitudes below the source, $z > z_s$, are:

$$\grave{\boldsymbol{\mathcal{R}}}^A = \left(\grave{\boldsymbol{R}}_b + \boldsymbol{I}\right)\left(\boldsymbol{I} - \acute{\boldsymbol{R}}_d\grave{\boldsymbol{R}}_b\right)^{-1}\grave{\boldsymbol{T}}_d\left(\boldsymbol{I} - \acute{\boldsymbol{R}}_s\grave{\boldsymbol{R}}_s\right)^{-1}\left(\boldsymbol{I} + \acute{\boldsymbol{R}}_s\right), \tag{5.128e}$$

$$\grave{\boldsymbol{\mathcal{R}}}^B = \left(\grave{\boldsymbol{R}}_b + \boldsymbol{I}\right)\left(\boldsymbol{I} - \acute{\boldsymbol{R}}_d\grave{\boldsymbol{R}}_b\right)^{-1}\grave{\boldsymbol{T}}_d\left(\boldsymbol{I} - \acute{\boldsymbol{R}}_s\grave{\boldsymbol{R}}_s\right)^{-1}\left(\boldsymbol{I} - \acute{\boldsymbol{R}}_s\right), \tag{5.128f}$$

$$\grave{\boldsymbol{\mathcal{R}}}^C = \left(\grave{\boldsymbol{R}}_b - \boldsymbol{I}\right)\left(\boldsymbol{I} - \acute{\boldsymbol{R}}_d\grave{\boldsymbol{R}}_b\right)^{-1}\grave{\boldsymbol{T}}_d\left(\boldsymbol{I} - \acute{\boldsymbol{R}}_s\grave{\boldsymbol{R}}_s\right)^{-1}\left(\boldsymbol{I} - \acute{\boldsymbol{R}}_s\right), \tag{5.128g}$$

$$\grave{\boldsymbol{\mathcal{R}}}^D = \left(\grave{\boldsymbol{R}}_b - \boldsymbol{I}\right)\left(\boldsymbol{I} - \acute{\boldsymbol{R}}_d\grave{\boldsymbol{R}}_b\right)^{-1}\grave{\boldsymbol{T}}_d\left(\boldsymbol{I} - \acute{\boldsymbol{R}}_s\grave{\boldsymbol{R}}_s\right)^{-1}\left(\boldsymbol{I} + \acute{\boldsymbol{R}}_s\right). \tag{5.128h}$$

The reflection and transmission can be calculated from the relations in equation 5.70 and 5.71. The single-interface reflection and transmission matrices are described by equation 5.63.

5.12.2 RT-responses and polarization modes

In TIV or isotropic media the wavenumber vector for a plane-wave constituent and the electric and magnetic field components form an orthogonal system (cf. Appendix 5.C). This means that in presence of an interface, the electromagnetic field can be decomposed into a transverse electric (TE) and transverse magnetic (TM) polarization mode. The interface normal and the wavenumber vector form the *plane of incidence*. The electromagnetic field component where the electric field is normal to the plane of incidence is referred to as the TE mode, and the field component where the magnetic field is normal to the plane of incidence is referred to as the TM mode.

For reflection and transmission between two TIV regions there is no coupling of the polarization modes as seen from equation 5.121, since the reflection and transmission matrices

are diagonal. From equation 5.119 it can be observed that the vertical slowness that corresponds to the TE mode is governed by anisotropy in the magnetic permeability, whereas the vertical slowness that corresponds to the TM mode is governed by anisotropy in the complex electric permittivity. The modes are obviously also decoupled for reflection and transmission at interfaces between TIV *and* isotropic media or between isotropic regions. For isotropic media the slownesses are equal, cf. equation 5.125.

At interfaces between media with more complicated anisotropy than TIV, the offdiagonal elements of the reflection and transmission matrices (cf. equations 5.63 and 5.114) are nonzero and thus the polarization modes are coupled. However, in a general anisotropic homogeneous region there are no pure TE- and TM-polarization modes since the propagation direction is not orthogonal to the field components (cf. Appendix 5.C). We will refer to the modes in such regions as quasi-TE (qTE) and quasi-TM (qTM). When the anisotropy simplifies into TIV, the qTE mode should then correspond to the TE mode, and likewise the qTM mode should give a TM mode.

Consider the matrix expressions in equation 5.128 which can be written as:

$$\boldsymbol{\mathcal{R}} = \begin{pmatrix} \mathcal{R}_{11} & \mathcal{R}_{12} \\ \mathcal{R}_{21} & \mathcal{R}_{22} \end{pmatrix}, \tag{5.129}$$

where the notation $\boldsymbol{\mathcal{R}}$ refers to all the eight different reflection and transmission responses in equation 5.128. Let equation 5.129 represent the RT-response in a TIV or isotropic layer from an anisotropic stack due to a source in a TIV or isotropic layer. The sorting of eigenvalues in equations 5.119 and 5.30 then means that subscript 1 in the matrix elements in equation 5.129 is related to the TE mode, whereas subscript 2 is related to the TM mode. Thus, the emitted TE polarization and the resulting TE-mode response is represented by $\mathcal{R}_{11}$, whereas $\mathcal{R}_{12}$ is the resulting TM mode from the TE radiation. In the same manner, the emitted TM polarization is represented by $\mathcal{R}_{21}$ and $\mathcal{R}_{22}$, where the latter is the TM mode in the resulting electromagnetic field, and $\mathcal{R}_{21}$ is the TE mode due to the radiated TM mode. In short, subscript 11 implies TE $\rightarrow$ TE, 12 is TE $\rightarrow$ TM, 21 is TM $\rightarrow$ TE, and 22 is TM $\rightarrow$ TM. Note however, that in a stack with general anisotropy, the $\mathcal{R}_{11}$-response will contain responses which have been converted from TM to TE and then back from TM to TE within the stack. In the same manner the $\mathcal{R}_{22}$-response is not a pure TM response. When all the layers in the stratified model are TIV or isotropic, there is no cross-coupling between the modes. Then the entries $\mathcal{R}_{12}$ and $\mathcal{R}_{21}$ are zero, and the calculation of the RT-response reduces to a scalar problem in terms of the TE and TM modes.

5.12.3 Horizontal electric dipole

For a HED in the x-direction, the source vector from equation 5.16 is $\boldsymbol{s} = (0 \;\; 0 \;\; J_x \;\; 0)^T$, where J_x is given by equation 5.17a and the delta function is accounted for in equation 5.45. Using

equation 5.126 this leads to

$$\grave{\boldsymbol{\Sigma}} = -\acute{\boldsymbol{\Sigma}} = -\frac{1}{\sqrt{2}}\boldsymbol{N}_E^T \begin{pmatrix} J_x \\ 0 \end{pmatrix} = -\frac{Il_x}{\sqrt{2}p_\rho} \begin{pmatrix} p_y \mathcal{E}_s \\ p_x \mathcal{M}_s^{-1} \end{pmatrix}, \tag{5.130}$$

where the eigenvector submatrix from equation 5.120 has been used since the source is assumed to be in a TIV layer, and where the variables

$$\mathcal{E} = \sqrt{\frac{\mu_h}{p_{z\mathrm{I}}}} \quad \text{and} \quad \mathcal{M} = \sqrt{\frac{\tilde{\varepsilon}_h}{p_{z\mathrm{II}}}}, \tag{5.131}$$

have been introduced to simplify notation. The subscript s implies material parameters within the source layer. The electromagnetic field is given by equation 5.127:

$$\boldsymbol{b}(z) = \frac{1}{\sqrt{2}} \begin{pmatrix} \boldsymbol{N}_E \boldsymbol{\mathcal{R}}^A \\ \boldsymbol{N}_H \boldsymbol{\mathcal{R}}^D \end{pmatrix} \grave{\boldsymbol{\Sigma}}(z_s). \tag{5.132}$$

The expression is valid for $z < z_s$, then $\boldsymbol{\mathcal{R}} \to \acute{\boldsymbol{\mathcal{R}}}$; and $z > z_s$, which implies that $\boldsymbol{\mathcal{R}} \to \grave{\boldsymbol{\mathcal{R}}}$. Written explicitly, the electric and magnetic field components in a TIV layer become:

$$E_x = -\frac{Il_x}{2p_\rho^2}\left[\mathcal{E}\mathcal{E}_s p_y^2 \mathcal{R}_{11}^A + \frac{\mathcal{E}}{\mathcal{M}_s} p_y p_x \mathcal{R}_{12}^A + \frac{\mathcal{E}_s}{\mathcal{M}} p_x p_y \mathcal{R}_{21}^A + \frac{1}{\mathcal{M}\mathcal{M}_s} p_x^2 \mathcal{R}_{22}^A\right], \tag{5.133a}$$

$$E_y = -\frac{Il_x}{2p_\rho^2}\left[-\mathcal{E}\mathcal{E}_s p_x p_y \mathcal{R}_{11}^A - \frac{\mathcal{E}}{\mathcal{M}_s} p_x^2 \mathcal{R}_{12}^A + \frac{\mathcal{E}_s}{\mathcal{M}} p_y^2 \mathcal{R}_{21}^A + \frac{1}{\mathcal{M}\mathcal{M}_s} p_y p_x \mathcal{R}_{22}^A\right], \tag{5.133b}$$

$$H_y = +\frac{Il_x}{2p_\rho^2}\left[\frac{\mathcal{E}_s}{\mathcal{E}} p_y^2 \mathcal{R}_{11}^D + \frac{1}{\mathcal{E}\mathcal{M}_s} p_y p_x \mathcal{R}_{12}^D + \mathcal{M}\mathcal{E}_s p_x p_y \mathcal{R}_{21}^D + \frac{\mathcal{M}}{\mathcal{M}_s} p_x^2 \mathcal{R}_{22}^D\right], \tag{5.133c}$$

$$H_x = -\frac{Il_x}{2p_\rho^2}\left[-\frac{\mathcal{E}_s}{\mathcal{E}} p_x p_y \mathcal{R}_{11}^D - \frac{1}{\mathcal{E}\mathcal{M}_s} p_x^2 \mathcal{R}_{12}^D + \mathcal{M}\mathcal{E}_s p_y^2 \mathcal{R}_{21}^D + \frac{\mathcal{M}}{\mathcal{M}_s} p_y p_x \mathcal{R}_{22}^D\right]. \tag{5.133d}$$

The z-components of the electric and magnetic fields are found using equation 5.15a and 5.15b, respectively; and they become:

$$E_z = -\frac{Il_x}{2\tilde{\varepsilon}_v}\left[\mathcal{M}\mathcal{E}_s p_y \mathcal{R}_{21}^D + \frac{\mathcal{M}}{\mathcal{M}_s} p_x \mathcal{R}_{22}^D\right], \tag{5.133e}$$

$$H_z = \frac{Il_x}{2\mu_v}\left[\mathcal{E}\mathcal{E}_s p_y \mathcal{R}_{11}^A + \frac{\mathcal{E}}{\mathcal{M}_s} p_x \mathcal{R}_{12}^A\right]. \tag{5.133f}$$

The electromagnetic field from a HED in the y-direction is found by letting $p_x J_x \to p_y J_y$ and $p_y J_x \to -p_x J_y$ in the equations above. When performing the substitution in expressions where both p_x and p_y are present, it is the rightmost slowness parameter that must be used (i.e., by the notation used here it is this slowness parameter that can be ascribed to the source transformation).

In cases where all the layers are TIV (or isotropic), the RT-response simplifies. The cross-coupling coefficients are $\mathcal{R}_{12} = 0$ and $\mathcal{R}_{21} = 0$ in this case. The responses for the TE

and TM modes ($\mathcal{R}_{11}$ and $\mathcal{R}_{22}$, respectively) are then given by the same scalar expression. For $z > z_s$ the RT-amplitudes are

$$\grave{\mathcal{R}}_A = \grave{T}_d \frac{\grave{R}_b + 1}{1 - \acute{R}_d \grave{R}_b} \frac{1 + \acute{R}_s}{1 - \acute{R}_s \grave{R}_s}, \tag{5.134a}$$

$$\grave{\mathcal{R}}_D = \grave{T}_d \frac{\grave{R}_b - 1}{1 - \acute{R}_d \grave{R}_b} \frac{1 + \acute{R}_s}{1 - \acute{R}_s \grave{R}_s}, \tag{5.134b}$$

and for $z < z_s$ the RT-amplitudes are

$$\acute{\mathcal{R}}_A = \acute{T}_u \frac{1 + \acute{R}_a}{1 - \grave{R}_u \acute{R}_a} \frac{1 + \grave{R}_s}{1 - \grave{R}_s \acute{R}_s}, \tag{5.134c}$$

$$\acute{\mathcal{R}}_D = \acute{T}_u \frac{1 - \acute{R}_a}{1 - \grave{R}_u \acute{R}_a} \frac{1 + \grave{R}_s}{1 - \grave{R}_s \acute{R}_s}. \tag{5.134d}$$

5.12.4 Horizontal magnetic dipole

A HMD implies that the source term from equation 5.16 becomes $\boldsymbol{s} = (0 \;\; J_x^M \;\; 0 \;\; 0)^T$. In TIV media the HMD source in equation 5.17d reduces to $J_x^M = -i\omega\mu_h I a_x \delta(z - z_s)$. The source in the mode-domain can thus be written:

$$\grave{\boldsymbol{\Sigma}} = \acute{\boldsymbol{\Sigma}} = \frac{1}{\sqrt{2}} \boldsymbol{N}_H^T \begin{pmatrix} 0 \\ J_x^M \end{pmatrix} = \frac{-i\omega\mu_h^s I a_x}{\sqrt{2} p_\rho} \begin{pmatrix} -p_x \mathcal{E}_s^{-1} \\ p_y \mathcal{M}_s \end{pmatrix}, \tag{5.135}$$

where the superscript s on μ_h refers to the permeability in the source layer. To obtain the electromagnetic field, the expression in equation 5.127 is used:

$$\boldsymbol{b}(z) = \frac{1}{\sqrt{2}} \begin{pmatrix} \boldsymbol{N}_E \boldsymbol{\mathcal{R}}^B \\ \boldsymbol{N}_H \boldsymbol{\mathcal{R}}^C \end{pmatrix} \grave{\boldsymbol{\Sigma}}(z_s). \tag{5.136}$$

Written explicitly the electric and magnetic fields become:

$$E_x = -\frac{i\omega\mu_h^s I a_x}{2p_\rho^2} \left[-\frac{\mathcal{E}}{\mathcal{E}_s} p_y p_x \mathcal{R}_{11}^B + \mathcal{E}\mathcal{M}_s p_y^2 \mathcal{R}_{12}^B - \frac{1}{\mathcal{M}\mathcal{E}_s} p_x^2 \mathcal{R}_{21}^B + \frac{\mathcal{M}_s}{\mathcal{M}} p_x p_y \mathcal{R}_{22}^B \right], \tag{5.137a}$$

$$E_y = -\frac{i\omega\mu_h^s I a_x}{2p_\rho^2} \left[\frac{\mathcal{E}}{\mathcal{E}_s} p_x^2 \mathcal{R}_{11}^B - \mathcal{E}\mathcal{M}_s p_x p_y \mathcal{R}_{12}^B - \frac{1}{\mathcal{M}\mathcal{E}_s} p_y p_x \mathcal{R}_{21}^B + \frac{\mathcal{M}_s}{\mathcal{M}} p_y^2 \mathcal{R}_{22}^B \right], \tag{5.137b}$$

$$H_y = +\frac{i\omega\mu_h^s I a_x}{2p_\rho^2} \left[-\frac{1}{\mathcal{E}\mathcal{E}_s} p_y p_x \mathcal{R}_{11}^C + \frac{\mathcal{M}_s}{\mathcal{E}} p_y^2 \mathcal{R}_{12}^C - \frac{\mathcal{M}}{\mathcal{E}_s} p_x^2 \mathcal{R}_{21}^C + \mathcal{M}\mathcal{M}_s p_x p_y \mathcal{R}_{22}^C \right], \tag{5.137c}$$

$$H_x = -\frac{i\omega\mu_h^s I a_x}{2p_\rho^2} \left[\frac{1}{\mathcal{E}\mathcal{E}_s} p_x^2 \mathcal{R}_{11}^C - \frac{\mathcal{M}_s}{\mathcal{E}} p_x p_y \mathcal{R}_{12}^C - \frac{\mathcal{M}}{\mathcal{E}_s} p_y p_x \mathcal{R}_{21}^C + \mathcal{M}\mathcal{M}_s p_y^2 \mathcal{R}_{22}^C \right]. \tag{5.137d}$$

The z-components are found using equation 5.15:

$$E_z = -\frac{i\omega\mu_h^s I a_x}{2\tilde{\varepsilon}_v} \left[-\frac{\mathcal{M}}{\mathcal{E}_s} p_x \mathcal{R}_{21}^C + \mathcal{M}\mathcal{M}_s p_y \mathcal{R}_{22}^C \right], \tag{5.137e}$$

$$H_z = -\frac{i\omega\mu_h^s I a_x}{2\mu_v} \left[\frac{\mathcal{E}}{\mathcal{E}_s} p_x \mathcal{R}_{11}^B - \mathcal{E}\mathcal{M}_s p_y \mathcal{R}_{12}^B \right]. \tag{5.137f}$$

It can be seen from equations 5.133 and 5.137 that there is a duality between the electromagnetic field from a magnetic and an electric dipole, a subject that is treated in Appendix 5.B. The field from a source in the y-direction can be found by letting $p_x J_x^M \rightarrow p_y J_y^M$ and $p_y J_x^M \rightarrow -p_x J_y^M$.

If all the layers are TIV or isotropic, the cross-coupling terms are zero and the TE-mode and TM-mode responses are both given by:

$$\grave{\mathcal{R}}_B = \grave{T}_d \frac{\grave{R}_b + 1}{1 - \acute{R}_d \grave{R}_b} \frac{1 - \acute{R}_s}{1 - \acute{R}_s \grave{R}_s}, \tag{5.138a}$$

$$\grave{\mathcal{R}}_C = \grave{T}_d \frac{\grave{R}_b - 1}{1 - \acute{R}_d \grave{R}_b} \frac{1 - \acute{R}_s}{1 - \acute{R}_s \grave{R}_s}, \tag{5.138b}$$

when $z > z_s$. For $z < z_s$ the RT-amplitudes are

$$\acute{\mathcal{R}}_B = \acute{T}_u \frac{1 + \acute{R}_a}{1 - \grave{R}_u \acute{R}_a} \frac{\grave{R}_s - 1}{1 - \grave{R}_s \acute{R}_s}, \tag{5.138c}$$

$$\acute{\mathcal{R}}_C = \acute{T}_u \frac{1 - \acute{R}_a}{1 - \grave{R}_u \acute{R}_a} \frac{\grave{R}_s - 1}{1 - \grave{R}_s \acute{R}_s}. \tag{5.138d}$$

5.12.5 Vertical electric dipole

The source term for a VED is given by equation 5.16 as $\boldsymbol{s} = (p_x J_z/\tilde{\varepsilon}_v \;\; p_y J_z/\tilde{\varepsilon}_v \;\; 0 \;\; 0)^T$ where J_z is given by equation 5.17c. Thus,

$$\grave{\boldsymbol{\Sigma}} = \acute{\boldsymbol{\Sigma}} = \frac{J_z}{\sqrt{2}\tilde{\varepsilon}_v^s} \boldsymbol{N}_H^T \begin{pmatrix} p_x \\ p_y \end{pmatrix} = \frac{I l_z p_\rho}{\sqrt{2}\tilde{\varepsilon}_v^s} \begin{pmatrix} 0 \\ \mathcal{M}_s \end{pmatrix}, \tag{5.139}$$

where the superscript s on $\tilde{\varepsilon}_h$ refers to the complex permittivity in the source layer. Since the upgoing radiation of the mode-source vector equals the downgoing radiation, the VED has the same scattering coefficients as the HMD in equation 5.136. Since the uppermost element in equation 5.139 is zero, this means that

$$E_x = \frac{I l_z}{2\tilde{\varepsilon}_v^s} \left[\mathcal{E}\mathcal{M}_s p_y \mathcal{R}_{12}^B + \frac{\mathcal{M}_s}{\mathcal{M}} p_x \mathcal{R}_{22}^B \right], \tag{5.140a}$$

$$E_y = \frac{I l_z}{2\tilde{\varepsilon}_v^s} \left[-\mathcal{E}\mathcal{M}_s p_x \mathcal{R}_{12}^B + \frac{\mathcal{M}_s}{\mathcal{M}} p_y \mathcal{R}_{22}^B \right], \tag{5.140b}$$

$$H_y = -\frac{I l_z}{2\tilde{\varepsilon}_v^s} \left[\frac{\mathcal{M}_s}{\mathcal{E}} p_y \mathcal{R}_{12}^C + \mathcal{M}\mathcal{M}_s p_x \mathcal{R}_{22}^C \right], \tag{5.140c}$$

$$H_x = \frac{I l_z}{2\tilde{\varepsilon}_v^s} \left[-\frac{\mathcal{M}_s}{\mathcal{E}} p_x \mathcal{R}_{12}^C + \mathcal{M}\mathcal{M}_s p_y \mathcal{R}_{22}^C \right]. \tag{5.140d}$$

The vertical electric and magnetic components become, using equation 5.15:

$$E_z = \frac{Il_z p_\rho^2}{2\tilde{\varepsilon}_v^s \tilde{\varepsilon}_v} \mathcal{M}\mathcal{M}_s \mathcal{R}_{22}^C + \frac{1}{i\omega\tilde{\varepsilon}_v^s} Il_z \delta(z_s), \tag{5.140e}$$

$$H_z = -\frac{Il_z p_\rho^2}{2\tilde{\varepsilon}_v^s \mu_v} \mathcal{E}\mathcal{M}_s \mathcal{R}_{12}^B. \tag{5.140f}$$

When all the layers are TIV or isotropic, the VED has pure TM-polarization components only, and there is no vertical magnetic field ($H_z = 0$).

5.12.6 Vertical magnetic dipole

The VMD source is described by equation 5.16 as $\boldsymbol{s} = (0\ 0\ -p_y J_z^M/\mu_v\ \ p_x J_z^M/\mu_v)^T$. By using the expression for J_z^M from equation 5.17f, which in TIV-media reduces to $J_z^M = -i\omega\mu_v I a_z \delta(z - z_s)$, one gets

$$\grave{\boldsymbol{\Sigma}} = -\acute{\boldsymbol{\Sigma}} = -\frac{J_z^M}{\sqrt{2}\mu_v^s} \boldsymbol{N}_E^T \begin{pmatrix} -p_y \\ p_x \end{pmatrix} = \frac{-i\omega I a_z p_\rho}{\sqrt{2}} \begin{pmatrix} \mathcal{E}_s \\ 0 \end{pmatrix}. \tag{5.141}$$

Since $\grave{\boldsymbol{\Sigma}} = -\acute{\boldsymbol{\Sigma}}$, the VMD has the same scattering coefficients as the field from a HED, cf. equation 5.132. Then

$$E_x = -\frac{i\omega I a_z}{2} \left[\mathcal{E}\mathcal{E}_s p_y \mathcal{R}_{11}^A + \frac{\mathcal{E}_s}{\mathcal{M}} p_x \mathcal{R}_{21}^A \right], \tag{5.142a}$$

$$E_y = -\frac{i\omega I a_z}{2} \left[-\mathcal{E}\mathcal{E}_s p_x \mathcal{R}_{11}^A + \frac{\mathcal{E}_s}{\mathcal{M}} p_y \mathcal{R}_{21}^A \right], \tag{5.142b}$$

$$H_y = \frac{i\omega I a_z}{2} \left[\frac{\mathcal{E}_s}{\mathcal{E}} p_y \mathcal{R}_{11}^D + \mathcal{M}\mathcal{E}_s p_x \mathcal{R}_{21}^D \right], \tag{5.142c}$$

$$H_x = -\frac{i\omega I a_z}{2} \left[-\frac{\mathcal{E}_s}{\mathcal{E}} p_x \mathcal{R}_{11}^D + \mathcal{M}\mathcal{E}_s p_y \mathcal{R}_{21}^D \right]. \tag{5.142d}$$

The z-components are found using equation 5.15:

$$E_z = -\frac{i\omega I a_z p_\rho^2}{2\tilde{\varepsilon}_v} \mathcal{M}\mathcal{E}_s \mathcal{R}_{21}^D, \tag{5.142e}$$

$$H_z = \frac{i\omega I a_z p_\rho^2}{2\mu_v} \mathcal{E}\mathcal{E}_s \mathcal{R}_{11}^A - I a_z \delta(z_s). \tag{5.142f}$$

When all the layers are TIV or isotropic, the VMD produces pure TE-polarization components, and the vertical electric field is zero ($E_z = 0$).

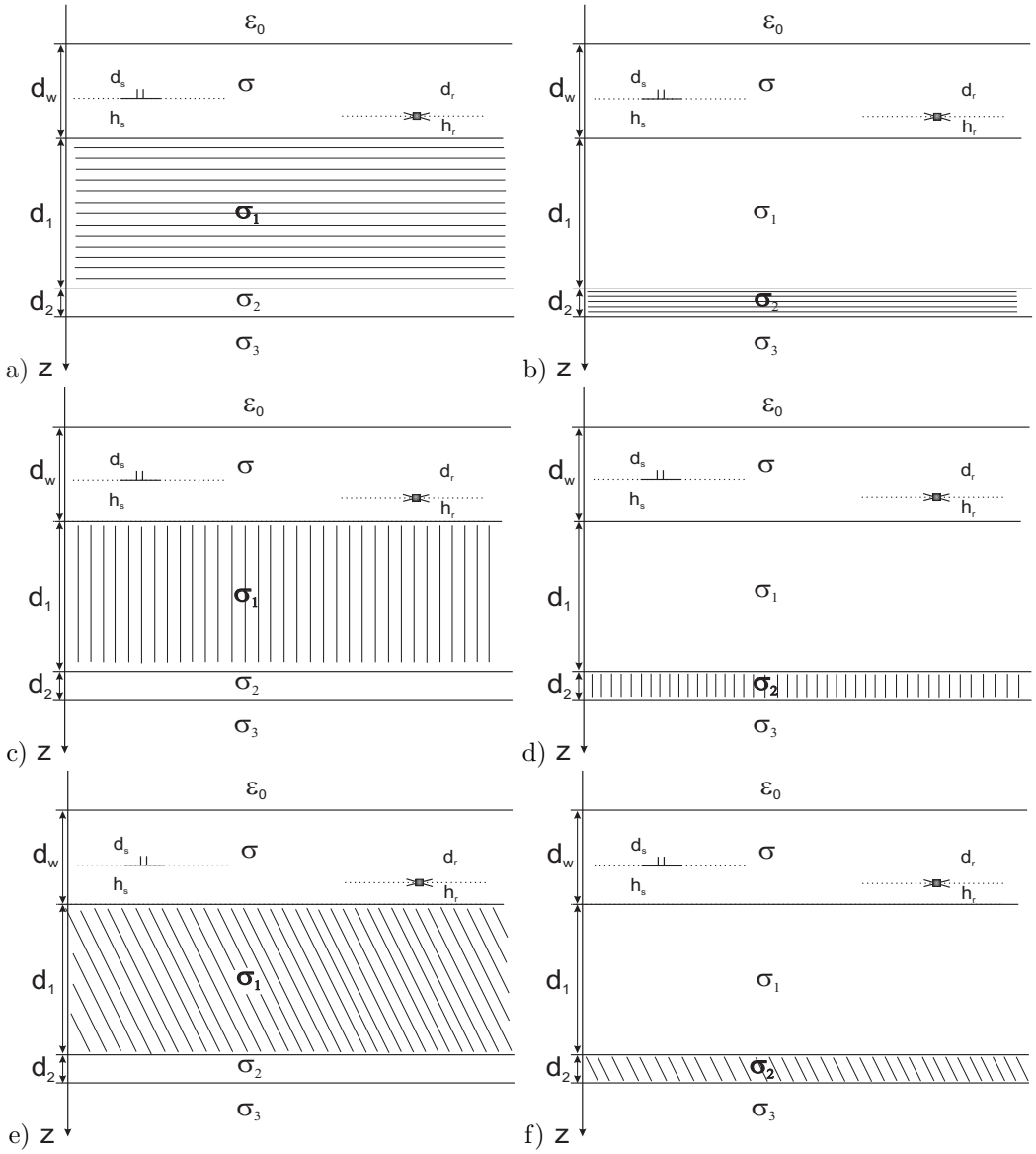

Figure 5.5: Anisotropy models for some idealized CSEM/SBL scenarios. The figures to the left (right) illustrate anisotropy in the overburden (reservoir). Three basic uniaxial models are considered. Figures a and b show TIV media, c and d illustrate TIH media, and in e and f, media with dipping anisotropy (TID) are sketched.

5.13 Numerical results

The theory for electromagnetic field propagation in stratified anisotropic media has been presented in a rather general form. As long as the constitutive relations are as given in equation 5.2, the formalism can be applied to electromagnetic problems in geophysics from e.g., ground penetrating radar (GPR) to marine controlled source electromagnetics (CSEM) or SeaBed Logging (SBL). The expressions in equations 5.76 and 5.81 can be used to model electromagnetic fields from electric and magnetic dipole sources in stratified media with arbitrary anisotropy. Here, we apply the method to plane-layer marine CSEM modelling. We assume that the source and receiver layers are TIV, and thus, equations 5.133, 5.137, 5.140, and 5.142 can be used to calculate the electromagnetic fields. Other layers than the source and receiver layer(s) may then have arbitrary anisotropy.

The expressions in equations 5.133, 5.137, 5.140, and 5.142 are given in the frequency-wavenumber domain. In order to calculate the fields in the spatial domain, the 2-D inverse Fourier transform in equation 5.6b must be applied. We consider the frequency-domain field expressions since single-frequency components of the source signal are studied. If all the layers in the stratified model are limited to TIV, the 2-D Fourier transform can be reduced to a 1-D Hankel transform due to the rotational symmetry. Explicit formulas for this are given in Appendix 5.F.

The field expressions were implemented in FORTRAN 90. Since marine CSEM is a low-frequency application in conductive regions, the dielectric part of the permittivity dyad in equation 5.3 is totally dominated by the conductivity dyad in all of the homogeneous regions, except in the air halfspace. This implies that the wavenumber-domain field components will have large variations in strength, and in order to accurately calculate the fields in the spatial domain, the integration in the wavenumber domain requires large wavenumbers and careful sampling. We implemented the 2-D Fourier transform using adaptive Gauss-Legendre quadrature, and the integration was performed between zero crossings of the sine function (extrema of the cosine function). Series-summation acceleration was implemented using continued fractions and Euler's method as described in Hänggi et al. (1998) and Press et al. (1997), respectively. For the types of input functions encountered here, numerical solutions to the Fourier transform that use logarithmic spacing are often very efficient. The digital filter method described by e.g., Anderson (1979), Mohsen and Hashish (1994), and Christensen (1990), was thus implemented. The efficiency and accuracy of the two different methods (numerical quadrature and digital filter) depend on the input function (Anderson, 1989).

The various models that have been considered are shown in Figure 5.5. For simplicity, the permeability is taken to be constant. Thus, this dyad is diagonal with all entries equal. The seawater is isotropic. In all of the figures the water depth is 300 m, the source height is 30 m, the thickness of the overburden is 1 km, and the reservoir is 100 m thick. Anisotropy

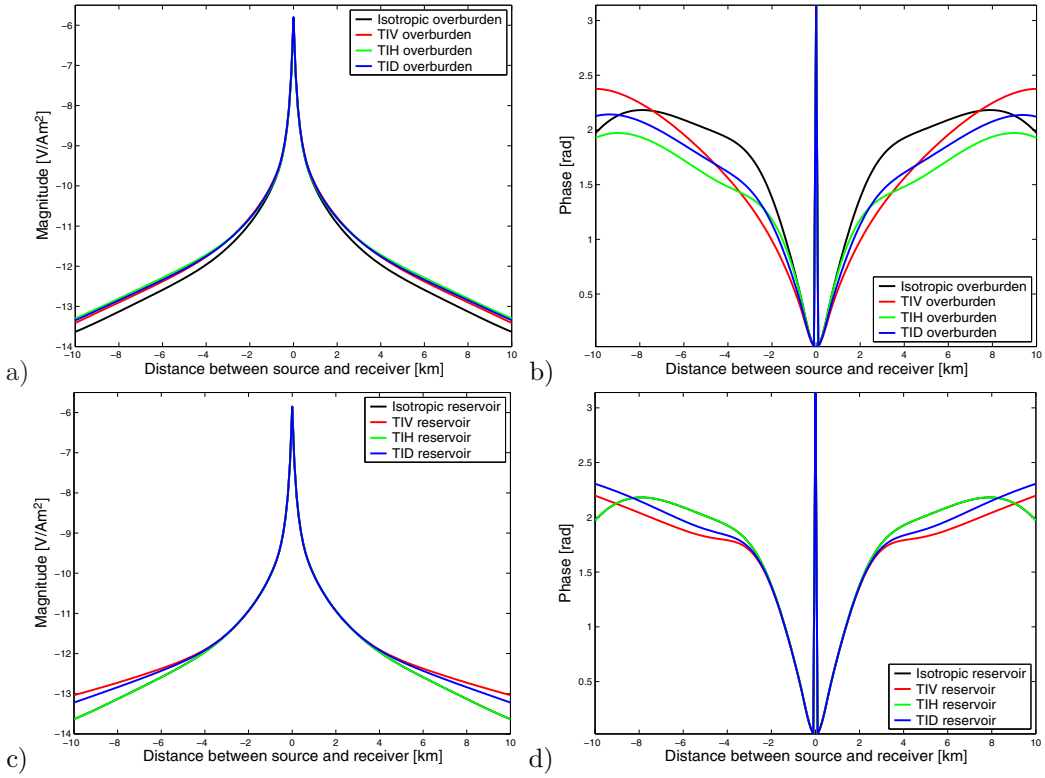

Figure 5.6: Modelling results for the anisotropic models in Figure 5.5. Figure a shows the amplitude response for various kinds of anisotropy in the overburden, whereas Figure b shows the phase response. Figures c and d are the corresponding responses for an anisotropic reservoir. In all the figures the isotropic conductivity contrast between the overburden and the reservoir is 100.

in the overburden and reservoir is considered separately and for the two different cases of having a resistive reservoir and a conductive reservoir. The isotropic conductivities are $\sigma = 3.2$ S/m for seawater and $\sigma_1 = 1.0$ S/m for the overburden and bottom halfspace ($\sigma_3 = \sigma_1$). The conductivity in the reservoir is $\sigma_2 = 0.01$ S/m for the resistive case and $\sigma_2 = 0.5$ S/m for the conductive case. To simplify interpretation, the anisotropy is taken to be transversely isotropic (uniaxial). We refer to the direction with different conductivity than the two other as the direction of anisotropy. In addition to the isotropic case, scenarios with transverse isotropy in the vertical direction (TIV), transverse isotropy in the horizontal direction (TIH), and dipping transverse isotropy (TID), are modelled. The conductivity in the anisotropy direction is taken to be one-fourth of the isotropic conductivity. This means for example that in the model with a TIV overburden, the vertical conductivity is

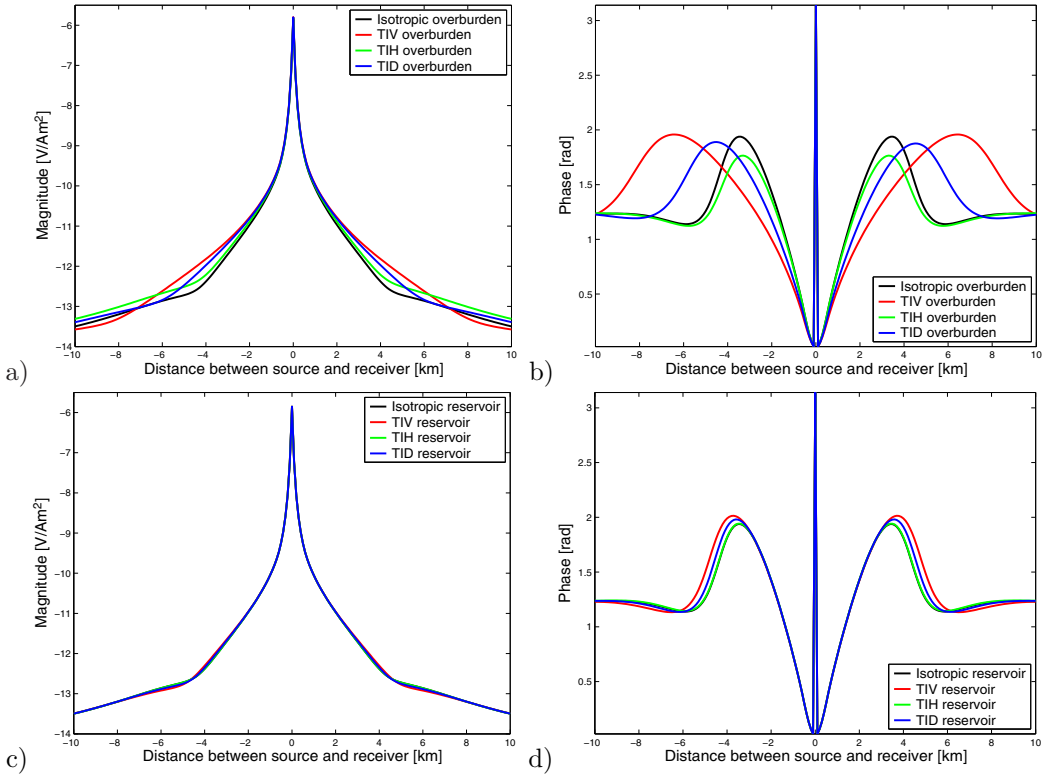

Figure 5.7: Modelling results for the anisotropic models in Figure 5.5. The isotropic conductivity contrast between the overburden and the reservoir is 2 in these simulations. Figures a and b show the effect of anisotropy in the overburden, and Figures c and d show the responses from an anisotropic reservoir with low resistivity.

$\sigma_{1v} = 0.25$ S/m whereas the horizontal conductivity is $\sigma_{1h} = 1.0$ S/m. For the resistive reservoir case, the vertical conductivity in a TIV model is $\sigma_{2v} = 0.0025$ S/m, whereas the horizontal conductivity is $\sigma_{2h} = 0.01$ S/m. In the TIH model, the azimuth angle between the direction of the source and anisotropy is 15° (cf. Figure 5.1). When the model has dipping transverse isotropy (TID), the anisotropy direction has a 30° tilt from the vertical axis. This dip is furthermore taken to be in the direction of the source antenna. The source frequency is 0.25 Hz.

For simplicity we consider the inline electric field from a HED (e.g., the field component in the same direction as the source dipole). The plots are shown in Figure 5.6 for the resistive reservoir case and Figure 5.7 for the conductive reservoir. In both cases, Figure a shows the magnitude versus offset (MVO) when the overburden is anisotropic, and Figure b shows the phase versus offset (PVO). Figures c and d show the MVO and PVO plots when the reservoir

is anisotropic.

In the resistive reservoir case, the MVO plot that describes anisotropy effects in the overburden shows an increase in response when anisotropy is present. This is due to the conductivity being less than in the isotropic case. Moreover, the response is largest for a TIH overburden since it is this direction that has the strongest support of field propagation between the seafloor and the reservoir. To this end, note that there is a cross-coupling of polarization modes in the TIH case. Using the same line of arguments, the effect of a dipping anisotropy should come out with magnitude in between the TIV and TIH cases as shown in the modelling. The phase behaviour is a bit more involved. The signals propagate faster when anisotropy is present since they experience less conductivity. In consistency with the amplitude responses, at far offsets the TIH model leads to faster propagation than the TID model, and the TID model implies faster propagation than the TIV model. At intermediate distances, the behaviour is a bit more complicated since, in this case, the responses from the guiding in the reservoir and the lateral field propagation along the seabed are nearly equal in magnitude.

A rough interpretation of the consequences of anisotropy in the reservoir can be made along the following lines: The response from the thin resistive layer is due to propagation in the horizontal direction of the reservoir, and the important conductivity parameter is the vertical conductivity. The TIV reservoir has less conductivity in the vertical direction than the isotropic model, and thus, the TIV case should be expected to give an increase in the reservoir response. The same effect, but less, should be expected for the TID reservoir, whereas TIH in the reservoir should not influence the response to any particular extent. From Figures 5.6c and d it can be observed that the behaviour of the modelled data has these characteristics. The dip in the phase curves for the isotropic case and TIH case is due to the sea-surface response.

In the conductive reservoir case the thin layer has almost the same resistivity as the surrounding overburden and underburden (half the value). From Figure 5.7 it can be observed that anisotropy in the overburden has pronounced effects on the response. The small variation in the isotropic conductivities leads to larger sensitivity to the anisotropy. The interplay between the lateral field propagation at the sea-surface and seafloor along with the reflection from the reservoir, leads to the TIV model having the strongest response for small distances and the TIH model having the strongest response for larger distances. As seen from Figures 5.7c and d, anisotropy in the reservoir has small effects on the response when the reservoir is conductive.

The purpose of the modelling examples is to illustrate some of the effects of anisotropy. Even if responses from isotropic models can be constructed to resemble more complicated anisotropy models (by carefully selecting the conductivity parameters in the direction normal to the propagation direction of the strongest signal contribution), isotropic models will seldom

account for all the anisotropic effects. With one more degree of freedom, a TIV model can obviously account for anisotropy better than an isotropic model, but not fully explain more complicated anisotropy phenomena. Another point to make by the simple modelling examples made here, is that anisotropy in the overburden might confuse the interpretation of the response from a reservoir if not carefully rendered.

5.14 Conclusions

Electromagnetic field propagation from electric and magnetic dipoles in planarly layered lossy anisotropic media has been considered. The set of first-order ordinary differential equations in terms of the horizontal electromagnetic field components in the frequency-wavenumber domain has been evaluated in terms of a system matrix. This matrix is dependent on the medium properties for a specific layer and the horizontal wavenumbers for a plane-wave component in the wavenumber spectrum.

By evaluating the eigenvalues and corresponding eigenvectors of the system matrix, it has been shown that the resulting diagonalization leads to two decoupled differential equations with upgoing and downgoing field constituents in a homogeneous region. The eigenvalues of the system matrix correspond to the vertical slownesses. The reflection and transmission (RT) at an interface can be calculated from the eigenvector matrices on each side, and a recursive scheme for calculating the RT-response across a stack of layers has been derived. Thus, we were able to obtain expressions for the field vector in any layer at any position in terms of eigenvalues, eigenvector matrices, RT-response matrices, and the source function.

The assumption that the property dyads are symmetric, and the energy-flux normalization of the eigenvector matrices, made it possible to obtain reciprocity relations for reflection and transmission responses. An example of an application of the reciprocity relations is that the number of calculations in the inverse Fourier transform can be reduced by 50%.

In addition to media with general anisotropy, configurations with simpler anisotropies have been studied. In anisotropic media the diagonalized system matrix is in general not up/down-symmetric. Up/down-symmetry follows if one of the principal axes of the anisotropic medium coincides with the coordinate axis normal to the planar interfaces. Then the diagonal submatrices in the system matrix are zero. In vertically transversely isotropic (TIV) media, the mode-field is decoupled in a TE and TM mode throughout the layered system.

For a source and receiver in a TIV medium, explicit expressions for the electromagnetic fields from the source dipoles HED, HMD, VED, and VMD have been derived. If the entire stratified medium is characterized by TIV or isotropy, the recursive relations for the RT-responses simplify to scalar equations. In this case the 2-D Fourier transform can be reduced to a 1-D Hankel transform.

A numerical implementation of the algorithms and a modelling study have been performed. The modelling example was taken from a marine CSEM setting. The obtained responses show different behaviour for different anisotropy configurations.

Finally, an application of the propagator method for isotropic media has been demonstrated in Appendix 5.G.

5.15 Acknowledgments

We are grateful to Lasse Amundsen, Rune Mittet, and Ola Hunderi for valuable discussions. L.O.L. would like to thank Statoil's VISTA programme for financial support. B.U. is appreciative to the Norwegian Research Council, Norsk Hydro ASA, Statoil ASA, and ElectroMagnetic GeoServices AS for supporting this research.

5.A Rotation of the anisotropy principal axes

The electromagnetic property dyads are determined by three values in their principal-axis system. The axes of the principal system are referred to as $(1, 2, 3)$, and in a medium with triclinic anisotropy, each of the property dyads may have their own set of principal axes. In order to rotate the principal coordinate system into the main coordinate frame (x, y, z), it is convenient to use Euler angles (ϕ, θ, ψ). The convention used by Goldstein (1980) is followed. Now, as seen in Figure 5.1, ϕ is the angle between the x-axis and the line of nodes, θ is the angle between the z-axis and the 3-axis, and finally, ψ is the angle between the line of nodes and the 1-axis. Note that the "line of nodes" is the line defined by the intersection of the xy-plane and the 12-plane (i.e., the horizontal planes of the coordinate frames). The entries of a property dyad in the main coordinate frame are then obtained by transforming the dyad from the principal system as follows:

$$\boldsymbol{\sigma} = \begin{pmatrix} \sigma_{xx} & \sigma_{xy} & \sigma_{xz} \\ \sigma_{yx} & \sigma_{yy} & \sigma_{yz} \\ \sigma_{zx} & \sigma_{zy} & \sigma_{zz} \end{pmatrix} = \begin{pmatrix} e_{11} & e_{12} & e_{13} \\ e_{21} & e_{22} & e_{23} \\ e_{31} & e_{32} & e_{33} \end{pmatrix} \begin{pmatrix} \sigma_1 & 0 & 0 \\ 0 & \sigma_2 & 0 \\ 0 & 0 & \sigma_3 \end{pmatrix} \begin{pmatrix} e_{11} & e_{21} & e_{31} \\ e_{12} & e_{22} & e_{32} \\ e_{13} & e_{23} & e_{33} \end{pmatrix}, \quad \text{(5.A-1)}$$

where

$$e_{11} = \cos\phi\cos\psi - \sin\phi\cos\theta\sin\psi, \quad \text{(5.A-2a)}$$
$$e_{12} = -\cos\phi\sin\psi - \sin\phi\cos\theta\cos\psi, \quad \text{(5.A-2b)}$$
$$e_{13} = \sin\phi\sin\theta, \quad \text{(5.A-2c)}$$
$$e_{21} = \sin\phi\cos\psi + \cos\phi\cos\theta\sin\psi, \quad \text{(5.A-2d)}$$
$$e_{22} = -\sin\phi\sin\psi + \cos\phi\cos\theta\cos\psi, \quad \text{(5.A-2e)}$$
$$e_{23} = -\cos\phi\sin\theta, \quad \text{(5.A-2f)}$$
$$e_{31} = \sin\theta\sin\psi, \quad \text{(5.A-2g)}$$
$$e_{32} = \sin\theta\cos\psi, \quad \text{(5.A-2h)}$$
$$e_{33} = \cos\theta. \quad \text{(5.A-2i)}$$

This procedure, $\boldsymbol{\sigma} = \boldsymbol{e}\boldsymbol{\sigma}_p\boldsymbol{e}^T$, where $\boldsymbol{e}$ is the coordinate rotation matrix with elements $e_{ij} = e_{ji}$, and $\boldsymbol{\sigma}_p$ is the dyad in the principal system, can be performed for all the three property dyads. In general, the principal axes may be different for all these dyads (which obviously requires different rotation angles for each property dyad).

The entries in the conductivity matrix in the main coordinate frame are given by the

rotation angles and the principal values as:

$$\sigma_{xx} = \sigma_1 e_{11}^2 + \sigma_2 e_{12}^2 + \sigma_3 e_{13}^2, \tag{5.A-3a}$$
$$\sigma_{xy} = \sigma_1 e_{11} e_{21} + \sigma_2 e_{12} e_{22} + \sigma_3 e_{13} e_{23}, \tag{5.A-3b}$$
$$\sigma_{xz} = \sigma_1 e_{11} e_{31} + \sigma_2 e_{12} e_{32} + \sigma_3 e_{13} e_{33}, \tag{5.A-3c}$$
$$\sigma_{yy} = \sigma_1 e_{21}^2 + \sigma_2 e_{22}^2 + \sigma_3 e_{23}^2, \tag{5.A-3d}$$
$$\sigma_{yz} = \sigma_1 e_{21} e_{31} + \sigma_2 e_{22} e_{32} + \sigma_3 e_{23} e_{33}, \tag{5.A-3e}$$
$$\sigma_{zz} = \sigma_1 e_{31}^2 + \sigma_2 e_{32}^2 + \sigma_3 e_{33}^2. \tag{5.A-3f}$$

In u/d-symmetric media, the relation between the principal and main coordinate systems is described by one rotation only (for each property dyad) in the horizontal plane (i.e., ϕ in equation 5.A-2). The conductivity dyad can in this case be written as

$$\begin{pmatrix} \sigma_{xx} & \sigma_{xy} & 0 \\ \sigma_{yx} & \sigma_{yy} & 0 \\ 0 & 0 & \sigma_v \end{pmatrix} = \begin{pmatrix} \cos\phi & \sin\phi & 0 \\ -\sin\phi & \cos\phi & 0 \\ 0 & 0 & 1 \end{pmatrix} \begin{pmatrix} \sigma_1 & 0 & 0 \\ 0 & \sigma_2 & 0 \\ 0 & 0 & \sigma_v \end{pmatrix} \begin{pmatrix} \cos\phi & -\sin\phi & 0 \\ \sin\phi & \cos\phi & 0 \\ 0 & 0 & 1 \end{pmatrix}, \tag{5.A-4}$$

whence

$$\begin{gathered} \sigma_{xx} = \sigma_1^2 \cos^2\phi + \sigma_2^2 \sin^2\phi, \quad \sigma_{yy} = \sigma_1^2 \sin^2\phi + \sigma_2^2 \cos^2\phi, \\ \sigma_{xy} = \sigma_{yx} = (\sigma_2 - \sigma_1) \sin\phi \cos\phi. \end{gathered} \tag{5.A-5}$$

The relations presented in this section in terms of the conductivity dyad are equally valid for the permittivity and permeability dyads.

5.B Duality in the field expressions

When magnetic sources are introduced into Maxwell's equations, Faraday's and Ampère's laws can be written as

$$\nabla \times \mathbf{E} = -\mathbf{J}_{0M} + i\omega\boldsymbol{\mu}\mathbf{H}, \tag{5.B-6a}$$
$$\nabla \times \mathbf{H} = \mathbf{J}_0 - i\omega\boldsymbol{\varepsilon}\mathbf{E}, \tag{5.B-6b}$$

where $\mathbf{J}_0$ is the electric source and $\mathbf{J}_{0M}$ is the magnetic source. Using the equations of charge conservation, the divergence equations can be written in terms of the source-current density as

$$\nabla \cdot (\boldsymbol{\varepsilon}\mathbf{E}) = -\frac{1}{i\omega} \nabla \cdot \mathbf{J}_0, \tag{5.B-6c}$$
$$\nabla \cdot (\boldsymbol{\mu}\mathbf{H}) = -\frac{1}{i\omega} \nabla \cdot \mathbf{J}_{0M}. \tag{5.B-6d}$$

From these equations one observes a simple relationship between the fields from a magnetic dipole and an electric dipole. Starting with Faraday's law (equation 5.B-6a) and the corresponding divergence equation (5.B-6c), one can arrive at Ampère's law (equation 5.B-6b) and its corresponding divergence equation (5.B-6d) by doing the following change of variables:

$$\mathbf{E} \rightarrow \mathbf{H}, \tag{5.B-7a}$$

$$\mathbf{H} \rightarrow -\mathbf{E}, \tag{5.B-7b}$$

$$\boldsymbol{\mu} \rightarrow \tilde{\boldsymbol{\varepsilon}}, \tag{5.B-7c}$$

$$\tilde{\boldsymbol{\varepsilon}} \rightarrow \boldsymbol{\mu}, \tag{5.B-7d}$$

$$\mathbf{J}_0 \rightarrow \mathbf{J}_{0M}. \tag{5.B-7e}$$

The opposite "transformation", from Ampère's law to Faraday's law and their corresponding divergence equations, also holds. In this case the relation

$$\mathbf{J}_{0M} \rightarrow -\mathbf{J}_0 \tag{5.B-7f}$$

is needed. In terms of the dipole sources used in equation 5.4 and 5.5, the source transformations become:

$$I\mathbf{l} \rightarrow -i\omega\boldsymbol{\mu} I\mathbf{a} \quad \text{and} \quad i\omega\boldsymbol{\mu} I\mathbf{a} \rightarrow I\mathbf{l}. \tag{5.B-8}$$

In the main text, RT-responses from a multilayered medium are considered. If a change of variables as described above is performed, a change in polarization modes and signs in the reflection coefficients must be taken into account due to the interchange of the electric and magnetic fields.

The explicit field expressions for the HMD and VMD (HED and VED) can be derived from the expressions for the HED and VED (HMD and VMD), respectively, by using the change of variables in equations 5.B-7a to 5.B-7d and 5.B-8. In addition, the following change of variables for the RT-response coefficients must be performed:

$$\mathcal{R}^A_{11} \leftrightarrow -\mathcal{R}^C_{22}, \qquad \mathcal{R}^A_{12} \leftrightarrow \mathcal{R}^C_{21}, \tag{5.B-9a}$$

$$\mathcal{R}^A_{21} \leftrightarrow \mathcal{R}^C_{12}, \qquad \mathcal{R}^A_{22} \leftrightarrow -\mathcal{R}^C_{11}, \tag{5.B-9b}$$

$$\mathcal{R}^B_{11} \leftrightarrow -\mathcal{R}^D_{22}, \qquad \mathcal{R}^B_{12} \leftrightarrow \mathcal{R}^D_{21}, \tag{5.B-9c}$$

$$\mathcal{R}^B_{21} \leftrightarrow \mathcal{R}^D_{12}, \qquad \mathcal{R}^B_{22} \leftrightarrow -\mathcal{R}^D_{11}. \tag{5.B-9d}$$

5.C Energy velocity of a plane-wave component

The energy velocity can be defined as (Kong, 2000; Carcione and Schoenberg, 2000):

$$\mathbf{v}_e = \frac{\mathrm{Re}(\mathbf{S})}{\mathrm{Re}(u_e + u_m)}, \tag{5.C-10}$$

where $\mathbf{S} = \frac{1}{2}\mathbf{E} \times \mathbf{H}^*$ is the complex Poynting vector, $u_e = \frac{1}{4}\mathbf{E} \cdot \mathbf{D}^*$ is the electric energy, and $u_m = \frac{1}{4}\mathbf{H} \cdot \mathbf{B}^*$ is the magnetic energy. Consider a plane electromagnetic wave in a homogeneous source-free medium. Then Maxwell's equations can be written as:

$$\mathbf{p} \cdot \mathbf{D} = 0, \tag{5.C-11a}$$

$$\mathbf{p} \cdot \mathbf{B} = 0, \tag{5.C-11b}$$

$$\mathbf{p} \times \mathbf{E} = \mathbf{B}, \tag{5.C-11c}$$

$$\mathbf{p} \times \mathbf{H} = -\mathbf{D}, \tag{5.C-11d}$$

where $\mathbf{p}$ is the slowness vector. From these equations it is seen that the slowness is in a direction perpendicular to both the $\mathbf{D}$- and $\mathbf{B}$-field. It is convenient to rotate the coordinate system so that one of the axes coincides with the direction of the slowness. Some caution must however be taken here; since the slowness vector is complex, the "rotation" must be performed with complex angles. Thus, the coordinate system is rather transformed into a new state. We will as in Kong (2000) refer to the system after the transformation as the kDB-system, in which the axes are denoted as 123. (cf. Figure 5.1 where $x'y'z'$ can be pictured as 123). Note that the axes in the kDB-system are not the same as any principal anisotropy axes. Now, an expression for the energy velocity in terms of the material and slowness parameters can be obtained. From Figure 5.1 it is seen that a rotation into the kDB-system described by the angles ϕ and θ can be written as:

$$\boldsymbol{e}_{\mathrm{kDB}} = \begin{pmatrix} e'_{11} & e'_{12} & e'_{13} \\ e'_{21} & e'_{22} & e'_{23} \\ e'_{31} & e'_{32} & e'_{33} \end{pmatrix}, \tag{5.C-12}$$

where

$$e'_{11} = \sin\phi, \qquad e'_{12} = -\cos\phi, \qquad e'_{13} = 0, \tag{5.C-13a}$$

$$e'_{21} = \cos\phi\cos\theta, \qquad e'_{22} = \sin\phi\cos\theta, \qquad e'_{23} = -\sin\theta, \tag{5.C-13b}$$

$$e'_{31} = \cos\phi\sin\theta, \qquad e'_{32} = \sin\phi\sin\theta, \qquad e'_{33} = \cos\theta. \tag{5.C-13c}$$

The angles would take the values $\phi \in [0, 360°)$, $\theta \in [0, 180°)$ in a lossless case, but here they are complex with

$$\cos\phi = \frac{p_x}{\sqrt{p_x^2 + p_y^2}} \quad \text{and} \quad \cos\theta = \frac{p_z}{\sqrt{p_x^2 + p_y^2 + p_z^2}}. \tag{5.C-14}$$

The material parameters in the kDB-system are obtained from the material parameters in the main coordinate frame by the dyadic transformation:

$$\boldsymbol{\chi}' = \boldsymbol{e}_{\mathrm{kDB}} \boldsymbol{\chi} \boldsymbol{e}_{\mathrm{kDB}}^T, \tag{5.C-15}$$

where the resulting matrix is symmetric after the orthogonal transformation. Next, a relation between $\mathbf{D}$ and $\mathbf{B}$ is needed. It is convenient to introduce the impermeability and the complex impermittivity, which are the inverses of the permeability and complex permittivity, respectively (Kong, 2000):

$$\mathbf{E} = \tilde{\boldsymbol{\varepsilon}}^{-1}\mathbf{D} = \boldsymbol{\kappa}\mathbf{D} \quad \text{and} \quad \mathbf{H} = \boldsymbol{\mu}^{-1}\mathbf{B} = \boldsymbol{\nu}\mathbf{B}. \tag{5.C-16}$$

From the curl equations in 5.C-11, the following relations between $\mathbf{D}$ and $\mathbf{B}$ can be obtained in the kDB-system:

$$D_1 = p(\nu'_{21}B_1 + \nu'_{22}B_2), \tag{5.C-17a}$$
$$D_2 = -p(\nu'_{11}B_1 + \nu'_{12}B_2), \tag{5.C-17b}$$
$$B_1 = -p(\kappa'_{21}D_1 + \kappa'_{22}D_2), \tag{5.C-17c}$$
$$B_2 = p(\kappa'_{11}D_1 + \kappa'_{12}D_2), \tag{5.C-17d}$$

where $p = |\mathbf{p}|$ is the slowness in the $\hat{\mathbf{e}}_3$-direction. Note that by definition, this is the direction of the total slowness. Note also that $B_3 = 0$ and $D_3 = 0$. From equation 5.C-17, the dispersion relation

$$u^2 = -\frac{1}{2}\left[b_u \pm \sqrt{b_u^2 - 4c_u}\right], \tag{5.C-18a}$$
$$b_u = \left(\kappa'_{21}\nu'_{21} + \kappa'_{12}\nu'_{12} - \kappa'_{11}\nu'_{22} - \kappa'_{22}\nu'_{11}\right), \tag{5.C-18b}$$
$$\begin{aligned} c_u = {} & \left(\kappa'_{21}\nu'_{21} - \kappa'_{11}\nu'_{22}\right)\left(\kappa'_{12}\nu'_{12} - \kappa'_{22}\nu'_{11}\right) \\ & - \left(\kappa'_{22}\nu'_{21} - \kappa'_{12}\nu'_{22}\right)\left(\kappa'_{11}\nu'_{12} - \kappa'_{21}\nu'_{11}\right), \end{aligned} \tag{5.C-18c}$$

and a relation between D_1 and D_2 can be obtained:

$$\frac{D_2}{D_1} = \frac{u^2 + \kappa'_{21}\nu'_{21} - \kappa'_{11}\nu'_{22}}{\kappa'_{12}\nu'_{22} - \kappa'_{22}\nu'_{21}} = \frac{\kappa'_{21}\nu'_{11} - \kappa'_{11}\nu'_{12}}{u^2 + \kappa'_{12}\nu'_{12} - \kappa'_{22}\nu'_{11}} = \Psi, \tag{5.C-18d}$$

where the complex velocity is the reciprocal of slowness, $u = 1/p$. The electric field in the kDB-system can then be written as

$$\mathbf{E}_{\mathrm{kDB}} = \boldsymbol{\kappa}'\mathbf{D}_{\mathrm{kDB}} = \begin{pmatrix} \kappa'_{11} + \kappa'_{12}\Psi \\ \kappa'_{21} + \kappa'_{22}\Psi \\ \kappa'_{31} + \kappa'_{32}\Psi \end{pmatrix} D_1, \tag{5.C-19}$$

whereas the magnetic field in the kDB-system is obtained using Faraday's law:

$$\mathbf{H}_{\mathrm{kDB}} = \boldsymbol{\nu}'(\mathbf{p} \times \mathbf{E}_{\mathrm{kDB}}) = p \begin{pmatrix} (\nu'_{12}\kappa'_{11} - \nu'_{11}\kappa'_{21}) + (\nu'_{12}\kappa'_{12} - \nu'_{11}\kappa'_{22})\Psi \\ (\nu'_{22}\kappa'_{11} - \nu'_{21}\kappa'_{21}) + (\nu'_{22}\kappa'_{12} - \nu'_{21}\kappa'_{22})\Psi \\ (\nu'_{32}\kappa'_{11} - \nu'_{31}\kappa'_{21}) + (\nu'_{32}\kappa'_{12} - \nu'_{31}\kappa'_{22})\Psi \end{pmatrix} D_1. \tag{5.C-20}$$

The complex Poynting vector in the kDB-system expressed in terms of D_1 then becomes:

$$\mathbf{S}_{\mathrm{kDB}} = \tfrac{1}{2}\mathbf{s}_{\mathrm{kDB}}p^* D_1 D_1^*, \tag{5.C-21}$$

where

$$\mathbf{s}_{\mathrm{kDB}} = \begin{pmatrix} s_{11} + s_{12}\Psi + s_{13}\Psi^* + s_{14}\Psi\Psi^* \\ s_{21} + s_{22}\Psi + s_{23}\Psi^* + s_{24}\Psi\Psi^* \\ s_{31} + s_{32}\Psi + s_{33}\Psi^* + s_{34}\Psi\Psi^* \end{pmatrix}, \tag{5.C-22a}$$

and

$$\begin{aligned}
s_{11} &= (\nu'_{32}\kappa'_{21} - \nu'_{22}\kappa'_{31})(\kappa'_{11})^* - (\nu'_{31}\kappa'_{21} - \nu'_{21}\kappa'_{31})(\kappa'_{21})^*, \\
s_{12} &= (\nu'_{32}\kappa'_{22} - \nu'_{22}\kappa'_{32})(\kappa'_{11})^* - (\nu'_{31}\kappa'_{22} - \nu'_{21}\kappa'_{32})(\kappa'_{21})^*, \\
s_{13} &= (\nu'_{32}\kappa'_{21} - \nu'_{22}\kappa'_{31})(\kappa'_{12})^* - (\nu'_{31}\kappa'_{21} - \nu'_{21}\kappa'_{31})(\kappa'_{22})^*, \\
s_{14} &= (\nu'_{32}\kappa'_{22} - \nu'_{22}\kappa'_{32})(\kappa'_{12})^* - (\nu'_{31}\kappa'_{22} - \nu'_{21}\kappa'_{32})(\kappa'_{22})^*, \\
s_{21} &= (\nu'_{12}\kappa'_{31} - \nu'_{32}\kappa'_{11})(\kappa'_{11})^* - (\nu'_{11}\kappa'_{31} - \nu'_{31}\kappa'_{11})(\kappa'_{21})^*, \\
s_{22} &= (\nu'_{12}\kappa'_{32} - \nu'_{32}\kappa'_{12})(\kappa'_{11})^* - (\nu'_{11}\kappa'_{32} - \nu'_{31}\kappa'_{12})(\kappa'_{21})^*, \\
s_{23} &= (\nu'_{12}\kappa'_{31} - \nu'_{32}\kappa'_{11})(\kappa'_{12})^* - (\nu'_{11}\kappa'_{31} - \nu'_{31}\kappa'_{11})(\kappa'_{22})^*, \\
s_{24} &= (\nu'_{12}\kappa'_{32} - \nu'_{32}\kappa'_{12})(\kappa'_{12})^* - (\nu'_{11}\kappa'_{32} - \nu'_{31}\kappa'_{12})(\kappa'_{22})^*, \\
s_{31} &= (\nu'_{22}\kappa'_{11} - \nu'_{12}\kappa'_{21})(\kappa'_{11})^* - (\nu'_{21}\kappa'_{11} - \nu'_{11}\kappa'_{21})(\kappa'_{21})^*, \\
s_{32} &= (\nu'_{22}\kappa'_{12} - \nu'_{12}\kappa'_{22})(\kappa'_{11})^* - (\nu'_{21}\kappa'_{12} - \nu'_{11}\kappa'_{22})(\kappa'_{21})^*, \\
s_{33} &= (\nu'_{22}\kappa'_{11} - \nu'_{12}\kappa'_{21})(\kappa'_{12})^* - (\nu'_{21}\kappa'_{11} - \nu'_{11}\kappa'_{21})(\kappa'_{22})^*, \\
s_{34} &= (\nu'_{22}\kappa'_{12} - \nu'_{12}\kappa'_{22})(\kappa'_{12})^* - (\nu'_{21}\kappa'_{12} - \nu'_{11}\kappa'_{22})(\kappa'_{22})^*.
\end{aligned} \tag{5.C-22b}$$

The energy densities in the kDB-system can be written as

$$u_m = \tfrac{1}{4}\mathbf{H}\cdot\mathbf{B}^* = \tfrac{1}{4}(H_1 B_1^* + H_2 B_2^*) = \tfrac{p^*}{4p}(E_1^* D_1 + E_2^* D_2) = \tfrac{p^*}{p}u_e^*, \tag{5.C-23a}$$

$$u_e = \tfrac{1}{4}\mathbf{E}\cdot\mathbf{D}^* = \tfrac{1}{4}(E_1 D_1^* + E_2 D_2^*) = \tfrac{1}{4}\left[(\kappa'_{11} + \kappa'_{12}\Psi) + (\kappa'_{21} + \kappa'_{22}\Psi)\Psi^*\right] D_1 D_1^*. \tag{5.C-23b}$$

The energy density is independent of the coordinate system in which it is calculated, whereas the Poynting vector must be transformed back to the main coordinate frame $\mathbf{S} = \boldsymbol{e}_{\mathrm{kDB}}^T \mathbf{S}_{\mathrm{kDB}}$. This leads to the following expressions for the energy velocity:

$$\mathbf{v}_e = n_v^{-1}\mathrm{Re}\big(p^* \boldsymbol{e}_{\mathrm{kDB}}^T \mathbf{s}_{\mathrm{kDB}}\big), \tag{5.C-24}$$

where

$$n_v = \mathrm{Re}\Big(\tfrac{1}{p}\Big)\mathrm{Re}[p(\kappa'_{11} + \kappa'_{12}\Psi) + p(\kappa'_{21} + \kappa'_{22}\Psi)\Psi^*)]. \tag{5.C-25}$$

If $\Psi \to \infty$, the Poynting vector and energy velocity can be calculated in terms of D_2, which implies multiplying the expressions with $\Psi^{-1}\left(\Psi^{-1}\right)^*$.

When the eigenvalues are found, their ordering into upgoing and downgoing constituents can be determined from the direction of the z-component of the corresponding energy velocity. Moreover, the ordering of modes can be determined by matching the eigenvalue and the

complex velocity in the dispersion relation in equation 5.C-18a. The choice of sign that corresponds to what mode can be established by considering what happens when the anisotropy simplifies into TIV. Then the fraction between D_1 or D_2 either approach zero or infinity depending on if the slowness corresponds to a TE or a TM mode.

5.D Mixing the qTE and qTM modes in a layer

Consider reflection and transmission through a stack of three layers [from region (3) to (1) through layer (2)], and assume that the qTE and qTM modes have been switched when sorting the eigenvalues into the upgoing eigenvalue submatrix in region (2). Then, in region (2), the "mixed" eigenvector submatrices and eigenvalue matrix are related to the corresponding "correct" matrices as

$$\acute{\boldsymbol{N}}'_E = \begin{pmatrix} n_{12} & n_{11} \\ n_{22} & n_{21} \end{pmatrix} = \acute{\boldsymbol{N}}_E \boldsymbol{K}, \tag{5.D-26a}$$

$$\acute{\boldsymbol{N}}'_H = \begin{pmatrix} n_{32} & n_{31} \\ n_{42} & n_{41} \end{pmatrix} = \acute{\boldsymbol{N}}_H \boldsymbol{K}, \tag{5.D-26b}$$

$$\acute{\mathbf{p}}'_{\mathbf{z}} = \boldsymbol{K} \acute{\mathbf{p}}_{\mathbf{z}} \boldsymbol{K}, \tag{5.D-26c}$$

where $\boldsymbol{K}$ is given by equation 5.19. By using equation 5.61, the $\boldsymbol{C}$ and $\boldsymbol{D}$ matrices between medium (3) and (2) become:

$$\acute{\boldsymbol{C}}' = \boldsymbol{K}\acute{\boldsymbol{C}}, \quad \acute{\boldsymbol{D}}' = \boldsymbol{K}\acute{\boldsymbol{D}}, \quad \hat{\boldsymbol{C}}' = \boldsymbol{K}\hat{\boldsymbol{C}}, \quad \text{and} \quad \hat{\boldsymbol{D}}' = \boldsymbol{K}\hat{\boldsymbol{D}}, \tag{5.D-27}$$

since layer (2) has the mixed modes. Thus, the reflection coefficients are

$$\acute{\boldsymbol{t}}' = 2\left(\boldsymbol{K}\acute{\boldsymbol{C}} + \boldsymbol{K}\acute{\boldsymbol{D}}\right)^{-T} = \boldsymbol{K}\acute{\boldsymbol{t}}, \tag{5.D-28a}$$

$$\acute{\boldsymbol{r}}' = -\left(\boldsymbol{K}\hat{\boldsymbol{C}} - \boldsymbol{K}\hat{\boldsymbol{D}}\right)^{T}\left(\boldsymbol{K}\acute{\boldsymbol{C}} + \boldsymbol{K}\acute{\boldsymbol{D}}\right)^{-T} = \acute{\boldsymbol{r}}, \tag{5.D-28b}$$

$$\grave{\boldsymbol{r}}' = \left(\hat{\boldsymbol{C}} - \hat{\boldsymbol{D}}\right)\left(\boldsymbol{K}\grave{\boldsymbol{C}} + \boldsymbol{K}\grave{\boldsymbol{D}}\right)^{-1} = \boldsymbol{K}\grave{\boldsymbol{r}}, \tag{5.D-28c}$$

$$\grave{\boldsymbol{t}}' = 2\left(\grave{\boldsymbol{C}} + \grave{\boldsymbol{D}}\right)^{-1} = \grave{\boldsymbol{t}}. \tag{5.D-28d}$$

When inserted into the recursive formula in equation 5.70, this leads to

$$\grave{\boldsymbol{R}}'_j = \boldsymbol{K}\mathrm{e}^{i\omega\acute{\mathbf{p}}_{\mathbf{z}}h_j}\boldsymbol{K}\left[\boldsymbol{K}\grave{\boldsymbol{r}}_j + \boldsymbol{K}\acute{\boldsymbol{t}}_j\grave{\boldsymbol{R}}_{j+1}\left(\boldsymbol{I} - \acute{\boldsymbol{r}}_j\grave{\boldsymbol{R}}_{j+1}\right)^{-1}\grave{\boldsymbol{t}}_j\right]\mathrm{e}^{i\omega\grave{\mathbf{p}}_{\mathbf{z}}h_j} = \boldsymbol{K}\grave{\boldsymbol{R}}_j. \tag{5.D-29}$$

In the propagation between medium (2) and (1), the same procedure yields the relations:

$$\check{\boldsymbol{C}}' = \check{\boldsymbol{C}}\boldsymbol{K}, \quad \check{\boldsymbol{D}}' = \check{\boldsymbol{D}}\boldsymbol{K}, \quad \check{\boldsymbol{C}}' = \check{\boldsymbol{C}}\boldsymbol{K}, \quad \text{and} \quad \check{\boldsymbol{D}}' = \check{\boldsymbol{D}}\boldsymbol{K}, \tag{5.D-30}$$

which give the reflection coefficients

$$\acute{\boldsymbol{t}}' = 2\left(\acute{\boldsymbol{C}}\boldsymbol{K} + \acute{\boldsymbol{D}}\boldsymbol{K}\right)^{-T} = \acute{\boldsymbol{t}}\boldsymbol{K}, \tag{5.D-31a}$$

$$\acute{\boldsymbol{r}}' = -\left(\hat{\boldsymbol{C}} - \hat{\boldsymbol{D}}\right)^{T}\left(\acute{\boldsymbol{C}}\boldsymbol{K} + \acute{\boldsymbol{D}}\boldsymbol{K}\right)^{-T} = \acute{\boldsymbol{r}}\boldsymbol{K}, \tag{5.D-31b}$$

$$\grave{\boldsymbol{r}}' = \left(\acute{\boldsymbol{C}}\boldsymbol{K} + \acute{\boldsymbol{D}}\boldsymbol{K}\right)^{-T}\left(\check{\boldsymbol{C}}\boldsymbol{K} - \check{\boldsymbol{D}}\boldsymbol{K}\right)^{T} = \grave{\boldsymbol{r}}, \tag{5.D-31c}$$

$$\grave{\boldsymbol{t}}' = 2\left(\grave{\boldsymbol{C}} + \grave{\boldsymbol{D}}\right)^{-1} = \grave{\boldsymbol{t}}. \tag{5.D-31d}$$

When inserted into the recursive formula, one gets

$$\grave{\boldsymbol{R}}'_{j-1} = \mathrm{e}^{i\omega\grave{\mathbf{p}}_{\mathbf{z}}h_{j-1}}\left[\grave{\boldsymbol{r}}_{j-1} + \acute{\boldsymbol{t}}_{j-1}\boldsymbol{K}\boldsymbol{K}\grave{\boldsymbol{R}}_j\left(\boldsymbol{I} - \acute{\boldsymbol{r}}_{j-1}\boldsymbol{K}\boldsymbol{K}\grave{\boldsymbol{R}}_j\right)^{-1}\grave{\boldsymbol{t}}_{j-1}\right]\mathrm{e}^{i\omega\grave{\mathbf{p}}_{\mathbf{z}}h_{j-1}} = \grave{\boldsymbol{R}}_{j-1}. \tag{5.D-32}$$

The proof for mixing the downgoing modes is similar and leads to the same conclusion.

5.E The Fresnel eigenvector matrix in TIV media

The flux-normalized eigenvector leads to a symmetry in the transmission coefficients in equation 5.121 that might not be appropriate for all purposes. In order to get the Fresnel transmission coefficients, a different scaling on the eigenvectors that make up the eigenvector matrix can be chosen:

$$\begin{aligned}
\boldsymbol{N}_F &= \frac{1}{\sqrt{2}p_\rho}\begin{pmatrix} p_y & p_x & p_y & p_x \\ -p_x & p_y & -p_x & p_y \\ p_y\frac{p_{z\mathrm{I}}}{\mu_h} & p_x\frac{\tilde{\varepsilon}_h}{p_{z\mathrm{II}}} & -p_y\frac{p_{z\mathrm{I}}}{\mu_h} & -p_x\frac{\tilde{\varepsilon}_h}{p_{z\mathrm{II}}} \\ -p_x\frac{p_{z\mathrm{I}}}{\mu_h} & p_y\frac{\tilde{\varepsilon}_h}{p_{z\mathrm{II}}} & p_x\frac{p_{z\mathrm{I}}}{\mu_h} & -p_y\frac{\tilde{\varepsilon}_h}{p_{z\mathrm{II}}} \end{pmatrix}, \\
\boldsymbol{N}_F^{-1} &= \frac{1}{\sqrt{2}p_\rho}\begin{pmatrix} p_y & -p_x & p_y\frac{\mu_h}{p_{z\mathrm{I}}} & -p_x\frac{\mu_h}{p_{z\mathrm{I}}} \\ p_x & p_y & p_x\frac{p_{z\mathrm{II}}}{\tilde{\varepsilon}_h} & p_y\frac{p_{z\mathrm{II}}}{\tilde{\varepsilon}_h} \\ p_y & -p_x & -p_y\frac{\mu_h}{p_{z\mathrm{I}}} & p_x\frac{\mu_h}{p_{z\mathrm{I}}} \\ p_x & p_y & -p_x\frac{p_{z\mathrm{II}}}{\tilde{\varepsilon}_h} & -p_y\frac{p_{z\mathrm{II}}}{\tilde{\varepsilon}_h} \end{pmatrix}.
\end{aligned} \tag{5.E-33}$$

With the choice in equation 5.E-33, the downgoing reflection matrix $\grave{\boldsymbol{r}}$ is as given in equation 5.121 with $\acute{\boldsymbol{r}} = -\grave{\boldsymbol{r}}$. The upgoing and downgoing transmission matrices are:

$$\grave{\boldsymbol{t}} = \begin{pmatrix} \frac{2\mu_h^+\, p_{z\mathrm{I}}^-}{\mu_h^+\, p_{z\mathrm{I}}^- + \mu_h^-\, p_{z\mathrm{I}}^+} & 0 \\ 0 & \frac{2\tilde{\varepsilon}_h^-\, p_{z\mathrm{II}}^+}{\tilde{\varepsilon}_h^-\, p_{z\mathrm{II}}^+ + \tilde{\varepsilon}_h^+\, p_{z\mathrm{II}}^-} \end{pmatrix}, \quad \acute{\boldsymbol{t}} = \begin{pmatrix} \frac{2\mu_h^-\, p_{z\mathrm{I}}^+}{\mu_h^+\, p_{z\mathrm{I}}^- + \mu_h^-\, p_{z\mathrm{I}}^+} & 0 \\ 0 & \frac{2\tilde{\varepsilon}_h^+\, p_{z\mathrm{II}}^-}{\tilde{\varepsilon}_h^-\, p_{z\mathrm{II}}^+ + \tilde{\varepsilon}_h^+\, p_{z\mathrm{II}}^-} \end{pmatrix}. \tag{5.E-34}$$

Note that the Fresnel transmission matrices are not symmetric, i.e., $\grave{\boldsymbol{t}} \neq \acute{\boldsymbol{t}}$, by contrast to the relation in equation 5.122.

5.F Electromagnetic fields in TIV media

When all the layers in the stratified model are either TIV or isotropic, the double Fourier integral over the horizontal wavenumbers k_x and k_y in equation 5.6b can be rewritten into a single integral in terms of Bessel functions and the polar horizontal wavenumber k_ρ. Thus, it is convenient to introduce cylindrical coordinates:

$$k_\rho = \sqrt{k_x^2 + k_y^2}, \qquad k_x = k_\rho \cos\alpha, \qquad k_y = k_\rho \sin\alpha, \tag{5.F-35a}$$

$$\rho = \sqrt{x^2 + y^2}, \qquad x = \rho \cos\beta, \qquad y = \rho \sin\beta, \tag{5.F-35b}$$

where α is the polar angle in the wavenumber domain, β is the angle in the spatial domain, and ρ is the polar radius. The inverse Fourier transform from the wavenumber domain back to the spatial domain (equation 5.6b without the time and frequency part), can then be rewritten as

$$\int_{-\infty}^{\infty}\int_{-\infty}^{\infty} dk_x dk_y\, \Phi\left(k_x, k_y\right)\, \mathrm{e}^{ik_x x + ik_y y} = \int_0^{2\pi}\int_0^{\infty} d\xi dk_\rho\, k_\rho\, \Phi\left(k_\rho, \xi\right)\, \mathrm{e}^{ik_\rho \rho \sin\xi}\,, \tag{5.F-36}$$

where $\xi = \alpha - \beta + \pi/2$. The exponential term that contains the sine function, can be expressed by a series of Bessel functions (Gradshteyn and Ryzhik, 1980):

$$\exp\left(ik_\rho \rho \sin\xi\right) = \sum_{n=-\infty}^{\infty} J_n(k_\rho\rho)\mathrm{e}^{in\xi}. \tag{5.F-37}$$

By using the property $J_{-n}\left(k_\rho\rho\right) = (-1)^n J_n\left(k_\rho\rho\right)$, one arrives at the representation:

$$J_0(k_\rho\rho) = \frac{1}{2\pi}\int_0^{2\pi} d\xi\, \mathrm{e}^{ik_\rho\rho\sin\xi}, \tag{5.F-38a}$$

$$J_1(k_\rho\rho) = \frac{1}{2\pi i}\int_0^{2\pi} d\xi\, \sin\xi\, \mathrm{e}^{ik_\rho\rho\sin\xi}, \tag{5.F-38b}$$

$$J_2(k_\rho\rho) = \frac{1}{2\pi}\int_0^{2\pi} d\xi\, \cos 2\xi\, \mathrm{e}^{ik_\rho\rho\sin\xi}, \tag{5.F-38c}$$

where the following relationship between J_0, J_1 and J_2 holds:

$$J_0(k_\rho\rho) + J_2(k_\rho\rho) = \frac{2}{k_\rho\rho} J_1(k_\rho\rho). \tag{5.F-39}$$

Since the RT-responses are symmetric about the vertical axis in TIV media, the angle α is *explicitly* present in the field expressions in equations 5.133, 5.137, 5.140, and 5.142 in this case. Thus, the angle dependence in the wavenumber domain can be accounted for by the higher orders of the Bessel functions. Now, rewrite the cosine and sine terms that contain α into expressions that contain ξ and β. Since terms involving $\cos\xi$ and $\sin 2\xi$ do not contribute to the Bessel expansion, this means that

$$\cos\alpha \to \sin\xi\cos\beta, \qquad \sin\alpha \to \sin\xi\sin\beta, \tag{5.F-40a}$$

$$\cos 2\alpha \to -\cos 2\xi\cos 2\beta, \qquad \sin 2\alpha \to -\cos 2\xi\sin 2\beta. \tag{5.F-40b}$$

The field components in cylindrical coordinates are furthermore obtained from the Cartesian components by the rotation:

$$\begin{pmatrix}\Psi_\rho\\ \Psi_\beta\\ \Psi_z\end{pmatrix} = \begin{pmatrix}\cos\beta & \sin\beta & 0\\ -\sin\beta & \cos\beta & 0\\ 0 & 0 & 1\end{pmatrix}\begin{pmatrix}\Psi_x\\ \Psi_y\\ \Psi_z\end{pmatrix}, \tag{5.F-41}$$

where $\mathbf{\Psi} = \{\mathbf{E}, \mathbf{H}\}$.

In the following subsections, the electromagnetic field expressions in a TIV medium for the four different source types are given in terms of cylindrical coordinates. In a numerical implementation cylindrical coordinates are advantageous since they imply evaluation of one integral instead of a double integral. The integral over the horizontal angles is contained within the Bessel functions as seen from equation 5.F-38. The vertical slownesses $p_{z\mathrm{I}}$ and $p_{z\mathrm{II}}$ that will be used in the following equations are dependent on $k_\rho = \omega p_\rho$ as described in equation 5.119.

5.F.1 Electromagnetic field from a HED

From the expressions in equation 5.133 the following field components from a HED is derived:

$$E_\rho = -\frac{Il_x}{4\pi}\cos\beta\left[\ \mathcal{I}^{TM}_{A0} + \frac{1}{\rho}\left(\mathcal{I}^{TE}_{A1} - \mathcal{I}^{TM}_{A1}\right)\right], \tag{5.F-42a}$$

$$E_\beta = -\frac{Il_x}{4\pi}\sin\beta\left[-\mathcal{I}^{TE}_{A0} + \frac{1}{\rho}\left(\mathcal{I}^{TE}_{A1} - \mathcal{I}^{TM}_{A1}\right)\right], \tag{5.F-42b}$$

$$H_\rho = +\frac{Il_x}{4\pi}\sin\beta\left[-\mathcal{I}^{TE}_{D0} + \frac{1}{\rho}\left(\mathcal{I}^{TE}_{D1} - \mathcal{I}^{TM}_{D1}\right)\right], \tag{5.F-42c}$$

$$H_\beta = -\frac{Il_x}{4\pi}\cos\beta\left[\ \mathcal{I}^{TM}_{D0} + \frac{1}{\rho}\left(\mathcal{I}^{TE}_{D1} - \mathcal{I}^{TM}_{D1}\right)\right], \tag{5.F-42d}$$

$$E_z = +\frac{Il_x}{4\pi}\frac{i\cos\beta}{\omega\tilde{\varepsilon}_v}\int_0^\infty dk_\rho k_\rho^2\, J_1(k_\rho\rho)\, g^{TM}_D(p_{z\mathrm{II}}), \tag{5.F-42e}$$

$$H_z = +\frac{Il_x}{4\pi}\frac{i\sin\beta}{\omega\mu_v}\int_0^\infty dk_\rho k_\rho^2\, J_1(k_\rho\rho)\, g^{TE}_A(p_{z\mathrm{I}}), \tag{5.F-42f}$$

where

$$\mathcal{I}^{TE}_{A0} = \int_0^\infty dk_\rho k_\rho\, J_0(k_\rho\rho)\, g^{TE}_A(p_{z\mathrm{I}}), \qquad \mathcal{I}^{TE}_{A1} = \int_0^\infty dk_\rho\, J_1(k_\rho\rho)\, g^{TE}_A(p_{z\mathrm{I}}), \tag{5.F-42g}$$

$$\mathcal{I}^{TM}_{A0} = \int_0^\infty dk_\rho k_\rho\, J_0(k_\rho\rho)\, g^{TM}_A(p_{z\mathrm{II}}), \qquad \mathcal{I}^{TM}_{A1} = \int_0^\infty dk_\rho\, J_1(k_\rho\rho)\, g^{TM}_A(p_{z\mathrm{II}}), \tag{5.F-42h}$$

$$\mathcal{I}^{TE}_{D0} = \int_0^\infty dk_\rho k_\rho\, J_0(k_\rho\rho)\, g^{TE}_D(p_{z\mathrm{I}}), \qquad \mathcal{I}^{TE}_{D1} = \int_0^\infty dk_\rho\, J_1(k_\rho\rho)\, g^{TE}_D(p_{z\mathrm{I}}), \tag{5.F-42i}$$

$$\mathcal{I}^{TM}_{D0} = \int_0^\infty dk_\rho k_\rho\, J_0(k_\rho\rho)\, g^{TM}_D(p_{z\mathrm{II}}), \qquad \mathcal{I}^{TM}_{D1} = \int_0^\infty dk_\rho\, J_1(k_\rho\rho)\, g^{TM}_D(p_{z\mathrm{II}}), \tag{5.F-42j}$$

and

$$g_A^{TE}(p_{z\mathrm{I}}) = \sqrt{\frac{\mu_h}{p_{z\mathrm{I}}}}\sqrt{\frac{\mu_h}{p_{z\mathrm{I}}}}^{s}\mathcal{R}_A^{TE}(p_{z\mathrm{I}}), \qquad g_A^{TM}(p_{z\mathrm{II}}) = \sqrt{\frac{p_{z\mathrm{II}}}{\tilde{\varepsilon}_h}}\sqrt{\frac{p_{z\mathrm{II}}}{\tilde{\varepsilon}_h}}^{s}\mathcal{R}_A^{TM}(p_{z\mathrm{II}}), \tag{5.F-43a}$$

$$g_D^{TE}(p_{z\mathrm{I}}) = -\sqrt{\frac{p_{z\mathrm{I}}}{\mu_h}}\sqrt{\frac{\mu_h}{p_{z\mathrm{I}}}}^{s}\mathcal{R}_D^{TE}(p_{z\mathrm{I}}), \qquad g_D^{TM}(p_{z\mathrm{II}}) = -\sqrt{\frac{\tilde{\varepsilon}_h}{p_{z\mathrm{II}}}}\sqrt{\frac{p_{z\mathrm{II}}}{\tilde{\varepsilon}_h}}^{s}\mathcal{R}_D^{TM}(p_{z\mathrm{II}}), \tag{5.F-43b}$$

where the RT-amplitudes are given by equation 5.134.

5.F.2 Electromagnetic field from a HMD

From the expressions in equation 5.137 the field components from a HMD can be calculated:

$$E_\rho = -\frac{i\omega\mu_h^s I a_x}{4\pi}\sin\beta\left[\ \mathcal{I}_{B0}^{TM} + \frac{1}{\rho}\left(\mathcal{I}_{B1}^{TE} - \mathcal{I}_{B1}^{TM}\right)\right], \tag{5.F-44a}$$

$$E_\beta = +\frac{i\omega\mu_h^s I a_x}{4\pi}\cos\beta\left[-\mathcal{I}_{B0}^{TE} + \frac{1}{\rho}\left(\mathcal{I}_{B1}^{TE} - \mathcal{I}_{B1}^{TM}\right)\right], \tag{5.F-44b}$$

$$H_\rho = -\frac{i\omega\mu_h^s I a_x}{4\pi}\cos\beta\left[-\mathcal{I}_{C0}^{TE} + \frac{1}{\rho}\left(\mathcal{I}_{C1}^{TE} - \mathcal{I}_{C1}^{TM}\right)\right], \tag{5.F-44c}$$

$$H_\beta = -\frac{i\omega\mu_h^s I a_x}{4\pi}\sin\beta\left[\ \mathcal{I}_{C0}^{TM} + \frac{1}{\rho}\left(\mathcal{I}_{C1}^{TE} - \mathcal{I}_{C1}^{TM}\right)\right], \tag{5.F-44d}$$

$$E_z = -\frac{I a_x}{4\pi}\frac{\mu_h^s}{\tilde{\varepsilon}_v}\sin\beta\int_0^\infty dk_\rho k_\rho^2\, J_1(k_\rho\rho)\, g_C^{TM}(p_{z\mathrm{II}}), \tag{5.F-44e}$$

$$H_z = +\frac{I a_x}{4\pi}\frac{\mu_h^s}{\mu_v}\cos\beta\int_0^\infty dk_\rho k_\rho^2\, J_1(k_\rho\rho)\, g_B^{TE}(p_{z\mathrm{I}}), \tag{5.F-44f}$$

where

$$\mathcal{I}_{B0}^{TE} = \int_0^\infty dk_\rho k_\rho\, J_0(k_\rho\rho)\, g_B^{TE}(p_{z\mathrm{I}}), \qquad \mathcal{I}_{B1}^{TE} = \int_0^\infty dk_\rho\, J_1(k_\rho\rho)\, g_B^{TE}(p_{z\mathrm{I}}), \tag{5.F-44g}$$

$$\mathcal{I}_{B0}^{TM} = \int_0^\infty dk_\rho k_\rho\, J_0(k_\rho\rho)\, g_B^{TM}(p_{z\mathrm{II}}), \qquad \mathcal{I}_{B1}^{TM} = \int_0^\infty dk_\rho\, J_1(k_\rho\rho)\, g_B^{TM}(p_{z\mathrm{II}}), \tag{5.F-44h}$$

$$\mathcal{I}_{C0}^{TE} = \int_0^\infty dk_\rho k_\rho\, J_0(k_\rho\rho)\, g_C^{TE}(p_{z\mathrm{I}}), \qquad \mathcal{I}_{C1}^{TE} = \int_0^\infty dk_\rho\, J_1(k_\rho\rho)\, g_C^{TE}(p_{z\mathrm{I}}), \tag{5.F-44i}$$

$$\mathcal{I}_{C0}^{TM} = \int_0^\infty dk_\rho k_\rho\, J_0(k_\rho\rho)\, g_C^{TM}(p_{z\mathrm{II}}), \qquad \mathcal{I}_{C1}^{TM} = \int_0^\infty dk_\rho\, J_1(k_\rho\rho)\, g_C^{TM}(p_{z\mathrm{II}}), \tag{5.F-44j}$$

and

$$g_B^{TE}(p_{z\mathrm{I}}) = \sqrt{\frac{\mu_h}{p_{z\mathrm{I}}}}\sqrt{\frac{p_{z\mathrm{I}}}{\mu_h}}^{s}\mathcal{R}_B^{TE}(p_{z\mathrm{I}}), \qquad g_B^{TM}(p_{z\mathrm{II}}) = \sqrt{\frac{p_{z\mathrm{II}}}{\tilde{\varepsilon}_h}}\sqrt{\frac{\tilde{\varepsilon}_h}{p_{z\mathrm{II}}}}^{s}\mathcal{R}_B^{TM}(p_{z\mathrm{II}}), \tag{5.F-45a}$$

$$g_C^{TE}(p_{z\mathrm{I}}) = -\sqrt{\frac{p_{z\mathrm{I}}}{\mu_h}}\sqrt{\frac{p_{z\mathrm{I}}}{\mu_h}}^{s}\mathcal{R}_C^{TE}(p_{z\mathrm{I}}), \qquad g_C^{TM}(p_{z\mathrm{II}}) = -\sqrt{\frac{\tilde{\varepsilon}_h}{p_{z\mathrm{II}}}}\sqrt{\frac{\tilde{\varepsilon}_h}{p_{z\mathrm{II}}}}^{s}\mathcal{R}_C^{TM}(p_{z\mathrm{II}}), \tag{5.F-45b}$$

where the RT-amplitudes are given by equation 5.138.

5.F.3 Electromagnetic field from a VED

The field components from a VED are obtained from equation 5.140:

$$E_\rho = +\frac{Il_z}{4\pi}\frac{i}{\omega\tilde{\varepsilon}_v^s}\int_0^\infty dk_\rho k_\rho^2\, J_1(k_\rho\rho)\, g_B^{TM}(p_{z\text{II}}), \tag{5.F-46a}$$

$$H_\beta = +\frac{Il_z}{4\pi}\frac{i}{\omega\tilde{\varepsilon}_v^s}\int_0^\infty dk_\rho k_\rho^2\, J_1(k_\rho\rho)\, g_C^{TM}(p_{z\text{II}}), \tag{5.F-46b}$$

$$E_z = -\frac{Il_z}{4\pi}\frac{1}{\omega^2\tilde{\varepsilon}_v\tilde{\varepsilon}_v^s}\int_0^\infty dk_\rho k_\rho^3\, J_0(k_\rho\rho)\, g_C^{TM}(p_{z\text{II}}) + \frac{Il_z}{4\pi}\frac{1}{i\omega\tilde{\varepsilon}_v^s}\delta(z-z_s)\delta(x)\delta(y). \tag{5.F-46c}$$

5.F.4 Electromagnetic field from a VMD

The field components from a VMD are obtained from equation 5.142:

$$E_\beta = -\frac{Ia_z}{4\pi}\int_0^\infty dk_\rho k_\rho^2\, J_1(k_\rho\rho)\, g_A^{TE}(p_{z\text{I}}), \tag{5.F-47a}$$

$$H_\rho = +\frac{Ia_z}{4\pi}\int_0^\infty dk_\rho k_\rho^2\, J_1(k_\rho\rho)\, g_D^{TE}(p_{z\text{I}}), \tag{5.F-47b}$$

$$H_z = +\frac{Ia_z}{4\pi}\frac{i}{\omega\mu_v}\int_0^\infty dk_\rho k_\rho^3\, J_0(k_\rho\rho)\, g_A^{TE}(p_{z\text{I}}) - \frac{Ia_z}{4\pi}\delta(z-z_s)\delta(x)\delta(y). \tag{5.F-47c}$$

5.F.5 RT-amplitudes with source and receiver in the same layer

Consider the responses in equation 5.F-43 and 5.F-45 with the source at $z_s = 0$, and the receiver within the same layer at z. The RT-responses in equation 5.134 and 5.138 can then be combined into a single expression for $z < z_s$ and $z > z_s$ and written in terms of a direct and reflected field contribution:

$$\mathcal{R}_A = \mathrm{e}^{i\omega p_z|z|} + R_A, \qquad R_A = \frac{\grave{R}_s(1+\acute{R}_s)\mathrm{e}^{-i\omega p_z z} + \acute{R}_s(1+\grave{R}_s)\mathrm{e}^{i\omega p_z z}}{1-\acute{R}_s\grave{R}_s}, \tag{5.F-48a}$$

$$\mathcal{R}_B = \mathrm{sgn}(z)\mathrm{e}^{i\omega p_z|z|} + R_B, \quad R_B = \frac{\grave{R}_s(1-\acute{R}_s)\mathrm{e}^{-i\omega p_z z} - \acute{R}_s(1-\grave{R}_s)\mathrm{e}^{i\omega p_z z}}{1-\acute{R}_s\grave{R}_s}, \tag{5.F-48b}$$

$$-\mathcal{R}_C = \mathrm{e}^{i\omega p_z|z|} + R_C, \qquad R_C = \frac{-\grave{R}_s(1-\acute{R}_s)\mathrm{e}^{-i\omega p_z z} - \acute{R}_s(1-\grave{R}_s)\mathrm{e}^{i\omega p_z z}}{1-\acute{R}_s\grave{R}_s}, \tag{5.F-48c}$$

$$-\mathcal{R}_D = \mathrm{sgn}(z)\mathrm{e}^{i\omega p_z|z|} + R_D, \quad R_D = \frac{-\grave{R}_s(1+\acute{R}_s)\mathrm{e}^{-i\omega p_z z} + \acute{R}_s(1+\grave{R}_s)\mathrm{e}^{i\omega p_z z}}{1-\acute{R}_s\grave{R}_s}. \tag{5.F-48d}$$

In the expressions, $p_z = p_{z\text{I}}$ for the TE mode, and $p_z = p_{z\text{II}}$ for the TM mode.

5.G Up/down-separation and free-surface removal

Consider an isotropic source medium in which the electromagnetic field from a dipole antenna e.g., HED is recorded. The propagator-matrix method with its implicit splitting of fields into upgoing and downgoing components can be useful in processing real data from e.g., a marine CSEM/SBL experiment in shallow water. A possible choice of the eigenvector matrix that diagonalizes the system matrix into upgoing and downgoing components of the electric field, is (Amundsen et al., 2006)

$$\boldsymbol{N}_A = \begin{pmatrix} \boldsymbol{I} & \boldsymbol{I} \\ \boldsymbol{N}_2 & -\boldsymbol{N}_2 \end{pmatrix}, \quad \boldsymbol{N}_A^{-1} = \frac{1}{2}\begin{pmatrix} \boldsymbol{I} & \boldsymbol{N}_2^{-1} \\ \boldsymbol{I} & -\boldsymbol{N}_2^{-1} \end{pmatrix}, \tag{5.G-49}$$

where in isotropic media

$$\boldsymbol{N}_2 = \frac{1}{\mu p_z}\begin{pmatrix} \mu\tilde{\varepsilon} - p_y^2 & p_x p_y \\ p_x p_y & \mu\tilde{\varepsilon} - p_x^2 \end{pmatrix}, \quad \boldsymbol{N}_2^{-1} = \frac{1}{\tilde{\varepsilon} p_z}\begin{pmatrix} \mu\tilde{\varepsilon} - p_x^2 & -p_x p_y \\ -p_x p_y & \mu\tilde{\varepsilon} - p_y^2 \end{pmatrix}. \tag{5.G-50}$$

In this case, the eigenvector matrix is normalized with respect to the electric amplitude which leads to the relations

$$E_x = E_x^U + E_x^D \quad \text{and} \quad E_y = E_y^U + E_y^D. \tag{5.G-51}$$

Now $\boldsymbol{b} = \boldsymbol{N}_A \boldsymbol{w}_A$, where $\boldsymbol{w}_A = \begin{pmatrix} E_x^U & E_y^U & E_x^D & E_y^D \end{pmatrix}^T$. The quantity E^U describes the part of the electric field that is upgoing, and E^D describes the downgoing electric field. From the equations for up/down-separation where $\boldsymbol{N}_A$ is arranged to give $E_x = E_x^U + E_x^D$, one then gets

$$E_x^U = \frac{1}{2}\left(E_x - \frac{p_x p_y}{\tilde{\varepsilon} p_z} H_x - \frac{\mu\tilde{\varepsilon} - p_x^2}{\tilde{\varepsilon} p_z} H_y\right), \tag{5.G-52a}$$

$$E_x^D = \frac{1}{2}\left(E_x + \frac{p_x p_y}{\tilde{\varepsilon} p_z} H_x + \frac{\mu\tilde{\varepsilon} - p_x^2}{\tilde{\varepsilon} p_z} H_y\right). \tag{5.G-52b}$$

When inserting the field expressions from equation 5.133 into equation 5.G-52 with the appropriate simplifications for isotropic media with source and receiver within the same layer (equation 5.F-48), one gets:

$$E_x^U = \frac{I l_x}{2}\left[\frac{\mu p_y^2}{p_\rho p_z} f(-z, R_A^{TE}, -R_D^{TE}) + \frac{p_x^2 p_z}{\tilde{\varepsilon} p_\rho} f(-z, R_A^{TM}, -R_D^{TM})\right], \tag{5.G-53a}$$

$$E_x^D = \frac{I l_x}{2}\left[\frac{\mu p_y^2}{p_\rho p_z} f(z, R_A^{TE}, R_D^{TE}) + \frac{p_x^2 p_z}{\tilde{\varepsilon} p_\rho} f(z, R_A^{TM}, R_D^{TM})\right], \tag{5.G-53b}$$

where

$$f(z, R_A, R_D) = \frac{1 + \operatorname{sgn}(z)}{2}\, \mathrm{e}^{i\omega p_z |z|} + \frac{R_A + R_D}{2}. \tag{5.G-54}$$

From equation 5.F-48a and 5.F-48d, the following relations can be derived:

$$\frac{R_A - R_D}{2} = \frac{1}{1 - \grave{R}_s \acute{R}_s} \grave{R}_s (1 + \acute{R}_s) \mathrm{e}^{-i\omega p_z z}, \tag{5.G-55a}$$

$$\frac{R_A + R_D}{2} = \frac{1}{1 - \grave{R}_s \acute{R}_s} \acute{R}_s (1 + \grave{R}_s) \mathrm{e}^{i\omega p_z z}. \tag{5.G-55b}$$

The TE and TM modes are not separated in these expressions. In order to derive expressions with separated modes, the eigenvector matrix can be chosen as in equation 5.E-33. Then the mode-field vector describes the upgoing and downgoing TE and TM mode. In isotropic media

$$\begin{pmatrix} U^{TE} \\ U^{TM} \\ D^{TE} \\ D^{TM} \end{pmatrix} = \boldsymbol{N}_F^{-1} \boldsymbol{b} = \frac{1}{\sqrt{2} p_\rho} \begin{pmatrix} p_y & -p_x & p_y \frac{\mu}{p_z} & -p_x \frac{\mu}{p_z} \\ p_x & p_y & p_x \frac{p_z}{\tilde{\varepsilon}} & p_y \frac{p_z}{\tilde{\varepsilon}} \\ p_y & -p_x & -p_y \frac{\mu}{p_z} & p_x \frac{\mu}{p_z} \\ p_x & p_y & -p_x \frac{p_z}{\tilde{\varepsilon}} & -p_y \frac{p_z}{\tilde{\varepsilon}} \end{pmatrix} \begin{pmatrix} E_x \\ E_y \\ -H_y \\ H_x \end{pmatrix}. \tag{5.G-56}$$

By inserting the field expressions from equation 5.133 with the appropriate simplifications for isotropic media with source and receiver within the same layer, one then gets

$$U^{TE} = \frac{I l_x}{2\sqrt{2} p_\rho} \left(\frac{\mu p_y}{p_z} \left\{ [1 - \mathrm{sgn}(z)] \mathrm{e}^{i\omega p_z |z|} + R_A^{TE} - R_D^{TE} \right\} \right), \tag{5.G-57a}$$

$$U^{TM} = \frac{I l_x}{2\sqrt{2} p_\rho} \left(\frac{p_z p_x}{\tilde{\varepsilon}} \left\{ [1 - \mathrm{sgn}(z)] \mathrm{e}^{i\omega p_z |z|} + R_A^{TM} - R_D^{TM} \right\} \right), \tag{5.G-57b}$$

$$D^{TE} = \frac{I l_x}{2\sqrt{2} p_\rho} \left(\frac{\mu p_y}{p_z} \left\{ [1 + \mathrm{sgn}(z)] \mathrm{e}^{i\omega p_z |z|} + R_A^{TE} + R_D^{TE} \right\} \right), \tag{5.G-57c}$$

$$D^{TM} = \frac{I l_x}{2\sqrt{2} p_\rho} \left(\frac{p_z p_x}{\tilde{\varepsilon}} \left\{ [1 + \mathrm{sgn}(z)] \mathrm{e}^{i\omega p_z |z|} + R_A^{TM} + R_D^{TM} \right\} \right). \tag{5.G-57d}$$

Here, the upgoing and downgoing mode-fields are a mix of the electric and magnetic field.

In a marine CSEM/SBL experiment, the receiver is normally situated below the receiver, i.e., $z > 0$ in equation 5.F-48. The reflection response from the lower stack can thus be obtained by dividing the upgoing mode-field by the downgoing mode-field. The reflection responses for the TE- and TM-polarization components hence become:

$$\frac{U^{TE}}{D^{TE}} = \grave{R}_b^{TE} \quad \text{and} \quad \frac{U^{TM}}{D^{TM}} = \grave{R}_b^{TM}, \tag{5.G-58}$$

where $\grave{R}_b$ is the reflection response from the lower stack at the receiver (cf. Figure 5.4). The decomposition matrix from equation 5.120 would give the same results since the difference between the eigenvectors lies within a normalization factor. By using the reflection response from the lower stack when calculating the electromagnetic field from an artificial source, one might say that one in this way has removed the free surface from the original data set. In order to do the free-surface removal with the procedure described here, a 2-D data set with $z > z_s$ and which contains all the horizontal components of the electromagnetic field is needed.

Bibliography

Abramowitz, M. and Stegun, I. A. (1962). *Handbook of Mathematical Functions*. Dover, New York, 9th edition.

Adler, R. B., Chu, L. J., and Fano, R. M. (1960). *Electromagnetic Energy Transmission and Radiation*. John Wiley & Sons, New York.

Altman, C. and Suchy, K. (1998). The Maxwell and adjoint systems for complex media: Physical significance and applications. *International Journal of Applied Electromagnetics and Mechanics*, 9(1):135–142.

Amundsen, L., Løseth, L. O., Mittet, R., Ellingsrud, S., and Ursin, B. (2006). Decomposition of electromagnetic fields into upgoing and downgoing components. *Geophysics*, 71(5):G211–G223.

Anderson, W. L. (1979). Computer program, numerical integration of related Hankel transforms of orders 0 and 1 by adaptive digital filtering. *Geophysics*, 44(7):1287–1305.

Anderson, W. L. (1989). A hybrid fast Hankel transform algorithm for electromagnetic modeling. *Geophysics*, 54(2):263–266.

Bannister, P. R. (1984). New simplified formulas for ELF subsurface-to-subsurface propagation. *IEEE Journal of Oceanic Engineering*, OE-9(3):154–163.

Baños, A. (1966). *Dipole Radiation in the Presence of a Conducting Half-Space*. Pergamon Press, Oxford.

Bender, C. M. and Orszag, S. A. (1999). *Advanced Mathematical Methods for Scientists and Engineers*. Springer-Verlag, New York.

Berremann, D. W. (1972). Optics in stratified and anisotropic media: $4 \times 4-$matrix formulation. *Journal of the Optical Society of America*, 62(4):502–510.

Born, M. and Wolf, E. (1999). *Principles of Optics*. University Press, Cambridge, 7th edition.

Brekhovskikh, L. M. (1960). *Waves in Layered Media*. Academic Press, New York.

Bremmer, H. (1949). *Terrestrial Radio Waves*. Elsevier, New York.

Brillouin, L. (1914). 2. Über die Fortpflanzung des Lichtes in dispergierenden Medien. *Annalen der Physik*, 44(10):203–240.

Bunse-Gerstner, A., Byers, R., and Mehrmann, V. (1992). A chart of numerical methods for structured eigenvalue problems. *SIAM Journal of Matrix Analysis and Its Applications*, 13:419–453.

Burrows, M. L. (1978). *ELF Communications Antennas*. Peter Peregrinus Ltd., Institution of Electrical Engineers.

Cagniard, L. (1953). Basic theory of the magneto-telluric method of geophysical prospecting. *Geophysics*, 18(3):605–635.

Carcione, J. M. (2006). A spectral numerical method for electromagnetic diffusion. *Geophysics*, 71(1):I1–I9.

Carcione, J. M. and Cavallini, F. (2001). A semianalytical solution for the propagation of electromagnetic waves in 3-D lossy orthotropic media. *Geophysics*, 66(4):1141–1148.

Carcione, J. M. and Schoenberg, M. A. (2000). 3-D ground-penetrating radar simulation and plane-wave theory in anisotropic media. *Geophysics*, 65(5):1527–1541.

Červený, V. and Hron, F. (1980). The ray series method and dynamic ray tracing system for three dimensional inhomogeneous media. *Bulletin of Seismological Society of America*, 70:47–77.

Chapman, C. (2004). *Fundamentals of Seismic Wave Propagation*. University Press, Cambridge.

Chapman, C. H. (1994). Reflection/transmission coefficient reciprocities in anisotropic media. *Geophysical Journal International*, 116:498–501.

Chave, A. D., Constable, S., and Edwards, R. N. (1991). Electrical exploration methods for the seafloor. In Nabighian, M. N., editor, *Electromagnetic Methods in Applied Geophysics*, volume 2: Application, pages 931–366. Society of Exploration Geophysicists, Oklahoma.

Chave, A. D. and Cox, C. S. (1982). Controlled electromagnetic sources for measuring electrical conductivity beneath the oceans. 1. Forward problem and model study. *Journal of Geophysical Research*, 87:5327–5338.

Chave, A. D., Flosadottir, A. H., and Cox, C. S. (1990). Some comments on the seabed propagation of VLF/ULF electromagnetic fields. *Radio Science*, 25:825–836.

Chew, W. C. (1995). *Waves and Fields in Inhomogeneous Media*. IEEE Press, New York.

Chlamtac, M. and Abramovici, F. (1981). The electromagnetic fields of a horizontal dipole over a vertically inhomogeneous and anisotropic earth. *Geophysics*, 46:904–915.

Christensen, N. B. (1990). Optimized fast Hankel transform filters. *Geophysical Prospecting*, 38:545–568.

Claerbout, J. F. (1971). Toward a unified theory of reflector mapping. *Geophysics*, 36(3):467–481.

Constable, S. and Cox, C. (1996). Marine controlled source electromagnetic sounding - II: The PEGASUS experiment. *Journal of Geophysical Research*, 97:5519–5530.

Constable, S., Orange, A. S., Hoversten, G. M., and Morrison, F. (1998). Marine magnetotellurics for petroleum exploration, part I: A sea-floor equipment system. *Geophysics*, 63:816–825.

Constable, S. and Weiss, C. J. (2006). Mapping thin resistors and hydrocarbons with marine EM methods: Insights from 1D modeling. *Geophysics*, 71(2):G43–G51.

Cox, C. S., Constable, S. C., Chave, A. D., and Webb, S. C. (1986). Controlled source electromagnetic sounding of the oceanic lithosphere. *Nature*, 320:52–54.

Cox, C. S., Filloux, J. H., and Larsen, J. (1971). Electromagnetic studies of ocean currents and electrical conductivity below the ocean floor. In Maxwell, A., editor, *The Sea*, volume 4, part I, pages 637–693. John Wiley, New York.

Crank, J. (1975). *The Mathematics of Diffusion*. Clarendon Press, Oxford, 2nd edition.

Darrigol, O. (2000). *Electrodynamics from Ampère to Einstein*. University Press, Oxford.

Davison, M. and Doeschl, A. (2004). A hyperbolic PDE with parabolic behavior. *SIAM Review*, 46(1):115–127.

DeSanto, J. A. (1992). *Scalar Wave Theory*. Springer-Verlag, Heidelberg.

Edwards, R. N., Nobes, D. C., and Gómes-Treviño, E. (1984). Offshore electrical exploration of sedimentary basins: The effects of anisotropy in horizontally isotropic, layered media. *Geophysics*, 49(5):566–576.

Eidesmo, T., Ellingsrud, S., MacGregor, L. M., Constable, S. C., Sinha, M. C., Johansen, S., Kong, F. N., and Westerdahl, H. (2002). SeaBed Logging (SBL), a new method for remote and direct identification of hydrocarbon filled layers in deepwater areas using controlled source electromagnetic sounding. *First Break*, 20:144–152.

Ellingsrud, S., Eidesmo, T., Schaug-Pettersen, T., and Pedersen, H. M. (2000). Method and apparatus for determining the nature of subterranean reservoirs. European Patent Office. EP 1 309 887 B1, March 31st, 2004, filed August 2nd 2001 (priority date August 14th, 2000).

Ellingsrud, S., Eidesmo, T., Sinha, M. C., MacGregor, L. M., and Constable, S. C. (2002). Remote sensing of hydrocarbon layers by SeaBed Logging (SBL): Results from a cruise offshore Angola. *Leading Edge*, 20(10):972–982.

Evans, R. L., Sinha, M. C., Constable, S., and Unsworth, M. J. (1994). On the electrical nature of the axial melt zone at 13N on the East Pacific Rise. *Journal of Geophysical Research*, 99:577–588.

Everett, M. E. and Constable, S. (1999). Electric dipole fields over an anisotropic seafloor: Theory and application to the structure of 40 Ma Pacific Ocean lithosphere. *Geophysical Journal International*, 136:41–56.

Faßbender, H., Mackey, D. S., and Mackey, N. (2001). Hamilton and Jacobi come full circle: Jacobi algorithms for structured Hamiltonian eigenproblems. *Linear Algebra and Its Applications*, 332-334:37–80.

Felsen, L. B. and Marcuvitz, N. (2003). *Radiation and Scattering of Waves*. John Wiley & Sons, New York.

Goldstein, H. (1980). *Classical Mechanics*. Addison-Wesley, London, 2nd edition.

Gradshteyn, I. S. and Ryzhik, I. M. (1980). *Table of Integrals, Series, and Products*. Academic Press, San Diego, CA.

Green, G. (1828). *An Essay on the Application of Mathematical Analysis to the Theories of Electricity and Magnetism*. T. Wheelhouse, Nottigham.

Griffiths, D. J. (1999). *Introduction to Electrodynamics*. Prentice Hall, New Jersey.

Griffiths, D. J. and Steinke, C. A. (2000). Waves in locally periodic media. *American Journal of Physics*, 69(2):137–154.

Hänggi, P., Roesel, F., and Trautman, D. (1998). Evaluation of infinite series by use of continued fraction expansions: A numerical study. *Journal of Computational Physics*, 37:242–258.

Helbig, K. and Thomsen, L. (2005). 75-plus years of anisotropy in exploration and reservoir seismics: A historical review of concepts and methods. *Geophysics*, 70(6):9ND–23ND.

Hill, D. A. and Wait, J. R. (1980). Ground wave attenuation function for a spherical earth with arbitrary surface impedance. *Radio Science*, 15(3):637–643.

Hofmann, J. R. (2006). *André-Marie Ampère: Enlightenment and Electrodynamics*. University Press, Cambridge.

Horn, R. A. and Johnson, C. A. (1985). *Matrix Analysis*. Cambridge University Press, Cambridge.

Hoversten, G. M., Newman, G. A., Geier, N., and Flanagan, G. (2006). 3D modeling of a deepwater EM exploration survey. *Geophysics*, 71(5):G239–G248.

Huard, S. (1997). *Polarization of Light*. John Wiley & Sons, New York.

Jackson, J. D. (1998). *Classical Electrodynamics*. John Wiley & Sons, New York, 3rd edition.

Johnson, H. M. (1962). A history of well logging. *Geophysics*, 27(4):507–527.

Kennedy, W. D. and Herrick, D. C. (2004). Conductivity anisotropy in shale-free sandstone. *Petrophysics*, 45(1):38–58.

Kennett, B. L. N. (1983). *Seismic Wave Propagation in Stratified Media*. Cambridge University Press, Cambridge.

King, R. W. P., Owens, M., and Wu, T. T. (1992). *Lateral Electromagnetic Waves*. Springer-Verlag, New York.

Kong, J. A. (1972). Electromagnetic fields due to dipole antennas over stratified anisotropic media. *Geophysics*, 37(6):985–996.

Kong, J. A. (2000). *Electromagnetic Wave Theory*. EMW Publishing, Cambridge, Massachusetts.

Kraichman, M. B. (1970). *Handbook of Electromagnetic Propagation in Conducting Media*. U.S. Government Printing Office, Washington D.C.

Lee, K. H., Liu, G., and Morrison, H. F. (1989). A new approach to modeling the electromagnetic response of conductive media. *Geophysics*, 54(9):1180–1192.

Li, X. and Pedersen, L. B. (1991). The electromagnetic response of an azimuthally anisotropic half-space. *Geophysics*, 56(9):1462–1473.

Løseth, L. O. (2000). Electromagnetic waves in layered media. M.Sc. Thesis, NTNU.

Løseth, L. O. (2007). Asymptotic evaluations of the marine CSEM field integrals. *IEEE Transactions on Geoscience and Remote Sensing, Submitted for publication*.

Løseth, L. O., Pedersen, H. M., Schaug-Pettersen, T., Ellingsrud, S., and Eidesmo, T. (2006a). The first test of the SeaBed Logging method. *Journal of Applied Geophysics, Submitted for publication*.

Løseth, L. O., Pedersen, H. M., Ursin, B., Amundsen, L., and Ellingsrud, S. (2006b). Low-frequency electromagnetic fields in applied geophysics: Waves or diffusion? *Geophysics*, 71(4):W29–W40.

Løseth, L. O. and Ursin, B. (2007). Electromagnetic fields in planarly layered anisotropic media. *Geophysical Journal International, Accepted for publication*.

MacGregor, L. M. and Sinha, M. C. (2000). Use of marine controlled source electromagnetic sounding for sub-basalt exploration. *Geophysical Prospecting*, 48:1091–1106.

Maillet, R. (1947). The fundamental equations of electrical propspecting. *Geophysics*, 12(4):529–556.

Mohsen, A. A. and Hashish, E. A. (1994). The fast Hankel transform. *Geophysical Prospecting*, 34:131–139.

Morse, P. M. and Feshbach, H. (1953). *Methods of Theoretical Physics*. McGraw-Hill, New York.

Nabighian, M. N. (1987). *Electromagnetic Methods in Applied Geophysics, Vol. 1: Theory, Vol. 2: Applications, Series: Investigations in Applied Geophysics; No. 3*. Society of Exploration Geophysicists, Oklahoma.

Negi, J. G. and Saraf, P. D. (1989). *Anisotropy in Geoelectromagnetism*. Elsevier, New York.

Nekut, A. G. (1994). Electromagnetic ray-trace tomography. *Geophysics*, 59(3):371–377.

O'Brien, D. P. and Morrison, H. F. (1967). Electromagnetic fields in an N-layer anisotropic half-space. *Geophysics*, 32(4):668–677.

Onsager, L. (1931). Reciprocal relations in irreversible processes I. *Physical Review*, 37:405–425.

Ott, H. (1942). Reflexion und Brechung von Kugelwellen; Effekte 2. Ordnung. *Annalen der Physik*, 41:443–466.

Press, W. H., Teukolsky, S. A., Vetterling, W. T., and Flannery, B. P. (1997). *Numerical Recipes in Fortran 77*. Cambridge University Press, New York, 2nd edition.

Raiche, A. P. and Gallagher, R. G. (1985). Apparent resistivity and diffusion velocity. *Geophysics*, 50(10):1628–1633.

Sinha, A. K. and Bhattacharyya, P. K. (1967). Electric dipole over an anisotropic and inhomogeneous earth. *Geophysics*, 32(4):652–667.

Sommerfeld, A. (1909). 1. Über die Ausbreitung der Wellen in der drahtlosen Telegraphie. *Annalen der Physik*, 28(4):665–736.

Sommerfeld, A. (1914). 1. Über die Fortpflanzung des Lichtes in dispergierenden Medien. *Annalen der Physik*, 44(10):177–202.

Sommerfeld, A. (1967). *Partial Differential Equations in Physics*. Academic Press, New York.

Spies, B. (1989). Depth of investigation in electromagnetic sounding methods. *Geophysics*, 54(7):872–888.

Stamnes, J. J. (1986). *Waves in Focal Regions*. Adam Hilger, Bristol.

Stamnes, J. J. and Sithambaranathan, G. S. (2001). Reflection and refraction of an arbitrary electromagnetic wave at a plane interface separating an isotropic and a biaxial medium. *Journal of Optical Society of America A*, 18(12):3119–3129.

Stovas, A. and Ursin, B. (2003). Reflection and transmission responses of layered transversely isotropic viscoeleastic media. *Geophysical Prospecting*, 51:447–477.

Stratton, J. A. (1941). *Electromagnetic Theory*. McGraw-Hill, New York.

Suchy, K. and Altman, C. (1975). The Maxwell field, its adjoint field and the 'conjugate' field in anisotropic absorbing media. *Journal of Plasma Physics*, 13, part 2:299–316.

Svendsen, I. A. and Jonsson, I. G. (1976). *Hydrodynamics of Costal Regions*. Technical University of Denmark, DK-2800 Lyngby.

Tai, C.-T. (1994). *Dyadic Green Functions in Electromagnetic Theory*. IEEE Press, New York.

Ulaby, F. T. (2001). *Fundamentals of Applied Electromagnetics*. Prentice Hall, New Jersey.

Ursin, B. (1983). Review of elastic and electromagnetic wave propagation in horizontally layered media. *Geophysics*, 48:1063–1081.

Ursin, B. and Stovas, A. (2002). Reflection and transmission responses of a layered isotropic viscoelastic medium. *Geophysics*, 67(1):307–323.

Vašíček, A. (1960). *Optics in Thin Films*. North Holland Publishing Company, Amsterdam.

Virieux, J., Flores-Luna, C., and Gibert, D. (1994). Asymptotic theory for diffusive electromagnetic imaging. *Geophysical Journal International*, 119:857–868.

Wait, J. R. (1961). The electromagnetic fields of a horizontal dipole in the presence of a conducting half-space. *Canadian Journal of Physics*, 39:1017–1028.

Wait, J. R. (1962). *Electromagnetic Waves in Stratified Media*. Pergamon Press, Oxford.

Wait, J. R. (1966). Electromagnetic propagation in an idealized earth crust waveguide. *Radio Science*, 1:913–924.

Wait, J. R. (1998). The ancient and modern history of EM ground-wave propagation. *IEEE Antennas and Propagation Magazine*, 40(5):7–23.

Ward, S. H. (1980). Electrical, electromagnetic, and magnetotelluric methods. *Geophysics*, 45(11):1659–1666.

Ward, S. H. and Hohmann, G. W. (1987). Electromagnetic theory for geophysical applications. In Nabighian, M. N., editor, *Electromagnetic Methods in Applied Geophysics*, volume 1: Theory, pages 131–311. Society of Exploration Geophysicists, Oklahoma.

Weyl, H. (1919). Ausbreitung elektromagnetischer Wellen über einem ebenen Leiter. *Annalen der Physik*, 60:481–500.

White, B. S. and Zhou, M. (2006). Electroseismic prospecting in layered media. *SIAM Journal on Applied Mathematics*, 67(1):69–98.

Yin, C. (2006). MMT forward modeling for a layered earth with arbitrary anisotropy. *Geophysics*, 71(3):G115–G128.

Yin, C. and Maurer, H. M. (2001). Electromagnetic induction in a layered earth with arbitrary anisotropy. *Geophysics*, 66(5):1405–1416.

Yin, C. and Weidelt, P. (1999). Geoelectrical fields in a layered earth with arbitrary anisotropy. *Geophysics*, 64(2):426–434.

Young, P. D. and Cox, C. S. (1981). Electromagnetic active source sounding near the East Pacific Rise. *Geophysical Research Letters*, 8:1043–1046.

Yu, L. and Edwards, R. N. (1992). The detection of lateral anisotropy of the ocean floor by electromagnetic methods. *Geophysical Journal International*, 108:433–441.

Yu, L., Evans, R. L., and Edwards, R. N. (1997). Transient electromagnetic responses in seafloor with triaxial anisotropy. *Geophysical Journal International*, 129:292–304.

Zenneck, J. (1907). Fortpflanzung ebener elektromagnetischer Wellen längs einer ebenen Leiterfläche. *Annalen der Physik*, 23:846–866.